

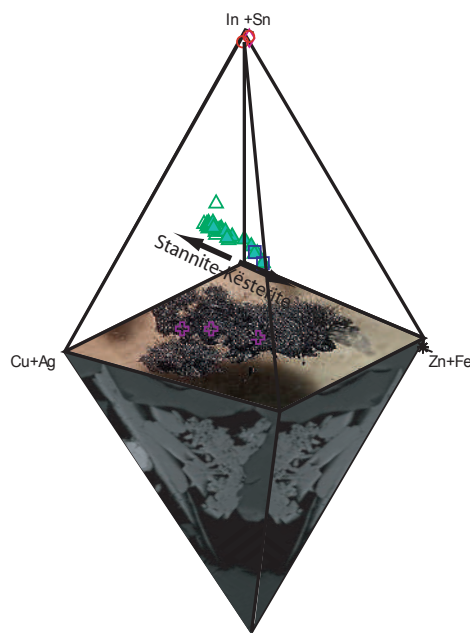


Escola Politècnica Superior  
d'Enginyeria de Manresa

UNIVERSITAT POLITÈCNICA DE CATALUNYA

# GEOCHEMICAL AND METALLOGENIC MODEL OF THE SANTA FE SN-ZN-PB-AG-(IN) DEPOSIT IN THE CENTRAL ANDEAN TIN BELT

**PhD Thesis by  
Ma. Abigail Jiménez Franco**





**Escola Politècnica Superior  
d'Enginyeria de Manresa**

UNIVERSITAT POLITÈCNICA DE CATALUNYA

**Thesis for the Doctor of Philosophy Degree at the  
Polytechnic University of Catalonia within Doctoral  
Program of Natural Resources and Environment**

**Advisors: Dr. Ma. Pura Alfonso Abella  
Dr. Carles Canet Miquel**



# ACKNOWLEDGEMENTS

I would like to express my gratitude to my doctoral thesis supervisors Dr. Pura Alfonso Abella and Dr. Carles Canet Miquel for his guidance, support and belief during this process. I must also acknowledge to Marc Bascompte Massanés and H. Francisco Anticoi Sudzuki for their support but above all for friendship without which this thesis would not have been possible.

I gratefully acknowledge to Dra. Maite Garcia-Valles of the *Universitat de Barcelona (UB)* for her important contributions on different aspects of this work. In addition, I want to express my gratitude to the staff of the Japo, Santa Fe and Morococala mines for their kind guidance. Finally, I would like to thank the *Departament d'Enginyeria Minera, Industrial i TIC, of the Universitat Politècnica de Catalunya (UPC)*.

This work was partly financed by the project AECID: A3/042750/11, the *Centre de Cooperació per al Desenvolupament of the UPC (CCD 2013UO010, 2014U002)* and the SGR 2014 SGR 1661. This work is possible because a grant from the Mexican Secretariat of Education (SEP) and the National Council on Science and Technology (CONACYT) of Mexico. The EPMA analyses were obtained at the *Serveis Científics i Tecnològics de la UB (CCiT-UB)* and the *Laboratorio Universitario de Petrología, of the Instituto de Geofísica, UNAM*. I thank Xavier Llovet and Carlos Linares López for their assistance during the EPMA analyses. Isotopic analyses were also performed in the CCiT-UB. The relationship with the *Instituto de Geofísica* of the UNAM has been key to carry on an essential part of the analysis of laboratory indispensable to development of this work. Fluid Inclusion study was carried on at the Campus Juriquilla of the UNAM, this has been possible due to collaboration of Dr. Eduardo Gonzalez-Partida.

---

---

# ABSTRACT

The Santa Fe mining district is located in the Central Andean tin belt and contains several Sn-Zn-Pb-Ag deposits. From the economic point of view, the most important deposits of the district are Japo, Santa Fe and Morococala. Beyond the traditional metal commodities, the Central Andean Tin Belt could become an exploration target for indium, owing to the potential of the ore-bearing paragenesis to contain high concentrations of this technology-critical element. Notwithstanding the foregoing, important features about genesis and fluids evolution have been poorly studied. This work presents a reinterpretation of the Santa Fe deposit as a greisen deposit based in fluid inclusions and isotopic data, as well as an extensive and accurate fieldwork. In the Santa Fe district, the ore mineralization occurs as two main styles: (a) Sn-rich mineralization, represented by cassiterite-quartz veins, and (b) Zn-Pb-Ag mineralization, represented by sphalerite, galena and stannite group phases. The In contents in igneous rocks are between 1.5 and 2.5 ppm, whereas in the ore concentrate it attains up to 200 ppm. The  $1000 \times \text{In}/\text{Zn}$  ratio ranges from 25 up to 4000.

Exceptionally high In values were found in sakuraiite (2.03 wt.%). Sakuraiite in this deposit show evidences for a link between stannite-k esterite solution. Thus, there is an important relationship between stannite group and and the others sulfosalts in this deposit.

Likewise, an important number of metal associations, including base, alloy, noble and critical metals, have been found in this ore deposit. There is a noteworthy exploration potential for these metals in the Santa Fe District and even in similar deposits elsewhere in the Central Andean tin belt.

*Keywords:* Indium; tin; greisen; stannite; sakuraiite; sulfosalts.

---

# RESUMEN

El distrito minero de Santa Fe se encuentra ubicado en la faja estannífera de la cordillera central andina, la cual contiene importantes depósitos de Sn-Zn-Pb-Ag. Desde el punto de vista económico, los depósitos más importantes de este distrito son los de Japo, Santa Fe y Morococala. Más allá de los productos metálicos tradicionales, la faja estannífera podría convertirse en un potencial blanco de exploración para elementos tecnológicamente estratégicos como el indio.

No obstante lo anterior, el conocimiento de los aspectos más destacados respecto a la evolución y la génesis de los fluidos mineralizantes en este sector andino continúan siendo incipiente. Por ello, este trabajo pretende esclarecer y reinterpretar la historia y evolución geológica del yacimiento de Santa Fe, el cual en el presente trabajo se ha clasificado como un depósito tipo greisen con base fundamentalmente en el estudio de las asociaciones minerales y su química mineral; así como, en el estudio geotermométrico y considerando los datos isotópicos obtenidos, sin dejar de lado un exhaustivo y sistemático trabajo de campo.

En el distrito de Santa Fe, las menas metálicas se presentan en dos estilos principales: (a) la mineralización rica en Sn, representada por las vetas de cuarzo y casiterita y (b) la mineralización de Zn-Pb-Ag, representada por esfalerita, galena y minerales del grupo de la estannita.

La geoquímica de la suite de rocas encajantes también fue analizado. El contenido de In en rocas ígneas resulta ser de entre 1.5 y 2.5 ppm, mientras que en el concentrado de mineral alcanza hasta 200 ppm. La relación  $1000 \times \text{In} / \text{Zn}$  oscila entre 25 y 4000. Aunado a estos resultados, valores excepcionalmente altos de In fueron encontrados en cristales de sakuraiita (2,03 % en peso).

La sakuraiita en este depósito representa un vínculo entre la solución de stannite-kästerite, de lo cual puede inferirse una relación genética entre el grupo de la estannita y otras sulfosales en este depósito.

Asimismo, el yacimiento de Santa Fe también muestra un importante número de asociaciones metálicas, incluyendo metales bases, aleaciones, metales nobles y metales críticos. Hay un evidente potencial de exploración para estos metales en el Distrito de Santa Fe e incluso en depósitos similares también en otras zonas en la faja estannífera y en la cordillera central andina.

*Palabras clave:* indio; estaño; greisen; estannita; sakuraiita; sulfosales.

# RESUM

**E**l districte miner de Santa Fe està situat a la faixa estannífera de la serralada central andina, la qual conté importants dipòsits de Sn-Zn-Pb-Ag. Des del punt de vista econòmic, els dipòsits més importants d'aquest districte són els de Japo, Santa Fe i Morococala. Més enllà dels productes metàl·lics tradicionals, la faixa estannífera podria convertir-se en un potencial objectiu d'exploració degut als elements estratègics que conté, entre ells 'indi.

No obstant això, el coneixement dels aspectes més destacats de l'evolució i la gènesi dels fluids mineralitzadors en aquesta zona és incipient. Per aquesta raó, aquest treball pretén aclarir i reinterpretar la història i evolució geològica del jaciment de Santa Fe, classificant-lo com un dipòsit tipus greisen a partir de les associacions minerals i el seu quimisme. Així com, en l'estudi geotermomètric i considerant les dades isotòpiques obtingudes i amb base en un treball exhaustiu i sistemàtic de camp.

Les menes metàl·liques del jaciment es presenten en dos tipus principals: (a) mineralització rica en Sn, representada per les vetes de quarz i cassiterita, i (b) mineralització de Zn-Pb-Ag, representada per esfalerita, galena i minerals del grup de l'estannita.

La geoquímica del conjunt de roques ígnies encaixants també va ser analitzada. El contingut d'indi és d'entre 1,5 i 2,5 ppm, el concentrat arriba fins a 200 ppm i la relació  $1000 \times \text{In}/\text{Zn}$  oscil·la entre 25 i 4000. Addicionalment, s'han trobat valors excepcionalment alts d'indi en cristalls de sakuraiita (2.03% en pes), mostrant l'evidència d'un vincle entre la solució d'estannita-kësterita, de la qual es pot inferir una relació genètica entre el grup de l'estannita i altres sulfosals en aquest dipòsit.



El jaciment de Santa Fe també mostra un important nombre d'associacions metàl·liques, incloent-hi metalls base, aliatges, metalls nobles i metalls crítics. Hi ha un evident potencial d'exploració per aquests metalls al Districte de Santa Fe i fins i tot en dipòsits similars en altres zones de la faixa estannífera i en la serralada central andina.

*Paraules clau:* indi; estany; greisen; estannita; sakuraiïta; sulfosals.

# TABLE OF CONTENTS

Acknowledgements.....	i
Abstract.....	ii
Resumen.....	iii
Resum.....	v
Table of contents.....	vii
Figures Index.....	ix
Tables Index.....	xiii
1. Introduction.....	1
1.1. Goals.....	3
1.2. Specific goals.....	4
2. State of the art.....	7
2.1. Tin and metal sources .....	7
2.2. Tin deposits and magmatism.....	11
2.3. Geodynamic context.....	14
2.4. Greisen ore systems.....	16
2.5. Indium and world scenery.....	18
3. Regional Framework. The Central Andean Tin Belts.....	25
4. The Santa Fe Mining District.....	29
4.1. Previous works.....	30
4.2. Geology of the Santa Fe Mining District.....	34
4.3. Stratigraphy.....	35
Paleozoic.....	35
Cenozoic.....	38
4.4. Ore mineralization.....	41
The Japo deposit.....	41
The Santa Fe-Morococala deposit.....	42
5. Sampling and methods.....	45
5.1. Sampling and description.....	45
5.2. Petrographic study.....	46
5.3. X-ray powder diffraction.....	46
5.4. Scanning electron microscopy (SEM), with X-ray dispersive energy analyzer (EDS) and EMPA.....	48
5.5. Bulk chemical analyses.....	51
5.6. Micro-thermometric study of fluid inclusions.....	51
5.7. Sulfur isotopes.....	54
6. Results.....	57

6.1. Petrography.....	57
6.2. Geochemistry of metal and metalloid elements.....	62
6.3. REE Geochemistry.....	65
6.4. Mineralogical study and mineral chemistry.....	67
6.5. Alteration.....	80
6.6. Ore distribution in mineral processing.....	81
6.7. Fluids characterization.....	83
7. Discussion: The greisen deposit of the Santa Fe Mining District and its Indium potential.....	89
7.1. Paragenetic sequence.....	89
7.2. Fluids evolution and sulfur source.....	91
7.3. Type of deposit.....	93
7.4. Indium-bearing in the Santa Fe Mining District.....	100
Conclusions remarks and recommendations.....	105
REFERENCES.....	107

# FIGURES INDEX

Figure 1. Diagram showing relationships between oxidation state of magmas, Fe content and associated metal assemblages. After Lang and Baker (2001).....	12
Figure 2. Indium sits in Group 13, Row 5 of the periodic table. When indium is added to gallium nitride in LEDs, violet, blue and green colors can be produced (image by Berkeley Lab).....	19
Figure 3. Updated criticality assessments for the EU for 2013, using the highest value for supply risk. After European Commission, 2014).....	22
Figure 4. Indium price from 2012 to 2017 (data obtained of kitcometals.com).....	23
Figure 5. Distribution of In-bearing ore deposits in the world. After Schwarz-Schampera and Herzig, (2002) and Murakami and Ishihara (2013).....	24
Figure 6 Principal tectonic features and relationship with metallogenic of the Central Andes (after Mlynarczyk and William-Jones, 2005). a) Plate tectonics, volcanism and lithospheric thickness; b) Relevant ore deposit with time in the Central Andean tin belt; c) Schematic cross-section of the Andean continental margin, showing the relationships between convergence, subduction features, and the magmatic arc.....	26
Figure 7. Main access roads to study area.....	29
Figure 8. Outcrops of stratigraphic units in the Santa Fe District. A) Slate of the Llagagua formation in the Japo area; B) shales and sandstones sequence of the Uncia formation; C) Riolitic lava flow of the Morococala formation in the Santa Fe area; D) andesitic dome of the Morococal formation; E) Paleozoic metasedimentary sequence of the of the east limb of Santa Fe anticline intruded by dikes of Miocene age.....	36
Figure 9. Location and detailed geological map of the Santa Fe mining District. The schematic stratigraphic section (right) is based in Sugaki, et al. (1981), A, B, C and D indicate the location of the geological cross-sections shown in Fig. 10.....	39
Figure 10. Schematic A-B (east-west) and C-D (north-south) geological sections in the Santa Fe mining District (location shown on Fig. 9).....	40
Figure 11. View of the Santa Fe Mining District. A) Adit of the Japo mine hosted in Paleozoic shales; B) adit of the Santa Fe mine hosted in pyroclastic of the Morococala formation; C) panoramic view of the Morococala mine, also hosted in rocks of the Morococala Formation; D) East limb of the Santa Fe anticline, Japo town is at the bottom.....	41
Figure 12. Ore mineralization style. A) Mineralization in share zone; B) veins hosted in meta-sedimentary rocks; C) massive mineralization; D) ore mineralization in breccia; E) dissemination and replacement of phenocrystals.....	43
Figure 13. Logging of the drill-core JDC-06-006.....	46

Figure 14. Map of drill-holes location in the Santa Fe District.....	47
Figure 15. (Left) WDS spectra illustrating the interference between In-La and Sn-Lh within stannites (stn), cassiterites (cst) and a sphalerite (sph); after (Benzaazoua et al., 2003). (Right) Interference correction for Sn on In. The interference was calculated from the minimum measured signal for In-Ka for stannite group minerals and cassiterite and approximates 22 ppm In for 1 wt% Sn. After Andersen et al. (2016).....	50
Figure 16. Vapor-saturated phase relations in the NaCl-H <sub>2</sub> O system at low temperatures. After Bodnar and Vityk (1994) based in Hall et al. (1988); Sterner et al. (1988) and Bodnar et al. (1989). I = ice; L = liquid; HH = hydrohalite; H = halite; P = peritectic (0.1 °C, 26.3 wt.% NaCl); E = eutectic (-21.2 °C, 23.2 wt.% NaCl).....	53
Figure 17. Diagram of homogenization temperature vs salinity, showing four typical trends of distribution of fluid inclusion populations, according to their temperature (A) Boiling, in a volatile-free system; (B) dilution due to mixing with cold groundwater; (C) boiling with effervescence, in a volatile-rich system; (D) cooling or pressurization (after Hedenquist and Henley, 1985; Wilkinson, 2001; Canet et al., 2011).....	54
Figure 18. Petrography of intrusive rocks. A) drill-cores sample of the San Pablo stock; B) Photomicrograph (transmitted light) of altered phenocrystals in an aphanitic matrix; C) Photomicrograph (plane polarized light) altered k-feldspars and micas; D) drill-core sample of porphyry dike; E) Photomicrograph (transmitted light) shown porphyry texture; F) Photomicrograph (plane polarized light) altered k-feldspars and micas in cryptocrystalline matrix.....	59
Figure 19. Petrography of meta-sedimentary rocks. A) drillcore sample of shale with ore mineralization in micro-fractures; B) Photomicrograph (reflected light) of sulfides in micro-fracture plane: pyrite, chalcopyrite, arsenopyrite and oxides; C) Photomicrograph (reflected light) of pyrite and arsenopyrite with anomalous anisotropy; D) drill-core sample of greywacke; E) Photomicrograph (reflected light) shown sulfides infilling porosity between quartz grains; F) Photomicrograph (reflected light) of agglomerate of pyrite, chalcopyrite, chalcosite and arsenopyrite.....	61
Figure 20. Petrography of meta-sedimentary rocks. A) drill-core sample of sandstone with fine sand grain; B) Photomicrograph (plane polarized light) shown equigranular texture and alteration to clay-minerals; C) Photomicrograph (reflected light) of pyrite with some oxidation; D) drill-core sample of quartzite; E) Photomicrograph (plane polarized light) shown equigranular texture of quartz grains; F) Photomicrograph (reflected light) of micro-vein with sulfides mineralization.....	63
Figure 21. Binary diagrams of Sn, Pb, As, Cu, Ag and Zn vs In of igneous rocks and ore in the Santa Fe mining District.....	65

Figure 22. Chondrite-normalized rare earth elements (REE) of the SFD plots and distribution patterns of samples from Llallagua, Chorolque, San José, Oruro and Cerro Rico (Dietrich, 2000). Comparing with unaltered and altered fields after Van Kranendonk and Pirajno, 2004). Llallagua and Cerro Rico patterns correspond to pink color, Chorolque and San José with blue and unaltered felsic camp is shown in black tone.....66

Figure 23. Ore mineralization. A) Microphotography of the main mineral assemblage in the SFD under petrographic microscopy; B) Backscattered SEM images of the ore assemblage in the SFD; C) Microphotography of sphalerite and galena under petrographic microscopy; D) Backscattered electron SEM images of sulfosalts associated with galena, sphalerite and pyrite. Arg: argentite; Cst: cassiterite; Gn: galena; Py: pyrite; Sp: sphalerite; Stn: stannite; Tenn: tennantite.....69

Figure 24. Backscattered electron SEM images of sulfosalts of the SFD. A) Association of sulfosalts with galena and pyrite; B) Laitakarite filling a cavity in a pyrite crystal; C) Matildite associated to galena in a cavity of a sphalerite crystal; D) Acicular crystals of boulangerite. Bou: boulangerite; Cst: cassiterite; Gn: galena; Ltk: laitakarite; Py: pyrite; Ss: sulfosalts; Mat: matildite.....71

Figure 25. Binary plots of Fe+Cd+In vs. Zn (top), and frequency diagram of indium contents in sphalerite from the SFD. Histogram showing In wt.% in sphalerite from the SFD. Electron microprobe measurements n =51 (below). In wt% was estimated not considering interference correction of 22 ppm of In per 1% of Sn.....73

Figure 26. Backscattered SEM images of A) Stannite crystals filling cavities; B) Stannite crystals inside exfoliation of a pyrite crystal; C) Prismatic crystals of stannite associated with pyrite; D) Ore minerals associated to euhedral quartz; E) Euhedral crystals of stannite showing tetrahedral prisms, and F) minerals of stannite group with composition variable. Gn: galena; Py: pyrite; Qtz: quartz; Stn: stannite.....75

Figure 27. Backscattered SEM images of: A) Ourayite filling cavities in a pyrite crystal; B) Acicular crystals of andorite; C) Bismuthinite crystals in a galena crystal; D) Acicular monazite crystals associated to ore mineralization.....79

Figure 28. Content (wt.%) of ore minerals before and after recovery concentration. Concentrate shows poor efficiency in recovery of cassiterite and total loss of stannite. Most of the “others” are gangue minerals.....83

Figure 29. Photomicrographs of fluid inclusions from the SFD. A) Fluid inclusions associate with ore mineralization; B) sphalerite with quartz; C) primary fluid inclusions (negative crystals) on quartz and ore associate; D) primary fluid inclusion on growth zoning from Japo; E) primary fluid inclusion on growth zoning from Santa Fe; F) liquid+vapor inclusion in heterogeneous trapping zone from Japo; G) liquid+vapor inclusion in heterogeneous trapping zone from Santa Fe; H) liquid+vapor+solid, from Japo; (I) fluid inclusion with liquid+vapor+solid, from Santa Fe.....85

Figure 30. Diagram showing salinity (wt.% NaCl eq.) vs. homogenization temperatures ( $T_H$ ) of the individual fluid inclusions analyzed in the SFD.....	87
Figure 31. Histograms showing $\delta^{34}\text{S}_{\text{CDT}}$ (in ‰) values of sulfides from the SFD... ..	87
Figure 32. Paragenetic sequence of the Santa Fe District.....	90
Figure 33. Range of $\delta^{34}\text{S}_{\text{CDT}}$ (‰) values of sulfides in selected ore systems and reservoirs, compiled by Pirajno (2009).....	92
Figure 34. Ore systems and metal associations in relation to the nature of magma and redox conditions. After Barton (1996), Thompson et al. (1999), and Lang and Baker (2001).....	95
Figure 35. Temperature-salinity fields and mean gradient curve for a range of hydrothermal ore systems: 1) Archaean orogenic Au; 2) Epithermal Au-Ag; 3) volcanogenic massive sulfides and 4) Porphyry Cu-Au. After Large et al. (1988). Dots in black represent FI values from The SFD.....	97
Figure 36. Conceptual genetic model of the Santa Fe District, illustrates the three different stages in deposit evolution. In this model, volatile-rich granitic cupola-like intrusions are emplaced in metasedimentary rocks. Stages of degassing and fluids evolution range from incipient through to advanced, from left to right in the figure, resulting in different levels of mineralization-alteration above the San Pablo stock. 1 to 4 represent different pulses of mineralization and dotted line the isothermal curves according to the fluid inclusions results in this work.....	99
Figure 37. A) Ternary Cu+Ag-Sn+In-Zn+Fe plot of indium-rich minerals from the SFD; B) Ternary diagram Fe-Cu-Zn, plot compositional difference between Stannite-Sakuraiite-Petrurkrite-K�esterite-Sphalerite phases.....	102
Figure 38. Summary of the major Indium deposit around the world (Valkama et al., 2016; Murakami and Ishihara, 2013; Dill et al., 2013; Ishihara et al., 2011; Cook et al., 2011b; Sinclair et al., 2006; Murao and Furuno, 1991; Murao et al., 2008, Ohta, 1989; Seifert and Sandmann, 2006).....	103

# TABLE INDEX

Table 1. Indium Estimated World Refinery Production and primary production capacity in metric tons.....	21
Table 2. Geochemical summary of intrusive rocks and ore minerals in the Santa Fe District.....	64
Table 3. Chemical composition (wt.%) and atomic proportions (apfu) of representative cassiterite from the Santa Fe District (EMPA).....	70
Table 4. Chemical composition (wt.%) and atomic proportions (apfu) of representative sphalerite from the Santa Fe District (EMPA).....	72
Table 5. Chemical composition (wt.%) and atomic proportions (apfu) of representative stannite from the Santa Fe District (EMPA).....	76
Table 6. Chemical composition (wt.%) and atomic proportions (apfu) of composition and atomic proportions of representative sakuraiite and k�rsterite from the Santa Fe District (EMPA).....	77
Table 7. Summary of sulfosalts from the Santa Fe District (EMPA) and their structural formula.....	78
Table 8. Alteration assemblages recognized in selected samples from the Santa Fe District.....	82
Table 9. Summary of microthermometric data of fluid inclusions of the Santa Fe District.....	84
Table 10. Summary of isotopic values of $\delta^{34}\text{S}\text{‰}$ of the Santa Fe District.....	88





# 1. INTRODUCTION

**T**raditional mineral resources are an important part of the basis in the Bolivian economy. center in 1994 (Espinoza-Morales, 2010) and nowadays, artisanal miners exploit it.

Mining is the main industry in Bolivia and in the production of ores such as tin, lead, zinc, copper antimony, tungsten, bismuth, silver and gold. Traditionally, Bolivia was one of the main producers of tin around the world. In 2016 Bolivia was the 5th producer of tin, after China, Indonesia, Myanmar and Brazil (USGS, 2017). Due to the exceptional extractive potential of the Bolivian deposits, several Sn-bearing minerals have been discovered and studied in Bolivia (e.g. potosíite, franckeite, cylindrite, cassiterite). Thus, this and most of the Andean deposits represent a chronic research target in ore deposits fields. The ore deposits in the Andean region also act to a key factor in the study

Accordingly, many Bolivian mines are tin world-class deposits. Such is the case of the Santa Fe Mining District. This district is located in the Oruro department, at 4360 meters above sea level. Santa Fe was one of the most important mining centers of Bolivia; in 1939, only in the Morococala mine more than 5000 Ton of tin were extracted. The Santa Fe mining district finished operations as governmental mining of the link between subduction-magmatism, hydrothermal ore deposits, conventional (Zn, Cd, Al, Bi, Cu, Au, Ag, Fe, Ni, Cr, Mn, Pb and Sn) and no-conventional (In, platinum group elements, PGE; rare earth elements, REE) elemental crust distribution.

Recently, several no conventional elements as In, PGE, REE, Nb and Co have taken importance because different authors (e.g. Duclos et al.,

2010; DOE, 2010; European Commission, 2014) have designed them as critical raw materials (CRMs). CRMs are defined according to availability (supply risk) and economic importance. The study of this issue is especially relevant because the rise of the Chinese economy.

The spatial distribution of ore deposit in Bolivia, and in the west of South America, is not accidental. Here ore deposits are distributed in metallogenic provinces parallel to subduction Nazca trench (Sillitoe, 1976; Lehmann, 1979; Mlynarczyk and William-Jones, 2005). The Santa Fe mining district is hosted in the Central Andean Tin Belt. The Central Andean Tin Belt is extended from Peru to Chile. It is an important metallogenic province, which allows many world-class deposits (e.g. Cerro Rico, Huanuni, Colquechaca, Llallagua, Pirquitas and San José). The most important deposits of this belt are located in the Bolivian territory, especially polymetallic deposits of Sn Pb, Zn, W and Ag located in the districts of Potosí, Oruro, Llallagua

and Huanuni. These are well-known ore deposits for the economic potential that represents, however the genesis and particular characteristics of most of these deposits have been poorly studied.

In the Santa Fe Mining District (SFD), the Santa Fe, Morococala and Japo deposits are the most representative, not only in economic terms but also from the point of view of the metallogenic knowledge in this sector of the Andean context. On the other hand, in the last years, Critical Raw Materials study has become relevant because the knowledge and abundance of most of these materials is scarce. In this sense, the SFD is also attractive because its unrevealed indium content.

The present work has been conducted as a cooperation project, thus the results present here also aim to contribute with the artisanal mining in the study area. The knowledge of these aspects will allow establishing criteria to propose new exploration/exploitation strategies not only in this district but also in analog deposits.

---

It is important to highlight, this work was developed as an international cooperation project between the *Escola Politècnica Superior d'Enginyeria de Manresa (EPSEM)* through of the *Centre de Cooperació al Desenvolupament (CCD)* of the *Universitat Politècnica de Catalunya (UPC, Spain)* and the *Universidad Técnica de Oruro (UTO, Bolivia)*. The CCD has as mission to promote cooperation and supporting implementation of initiatives in this area by all members of the UPC. Cooperation projects in the EPSEM are conducted by a non-governmental organization called *Mineria per el desenvolupament (Mining for development, MpD)*. The main MpD goal is to provide technical assistance in underdeveloped countries in order to perform a more sustainable extraction of mineral resources. In addition, it aims to achieve safe working conditions and reduce environmental impact.

Meanwhile, the UTO managed all relations with artisanal mines were this

project was done. The most important contribution of the UPC delegates is to provide technical advice to local miners and in this way, students of both universities gain experience. At the same time, members of both universities can develop research work to contribute to scientific knowledge.

### 1.1. Goals

The main purpose of this study is presenting a metallogenic and geochemistry model of the Santa Fe mining District —Japo, Santa Fe and Morococala mines—, based on pressure, temperature, sulfur origin, paragenetic and mineral chemistry data of three deposits. To do so, the mineralogy, geochemistry and conditions of formation of the fluids involved in the evolution of this ore deposit and similar deposits in the Central Andean Tin Belt were studied.

Likewise, the ore assemblages were meticulously investigated in order to know the concentration and

distribution of conventional and no-conventional elements, and thus to point out the exploration potential of the SFD. The metallogenic model of the Santa Fe Mining District based on the detailed study of the geology, mineralogy, mineral chemistry, isotopic and thermometric features of this ore deposit, including (a) the relationship with magmatism, (b) the physico-chemical characteristics of the mineralizing fluids and their origin.

Additionally, the extensive variety of mineral phases will provide a chemical and mineralogical description of minerals poorly studied or even unknown. This study is particularly focus in the study of the stannite group to know the concentration, distribution and indium content as a potential exploration-exploitation target.

## 1.2. Specific goals

Several specific goals have been established to achieve such purpose. However, each one requires a particular

methodology. In accordance with the above, the specific objectives are:

- To perform a detailed geological study of the Santa Fe Mining District, including a local mapping of the deposit area.
- To sample and logg of both the ore mineralization and the host rocks.
- To characterize the mineralogy and geochemistry of the ore bodies, with emphasis on the study of ore minerals and alterations. Determination of content of non-conventional elements (particularly Indium) in specific mineral phases.
- To characterize the chemistry of the ore minerals.
- To characterize the fluids responsible of ore mineralization by a fluid inclusion study and analysis of sulfur isotopes to determinate the origin of metals and sulfur.
- To determine the physic-chemical conditions of formation of the phases associated to metals.

- To characterize the different events of magmatism linked to ore mineralization, in order to determine the temporality of events.
- To compare with other deposits in the Bolivian Tin Belt to determine similarities and differences in this geotectonic context.
- Based on the results obtained, to make proposals for the optimization of the processing of these deposits.
- To clarify and establish the evolution model of the Santa Fe Mining District.



## 2. STATE OF THE ART

### 2.1. Tin and metal sources

The use of the tin back to the Bronze Age. Bronze contains around ninety percent copper and ten percent tin. The tin addition to bronze alloys improves their properties compared with pure copper: for example, bronze is harder and easier cast than copper. The ancient Greeks referred to the tin source as “the cassiterides”, meaning Tin Islands. These islands were most likely to have been in the Scilly Islands, Cornwall (Great Britain) and north-west Iberia (Spain) where there are large tin deposits. Robert Boyle published a work about the oxidation of tin in 1673. Chemical symbol of tin (Sn) comes from its Latin root, stannum (Chemicool, 2015).

Nowadays, tin is used as a coating on the surface of other metals to prevent corrosion; also, it can be rolled into thin foil sheets (tin foil). Alloys of tin are

commercially important in soft solder, pewter and bronze. Tin chloride ( $\text{SnCl}_2$ ) is used as a mordant in dyeing textiles, for increasing the weight of silk, and stannous fluoride ( $\text{SnF}_2$ ) is used in some toothpastes. One of the most relevant uses of tin is in the artificial complex indium-tin oxide (ITO) used as a thin-film coating on flat-screens (LCDs) (Tolcin, 2013).

In a global context, the Sn deposits are distributed in several tectonic environment. The main Sn deposits are sitting in continental arc, collisional or backarc tectonic settings presented in the next section. The study of source of metals (Sn included) is in continuous discussion and it is difficult to assess, but in general, metal-bearing minerals contain these elements in their lattices, which are released following the breakdown of the host mineral during magmatic-hydrothermal processes. In



addition, Lehmann (1982) pointed out that exsolved magmatic-hydrothermal fluids have the capacity to dissolve and transport metals from the surrounding rocks. Furthermore, crustal materials that contain pre-existing metal concentrations can also provide a rich source of metals during episodes of partial melting. In this respect, there are limited data on the partitioning of metals such as In, Sn and W within major silicate minerals. Several authors suggest that muscovite is the dominant host of Sn and W over biotite and that biotite may contain In (Miroshnichenko, 1965; Alderton and Moore, 1981; Neiva et al., 2002). Incorporation of trace elements, with variable ionic ratio and charge, into micas is well established (Ivanova, 1969; Tischendorf et al., 2001). Tourmaline can also incorporate such elements as Sn and W (Marks et al., 2013; Simons et al., 2017).

Moreover, metal concentrations in the hydrothermal fluids need not necessarily be high in order to form an

ore deposit, and therefore the critical factors for ore deposition must therefore be time and deposition rate. Although difficult to identify with absolute certainty, it is fair to assume that the source of these constituents can be the cooling magmas and/or the rocks through which the solutions pass. Metals such as Zn, Cu, Sn and W are present in various amounts in micas, pyroxenes and amphiboles. Sn and W concentrations of up to 500 ppm have been found in biotite and muscovite (Ivanova, 1969). Likewise, the partition coefficients for In, Sn, Sb, W and Bi in biotite and garnet in a basanite indicate incompatible behavior of these elements during melting, with the exception of In, which displays compatibility in garnet (Adam and Green, 2006). Approximations of mineral/melt partition coefficients using phenocryst/matrix measurements indicate that micas host Sn and W, whereas feldspar and quartz can exceptionally host Sn and W. Quartz from rare metal granite (RMG)

pegmatites contains less than 1 ppm Sn (Breiter, 2014; Simons et al., 2017).

Otherwise, the solubility of Cl<sup>-</sup> varies strongly with melt composition for mainly anhydrous aluminosilicate melts ranging from granite to basalt. Cl<sup>-</sup> increases with increasing concentrations of Al, Na, Ca, and Mg and decreasing concentrations of Si in melts. The crystallization of water- and chloride-free phases increases the volatile content of residual fractions of silicate melt until the volatile solubility limits are exceeded, and then vapor, liquid, or supercritical fluid exsolve. More importantly, extended fractional crystallization also leads to increasing activities of silica and decreasing activities of Ca, Al, and Mg in residual melt, which produces a fall in the maximum Cl<sup>-</sup> content of the melt that is required before Cl<sup>-</sup>-enriched volatile phases will exsolve (Webster et al., 1999).

The addition of gases decreases the solubility of H<sub>2</sub>O and CO<sub>2</sub> in the melt

by decreasing their activity in the fluid phase(s), resulting in fluid saturation with even lower concentrations of gases dissolved in the melt. At shallow crustal depths, metal partitioning becomes more complicated because magma may contain more than one silicate fluid phase. Addition of CO<sub>2</sub> and SO<sub>2</sub> will increase the field of immiscibility so that two aqueous phases may coexist over wide range of crustal conditions (Hedenquist and Lowenstern, 1994). The large density contrast between the vapor and hypersaline liquid commonly results in two phases separating within the magmatic chamber or its adjacent hydrothermal system. The dense hypersaline liquid remaining at depth will be richer in chalcophile elements than the low-salinity vapor (Hemley and Hunt, 1992). Evidence of these two different fluids are trapped as inclusions in minerals.

During anatexis of crustal rocks containing a sulfide minerals, polymetallic melts are entrained

into the leucosome that eventually coalesce to form granitic plutons. Once the melt approaches water saturation and the magma reaches its site of emplacement, the silicate melt exsolves a metal-rich hydrothermal fluid. Chlorine and fluorine jointly with sulfur are the major components that form halide ligands for stable metal complexes and are responsible for the transport of metals in solution (Pirajno, 2009).

Most ore metals can be partitioned into a magmatic-hydrothermal fluid as chloride, bisulfide and hydroxyacid complexes (Holland, 1972; Hemley and Hunt, 1992). At magmatic temperatures and pressures, insufficient data exist to define the conditions for partitioning of any given metal from a magma into an exsolved hydrothermal fluid. However, Urabe (1987) indicated that exsolving magmatic fluids, especially at low magmatic pressures, could scavenge metals.

Tomkins and Mavrogenes (2003) pointed out that metallogenic regions or provinces that are well endowed with certain metals may owe their metal enrichment to the presence of disseminated or massive sulfide deposits in parts of the oceanic crust undergoing subduction. The Southeast Asian Sn belt is a notable example of a metal-specific region (Lehmann, 1982; Schwartz et al. 1995).

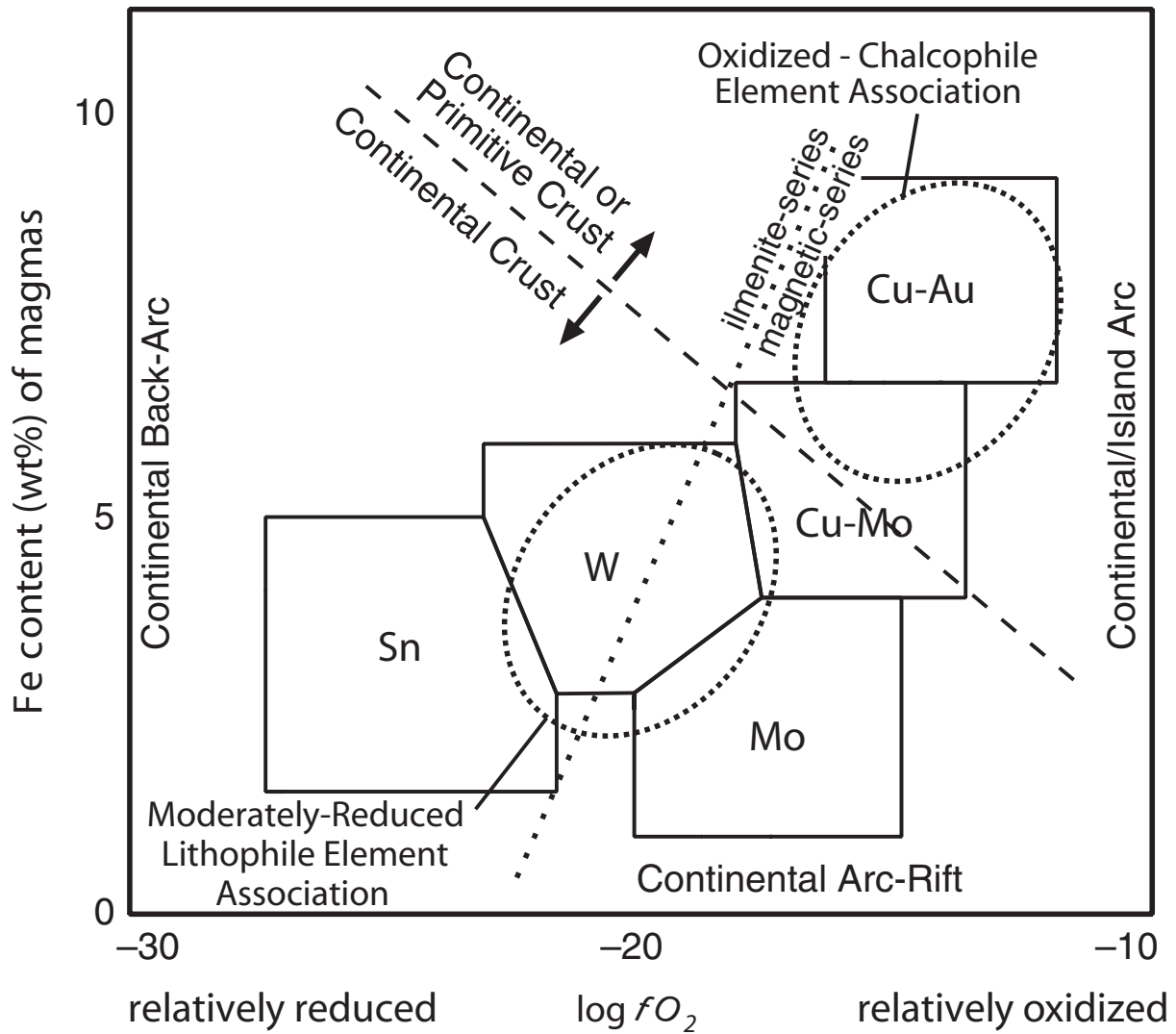
According to literature review (e.g. Schwartz et al. 1995, Pirajno, 2009, Simons et al., 2017) Sn deposits are specifically related to intrusion-associated hydrothermal systems; which include greisens, vein systems, mineral systems associated with anorogenic, ring complexes, and breccia pipes and vein deposits that are peripheral to large intrusions. In some cases, there may be spatial, temporal and genetic relationships with porphyry systems and even with epithermal systems. Although the emphasis in Au, intrusion-related

hydrothermal systems exhibit a spectrum of polymetallic ore assemblages, with the causative intrusions being surrounded by regional aureoles, characterized by arrays of polymetallic veins, replacement, breccia pipes, disseminated, sedimentary rock-hosted to greisen and skarn systems. Greisen system is the most representative ore model for Sn deposits.

## 2.2. Tin deposits and magmatism

There is a considerable literature on the association of tin deposits and magmatic rocks (e.g. Flinter, 1971; Groves, 1972; Ishihara, 1981; William-Jones and Heinrich 2005, Simons et al., 2017). Sn mineralization is commonly associated to intrusion-related systems. Elements in magmas need a transport to ascent through the shadow crustal and found a deposition mechanics; this transport is through hydrothermal fluids. The circulation of hydrothermal fluids in the crust results in the development of hydrothermal systems. Ore-fluids may

occur as either molecular or colloidal solutions. In ore-forming colloidal systems, solid phases are dispersed in liquid/gaseous fluids. The redox potential (Eh) as an important parameter that governs metal behavior in solutions in magmatic environment, as much as gas fugacity, which is a measure of the escaping tendency of a vapor or gas and its departure from ideal behavior (Pirajno, 2009). Eh is also important in determining the composition of fluids associated with igneous and metamorphic process (Frost, 1991). The Fe content of magmas determines the oxidized (magnetite series or I type) or reduced (ilmenite series or S type) character of magmatic fluids, which in turn determines the type of ore system. The diagram of Fig. 1 shows the relationship of the Fe content versus oxygen fugacity ( $fO_2$ ) and the position of reduced, mantle derived alkaline magmas with Sn and W mineralization and of oxidized calc-alkaline magmas with Cu-Mo, or Cu mineralization (Lang and Baker, 2001).



**Figure 1.** Diagram showing relationships between oxidation state of magmas, Fe content and associated metal assemblages. After Lang and Baker (2001).

It is of interest that peraluminous (Lehmann, 1982; Taylor and Wall, 1992; granites are a major global source Haapala, 1997; Romer and Kroner, of magmatic and magmatic- 2014).

hydrothermal ore deposits, particularly A very recent study about fractionating for lithophile elements (Simons et and distribution of lithophile elements al., 2017). Factors such as source as Li, Be, Ga, Nb, Ta, In, Sn, Sb, W and composition, degree of fractionation Bi was conducted by Simons et al. and hydrothermal overprinting control (2017). Approximations of mineral/enrichment of these metals in granites melt partition coefficients indicate

that micas host Sn and W, as Ivanova (1969) had determined. Mineral/melt ratios of Sn and W in micas implying that fractionation of an assemblage with a significant modal abundance of feldspar (+ quartz) over mica will result in a melt with higher Sn and W than the parental melt. Accessory minerals are also an important host of Nb, Ta, Sn and W within the source region, particularly Fe–Ti oxides (e.g. Stepanov and Hermann, 2013; Romer and Kroner, 2016). Tin partitioning during melting and fractionation is also partially influenced by the oxidation state of the melt.

Meanwhile, Ishihara (1977, 1981) and Ishihara et al. (1979) proposed that in the case of magnetite-series granites, characterized by high  $Fe^{+3}/Fe^{+2}$  ratios, Sn is also in the tetravalent state ( $Sn^{+4}$ ) and so it may substitute Ti or Fe, thus entering the lattice of the early crystallizing, rock-forming minerals (e.g. titanite, magnetite, hornblende, biotite). Its availability in the remaining

liquid would hence be limited; with the further consequence that accumulation of Sn in the residual melt would be insufficient to produce an ore deposit. In the case of the ilmenite-series granites (low  $Fe^{+3}/Fe^{+2}$ ), Sn is in the divalent state ( $Sn^{+2}$ ) and would be more available for accumulation in the residual melts, leading to a Sn-rich, and hence specialized, highly-fractionated leucocratic granite.

Taylor and Wall (1992) proposed that, in oxidizing melts, Sn is stabilized as  $Sn^{4+}$ , which should result in partitioning into minerals such as biotite, hornblende and magnetite, and therefore it would be more readily depleted during fractionation. However, Simons et al. (2017) found that in the Cornubian granites (South West England) ilmenite contains rather than magnetite, implying that Sn is relatively incompatible during fractionation.

William-Jones and Heinrich (2005) proposed that vapor phases are

potentially important agents for the transport of metallic elements in hydrothermal systems, beyond the usually accepted role of boiling fluids. Felsic magmas used to have high concentrations of Sn and Mo. The fundamental role of volatiles in granitic melts is two-fold. Firstly, they modify the physico-chemical behavior of the melt and its crystallization products. Secondly, because of the volatiles tendency to partition into the residual fluid phases, they are instrumental in the complexing and transport of metallic elements.

Adding volatiles to a mineral assemblage undergoing high-grade metamorphism lowers the melting temperature of the assemblage, and the addition of volatiles to a melt phase has the effect of lowering its solidus temperature. The behavior of volatiles (B, F, Cl) in a melt is similar to that of water, in that they react with the bridging oxygens of the silicate

tetrahedral by breaking the Si-O bridges and depolymerizing the melt (Burnham, 1997).

Literature review pointed out that there is a strong association between W-Sn over other metal association (e.g. Ishihara, 1981; Schwartz et al., 1995; Lang and Baker, 2001; Pirajno, 2009; Simons et al., 2017). Metals partition in muscovite represents sources of Sn, where P and F cause the retention in the melt of Nb, Ta, Sn, W and, to a lesser extent, In. However, the knowledge of mechanics of In-magmatic distributions is still scarce.

### 2.3. Geodynamic context

The Geodynamic environment is a key factor to consider in ore deposit models. Arc-related magmatic-hydrothermal and hydrothermal mineral deposits have been object of many studies. The deposit styles characteristic of continental arc and even intra-oceanic arc environments are porphyry Cu-

Au–Mo deposits, which are the most emblematic ore deposit of the Andes, the North American Cordillera, and the SW Pacific. These deposits tends to be Mesozoic or Cenozoic in age because of susceptibility to be eroded of older deposits. Deposits in more primitive intra-oceanic arcs tend to be more enriched in Mo, or even Sn (Bolivia) or W (New Brunswick, Canada) in rare cases (Groves and Bierlein, 2007). Porphyry deposits arguably show the clearest relationship to subduction processes of all, being related to dehydration of the subducting oceanic slab, and related high fluid flux into the overlying mantle wedge, which resulted in its metasomatism and generation of evolved, high-level granitic magmas from the hydrous, metal-enriched basaltic magmas produced by melting of this metasomatized mantle (Kerrich et al., 2005).

Several deposit types are sited in far back-arc settings, normally within deformed sedimentary sequences on

the margins of Precambrian cratons. Far back-arc settings include Sn-W deposits in S-type granites, usually associated to continent-continent collisional orogens that close an internal ocean (e.g. Tethys and the Alpine-Himalayan orogen; Kerrich et al., 2005). Far back-arc settings also include W skarns and the Sn-W deposits of the Tasman orogen in eastern Australia (e.g. Solomon and Groves 1994). Tin deposits also occur on the continental margin of accretionary orogens such as those of Bolivia (Groves and Bierlein, 2007).

In collisional tectonic settings, according to Kerrich et al. (2005), reworking of older and already devolatilized crust and limited development of magmatic arcs during collisions are not conducive to the formation of ore systems, except for Sn-W deposits associated with highly fractionated, ilmenite-type or S-type granites. These granites are highly enriched in incompatible and volatile elements (Rb, Th, U, Ta, Sn, W, Mo, B,



and F) and generated in the thickened crust that results from the collision of two continents. Continent-continent orogens have some of the largest Sn-W provinces, such as southwest England and Panasqueira (Portugal) of the Variscan Orogen.

Mantle plumes and delamination tectono-thermal events were responsible for widespread anorogenic magmatism that culminated with the emplacement of the A-type granites and gabbro-anorthosite complexes at 1.75–1.55 Ga and 1.0 Ga. These complexes are associated with Olympic Dam style mineralization of Iron oxide- copper- gold (IOCG) deposits, anorthosite-hosted Fe-Ti-V as well as Sn, W, Zn late stage mineralization (Pirajno, 2009).

#### 2.4. Greisen ore systems

The term greisen refers to an assemblage of quartz + muscovite, accompanied by varying amounts of

other distinctive minerals such as fluorite, topaz and tourmaline. Greisenization was defined by Shcherba (1970) as the high-temperature, post-magmatic alteration of rocks by volatile-rich solutions associated to the cooling of granitic intrusives. Greisen systems are normally associated with Sn, W, U, Mo, Be, Bi, Li and F mineralization.

According to Pirajno (2009) greisenization is typically linked with highly fractionated magmas that have intruded into crustal depths ranging from 3 to 5 km, and takes place in the apical portions of granitic intrusive bodies (cupolas), emanating from deep-seated granite batholiths. The highly evolved granitic melts that promote the development of greisenization and associated mineralization are strongly enriched in volatile components as Cl, B, F, and the above mentioned metallic elements. Taylor (1979) estimated Sn content of mineral phases of stanniferous granites as: titanite 230–260

ppm, ilmenite 15–80 ppm and biotite 50–500 ppm; whereas, according to Eugster (1985), ilmenite may contain up to 1000 ppm and biotite 1000 ppm Sn, respectively.

Greisen systems are typically associated with Sn and W mineralization, usually accompanied by other ore elements such as Cu, Zn, Bi, Mo, U, F. Common ore minerals are cassiterite, stannite, wolframite, scheelite, arsenopyrite, pyrite, chalcopyrite, molybdenite, sphalerite, bismuth and bismuthinite. Other important minerals are topaz, fluorite and apatite.

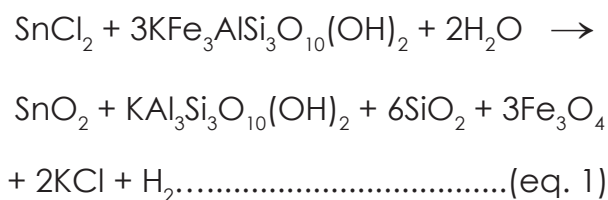
Most greisen-affiliated Sn and W deposits are spatially and genetically related to S-type granitic rocks, or the ilmenite-type, forming dome-like (cupolas), or ridge-like intrusion (Ishihara, 1977). This mineralization occurs as lenses, generally close to contacts of the granitic intrusion with the enclosing country rocks. Greisen may have distinct metal zonation. These are usually manifested by a lower

zone of Sn-Mo, extending upward and sometimes laterally through W-Bi to Cu, Zn, and Pb; in some cases, Au may also be presented. Ore deposition usually starts with an oxide phase (cassiterite, wolframite), followed by sulfides (pyrite, chalcopyrite, pyrrhotite, arsenopyrite, molybdenite, bismuthinite), and a late, lower temperature, carbonate-oxide stage characterized by calcite, siderite and iron oxides (Pirajno, 2009).

The world distribution of the Sn-W deposits of greisen affiliation tends to form either in collisional tectonic settings or in anorogenic intraplate settings (Mitchell and Garson, 1981). Sn transport because of hydroxyl and hydroxyfluoride complexing is thought to take place in high-temperature, alkaline fluids (Eadington, 1983).

Fluoride and chloride complexes are significant for the transport of Sn in hydrothermal solutions. It appears that F is more likely to transport Sn in highly saline solutions. Sn is considered transported as a stannous chloride complex ( $\text{SnCl}_2$ )

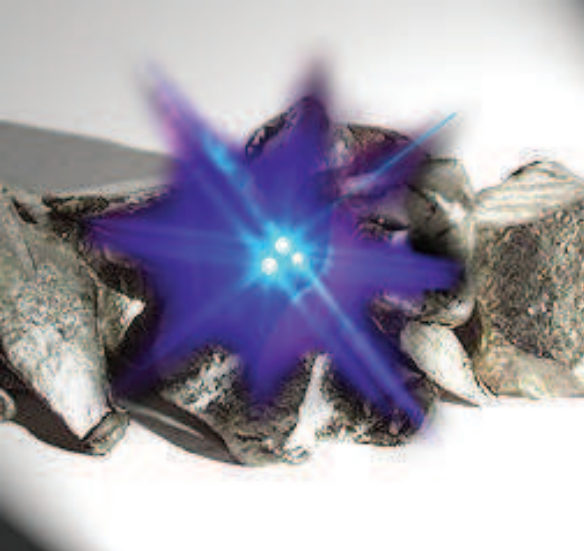
under conditions of low pH and low  $fO_2$  (Paterson et al., 1981). Precipitation of cassiterite due to the destabilization of the transporting complexes would then occur by either  $fO_2$  increase, an increase in pH, a decrease in temperature or a combination of these factors. Sn precipitates earlier under slightly more less acidic conditions. The precipitation of cassiterite also depends on the nature of the rocks with which fluids interact. The metal chloride solutes are converted to oxides and/or sulphides and HCl and  $H^+$  are released (Eugster, 1985). In pelitic rocks, conversion of feldspar and biotite to muscovite that may induce precipitation of cassiterite; Eugster (1985) proposed the next reaction:



## 2.5. Indium and world scenery

The invention of the spectroscope in 1860 led to the discovery of several new elements. In 1863, Ferdinand Reich discovered indium in Freiberg, Germany. Later, Hieronymus T. Richter, look in the same Freiberg sample the flame colors produced, He observed a brilliant indigo line, which did not match the spectral line of any known element know then. The element was named after its characteristic spectral line – the 'indi' coming from the indigo color (Schwarz-Schampera and Herzig, 2002, Chemicool, 2012).

Indium is an element of subgroup IIIA of the periodical table. According to Schwarz-Schampera and Herzig (2002) indium tends to occur in nature with base metal groups I-B (cooper, silver) II-B (zinc, cadmium), IV-A (tin, led) and V-A (bismuth) of the periodic table (Fig. 2).



	Group 12	Group 13	Group 14
Row 4	<b>30 Zn</b>	<b>31 Ga</b>	<b>32 Ge</b>
Row 5	<b>48 Cd</b>	<b>49 In</b>	<b>50 Sn</b>
Row 6	<b>80 Hg</b>	<b>81 Tl</b>	<b>82 Pb</b>

**Figure 2.** Indium sits in Group 13, Row 5 of the periodic table. When indium is added to gallium nitride in LEDs, violet, blue and green colors can be produced (image by Berkeley Lab).

Tolcin (2013) includes an indium history section, in the metal prices in the United States through 2010, science report by United States Geological Service (USGS). A summary of this work is explained in the next lines. Indium is produced mainly from residues generated during zinc ore processing. Before to 1940, indium was used almost for experimental purposes, although domestic production had begun in 1926. The first commercial application was in 1933, when small amounts of indium were added to certain dental alloys. The Indium Corporation of America (ICA) was founded in 1934 and became the first producer.

From 1940 to 1945, prices were usually determined through individual negotiations between the producer and consumer (Ludwick, 1959). The first large-scale application for indium was as a coating for bearings in high-performance aircraft engines during World War II (Slattery, 1995). After the war, new uses were found in fusible alloys, solders, and electronics. A producer price for indium was first established by ICA in 1946.

From 1973 to 1980, demand increased, especially for use in nuclear control rods, and easily accessible supplies of raw materials gradually decreased. ICA depleted its source of

feedstock in Bolivia and then obtained source material from Europe. To increase supply, world producers expanded production capacities. Orders for nuclear control rods dropped when the rate of nuclear power expansion decreased in the United States following the Three Mile Island accident of 1979. In 1988, demand grew up because the Japanese electronics industry. In the middle and late 1980s, the development of indium phosphide semiconductors and indium-tin-oxide (ITO) thin films for LCDs maximize interest (Tolcin, 2013). In 1989, indium was included in the list of materials to be added to the National Defense Stockpile (NDS) (Schmitt, 1989).

In 1998, indium demand declined owing to the second successive year of less LCD production and ITO the introduction of a new thin-film coating technology that requires only one-third as much indium per unit as the older process. Annual average prices continued to decline through 2002 owing to an oversupply in the metal

market, which was largely attributed to excessive Chinese production in the late 1990s and early 2000s and stagnant demand. In 2003, demand for indium began to increase significantly, especially in Japan and the Republic of Korea, owing to considerable growth in the LCD market. As LCD technology and manufacturing matured, prices for devices containing LCDs fell, which bolstered consumer demand for the technology. On the supply side, indium production was constricted owing to shortages of primary raw material in China and the closure of a primary indium production facility in France. This led to a shortage of metal, causing prices to rise during 2003 to 2005 (Tolcin, 2013).

In the 2000's Tolcin explains that the price of indium in 2005 reached historical peaks before declining to yearend. A brief price leveling that took place at the end of 2005 was attributed to industry stockpiling. Japanese ITO producers in particular were thought

to hold large stocks of indium bought in the 2004–2005. In 2006, indium prices increased during the first quarter and then declined rapidly through yearend. Although the availability of primary indium feedstock was further reduced and production capacity at ITO refineries and LCD plants in China, Japan, the Republic of Korea, and Taiwan increased, continued recycling efforts, especially in Japan, compensated for primary supply shortages and alleviated price pressures. By 2007, global secondary indium production significantly increased and accounted for a greater share of indium production than primary. In mid-2008, indium prices

rebounded after generally declining during 2007. However, as the recession set in globally, prices once again declined in late 2008 through the first half of 2009.

In the second half of 2009, ITO demand began to increase, particularly in the Republic of Korea, where exports of flat-panel displays increased significantly owing to China's household appliance subsidy program and the weaker won, causing stability in indium price. In 2014, the world's total production of primary indium was estimated to be 881 t, 8% more than that in 2013 (table 1). China was the leading producer, followed by the Republic of Korea, Japan, and

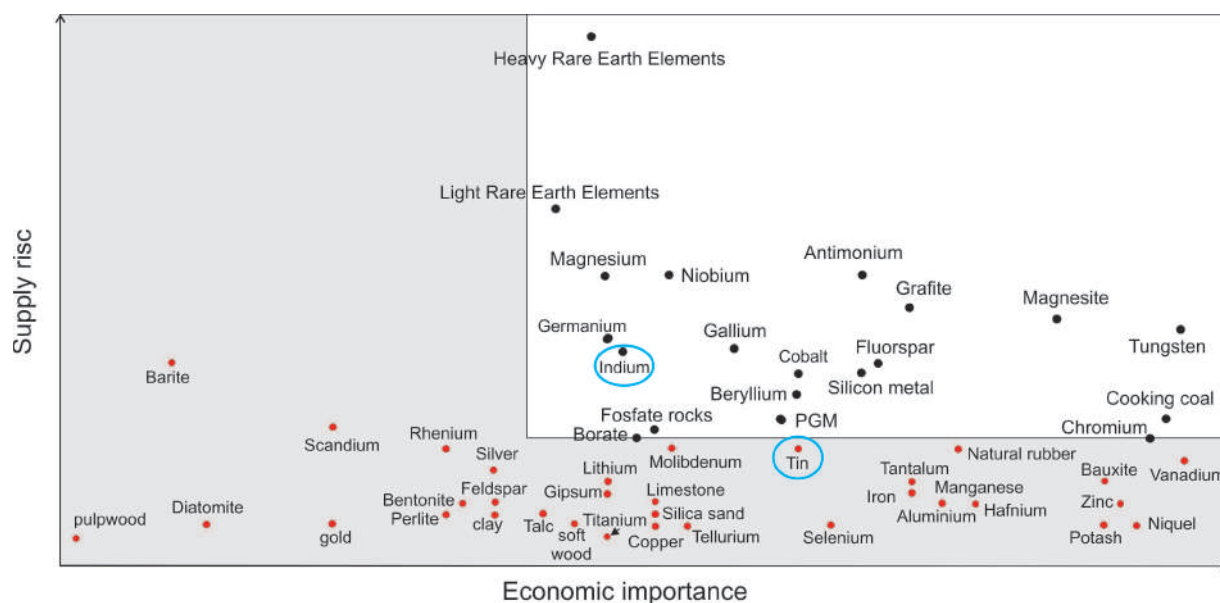
**Table 1.** Indium Estimated World Refinery Production and primary production capacity in metric tons (After Tolcin, 2016)

Country	2010	2011	2012	2013	2014	Production Capacity
Belgium	30,000	30,000	30,000	30,000	28,000	50
Canada	60,000	77,000	65,000	70,000	67,000	75
China	330,000	380,000	405,000	415,000	460,000	817
France	0	0	13,000	33,000	43,000	48
Japan	69,000	70,000	71,000	72,000	70,000	70
Korea	145,000	155,000	180,000	175,000	195,000	190
Peru	0	2,499	11,080	14,000	14,000	55
Russia	9,500	6,000	9,000	9,500	4,000	20
Total	643,500	720,499	784,080	818,500	881,000	-----

Canada (Table 1). Primary indium was recovered mainly from the residues generated during the smelting of zinc concentrates (Tolcin, 2016). In addition to the countries listed in the table 1, Kazakhstan and Ukraine are known to have produced indium; Italy, the Netherlands, may have produced secondary indium, but information is not enough to estimate output levels.

Meanwhile, The European Commission of Critical Raw Materials (CRMs) considerate that these are fundamental to Europe's economy, and they are essential for maintaining and improving quality of life. Therefore, the Raw Materials European Initiative was instigated to manage responses to raw materials issues at an EU level. Indium is included in the list of CRMs of the European Commission (Fig. 3). These CRMs have a high economic

Although an important factor, global changes in zinc mine production may not be an indicator of a corresponding change in the supply of indium. It has been estimated that about 35% of

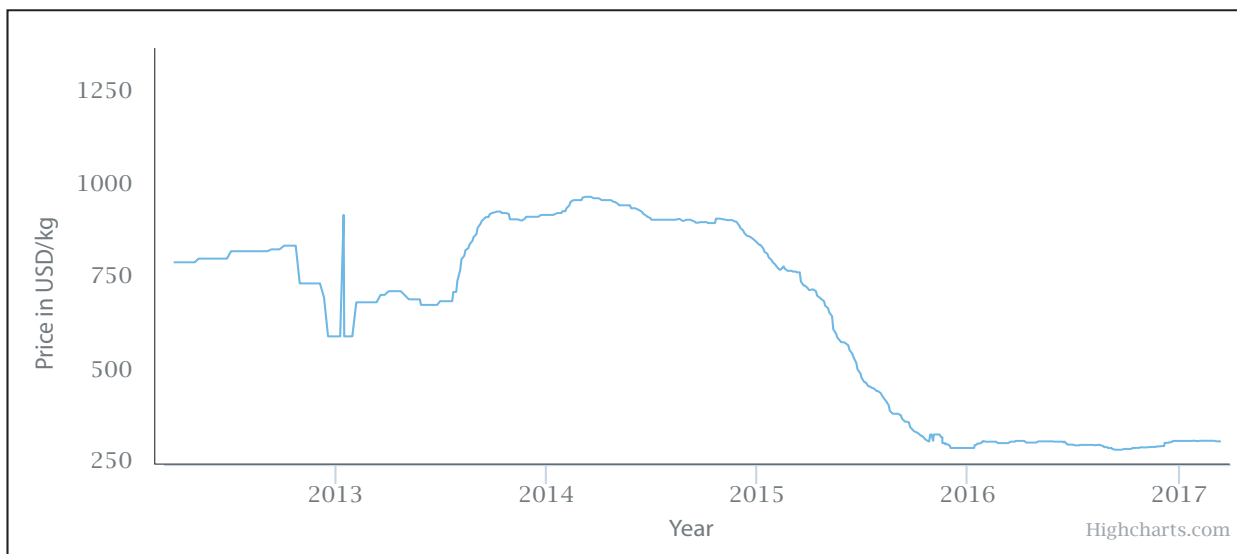


**Figure 3.** Updated criticality assessments for the EU for 2013, using the highest value for supply risk (After European Commission, 2014)..

importance to the EU combined with a high risk associated with their supply. The fluctuation of annual average indium prices since 2012 to 2017 is shown in Fig. 4 (Kitco, 2017).

Furthermore, Werner et al. (2017) point the fact that higher grades of Sn are associated with higher grades of Indium suggests that this correlation may be used to more accurately estimate the grade of indium where Sn grades are reported. They also propose that indium grades can be highly variable

within particular mineral hosts, and that a greater number of reporting deposits do not reduce statistical uncertainty. In addition, they recommend for mineralogical information to be reliable, it would then need to link it to other geological factors that would be more likely known about a deposit. In this sense, Murakami and Ishihara (2013), presented a very illustrative word scenery in the most important In-bearing and the ore deposit typology associated (Fig. 5).



**Figure 4.** Indium price from 2012 to 2017 (data obtained of kitcometals.com).



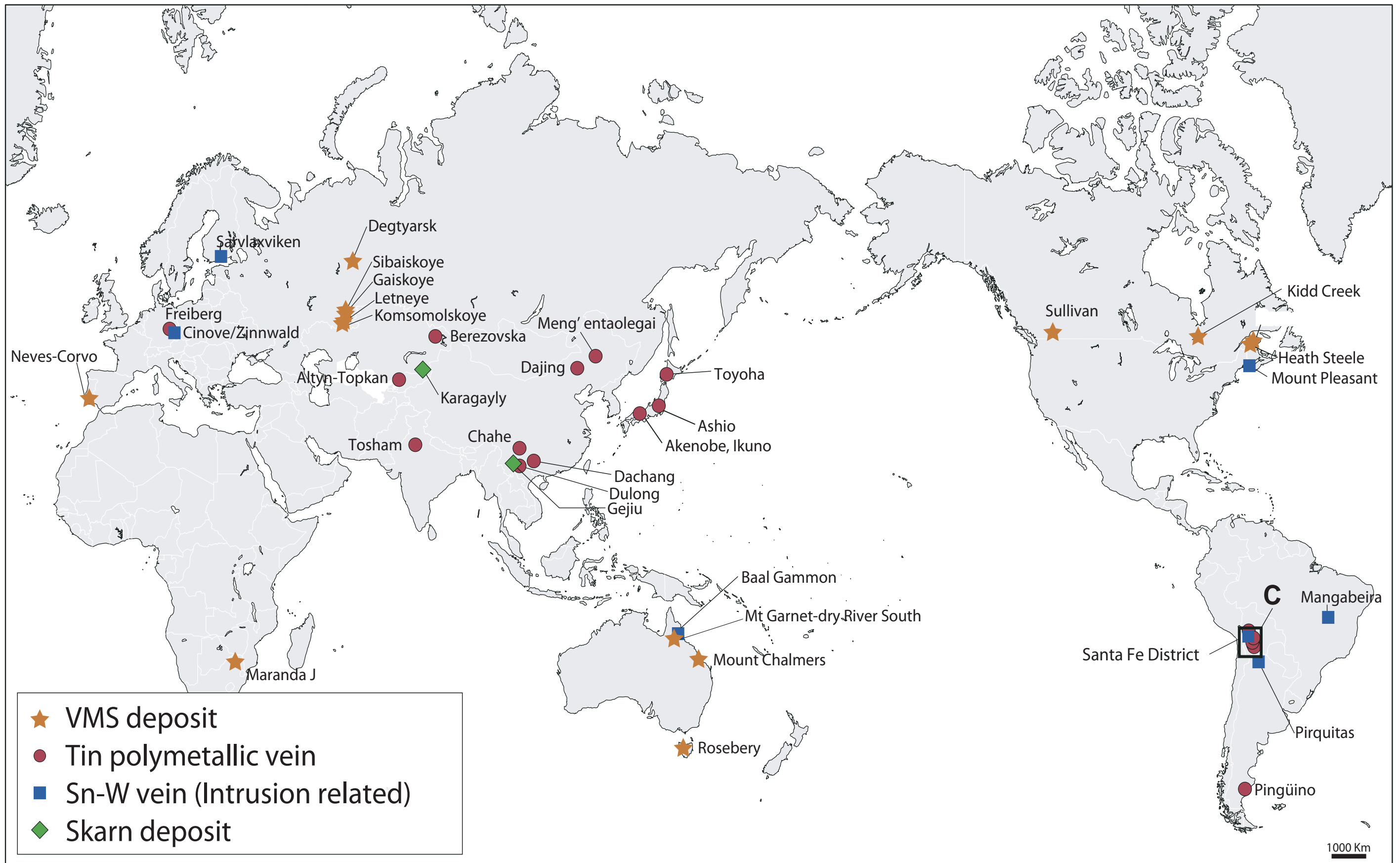
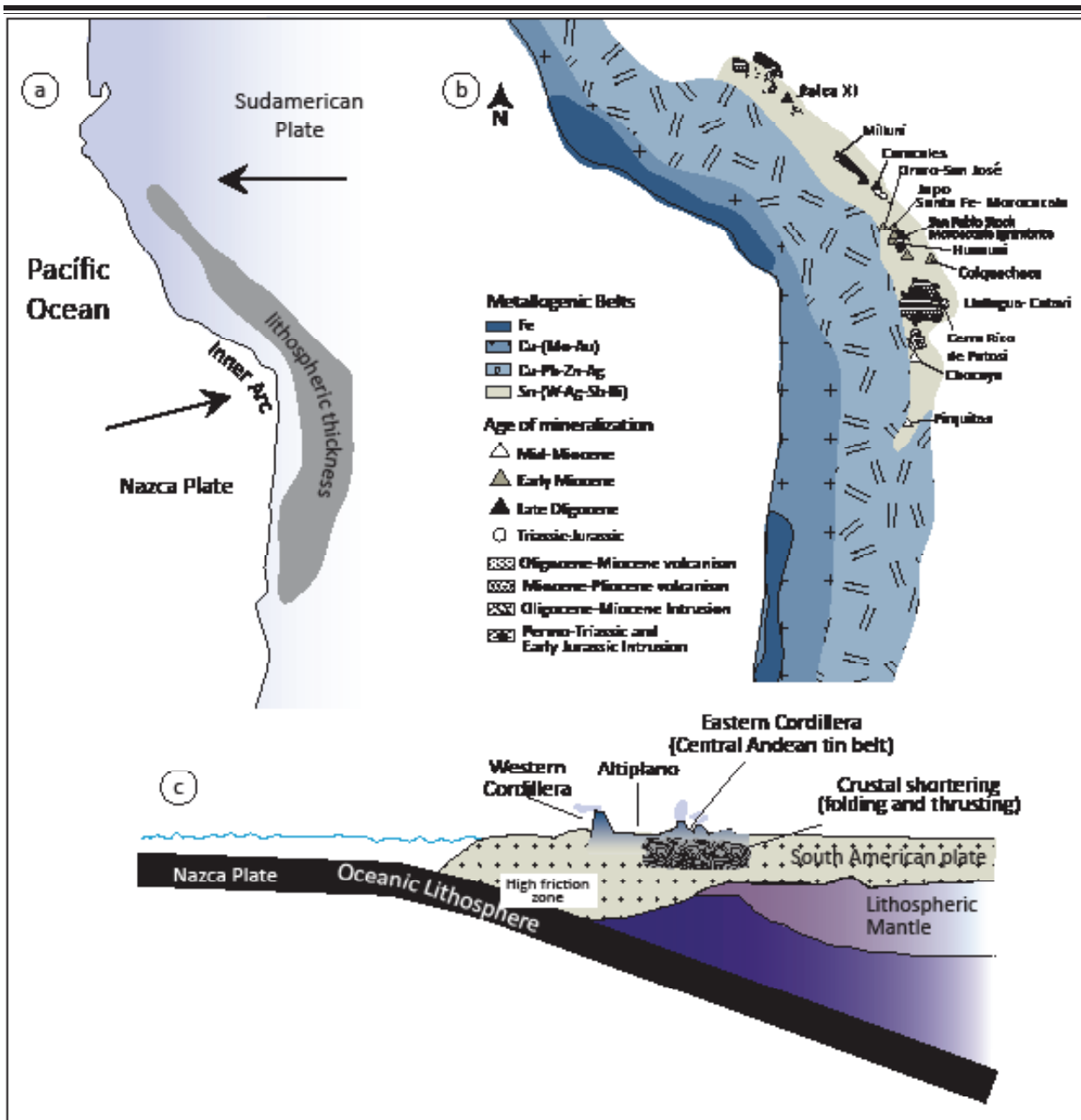


Figure 5. Distribution of In-bearing ore deposits in the world (after Schwarz-Schampera and Herzig, 2002; Murakami and Ishihara, 2013).

### 3. REGIONAL FRAMEWORK. THE CENTRAL ANDEAN TIN BELT

The Central Andean tin belt (also referred to as the Bolivian tin belt) extends along approximately 900 km in a NW trending toward Eastern Bolivia. This belt is extent through Peru and Chile as an extension of the Eastern Cordillera (Kontak et al., 1984a, b). There is an important geographic feature of the Central Andean tin belt precisely in the central segment of an arcuate mountain range, which represents a marked landward broadening of the Andean orogen (Fig. 6a). This region, referred to as the Inner Arc (Clark et al., 1990), is restricted to the Eastern Cordillera of the centermost Andes, and lies to the east of the zone of high intra-Andean plateaus (Altiplano-Puna), which marks an interface between the oceanward, Main Arc (Western Cordillera) and the South American craton (Fig. 6a). According to Mlynarczyk and William-Jones (2005), the Inner Arc is composed of early Paleozoic, marine sedimentary rocks, experienced extensive Cenozoic crustal deformation and anataxis; and it is because these processes that ultimately occurred the accumulation of large amounts of metals distributed in metallogenic belts (Sillitoe, 1976 and Lehmann, 1979; Fig. 6b). The Central Andean tin belt is, therefore, located in the segment of the Andean orogen, which experienced the greatest compression and resulting horizontal shortening, vertical thickening and a magmatic arc broadening. This phenomena was a result of a collisional episode between the continental and oceanic plates leads to shallower subduction (Fig. 6c).



**Figure 6.** Principal tectonic features and relationship with metallogenic of the Central Andes, a) Plate tectonics, volcanism and lithospheric thickness (~10-15 km); b) Relevant ore deposit with time in the Central Andean tin belt; c) Schematic cross-section of the Andean continental margin, showing the relationships between convergence, subduction features, and the magmatic arc (after Mlynarczyk and William-Jones, 2005; Sillitoe, 1976; Lehmann 1979, 1990).

The most important metallogenic epochs in this sector occurred at 26-20 Ma and 16-12 Ma because to migration of the arc (Clark et al., 1990; Soler and Bonhomme, 1990; Sébrier and Soler, 1991; Mlynarczyk and William-Jones, 2005).

According to Lehmann et al. (1990), there is an asymmetric metal zonation perpendicular to the Andean strike

that defines three major metallogenic belts, west to east: (a) Cu-Mo-Au-Fe, Western Cordillera, (b) Cu Pb-Zn-Ag-Au, Altiplano, and (c) Sn-W-Bi-Sb-Ag-Au, Eastern Cordillera.

Mlynarczyk and Williams-Jones (2005), proposed a chronology in the formation of major ore deposits related to magmatism. Considering that, Western Cordillera ore-causative magmatism could have started at 31 Ma, inducing a remarkable Sn-W metallogenic event in many places along the Central Andean tin belt. In the SFD, Grant et al. (1979) assigned to the San Pablo stock an age of ~23.3 Ma, while the eruptive complexes of Llallagua and Colquechaca (~100 km SE from SFD) have been dated at

~21 and ~22.6 Ma, respectively. The ore mineralization in Morococala was established at  $20.1 \pm 1.1$  Ma (Sugaki et al., 2003). The magmatism and the Morococala formation age have been studied by several authors (e.g. Morgan et al., 1998, sugaki et al, 2003). The last volcanic suite from the Morococala represents a second, post-mineralization magmatic stage, which was is represented by rhyolitic and dacitic lava flow. Lavenu et al., (1985) established a K-Ar age of 5.8-6.4 Ma to dacite rocks. Meanwhile, Evernden et al. (1977) obtained also by K-Ar method a 7 Ma age. The rhyolitic sequence is the earliest in this sector of the Central Andean tin belt.



## 4. THE SANTA FE MINING DISTRICT

The Central Andean tin belt hosts many W-Sn-Ag-Cu-Zn-Pb deposits. The Santa Fe mining district (SFD) is located in the Bolivian sector of this province and contains several Sn-Zn-Pb-Ag deposits and occurrences; among them, the most important from the economic point of view are Japo, Santa Fe and Morococala. Santa Fe and Morococala mines are separated ~2 km each other, whereas Japo is located ~10 km farther, towards NW from them. The SFD is located about 30 km of the Oruro city. Despite Oruro is an important mining center, the area has been barely studied due to highly rugged (3800 meters above sea level) and bad



**Figure 7.** Main access roads to study area.

access conditions to the locations of Japo, Santa Fe and Morococala (Fig. 7).

The SFD is exploited by several artisanal mining associations as Machacamarcá, Puente Grande, Santa Bárbara, Morococala, El Porvenir Japo, Santa Fe, Unificada, Nueva San Pablo, El Porvenir Cachi Cachi, Nuevo Amanecer Juan Del Valle and La Tormenta. Until 1994, the SFD was working as an independent district. Nowadays, these and others mines in the region are part of the Oruro politic District. Due the mining tradition and extractive potential, the Japo, Santa Fe and Morococala mines are the most representative in the SFD. Most of the others mining groups are depending of these three centers. These mines mainly produce tin, silver, zinc, lead and cooper.

#### 4.1.Previous works

Mining work in the SFD is reported since 1888 (Espinoza-Morales, 2010).

The modern mining activity in the SFD started in Japo at the beginning of the 20th century. Later, in the 20s, Mr. Simón Iturri Patiño became the owner of all the mines in the SFD as he was in those days of most deposits in Bolivia. From 1950 the Bolivian government managed the SFD; historically, those times were the most productive. In the same decade, the German Geological Mission was carried out in Bolivia. In 1964 appears the first geological map of Oruro.

Despite the economic value and geopolitical importance of mineral resources in the Central Andes, most deposits there have been poorly studied, especially from the mineralogical and metallogenic points of view. Most of studies have been carried on in a regional context. On 1966, W. Thormann published *Investigaciones preliminares sobre la Geotectónica y metalogenesis de la zona Challapata- Caxata*. Meanwhile, Radelli in the same year presented a general tectonic study of the Andean range.

Ahlfeld (1967) described the main metallogenic provinces in the Altiplano. He separated Central Andean tin belt in Northern and Southern parts based on changes in the character of the mineral deposits, also he defined different metallogenic ages to each of them. He distinguished, for the Northern part, Au, W, Sb, Sn, Bi, Zn, Pb deposits. Meanwhile, in the Southern part he found additionally Ag.

The first ore deposit publication, where the SFD is mentioned, corresponds to that of Kelly and Turneure (1970), and includes a mineralogical and fluid inclusion characterization of many Sn and W deposits along the eastern Bolivian Andean Belt. This study suggests that all the deposits in the Central Andean tin belt are due to a single but temporary extensive event of mineralization. Sugaki et al. (1988) also contributed with new information from fluid inclusions in many ore deposits. They proposed that changes of temperature and salinity correspond with a zonal

arrangement of minerals observed in many polymetallic deposits in Bolivia.

Kelly and Turneure (1970) also notes that the Central Andean tin belt is located just where there is thickening continental crust. This region, was referred later to as the Inner Arc (Clark et al., 1990), it is restricted to the Eastern Cordillera of the centermost Andes. Lehmann (1978, 1979, 1981, 1982, 1985) and Lehmann et al. (1978, 1980, 1990) carried out different studies about the relationship with magmatism and the high content of precious metals in this sector, with emphasis in the evolution of the Inner arc and metallogeny process involved. Later, Grant et al. (1977, 1979 and 1980) carried on several works about age of the magmatic activity related to ore mineralization. They assigned the isotopic (K-Ar) ages to the main intrusive stocks in the Bolivian tin belt.

Meanwhile, Lehmann et al. (2000a and b) proposed approaches about tin mineralization in the Central Andean



tin belt, comparing the Chilean copper porphyry systems with similar tectonic sceneries in the tin Bolivian part. These authors attributed the high Sn concentration to the large-scale upper crustal melting process, which strongly modified the melt systems and allowed an advance degree of fractionation under low  $fO_2$  conditions. They interpreted metal enrichment because a mix between the roots of the Bolivian systems (magnetite-series gabbroic-dacitic melts) and the upper crustal partial melts (ilmenite-series affinity).

Mlynarczyk and William-Jones (2005) summarized the main geological features and the proposals about magmatism relationship with ore mineralization of the Central Andes and defined the metallogenic provinces. Meanwhile, Arce-Burgoa (2009) proposes that these metallogenic belts can be divided in four groups: i) Sn porphyry; ii) Sn-Ag-Pb-Zn volcanic rocks (including Ag-Sn); iii) Sn-Ag-Pb-Zn mineralization hosted in sedimentary

rocks and Sn-W-Au-Zn tin-polymetallic deposits intrusion related.

More recently, several studies focused on the potential of its ore associations as a source of indium (Ishihara et al., 2011; Murakami and Ishihara, 2013). Indium is considered as a strategic metal for European Union because of its technological applications and the risk of supply disruption (Chapman et al., 2013; European Commission, 2014). On the other hand, the USGS (Tolcin, 2016) reported that indium-tin oxide (ITO) is leading the use of this metal, accounting for 55% to 85% of the global consumption, and reflecting the strong relationship between indium and tin as commodities.

Throughout development of the present work, Betkowski et al. (2017) are carrying out a petrographic and geochemical characterization of phosphates at Llallagua one of the world's biggest tin deposits, the Siglo XX mine. The Llallagua tin deposit is

also one of the most representative deposits at the Central Andean tin belt. Analogous to most of deposits in the Central Andean tin Belt and despite numerous studies, there is still a debate over the timing and characteristics of mineralization history of these deposits.

Just a few specific studies about the Santa Fe District can be mentioned. Sillitoe et al. (1975) proposed that most Sn deposits in Bolivia as porphyry tin type; they included the San Pablo stock and the Japo mine as part of this study.

Dietrich et al. (2000) conducted a geochemical and petrological study about the Bolivian tin porphyry systems. These author based in previous proposal, studied several samples from Llallagua, Chorolque, and Cerro Rico porphyry rocks comparing the geochemistry of the bulk rock vs melt inclusions. They proposed that decompression and concomitant crystallization of the magma chamber trigger release of Sn-W-B-As-bearing magmatic vapor phases from undisturbed granitic melt

portions, possibly preserved in apical satellite intrusions. Also, pointed the possibility of the genetic concept of deriving volcanic rocks and magmatic vapor phases from different portions of a compositionally zoned and partially mixed magma chamber as an explanation of the exceptional metallogenic situation of the Bolivian tin mineralization in association with only moderately fractionated felsic host rocks.

Sugaki et al. (1981) carried out a geological study on hydrothermal deposits in the Oruro department. These authors proposed a genetic link between the Santa Fe, Morococala and Japo deposits. They described a Sn-Zn-Pb-Ag metallogenic association and reported the major geological structures of the area (Sugaki et al., 1981; Sugaki et al. 2003). (Morgan et al., 1998) conducted a petrochemistry study of the volcanic sequence of the Morococala formation. They suggested that analyzed samples pertaining to a

single zoned silicic magma chamber. Sugaki et al. (1981) reported a grade 1.15 wt.% Sn in Japo, 0.68 wt.% Sn in Santa Fe and 0.59 wt.% Sn in Morococala.

In the 80's many deposits in Bolivia started to be mined by artisanal miners grouped in cooperatives. Nowadays, Japo, Santa Fe and Morococala deposits are exploited by three different mining cooperatives.

#### 4.2. Geology of the Santa Fe Mining District

A spectacular scene of a wide meta-sedimentary sequence cover by volcanic rocks on the top of the range characterizes the geological scenery of the Santa Fe District. The Paleozoic metasedimentary sequence starts by the Amutara Fm., which is a shale and sandstone turbidite unit deposited in a deep marine environment. This unit is overlain by a Silurian group that includes the Cacañiri, Llallagua, Uncia and Catavi formations. The Cancañiri Fm. conformably covers the Amutara Fm. and is composed by micaceous

sandstones and siltstones that gradually change to quartzites, sandstones, siltstones and grey-green shales of the Llallagua and Uncia formations. The Silurian group ends with the Catavi Fm., which consists of shales and sandstones.

An intense tectonic activity in different periods deformed the Paleozoic sequence and formed NNW-SSE folds, the largest of which is the Santa Fe anticline. Thrusting in the study area also took place; a wide N<sup>o</sup>40 shear zone and two fracture systems were developed: (S1) N40<sup>o</sup>E fracture system, dipping 60<sup>o</sup>NW, and (S2) with the same direction but dipping 75<sup>o</sup>SE. The Paleozoic sedimentary sequence is unconformably covered by the volcanic complex of the Morococala Fm., mainly constituted by calc-alkaline lavas and tuffs of Miocene age (Sugaki et al., 1981; Morgan et al., 1998).

The economic mineralization in the SFD is spatially related to intrusive rocks, consisting of stocks and porphyritic intrusions of peraluminous

granites formed through different magmatic pulses, most of them during Oligocene-Miocene times (Grant et al., 1979). Intrusive rocks have a porphyritic texture, with phenocrystals of quartz, K-feldspars, biotite, monazite and tourmaline, many of which are replaced by sulfides, chlorite and epidote.

The main intrusive body is the San Pablo stock, which is exposed alongside of the Japo mine. The San Pablo stock is an irregular body of ~2 km in diameter that intrudes the Paleozoic metasedimentary sequence. Dikes and hydrothermal breccias occur at the margin of the stock, cut by tin-bearing quartz veins. Sillitoe et al. (1975) classified the San Pablo stock as a quartz latite porphyry, noticing that it is pervasively altered, with the formation of sericite, pyrite, tourmaline and monazite.

### 4.3. Stratigraphy

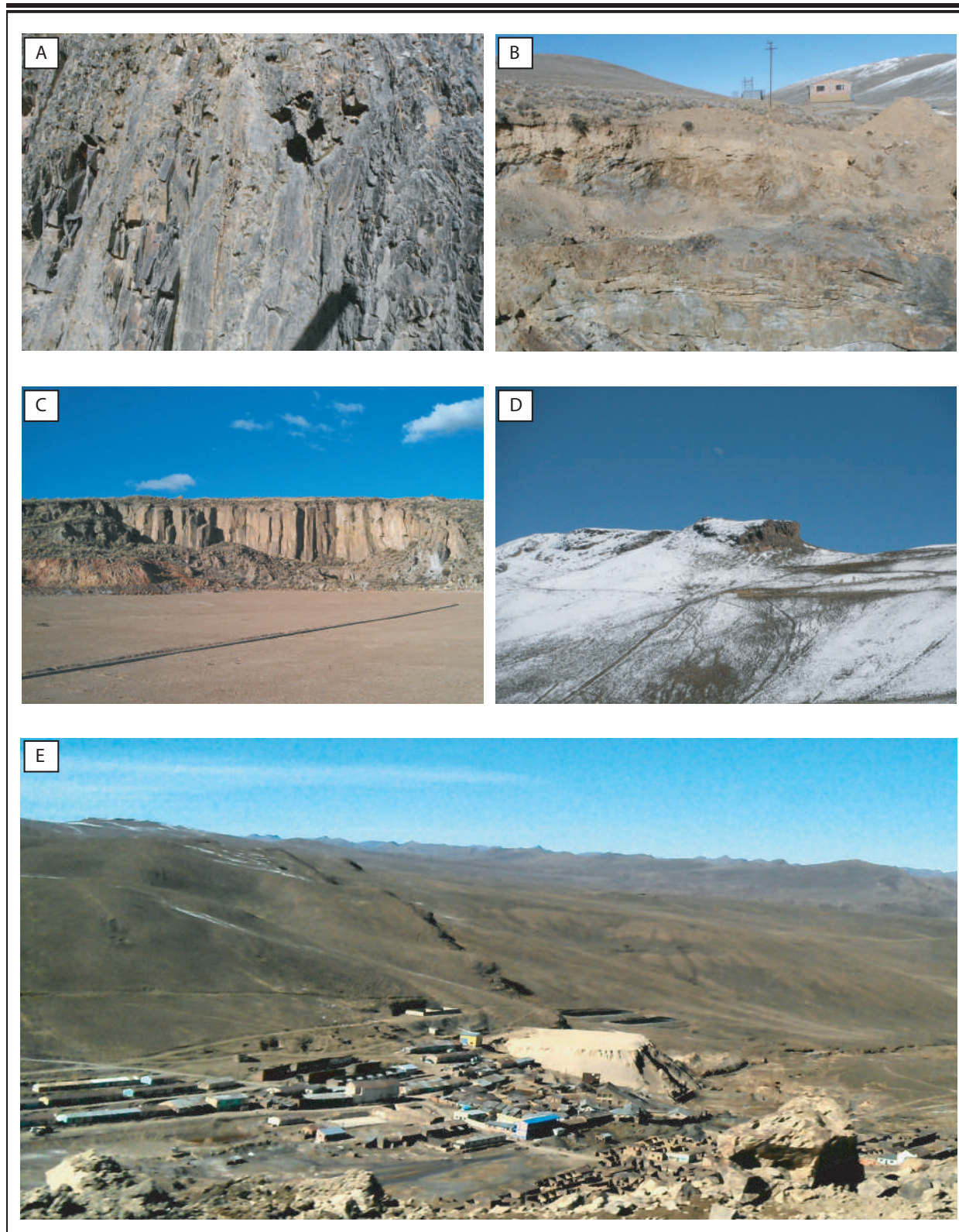
#### Paleozoic

#### Amutara Formation (Upper Ordovician)

The Amutara Fm is a Palaeozoic metasedimentary sequence. It is the basement of the stratigraphic sequence, which is a shale and sandstone turbidite deep marine unit. This unit is overlaid by a Silurian sequence of the Cacañiri, Lallagua Uncia and Catavi formations. Diaz-Martinez (1997) describes Amutara Formation as Sandstone of whitish to gray color with size of grain of fine to very fine. It presents layer of black shales of millimeter to decimetric thick with parallel laminations and ripples of currents, scarcely bioturbated and well cemented. It has >1000 m thickness (Fig. 8e).

#### Cancañuri Formation (Silurian Llandovery)

The Cancañiri Fm. covers the Amutara unit, has until 400 m thickness and micaceous sandstones and siltstones that gradually change to quartzites, sandstones, siltstones and



**Figure 8.** Outcrops of stratigraphic units in the Santa Fe District. A) Slate of the Llallagua formation in the Japo area; B) shales and sandstones sequence of the Uncia formation; C) Riolitic lava flow of the Morococala formation in the Santa Fe area; D) andesitic dome of the Morococala formation; E) Paleozoic metasedimentary sequence of the east limb of Santa Fe anticline intruded by dikes of Miocene age.

grey-green shales of the Lllagua and Uncia formations constitute it. It is exposed along anticline axis. In thin section Amutara formation looks as a sedimentary rock affected by a moderate metamorphism, with grain size of fine sand, supported by an altered cryptocrystalline matrix, which has resulted in micas and sillimanite (Fig. 8e).

### Lllagua Formation (Silurian Wenlock)

The Lllagua Formation exposes concordantly with the Uncia Formation in western and southern part of the district, and often forms steeper slope and cliff of mountain. It consists of phyllite, thick member of alternation of sandstone, slate and/or quartzite, and slate etc. Phyllite is found in lowest portion of this formation, and its thickness is within 100 m, but sometimes thinning out.

The alternation of sandstone, slate and quartzite is the principal member in the formation, and overlies phyllite

layer. Slate becomes predominant at upper part of the formation. Quartzite and sandstone are light gray to yellowish gray in color, while slate is grayish. The total thickness is approximate, 1,100 m. This formation becomes to principal country rocks of many ore veins in the district (Fig. 7a).

### Uncia Fm. (Ludlow)

The Uncia Fm., which cover conformably the Lllagua Fm. Uncia Fm is mostly conformed by shales and sandstones, with a total thickness about 1800m. These materials are conformably covered by the Fm Catavi, which is the top of the Silurian sequence (Fig. 7b).

### Catavi Fm. (Pridoli)

The Silurian sequence ends with Catavi Fm. It appears at synclinal structures. Catavi Fm is conformed mostly by sandstone of gray tones. These materials are unconformably covered by the volcanic complex part of the Morococala Fm., mainly constituted by calc-alkaline lavas and tuffs of Miocene age (Fig. 8e).

Cenozoic is now available (Fig. 9).

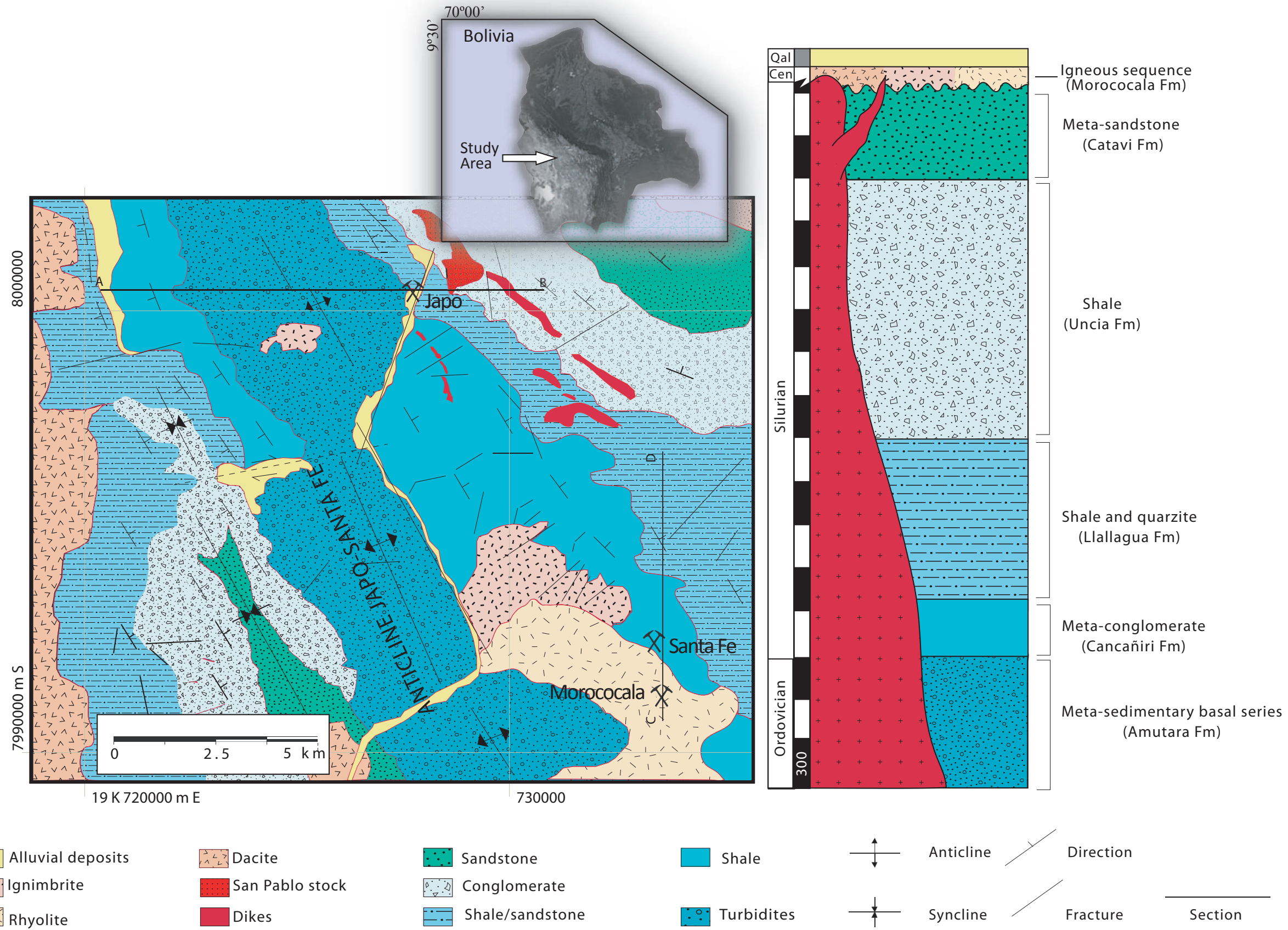
### Morococala Fm. (Cenozoic)

The Morococala Fm., with two important magmatic episodes, represents the Cenozoic sequence. On one hand, extrusive rocks are mostly represented by dacite of 5.8 to 6.4 m.y. (Lavenu et al., 1985) and rhyolite of 7 m.y. (Evernden et al. 1977). Generally, these are located in the top highland in Japo region, and they are more widely extended in Santa Fe-Morococala zone.

On the other hand, the intrusive rocks are represented by an intense plutonic activity as the San Pablo stock and some dikes related to it. The age of this plutonic suite is Miocene (Sugaki et al., 2003). According with Sugaki et al. (1981) the thickness of the Morococala Fm. is >150 m (Fig. 7c, d and e). As a result of the fieldwork, a more accurate geological map of the Santa Fe district

As well, two geological sections of Japo and Santa Fe-Morococala regions are showing in the Fig. 10. The section A-B represent a geological sketch, in east-west direction, of the Santa Fe anticline, where can be distinguished two parallel main faults, both belong to S2 system (N40°E / 75°S). The Japo mine is located in these faults. San Pablo stock emplaced also is following this NE-SW direction. Several dikes related to this stock were recognized in the Japo mine.

The C-D line is a north-south section, where the Santa Fe and the Morococala mines are located. Both are hosted in the east sector of the Santa Fe anticlinal, corresponding to Paleozoic sequence of the Uncia and Llallagua formations. Volcanic rocks of the Morococala formation cover unconformably them.



**Figure 9.** Location and detailed geological map of the Santa Fe mining District. The schematic stratigraphic section (right) is based in Sugaki, et al. (1981), A, B, C and D indicate the location of the geological cross-sections shown in Fig. 10.



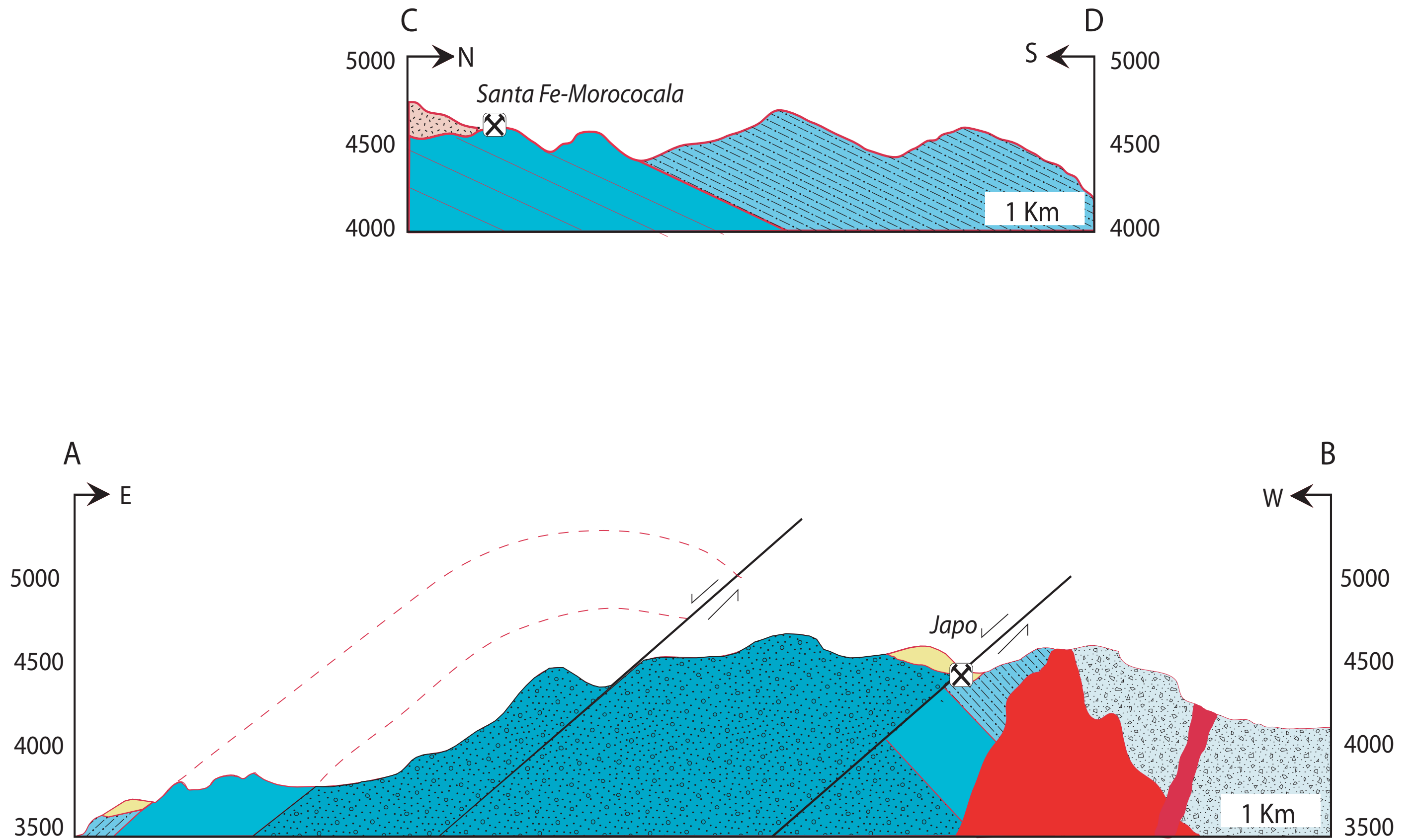


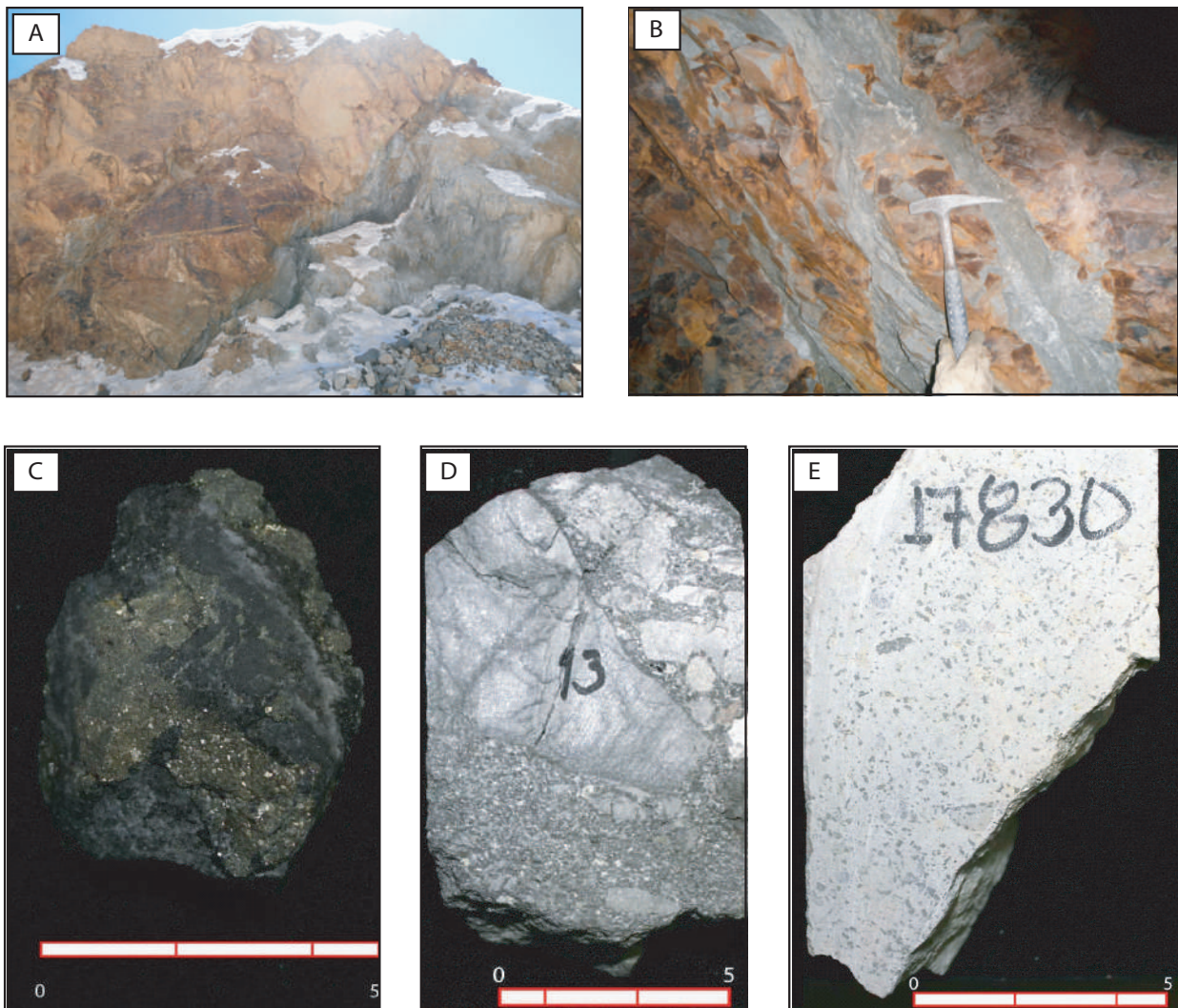
Figure 10. Schematic A-B (east-west) and C-D (north-south) geological sections in the Santa Fe mining District (location shown on Fig. 9).

4.4. Ore mineralization

The Japo deposit

In general, in The Santa Fe District ore mineralization occurs as veins and disseminations. The mineralization is mainly associated with felsic magmatism, represented by several generations of dykes and the felsic San Pablo stock (Fig. 11).

The Japo mine is located at 32 km southeast of the city of Oruro. The main mineralization in this deposit is situated at the east part of the Santa Fe anticline axis, which has NW-SE direction (Fig. 12a, d). The country rocks in the SFD are a Paleozoic meta-



**Figure 11.** Ore mineralization style. A) Mineralization in share zone; B) veins hosted in meta-sedimentary rocks; C) massive mineralization; D) ore mineralization in breccia; E) dissemination and replacement of phenocrysts.

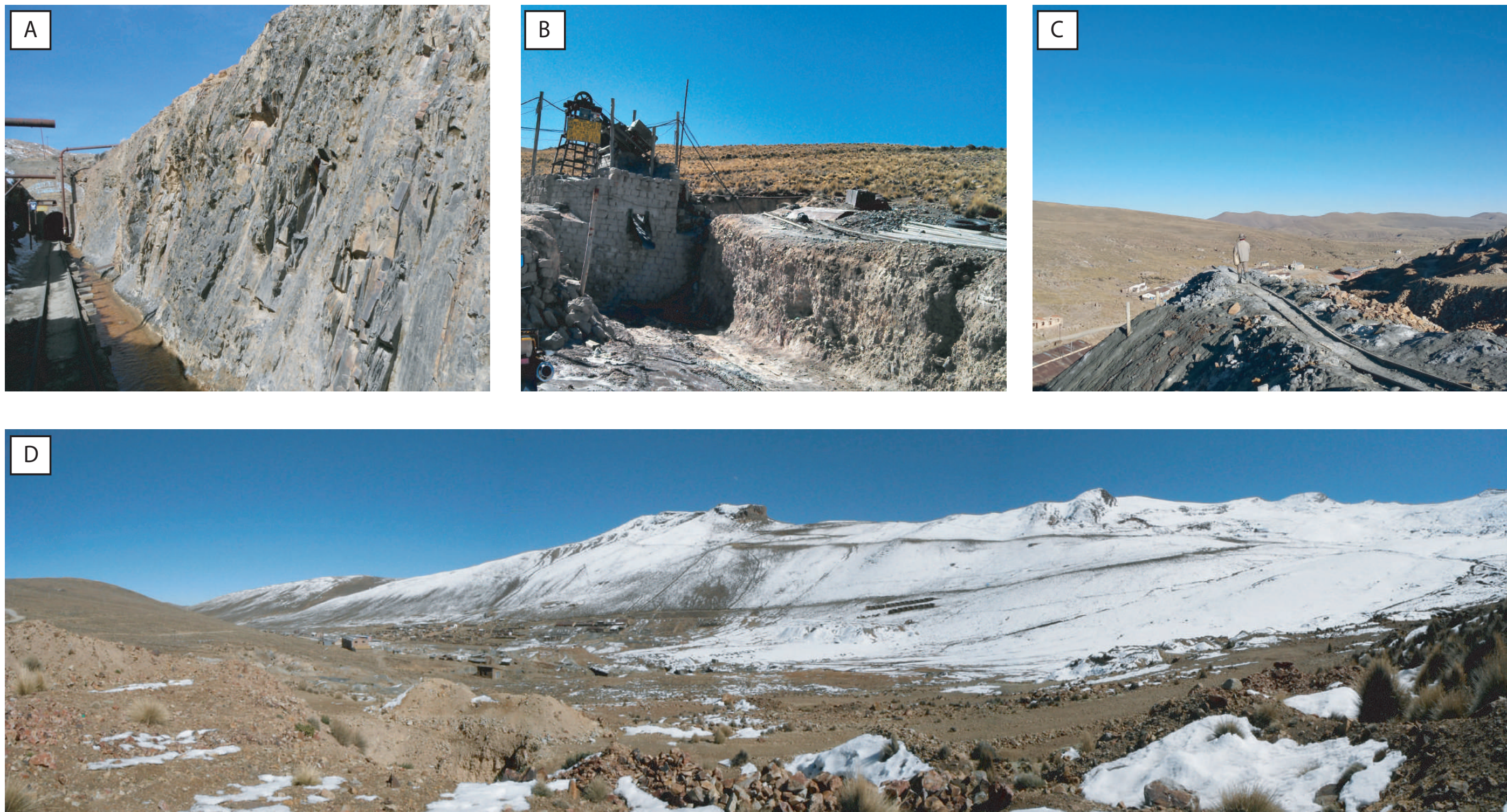
sedimentary sequence represented by the Cancañiri, Llallagua Uncia and Catavi formations. In general, the strata strike N35°W with a general dip of 40°NE and a secondary system follows an important fault strike of N20°E. The ore is hosted in veins of different widths, from a few centimeters to several meters.

In the Japo deposit most of the mineralization is represented by cassiterite and sulfides disseminated in intrusive rocks. Ore mineralization also occurs as veins of mostly sphalerite ± galena, pyrite, marcasite, arsenopyrite, chalcopyrite and chalcocite. Veins follow lithological and structural contacts, as fracture infillings, Mineralization also was found as replacements and breccias (Figs. 11 and 12). Alteration is developed (a) in plutonic rocks, where sericite, monazite, tourmaline and sulfides (mostly pyrite) formed; and (b) along the contact between host rocks and quartz veins, where alunite, plumbojarosite, vermiculite, kaolinite and dickite occur.

## The Santa Fe-Morococala deposit

The Santa Fe and Morococala mines are separated from each other by less than 2 km (Fig. 12b and c). The Santa Fe and Morococala mines are mainly hosted by rocks of the Cancañiri Fm., which is unconformably covered by the Morococala Fm. (Pliocene).

Mineralization in Santa Fe and Morococala occurs mostly as quartz veins, of few centimeters to 0.5 m thick, with cassiterite, sulfides and sulfosalts. Veins are associated to the above fracture systems ( $S_1$  and  $S_2$ ), so that  $S_1$  hosts mostly Sn ± sulfides ores whereas  $S_2$  is rich in Zn-Pb-Ag (Fig. 11a and b). Rutile is associated with the latest cassiterite and forms needle-like crystals. Among the supergene minerals, gypsum, calcite, melanterite and vivianite can be mentioned. The ore mineralization in Morococala mine was established at  $20.1 \pm 1.1$  m.y (Sugaki et al., 2003).



**Figure 12.** View of the Santa Fe Mining District. A) Adit of the Japo mine hosted in Paleozoic shales; B) adit of the Santa Fe mine hosted in pyroclastic of the Morococala formation; C) panoramic view of the Morococala mine, also hosted in rocks of the Morococala Formation; D) East limb of the Santa Fe anticline, Japo town is at the bottom.



# 5. SAMPLING AND METHODS

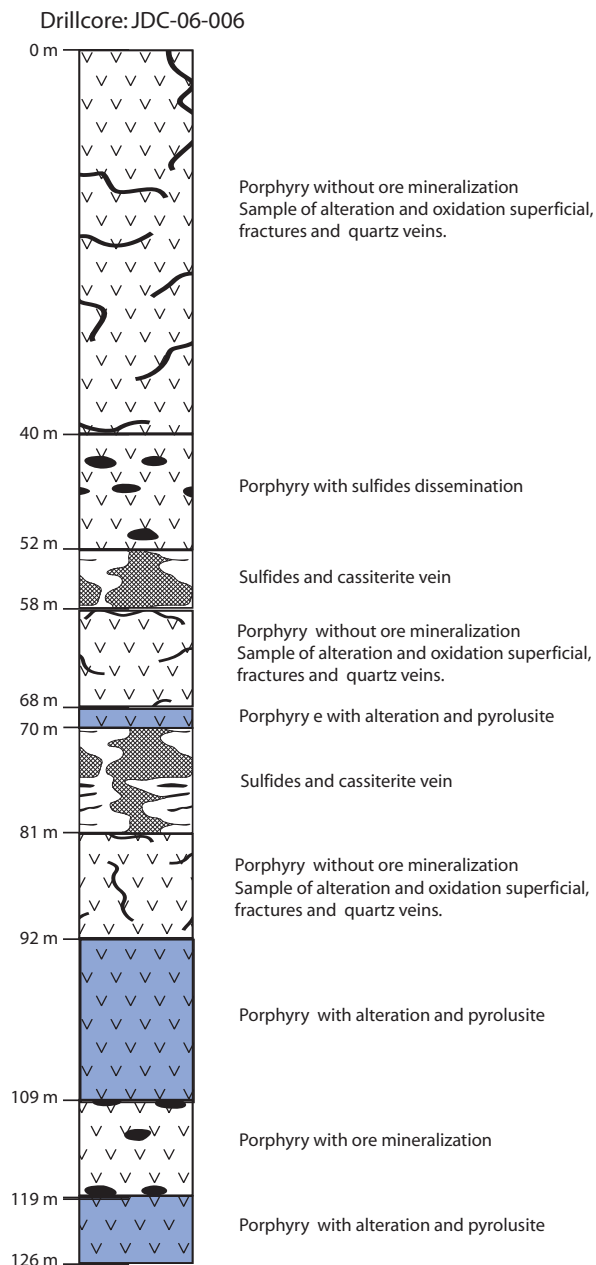
In the present study, different analytical techniques have been carried out in order to establish the stages of mineralization and its relative chronology and to determine the magmatic and structural controls of the mineralization. An extended explanation of conventional analytical technics can be consulted in Melgarejo et al. (2010).

## 5.1. Sampling and description

Fieldwork was conducted in three different stage on summer seasons of 2013, 2014 and 2015. Both, country rocks and ore mineralization were sampled in the Japo, Santa Fe and Morococala mines and outcrops. Drill-holes were performed by AITCOBOL during 2006 in an exploration project; this information allows having a very good space-structural control in different levels of this deposits.

More than 5000 m of drill-cores from the Japo mine were logged and sampled. A total of 169 rock samples were collected in the Santa Fe mining district, 108 from drill-cores, 38 in undermine and 23 in surface outcrops.

Subsequently, a selection of samples was made, which was based on the criterion that they were representative of the mineralized bodies studied and their respective host rocks. A macroscopic description of the hand samples was made. Samples (superficial, undermine and drill-core) relation and description can be consulted in the Appendix 1. Additionally, a very extensive drill-core logging was carried on. Description of a representative of the drill-core (JDC-06-006, scale 1:1000) is showing in Fig. 13. The drill-core logging and descriptions are attached in the Appendix 2.



**Figure 13.** Logging of the drill-core JDC-06-006.

This description allowed the macroscopic identification of the essential minerals, as well as textures. In this way, division of the samples into basic categories served to select a smaller set of representative samples. The Fig. 14 shows the map of drill-hole location.

## 5.2. Petrographic study

The petrographic study was carried out with the purpose of identifying the essential minerals and accessories, as well as their relative abundances. More than 40 samples were prepared by crushing and cutting from veins and host-rocks by two diamond saw. Subsequently, the selected samples were performance at the commercial laboratory Miekinia thin section labs, where samples were prepared as thin section from an integrated sample, not covered of 30 microns thickness. Mineral assemblages were studied in the polished thin sections using standard petrographic microscopy (Appendix 3).

Additionally, the stratigraphic information have been supplemented by the petrographic observations and logging drill-core.

## 5.3. X-ray powder diffraction

X-ray diffraction is a useful tool, especially to analyze cryptocrystalline mineral as clays or alteration minerals

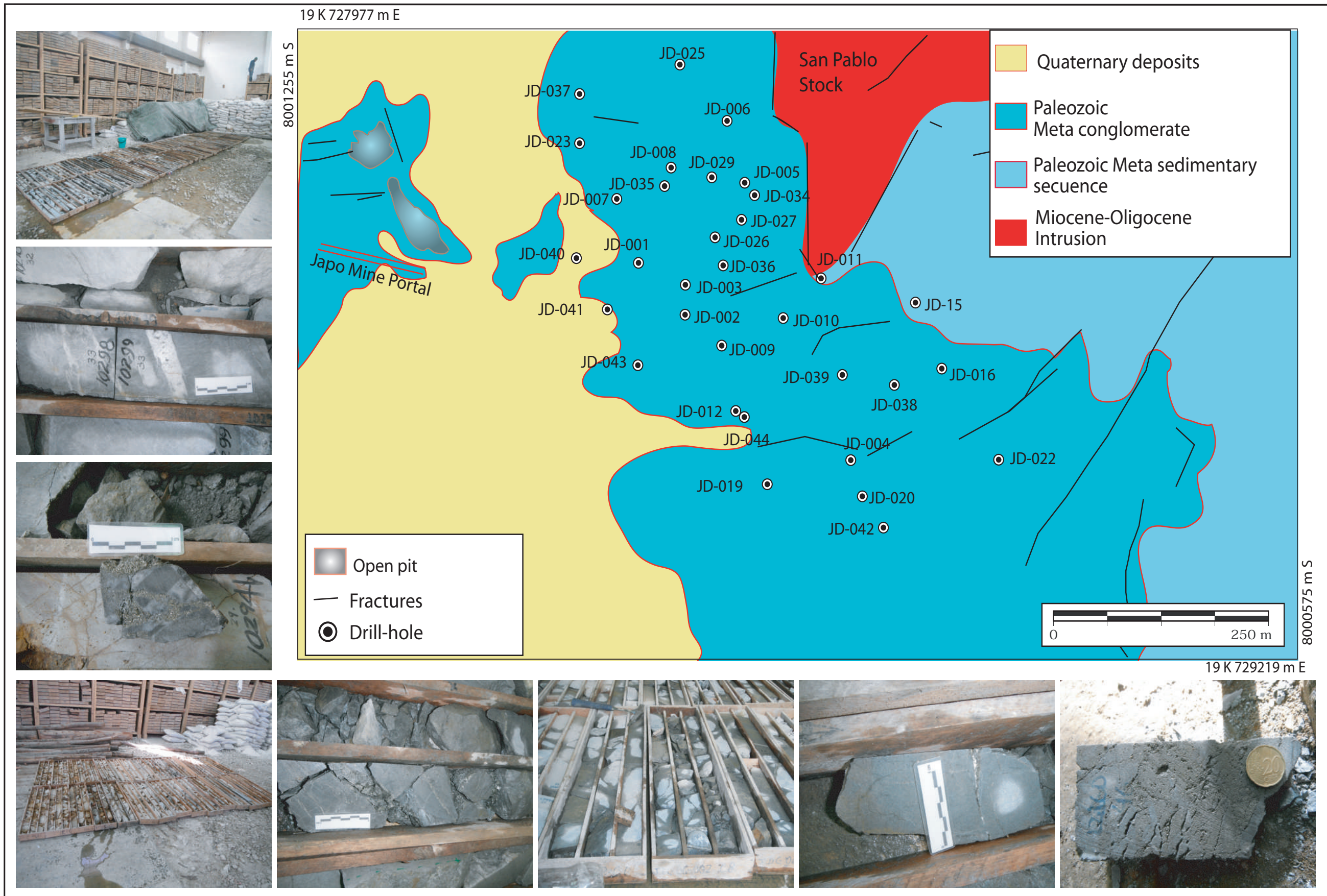


Figure 14. Map of drill-holes location in the Santa Fe District



that cannot be easily determined by microscopic techniques. Alteration association becomes important in hydrothermal systems, not only as a parameter to ore deposit classification type, but also as a good exploration target.

Selected samples from the SFD were carefully pulverized in an agate mortar, and the powder was placed in the sample holder. In general, some mm<sup>3</sup> is enough. Typically, the powder may be formed by forming a flat surface of 1-2 cm<sup>2</sup>, or alternatively by filling a non-absorbent glass capillary, with an inner diameter of about 0.5 mm.

Bulk mineralogy was confirmed in 37 samples by X-ray diffraction (XRD). Spectra were obtained from powdered samples (particles <math>126</math> under 45  $\mu\text{m}$ ) in a Bragg-Brentano PANAnalytical X'Pert 127 Diffractometer system (graphite monochromator, automatic 128-129 gap, K $\alpha$  radiation of Cu at  $k = 1.54061 \text{ \AA}$ , powered at 45 kV, 40 mA, scanning range 4–100 $^\circ$  with a 0.017 $^\circ$  2 $\theta$  step 130

scan and a 50-s measuring time) located at the CCiT-UB. The identification and semiquantitative evaluation of phases were conducted using 132 a PANAnalytical X'Pert HighScore software. The bulk of X-ray study can be consulted at Appendix 4.

#### 5.4. Scanning electron microscopy (SEM), with X-ray dispersive energy analyzer (EDS) and EMPA

A scanning electron microscope (SEM) was used to investigate smaller mineral grains and textures. More than 30 polished ore sections were analyzed using two different instruments: a Hitachi TM-1000 table-top scanning electron microscope (SEM), equipped with Energy Dispersive X-ray Spectroscopy (EDS) and Back-scattered Electron detector (BSE) at the *Departament d'Enginyeria Minera, Industrial i TIC of the Escola Politècnica Superior d'Enginyeria de Manresa*, (EPSEM) and also in the *Serveis Científics i Tecnològics of the Universitat de Barcelona*, (CCiT-UB).

This equipment allowed us to obtain back-scattered electron (BSE) images and qualitative chemical analyses by energy dispersive X-ray spectrometry (EDS). SEM-EDS is based on obtaining images as a result of interactions between incident electrons ray and sample. The back-scattered electrons and X-rays of the elements present in the sample are captured to know the chemical composition of the sample. The Hitachi TM-1000 table-top scanning electron microscope used in this study does not need carbon recover in samples, which represent an advantage over other conventional SEM. Unfortunately, many elements produce X-rays with energies close to those of other elements, because of the low spectral resolution of EDS spectrometers, the analyzes obtained are not always very precise. However, SEM can work with low current probe, it is a not destructive method, which makes it indispensable for analysis of crystals of very fine grain size (less

than 1  $\mu\text{m}$ ), even in rough samples. A catalog of the results obtained can be consulted in Appendix 5.

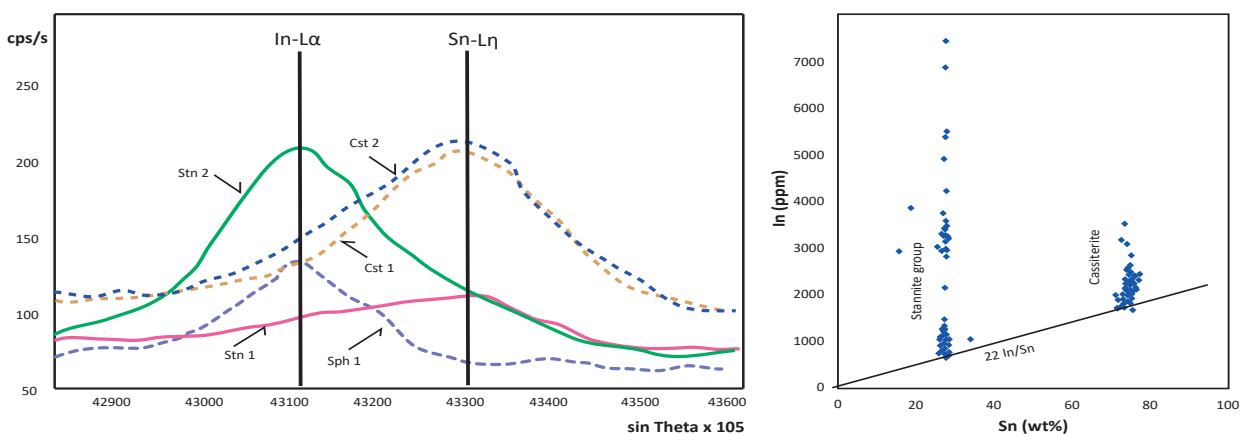
The electron probe micro-analyzer (EPMA) continues to be one of the most widely used methods for the routine chemical analysis of minerals. The electron microprobe analyzer (EPMA) can be considered as a scanning electron microscope that includes additional wavelength-dispersive spectrometer (WDS). Collection of quantitative analysis is the main characteristic of EPMA technic. WDS spectrometers separate the characteristic X-rays by their wavelength. Analyzer crystals are used to separate X-rays and radiation detectors to measure the X-rays dispersed by the crystals, and the X-ray intensities emitted by the sample are compared with standards of known composition. The analyzed samples were previously converted to electrically conductive, by a thin cover of graphite. Covering can be also of aluminum or gold. EPMA

allows quantitative chemical analysis of very small quantities ( $\sim 1 \mu\text{m}^3$ ), which allow to analyze heterogeneous grains, zonations, and exsolutions.

However, analysis of In-tin minerals by EPMA is problematic, due to interference of Sn-L $\eta$  ( $l=3.789 \text{ \AA}$ ) and interference on the In-L $\alpha$  ( $l=3.772 \text{ \AA}$ ) intensity (Schwarz-Schampera and Herzig, 2002; Benzaazoua et al., 2003). Andersen et al. (2016) found in samples from England that this interference to contribute 22 ppm of In per 1 wt% of Sn by linear approximation to the minimum measured In concentrations in stannite and cassiterite (Fig. 15). Indium contribute reported by Benzaazoua et

al. (2003) in samples from the Neves Corvo deposit is higher.

Quantitative analyses were obtained with an EPMA JEOL JXA-8230, at the CCiT-UB. Analyses were carried out under the following conditions: 20 KeV, 20 nA, beam diameter of 1  $\mu\text{m}$ , and a counting time of 30 s; the used standards were skutterudite (NiK $\alpha$ , AsK $\alpha$ , FeK $\alpha$ , CoK $\alpha$ ), sphalerite (ZnK $\alpha$ , SnL $\alpha$ ), cuprite (CuK $\alpha$ ), marcasite (SK $\alpha$ ), stibnite (SbL $\alpha$ ), Ag (AgL $\alpha$ ) and crocoite (PbM $\alpha$ ). The number of analyzed points were cassiterite, 60; sphalerite, 70; stannite, 78; sakuraiite, 10; k rsterite, 4; and sulfosalts; 32. The bulk of results of the chemical analysis mineral by EPMA are presented at the Appendix 6.



**Figure 15.** (Left) WDS spectra illustrating the interference between In-L $\alpha$  and Sn-L $\eta$  within stannites (stn), cassiterites (cst) and a sphalerite (sph); after (Benzaazoua et al., 2003). (Right) Interference correction for Sn on In. The interference was calculated from samples of England. The minimum measured signal for In-K $\alpha$  for stannite group minerals and cassiterite and approximates 22 ppm In for 1 wt% Sn. After Andersen et al. (2016).

### 5.5. Bulk chemical analyses

Bulk-rock analyses of element concentrations was carried out by a combination of instrumental neutron activation analysis (INAA), multi-acid digestion inductively coupled plasma (ICP) and inductively-coupled plasma emission mass spectrometry (ICP-MS) techniques at the commercial laboratory ACTLABS. The standards measurement conditions and detection limits are described in 4Litho report (Actlab Ltd., 2017). Milling samples was carried out at the Mineral Processing Lab of the EPSEM and at the Geology Faculty of the UB. Samples were performance an agate mill to avoid metals contamination. Concentrate samples were also analyzed in order to compare values between host rocks and ore to stablish the elemental distribution and mobility. Metal and metalloid contents (Ga, Cu, Zn, As, Ag, In, Sn, Sb, W, Pb and Bi) of all samples were analyzed. Additionally, REE (La, Ce, Pr, Nd, Sm, Eu, Gd, Tb, Dy, Ho,, Er, Tm, Yb, Lu) were measured in the intrusive rocks.

### 5.6. Micro-thermometric study of fluid inclusions

Fluid inclusions have many practical uses for ore deposits study, providing information on the temperature, pressure, density and composition of the fluids involved in ore mineralization. Previously, the fluid inclusions measurement, a specific petrographic study (following Van den Kerkhof and Hein, 2001 recommendations) about the characteristics of any fluid inclusion association is mandatory.

Fluid inclusions provide direct evidence of the nature and composition of hydrothermal solutions. Several studies about fluid inclusions (Roedder 1984; Roedder and Bodnar, 1997; Wilkinson, 2001; Van den Kerkhof and Hein, 2001) indicate that major solutes of hydrothermal fluids are cations of Na, K, Ca, Mg, Fe, Ba, Mn; anions of Cl, S, C, N, P, Si; metals such as Au, Ag, Cu, Pb, Zn, U; gaseous species ( $\text{CO}_2$ ,  $\text{CH}_4$ ,  $\text{N}_2$ ,  $\text{SO}_2$ ,  $\text{H}_2\text{S}$ ) and hydrocarbons. They represent samples of hydrothermal

fluids, and range in size from a single water molecule up to several millimeters with an average of about 0.01mm (Roedder, 1984).

The micro-thermometric study was carried on a Linkam THMSG-600 heating-freezing stage at the *Centro de Geociencias, of the Universidad Nacional Autónoma de México*. Calibration runs show that measurements are accurate to  $\pm 0.2^\circ\text{C}$  for  $T_m$  and to  $\pm 2^\circ\text{C}$  for  $T_H$ .

In the present study, fluid inclusions of primary origin were analyzed according to the criteria of Roedder (1984). Fluid inclusion were heated on heating-freezing stage mounted on a petrological microscope until the vapor and liquid phases homogenize. Homogenization of the liquid and gas phases will be seen to occur at a given temperature on heating of the inclusions. This homogenization temperature is equivalent to the minimum entrapment temperature, thus the real fluid could have occurred to higher temperature.

Salinity is measured in terms of NaCl wt.% equivalent and is based on freezing point depressions. The salinity of the inclusion is determined by first freezing the inclusion and then raising the temperature of the stage, observing the first and final melt temperatures ( $T_m$ ). The first melt temperature indicates the type of salt, while the temperature of the last melt indicates the degree of salinity, usually measured in equivalent NaCl. Decrepitation temperatures are obtained by crushing and bursting of inclusions by heating.

More than 470 fluid inclusions in calcite and quartz crystals were measured. Ice melting temperatures ( $T_m$ ), first, and then homogenization temperatures ( $T_H$ ) were obtained. Those fluid inclusions where leakage, decrepitation or other modifications were suspected were rejected, following the recommendations of Bodnar et al. (1985), and Van den Kerkhof and Hein (2001). Salinity values and isochores were calculated

$$\text{Salinity (wt.\%)} = 0.00 + 1.78\theta - 0.0442\theta^2 + 0.000557\theta^3 \dots \dots \dots (\text{eq.2})$$

$$\text{Salinity (wt.\%)} = 26.242 + 0.4928\Psi + 1.42\Psi^2 - 0.223\Psi^3 + 0.04129\Psi^4 + 6.295 \times 10^{-3}\Psi^5 - 1.967 \times 10^{-3}\Psi^6 + 1.1112 \times 10^{-4}\Psi^7 \dots \dots \dots (\text{eq.3})$$

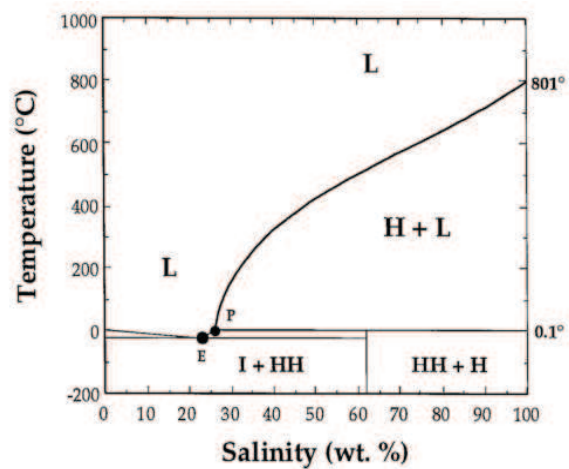
assuming an H<sub>2</sub>O—NaCl system, using the equations of state (eq, 2) of Bodnar and Vityk (1994):

Where  $\theta$  is the depression of the freezing point in degree Celsius. Equation 2 is correct to temperatures from 0.0 °C to -21.1 °C. To inclusions that containing >26.3 wt.% NaCl should show halite as the last solid phase to disappear during heating from low temperatures. The solubility of halite under vapor-saturated conditions is represented according to equation 3:

Where  $\Psi = T(^{\circ}\text{C})/100$ . Equation 3 accurately represents the solubility of NaCl in water from the peritectic temperature (0.1 °C) to the NaCl triple point (801 °C). Fig. 16 shows the H<sub>2</sub>O—NaCl phase relations in the low temperature region, including the relationships between the salinity and the ice-melting curve.

Likewise, fluid inclusions can also provide evidence of boiling. Canet et

al. (2011) described the main criterion is the presence of clusters of fluid inclusions that, belonging to a single paragenetic family, show variable liquid-to-vapor ratios, reflecting the coexistence of



**Figure 16.** Vapor-saturated phase relations in the NaCl—H<sub>2</sub>O system at low temperatures. After Bodnar and Vityk (1994) based in Hall et al. (1988); Sterner et al. (1988) and Bodnar et al. (1989).

I = ice; L = liquid; HH = hydrohalite; H = halite; P = peritectic (0.1 °C, 26.3 wt.% NaCl); E = eutectic (-21.2 °C, 23.2 wt.% NaCl).

vapor and liquid (Bodnar et al., 1985; Haas, 1971; Van den Kerkhof and Hein, 2001).

However, trapping of heterogeneous (vapor+liquid) fluids seems to not occur

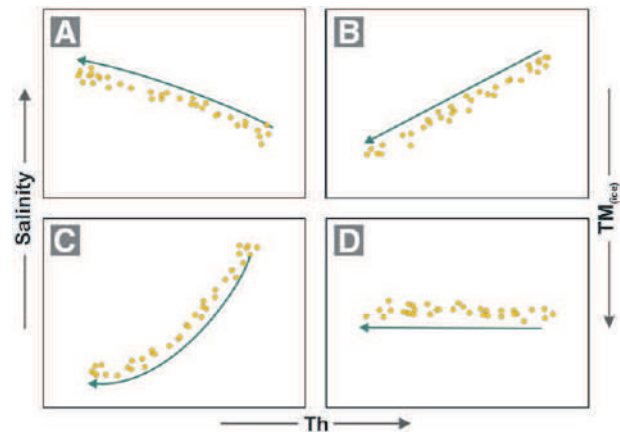
extensively. Fig. 17 illustrates cases where, boiling can only be inferred

from certain trends showed by fluid inclusion populations in a plot of  $T_H$  vs  $T_m$  (or alternatively the apparent salinity), in order that a progressive increase in salinity (or decrease in  $T_m$ ) along with a  $T_H$  decrease reflects the partitioning of the non-volatile solutes into the liquid phase during steam loss (Hedenquist and Henley, 1985; Wilkinson, 2001;).

### 5.7. Sulfur isotopes

Stable isotopes used for ore deposits usually are sulfur, oxygen, hydrogen and carbon. The study these isotopes on mineral deposits are useful to determine the origin, evolution, sources, temperature and mechanisms of ore deposition (Ohmoto and Goldhaber, 1997).

The interest of stable isotopes to understanding geological processes is because they may undergo fractionation when the phase in which they occur changes state due to equilibrium and kinetic effects. In general, heavier isotopes form more



**Figure 17.** Diagram of homogenization temperature vs salinity, showing four typical trends of distribution of fluid inclusion populations, according to their temperature (A) Boiling, in a volatile-free system; (B) dilution due to mixing with cold groundwater; (C) boiling with effervescence, in a volatile-rich system; (D) cooling or pressurization (after Hedenquist and Henley, 1985; Wilkinson, 2001; Canet et al., 2011).

stable bonds. Sulfur isotopes are very useful to determine the origin and evolution of fluids that formed ore deposits that contain sulfide minerals. Isotope ratios are usually expressed as the ratio of a minor isotope of an element to a major isotope of the element. Sulfur fractionation is with the relative variation of the sulphur isotopes  $^{32}\text{S}$  and  $^{34}\text{S}$ , usually expressed as a  $\delta$  notation, as parts per mil relative to a standard. The standard used is the Canyon Diablo Troilite meteorite, which has a  $\delta^{34}\text{S}$  value close to the mantle rocks. The expression used is (Ohmoto and Rye, 1979):

$$\delta^{34}\text{S} (\text{‰}) = \frac{^{34}\text{S}}{^{32}\text{S}}(\text{sample}) - \frac{\frac{^{34}\text{S}}{^{32}\text{S}}(\text{standard})}{\frac{^{34}\text{S}}{^{32}\text{S}}(\text{standard}) \times 1000} \dots(\text{eq. 4})$$

The main S-bearing compounds include sulfides, sulfates, H<sub>2</sub>S and SO<sub>2</sub>, and these are found in both magmatic and hydrothermal ore deposits, with the S originating from two main isotopically distinct reservoirs (1) mantle, with δ<sup>34</sup>S values of about 0‰; (2) seawater, where it occurs as dissolved sulfate with δ<sup>34</sup>S of about +20. The composition δ<sup>34</sup>S changed along the Earth history from about +9 to +39 (Claypool, 1980).

The seawater sulfate has to be reduced to form sulfide and precipitate as sulfide minerals. The mechanisms that control the fractionation of S isotopes (Ohmoto and Rye, 1979) are (1) bacterial reduction of sulfate to sulfide; (2) bacterial oxidation of sulfide to sulfate; (3) non-bacterial reduction of sulfate to sulfide (thermochemical sulfate reduction); and (4) evaporite deposition.

In general, biological activities produce the largest fractionations, as exemplified by up to 60‰ fractionation between seawater sulfate and biogenic sulfides since the beginning of the Phanerozoic, resulting in <sup>34</sup>S enrichment in seawater sulfate (Hoefs and Hoefs, 1997). In the case that an inorganic thermal reduction process produce reduction, the fractionation is considerably lower, due to meta-stability phenomena. For sulfides and sulfates of hydrothermal systems, the δ<sup>34</sup>S values are controlled by temperature, the isotopic composition of S in the fluids and the ratio of oxidized (SO<sub>4</sub><sup>2-</sup>) to reduced S (H<sub>2</sub>S) in the fluids, which are in turn dependent on pH and *f*O<sub>2</sub> of the ore fluids (Ohmoto and Lasaga, 1982; Ohmoto, 1986).

Sulfur isotope data were obtained from 99 mineral separates from the mineralization (number of analyses: pyrite, 38; sphalerite, 26; galena, 19; arsenopyrite, 10; chalcocite 2; sulfosalts, 3; chalcopyrite, 1). Two samples were



---

---

analyzed from pyrite grains enclosed in the host shales. Nearly pure sulfides were separated using a microdrill under a binocular microscope. Samples were analyzed by mass spectrometry using a Delta C Finnigan MAT continuous flow isotope-ratio mass spectrometer interfaced to a TC-EA+ elemental analyzer, at the CCiT-UB. The results are given as  $\delta^{34}\text{S}\text{‰}$  values, i.e. per mil deviations relative to the CDT standard. The analytical precision is within  $\pm 0.1\text{‰}$  at  $1\sigma$ .

# 6. RESULTS

## 6.1. Petrography

The study of the mineral phases has been carried out with the purpose of identifying the essential minerals and accessories, as well as their relative abundances and their textures, both host rocks and ore mineralization were studied of the SFD. The petrographic study, complemented by the geochemistry and SEM analysis, as well as by the analysis of EPMA and X-ray Diffraction has allowed to establish the paragenetic sequence and to determine with precision the suite of rocks in the district.

The petrographic description of this study is presented in Appendix 3. Macroscopically, there are two main types of host-rock in the SFD: Paleozoic meta-sedimentary suite and Miocene igneous suite. The igneous rocks were classified as granitic porphyry, aplite dyke, dacite, rhyolite and ignimbrite. Meanwhile, metasedimentary rocks

were classified as shale, meta-greywacke, meta-sandstone and quartzite.

Volcanic rocks are members of the Morococala formation, which is characterized by acid magmatism. Extrusive rocks were only classified in macroscopic samples since these are not relative to ore mineralization. Domes in Japo zone show aphanitic texture; quartz, plagioclase and k-feldspar can be differentiated. Plagioclase is more abundant than k-feldspar; this was classified as a dacite. Lava fronts are widely extent in Morocola and Santa Fe towns, in lava flows, the ratio of k-feldspar is greater than plagioclase, analyzed samples were classified as a rhyolite. Samples from plateaus are up to 70% of quartz composition and show typical ignimbrite texture with fiammes.

About the ore mineralization, macroscopically, can be recognized three different styles of mineralization:

i) veins of sulfide of Zn-Pb-Cu-As  $\pm$  Sn; ii) massive or semi-massive sulfides of Zn-Pb-Cu-As  $\pm$  Sn and iii) dissemination in intrusive bodies.

In general, the contacts between veins and the host-rocks are abrupt; the textures show evidence of replacement in phenocrystals and a complex mineralization in multiple stages. Additionally, breccias were also recognized, not only in magmatic rocks, but also in the sedimentary sequence.

### San Pablo stock

Several authors have described before the San Pablo stock, observations of the present work some precisions were made about it. The petrographic study was difficult to carry on because all samples shown different grades of alteration, which obstruct mineral recognition. Petrographic observations also point out to San Pablo stock as the main precursor of the ore mineralization in the Santa Fe mining District.

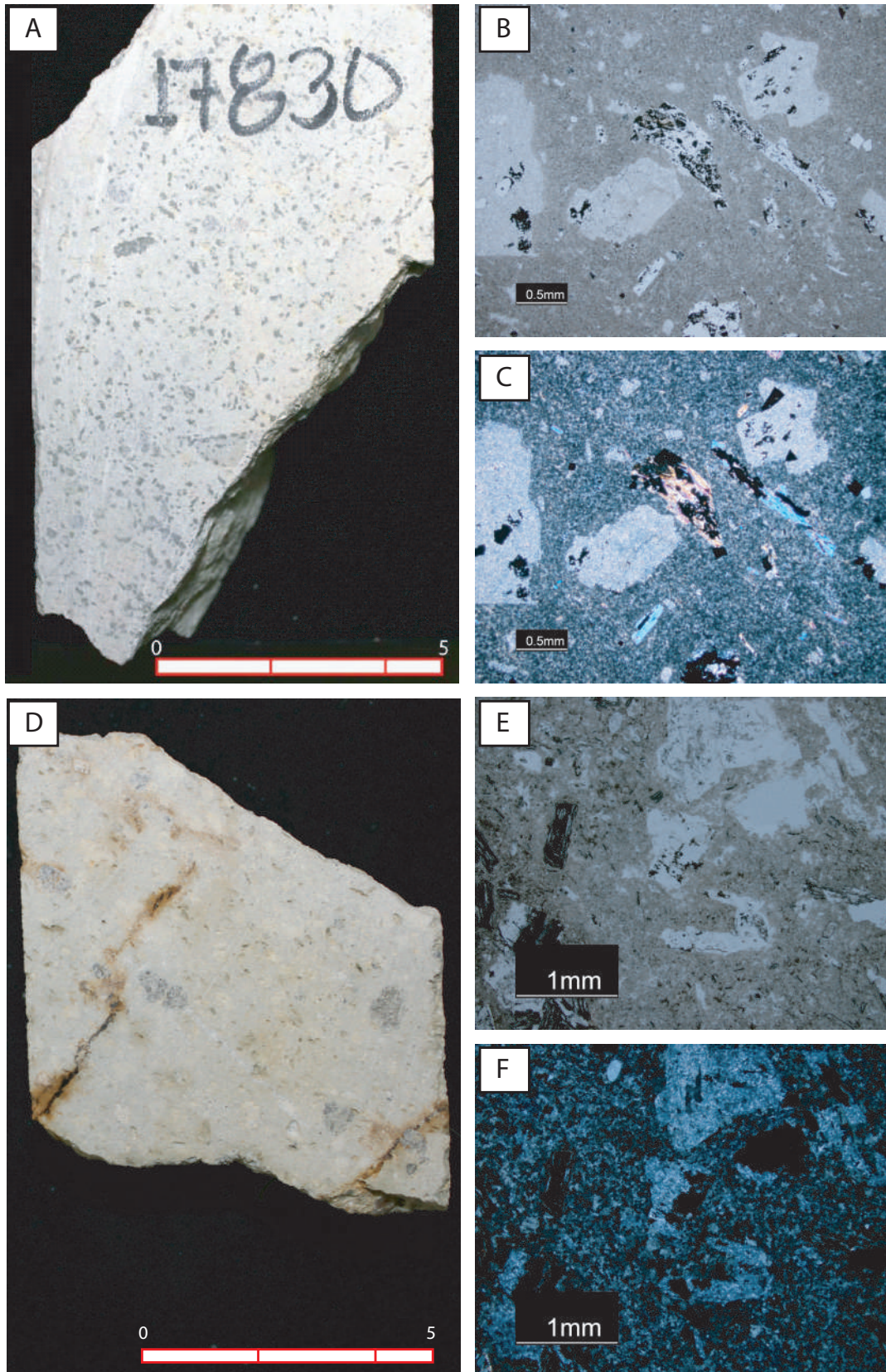
The San Pablo stock is a granitic porphyry composed by anhedral to

euhedral crystals of quartz, 200  $\mu$ m to 5mm; plagioclase, 500  $\mu$ m to 4mm; k-feldspar 300  $\mu$ m to 5 mm; and micas,  $\sim$ 50  $\mu$ m. Matrix is cryptocrystalline and it was found considerably altered to sericite (Fig. 18a).

The phenocrystals are also pervasively sericitized. Mica crystals have been replaced by illite and chlorite (Fig. 18b and c). Dark tourmaline with elongated forms or acicular crystals were found as accessory mineral. Tourmaline is more abundant in veins and altered zones (greisen). Monazite is also found as an accessory mineral, crystals are very fine (>10  $\mu$ m). Sulfide and cassiterite crystals were found replacing phenocrystals.

### Aplite dike

As in the San Pablo stock, samples from dikes are also altered. However, was possible to recognize the main petrographic characteristics in most of the samples. Dikes from the SFD in general present porphyritic texture in a cryptocrystalline matrix of quartz-feldespatic composition (Fig. 18d).



**Figure 18.** Petrography of intrusive rocks. A) drill-core sample of the San Pablo stock; B) Photomicrograph (transmitted light) of altered phenocrysts in an aphanitic matrix; C) Photomicrograph (plane polarized light) altered k-feldspars and micas; D) drill-core sample of porphyry dike; E) Photomicrograph (transmitted light) shown porphyry texture; F) Photomicrograph (plane polarized light) altered k-feldspars and micas in cryptocrystalline matrix.

Phenocrystals are mainly of quartz, plagioclase and k-feldspar of ~1 mm size. Scarcely apatite crystals up to 200  $\mu\text{m}$  are enclosed phenocrystals (Figs. 18e and f).

Some pyrite crystals replacing phenocrystals were found. Dikes show sericite alteration and oxides infilling fractures. Tourmaline crystals are found as accessory. Secondary quartz is also replaced phenocrystals and as micro-veins.

### Shale

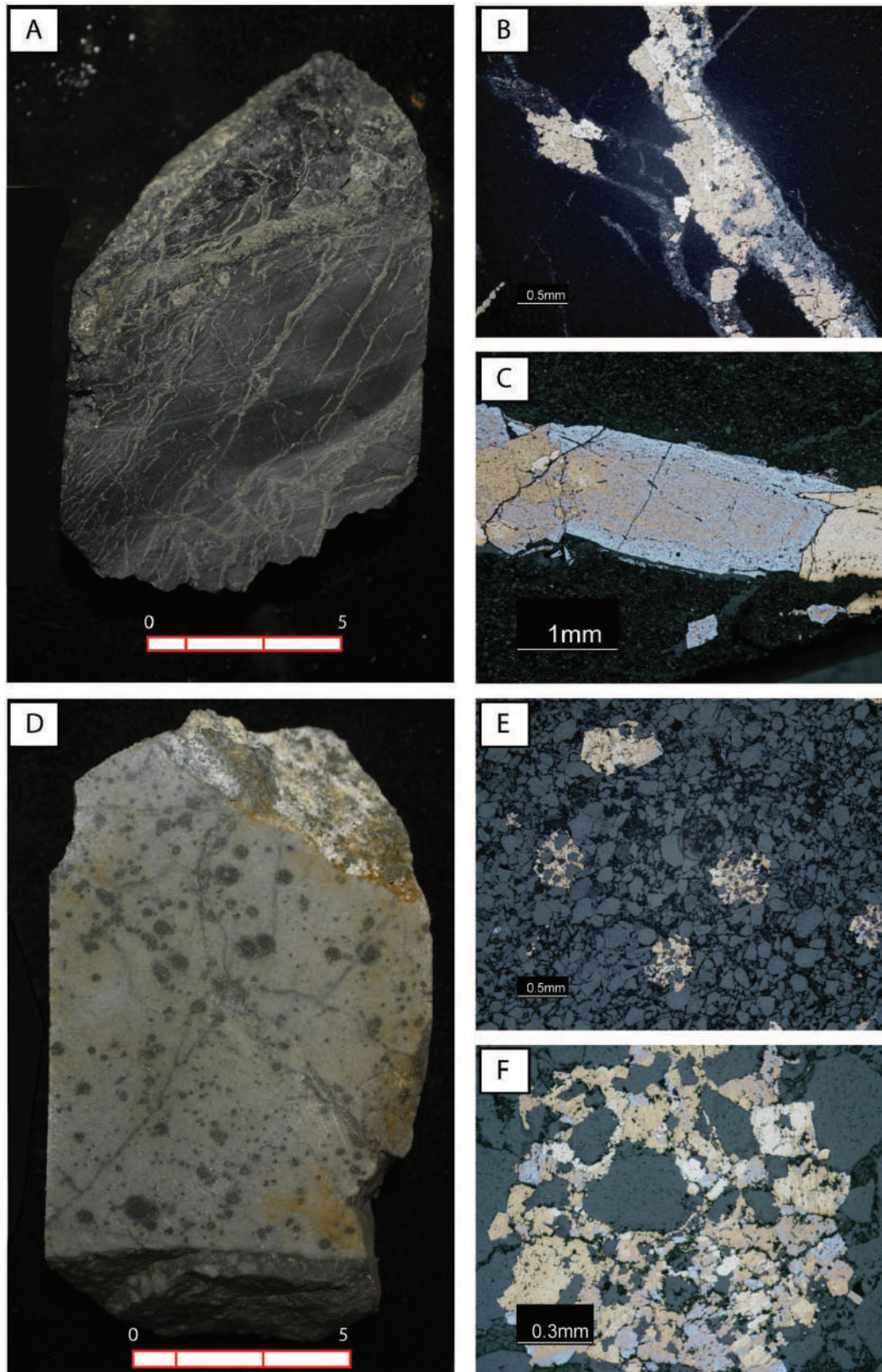
Shale rocks in the SFD are grey to black in color, grain fine-sized, these look texturally homogeneous, derived from an original shale-type sedimentary rock composed mainly by clay (Fig. 19a). In the analyzed rocks can be distinguished lamination as changes in the sedimentation regimen in different layers (change in the size of grain of clay to fine-sand). Infilling porosity and micro-fractures, acicular agglomerates of actinolite-tremolite crystals were

found (Figs. 19b and c) Two pyrite types were also observed, i) pyrite in different layer related to diagenesis process and ii) pyrite magmatic associated with ore mineralization in porosity zones and micro-veins.

### Meta-Greywacke

Meta-greywacke rocks are the most abundant in the SFD. These are of dark to gray color, with angular grains of quartz, k-feldspar, micas and lithic fragments in a compact, clay-fine matrix (35%).

Texturally, it is immature with moderate classification. Grains are sand-sized. Matrix is constituted by clay minerals of tabular and fibrous morphology. Quartz is willing in aggregates and isolate grains (Fig. 19d). Some crystals quartz are rounded, others show gulf morphology and overgrowth. Most of the k-feldspar are orthoclase; crystals show anhedral morphology with corroded limits. These present simple macles and alteration to sericite. Matrix is cryptocrystalline; in gray tones, some zones show crystal



**Figure 19.** Petrography of meta-sedimentary rocks. A) drillcore sample of shale with ore mineralization in micro-fractures; B) Photomicrograph (reflected light) of sulfides in micro-fracture plane: pyrite, chalcopyrite, arsenopyrite and oxides; C) Photomicrograph (reflected light) of pyrite and arsenopyrite with anomalous anisotropy; D) drill-core sample of greywacke; E) Photomicrograph (reflected light) shown sulfides infilling porosity between quartz grains; F) Photomicrograph (reflected light) of agglomerate of pyrite, chalcopyrite, chalcosite and arsenopyrite.

agglomeration. Most of sulfides crystals are pyrite and galena. These were found filling mainly in porosity forming aggregates and infilling veins (Figs. 19e and f).

### Meta-sandstone

Most sandstone rocks in the SFD, are yellow to gray color, composed mainly of fine sand-sized grains (<300  $\mu\text{m}$ ) (Fig. 20a). Grains are composed of quartz, k-feldspar and rock fragments. In general, these were found hardly fractured, show alteration in matrix. Some lytic fragments of quartzite (up to 5cm) were found. Can be distinguished dissemination of sulfides in porosity up to 5% of pyrite, chalcopyrite and sphalerite crystals (<50  $\mu\text{m}$ ) (Figs. 20b and c).

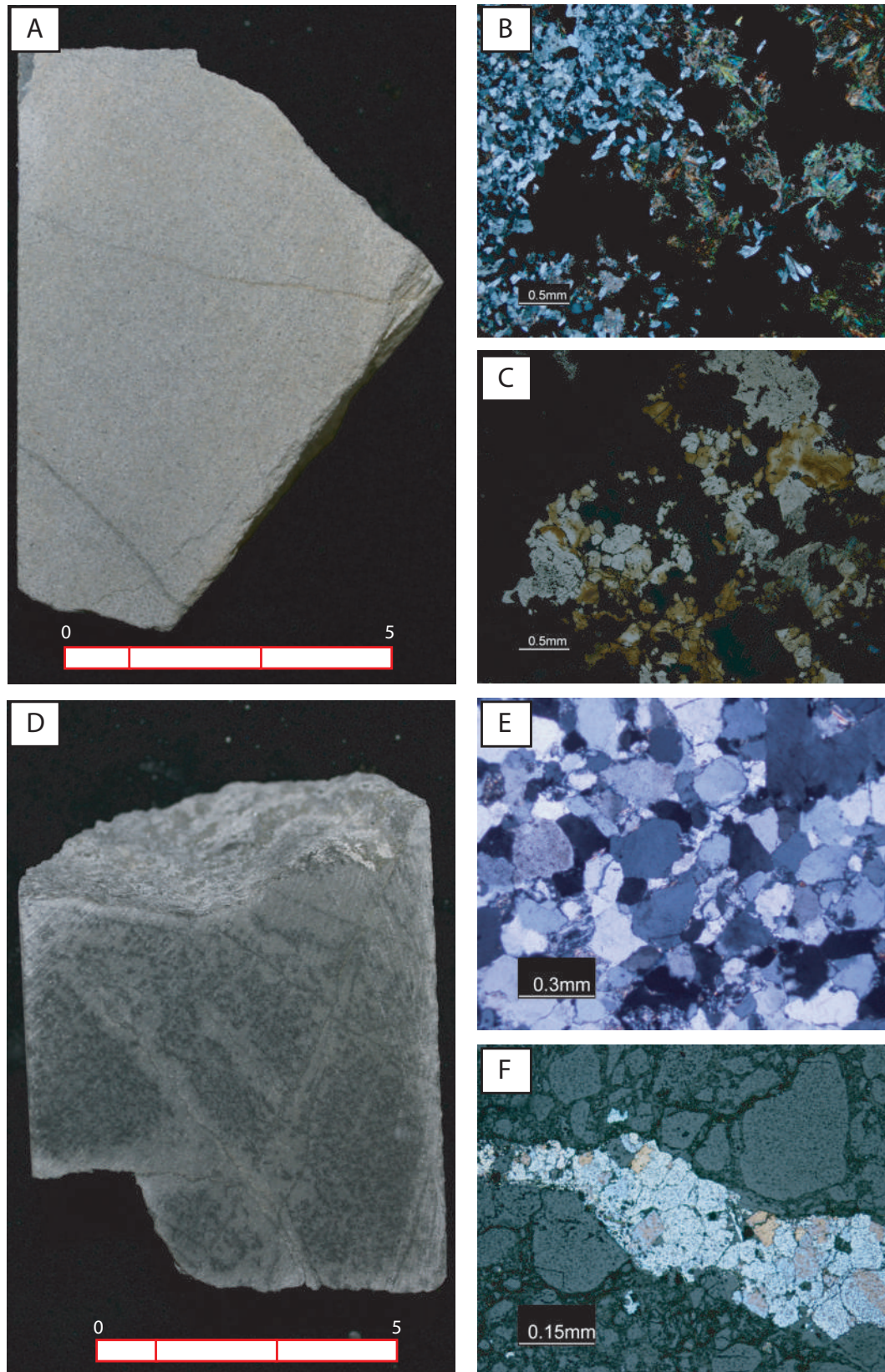
### Quartzite

Quartz-bearing sandstone was converted to quartzite. Quartzite is composed of mostly well-rounded

quartz grains cemented by silica with minor amounts of iron oxide, rutile and other acicular crystals (Fig. 20d). Fragments of organic material as fossils are present. The original texture and sedimentary structures are preserved. This shows poorly classification since grain size is very diverse. More than 50% of quartz grains show overgrowth with defined limits (Fig. 20e). In addition, micro-veins can be distinguished (Fig. 20f).

## 6.2 Geochemistry of metal and metalloid elements

The Morococala Fm represents the Miocene igneous activity in the Santa Fe District, with two main stages. The first one formed the San Pablo stock and a swarm of dikes related to it. The age of this plutonic suite is ~23.3 Ma (Grant et al., 1979; Sugaki et al., 2003). Extrusive rocks as dacite (5.8 to 6.4 Ma; Lavenu et al., 1985) and rhyolite (7 Ma; Evernden et al., 1977) represent the earliest magmatic event.



**Figure 20.** Petrography of meta-sedimentary rocks. A) drill-core sample of sandstone with fine sand grain; B) Photomicrograph (plane polarized light) shown equigranular texture and alteration to clay-minerals; C) Photomicrograph (reflected light) of pyrite with some oxidation; D) drill-core sample of quartzite; E) Photomicrograph (plane polarized light) shown equigranular texture of quartz grains; F) Photomicrograph (reflected light) of micro-vein with sulfides mineralization.



Metal and metalloid contents of the San Pablo granitic stock and related dikes, as well as of the extrusive rocks and ore mineralization of the SFD are provided in Table 2 and plotted in binary diagrams shown in Fig. 21. The San Pablo stock is anomalously enriched in the Sn, Ga, As, Cu, Ag, Zn, W and Pb content, between 50 and 100 ppm, with respect to with the average granitic rock (Turekian and Wedepohl, 1961; Hall, 1971).

The highest value of In (2.5 ppm) in the analyzed igneous rocks was obtained in samples from the San Pablo stock. The same sample shows Sn content

of 404 ppm. Meanwhile, hypabyssal rocks also show high content of Sn, in one of the analyzed dikes the content in this element up to 532 ppm. In consequence, in the ore concentrate, indium attains up to 200 ppm and tin exceeds 1000 ppm.

Moreover, the  $1000 \times \text{In}/\text{Zn}$  ratio ranges from 25 (dike) up to 4000 (concentrate). The  $1000 \times \text{In}/\text{Zn}$  ratio in the San Pablo stock is of 417. The In/Zn ratio can be used as an estimate of the ability to form proper In minerals; when Zn is abundant in an ore-forming system the ratios are likely low, thus In will precipitate in sulfides lattice. With less

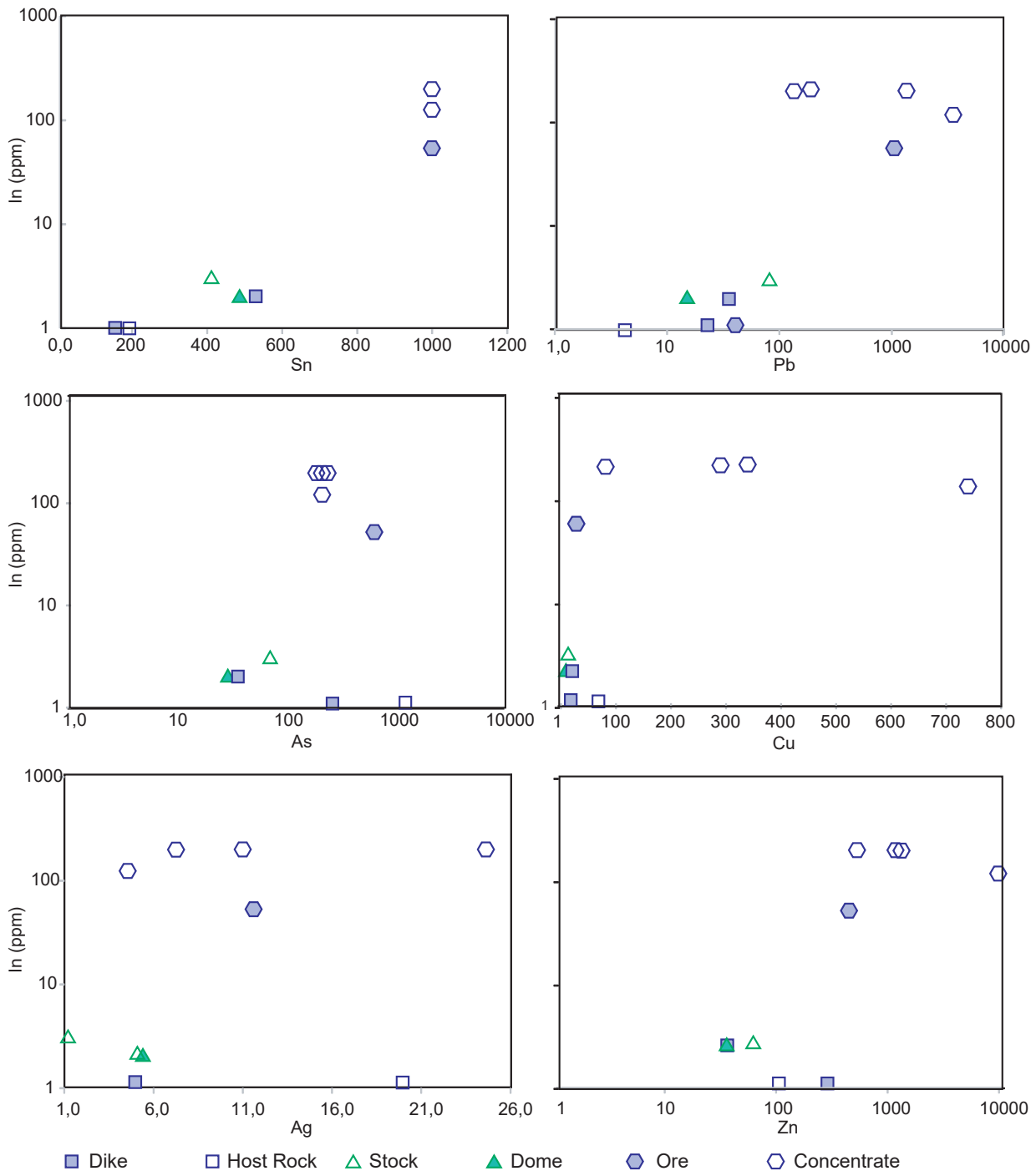
**Table 2.** Geochemical summary of intrusive rocks and ore minerals in the Santa Fe District.

Element	Ga	Cu	Zn	As	Ag	In	Sn	Sb	W	Pb	Bi	1000
Unit	ppm	ppm	wt %	ppm	ppm	ppm	ppm	ppm	ppm	ppm	ppm	In/Zn
Average granitic rocks (Hall, 1971)	1.0	10.0	0.0039	1.5	--	--	3.0	--	2.2	19.0	--	--
San Pablo Stock	47,0	< 10	0,01	67,0	0,7	2,5	404,0	29,1	21,0	82,0	2,4	417
Dome	5,0	< 10	0,00	26,0	5,3	1,6	485,0	8,0	12,0	15,0	0,9	533
Dike	7,0	20,0	0,00	34,0	5,0	2,2	532,0	4,8	16,0	35,0	9,1	733
Dike	9,0	20,0	0,03	248,0	5,0	0,7	153,0	3,0	11,0	23,0	10,5	26
Host Rock	15,0	70,0	0,01	1160,0	20,0	1,0	186,0	4,4	14,0	41,0	16,6	100
Morococala ore	35,0	30,0	0,04	593,0	11,6	54,5	> 1000	89,9	39,0	1060,0	101,0	1.298
Morococala concentrate	30,0	740,0	1,00	202,0	4,5	125,0	> 1000	41,8	31,0	3490,0	8,1	125
Morococala concentrate 2	33,0	80,0	0,11	176,0	24,6	200,0	> 1000	141,0	407,0	1330,0	69,0	1.852
Japo concentrate	21,0	340,0	0,12	189,0	7,3	200,0	> 1000	50,6	229,0	131,0	104,0	1.739
Japo concentrate 2	3,0	290,0	0,05	221,0	11,0	200,0	> 1000	40,6	154,0	174,0	62,0	4.000

Zn in the system, the ratios will become higher, leading to oversaturation of indium and providing a high potential for other minerals to be formed (Cook et al., 2011a, Valkama et al., 2016).

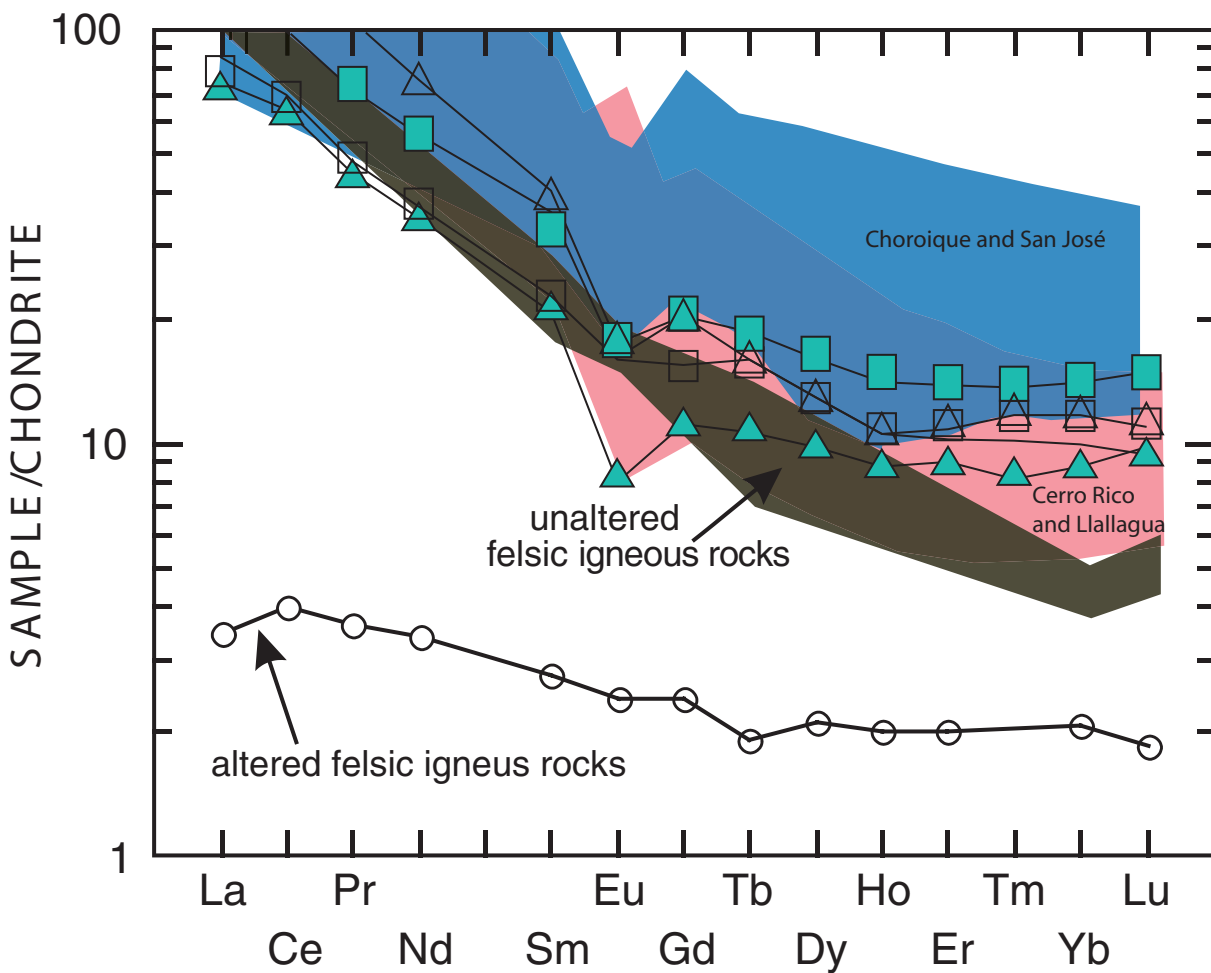
### 6.3. REE Geochemistry

REE are contained in more than 200 minerals including various phosphates as monazite (light REE) or xenotime



**Figure 21.** Binary diagrams of Sn, Pb, As, Cu, Ag and Zn vs In of igneous rocks and ore in the Santa Fe mining District.

(heavy REE). Common rock-forming fluids in unaltered and altered rocks minerals can be REE-bearing by is a useful monitor of changing fluid replacement of other elements (e.g. conditions from dominantly magmatic brabantite, zircon, and apatite). For the to meteoric. Hydrothermal solutions purpose of graphical presentation, REE have low REE concentrations. abundances are usually normalized Hydrothermal activity is not expected to chondritic meteorite abundances to change the REE content of the (Sun and McDonough, 1989). The REE solid, unless the water-rock ratios are concentration of the hydrothermal very high. The REE concentrations of



**Figure 22.** Chondrite-normalized rare earth elements (REE) of the SFD plots and distribution patterns of samples from Llallagua, Chorolque, San José, Oruro and Cerro Rico (Dietrich, 2000). Comparing with unaltered and altered fields after Van Kranendonk and Pirajno, 2004). Llallagua and Cerro Rico patterns correspond to pink color, Chorolque and San José with blue and unaltered felsic camp is shown in black tone.

hydrothermal solutions increases as the pH decreases, independent of rock type and temperature. (Michard, 1989).

The Fig. 22 shows the REE content on the igneous suite rocks of the Morococala Fm in comparison with fields of altered and unaltered rocks (Van Kranendonk and Pirajno, 2004). Also are showing the REE distribution patterns of the Llallagua, Chorolque, and Oruro porphyries bodies, in these are relatively inconspicuous and show moderate La/Lu fractionation and weak negative Eu anomalies. The patterns of Dietrich et al. (2000) work displays a REE distribution with lower heavy REE contents. These patterns are very similar to samples analyzed in the present study. Both patterns match with the unaltered felsic igneous field.

#### 6.4. Mineralogical study and mineral chemistry

Mineral classification specially in sulfides and sulfosalts groups is always controversial. To the classification

of mineral phases in the SFD, the International Mineralogical Association (IMA) considerations were attended, also according to Strunz classification (2004). According to the above, the present work presents four general groups: oxides, simple sulfides, sulfosalts and phosphates. Due to importance of stannite group in the Santa Fe mining district, it is also studied as a particular mineralogical group through to be member of the sulfosalts group.

It should be noted that, especially to contradistinguish between simplesulfurs and sulfosalts, inasmuch as, several mineral species combine the structural properties of sulfides (chalcogenides) with those of the other chemical groups, and can be considered as borderline cases. Thus, the IMA systematic proposed to sulfosalts and sulfurs (Moëlo et al., 2008) were rigorously attended.

Simple sulfurs were named to compounds of one or more metallic elements combined with the non-

metallic element sulfur. The sulfur acts as a semi-metal when it combines to form a sulfide mineral.

Otherwise, in sulfosalts (or thiosalt), S is considered to play the role of oxygen to similarly form complex anions. The term sulfosalt has been preserved as a practical, working category in the field of ore mineralogy. According to Moëlo et al (2008), the main reason is that sulfosalt minerals form a well-defined group encountered in specific conditions of ore formation.

The sulfosalt group is heterogeneous from a crystal-chemical point of view. According to the chemical definition, most sulfosalts are thio-arsenites, thio-antimonites, thio-bismuthites and their combinations, i.e., sulfosalts in which As, Sb and Bi have the same oxidation state +3. A very limited number of natural sulfosalts correspond to thio-arsenates or thioanti-monates. There are about 15 thio-stannates ( $\text{Sn}^{4+}$ ) recognized by IMA, mainly related to

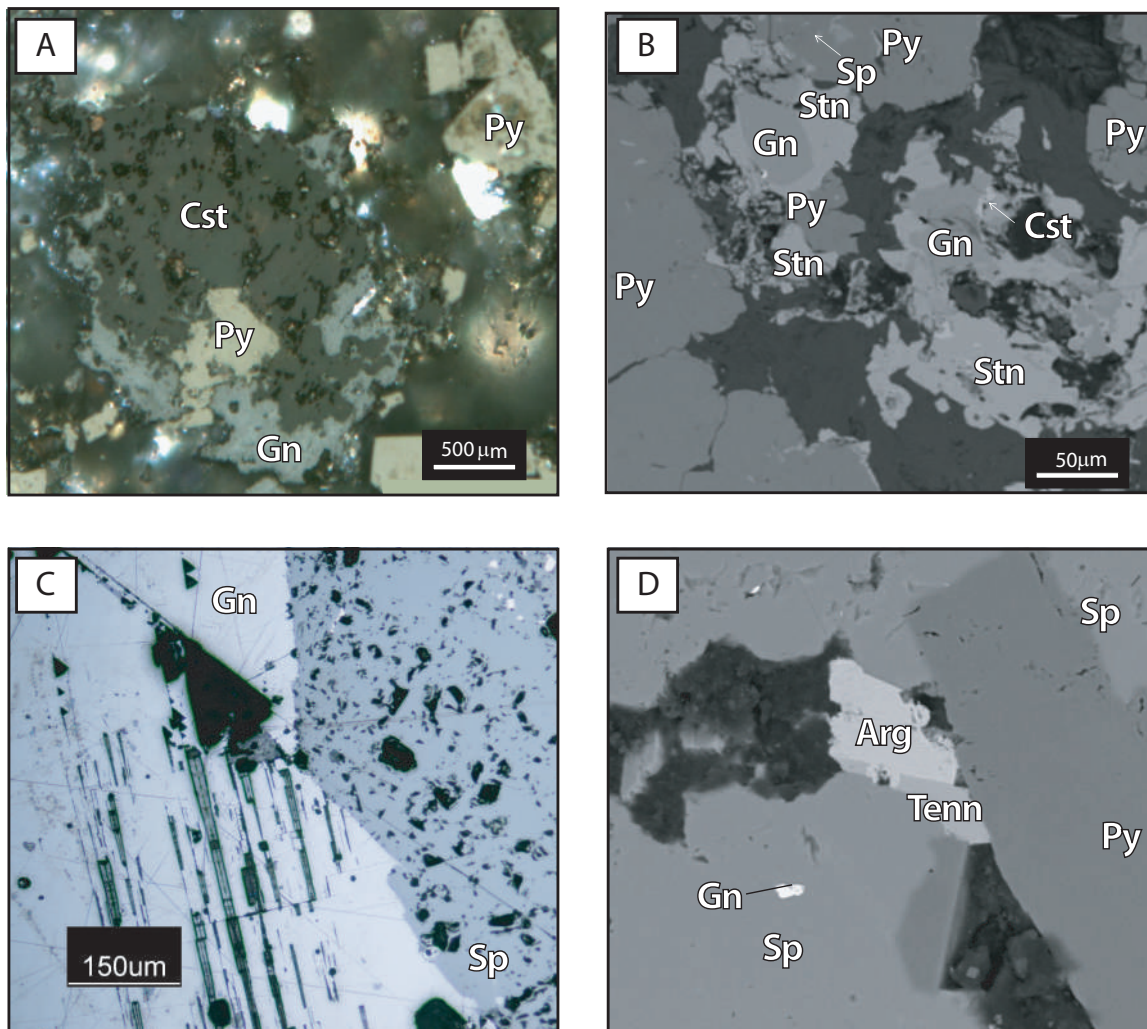
the ZnS archetypes (sphalerite and wurtzite), and a few thio-germanates. Sulvanite could be considered as a thio-vanadate, thio-tungstate and thio-molybdate are exceptional. Minerals corresponding to selenium- and tellurium-salts, with trivalent As, Sb or Bi, or, exceptionally,  $\text{Sb}^{5+}$  are uncommon. The IMA recognizes today more than 220 valid sulfosalts mineral species.

Moreover, according with field and petrographic observations, two stages of ore mineralization can be distinguished in the SFD: (1) Early, Sn-rich mineralization, represented by cassiterite-quartz veins and disseminations (Figs. 23a and b), and (2) late (more predominant), Zn-Pb-Ag mineralization, represented by veinlets with sphalerite, galena and stannite group phases (Figs. 23c and d). The former predominates in the Japo deposit, while in Santa Fe and Morococala different generations of Sn and Zn-Pb-Ag mineralization are found.

## Oxide Minerals

In the earliest stage of mineralization cassiterite occurs in drussy morphology in association with vuggy quartz, pyrite, arsenopyrite, chalcopyrite, chalcocite and, occasionally, with galena and stannite. However, the most common assemblage is quartz-pyrite-cassiterite.

In general, cassiterite crystals are irregular in shape. Crystals from Santa Fe and Morococala are finer (~10 µm) than those from Japo, where crystals of a few millimeters were found (Fig. 23a and b). Cassiterite from Morococala and Santa Fe is commonly in veinlets an intimate assemblage with sphalerite and pyrite.



**Figure 23.** Ore mineralization. A) Microphotography of the main mineral assemblage in the SFD under petrographic microscopy; B) Backscattered SEM images of the ore assemblage in the SFD; C) Microphotography of sphalerite and galena under petrographic microscopy; D) Backscattered electron SEM images of sulfosalts associated with galena, sphalerite and pyrite. Arg: argentite; Cst: cassiterite; Gn: galena; Py: pyrite; Sp: sphalerite; Stn: stannite; Tenn: tennantite.

In the Japo samples, cassiterite appears lesser extent than in the others deposits, in contrast, stannite is more abundant in Japo samples. Exceptionally, some cassiterite crystals from the Santa Fe deposit also assemble to sulfosalt such as franckeite and jamesonite. Apatite and tourmaline crystals in association with cassiterite also were found.

More than 60 EPMA analyses were carried out on cassiterite. The Table 3

shown the most representative results obtained. In general, cassiterite has high iron contents, with up to 3.23 wt.%. The In content is between 0.25 and 0.09 and 0.12 mean wt.%. Besides, Ti, Nb, Ta and W contents are negligible.

### Simple sulfide minerals

Galena, sphalerite and pyrite are the most common sulfides. Galena occurs as euhedral crystals up to 1 cm,

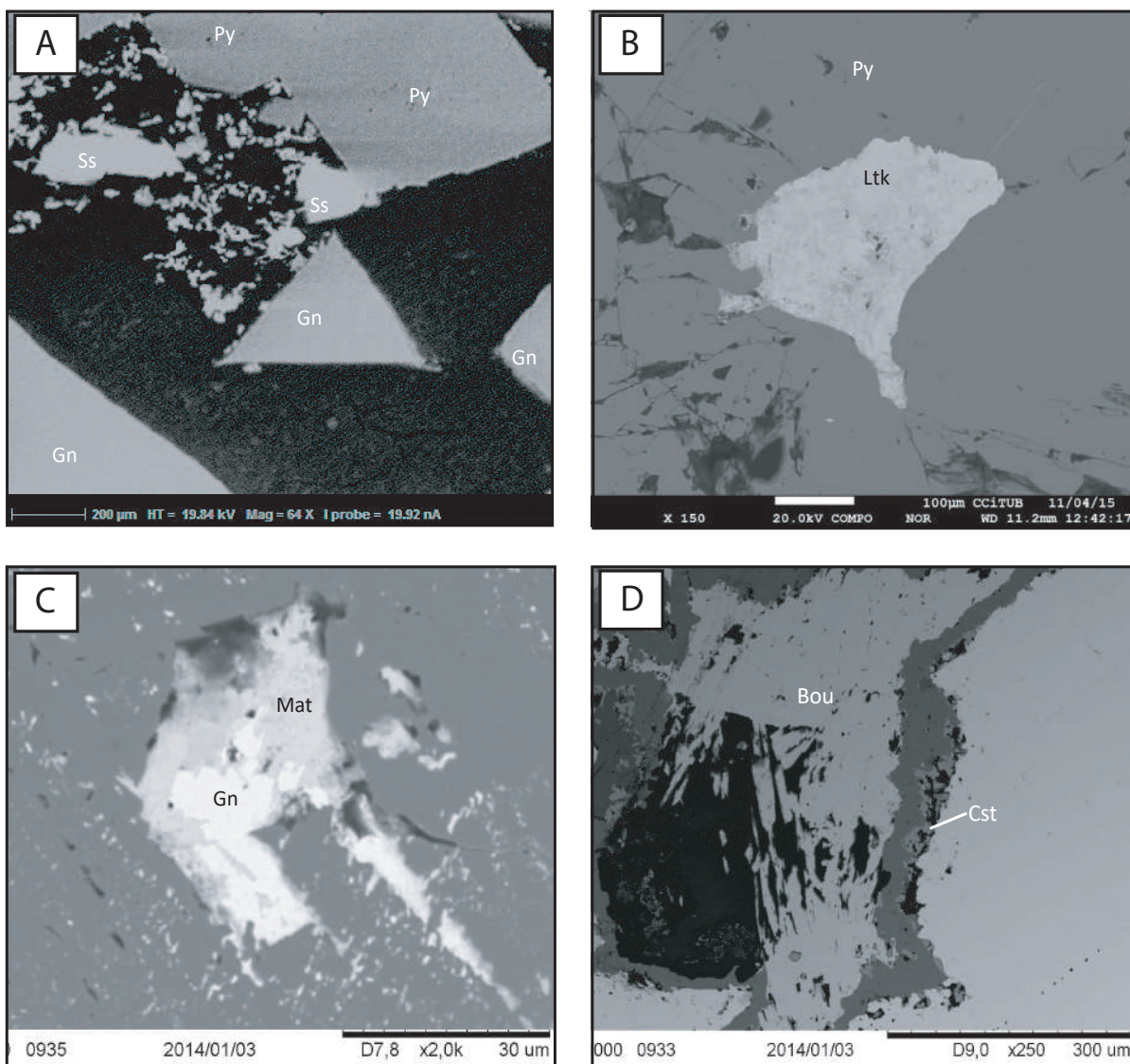
**Table 3.** Chemical composition (wt.%) and atomic proportions (apfu) of representative cassiterite from the Santa Fe District (EMPA).

	Cassiterite											
	1	2	3	4	5	6	7	8	9	10	11	12
S	0,09	0,46	0,50	0,42	0,26	0,72	0,04	0,36	0,07	0,05	0,08	0,90
Sn <sup>4+</sup>	74,21	73,02	70,34	77,41	75,11	73,62	75,96	74,87	77,50	76,14	75,16	75,40
Ti	0,03	0,03	0,00	0,00	0,01	0,00	0,00	0,00	0,01	0,00	0,00	0,00
Fe	0,38	0,91	3,23	0,01	0,26	0,15	0,14	0,24	0,08	0,18	0,25	0,40
Cu	0,00	0,00	0,02	0,02	0,06	0,01	0,00	0,02	0,00	0,01	0,00	0,09
Zn	2,60	3,35	0,07	0,00	2,56	1,24	1,94	3,52	0,17	0,03	2,56	3,28
As	0,01	0,00	0,00	0,00	0,00	0,00	0,00	0,00	0,00	0,00	0,00	0,00
Se	0,05	0,01	0,00	0,00	0,04	0,08	0,07	0,12	0,04	0,09	0,05	0,01
In	0,11	0,13	0,25	0,12	0,11	0,11	0,12	0,12	0,11	0,09	0,13	0,11
Pb	0,00	0,00	0,51	1,00	1,12	4,17	0,47	0,14	0,33	0,50	0,14	0,02
Total	77,49	77,91	73,74	78,98	79,53	80,09	78,74	79,40	78,31	77,08	78,38	80,21
SnO <sub>2</sub>	94,218	92,707	89,304	98,281	95,360	93,469	96,440	95,056	98,395	96,668	95,424	95,729
Ti	0,057	0,048	0,004	0,000	0,015	0,000	0,000	0,000	0,013	0,000	0,000	0,000
Fe	0,493	1,171	4,155	0,016	0,334	0,187	0,179	0,313	0,107	0,226	0,325	0,517
Cu	0,000	0,002	0,020	0,030	0,075	0,013	0,002	0,024	0,006	0,007	0,000	0,114
Zn	3,236	4,170	0,086	0,000	3,186	1,543	2,415	4,381	0,215	0,035	3,186	4,083
As	0,006	0,000	0,000	0,000	0,000	0,000	0,000	0,000	0,000	0,000	0,000	0,000
Se	0,087	0,008	0,000	0,000	0,074	0,130	0,116	0,206	0,059	0,145	0,083	0,009
In	0,138	0,157	0,302	0,145	0,137	0,129	0,142	0,148	0,128	0,114	0,155	0,137
PbO	0,000	0,000	0,548	1,074	1,206	4,492	0,507	0,153	0,353	0,538	0,156	0,025

commonly associated with sulfosalts and sometimes with cassiterite (Fig. 23b and 24a). Galena composition shows significant variations; EPMA analyses reveal an average silver content of 0.30 wt.% Ag. Often, Ag-rich sulfides as argentite  $Ag_2S$  and matildite  $AgBiS_2$  were

found associated with galena, forming fine-grained, complex intergrowths (Fig. 23c).

Sphalerite is the second ore mineral in abundance in the SFD, and occurs all through the mineralized zones. It develops anhedral grains, up



**Figure 24.** Backscattered electron SEM images of sulfosalts of the SFD. A) Association of sulfosalts with galena and pyrite; B) Laitakarite filling a cavity in a pyrite crystal; C) Matildite associated to galena in a cavity of a sphalerite crystal; D) Acicular crystals of boulangerite. Bou: boulangerite; Cst: cassiterite; Gn: galena; Ltk: laitakarite; Py: pyrite; Ss: sulfosalts; Mat, matildite.



to few cm across, with curvilinear equilibrium grain boundaries, forming mosaic aggregates and intergrowths with galena, pyrrhotite, pyrite and chalcopyrite (Figs. 23b, c, d). Some sphalerite grains show chalcopyrite disease.

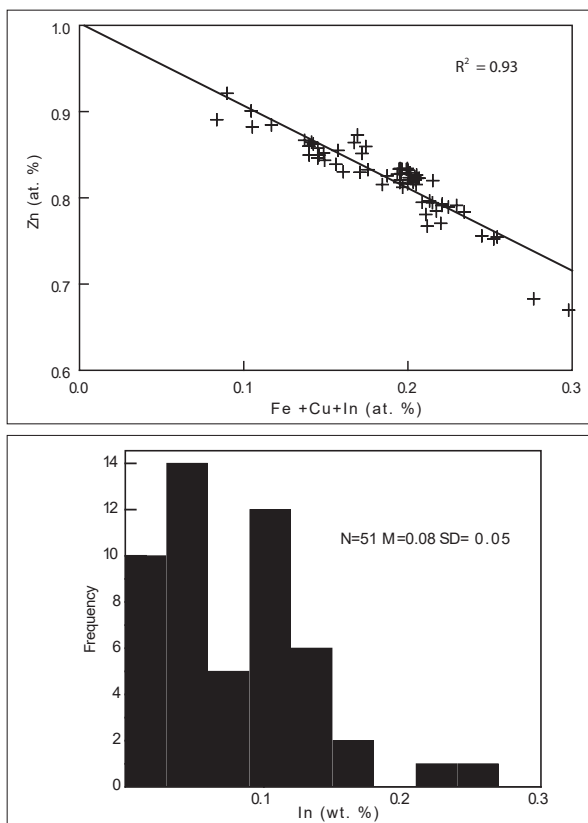
More than 50 EPMA analyzes were carried on in sphalerite crystals, these reveal In contents, up to 0.26 wt.%, however most of them show subordinated contents (Table 4). While for, contents of Cd up to 0.39 and Pb up to 0.29 wt.%. Sphalerite analyses

**Table 4.** Chemical composition (wt.%) and atomic proportions (apfu) of representative sphalerite from the Santa Fe District (EMPA).

	Santa Fe				Morococala							
	Sphalerite											
	1	2	3	4	5	6	7	8	9	10	11	12
S	33,63	32,76	34,62	33,90	34,72	34,49	34,34	34,34	34,55	34,37	35,36	34,49
Fe	9,58	9,27	8,64	5,65	7,71	11,04	10,89	10,82	11,36	11,35	11,93	11,11
Cu	0,16	0,21	0,37	0,21	0,12	0,13	0,00	0,04	0,04	0,02	0,05	0,09
Zn	56,22	57,09	54,31	58,92	56,54	53,86	54,55	54,51	53,69	53,93	51,96	54,10
As	0,00	0,00	0,02	0,00	0,00	0,00	0,00	0,00	0,00	0,00	0,00	0,00
Ag	0,03	0,34	0,00	0,00	0,00	0,01	0,00	0,01	0,00	0,02	0,01	0,00
Cd	0,06	0,00	0,01	0,05	0,00	0,39	0,35	0,33	0,39	0,37	0,36	0,33
Sn	0,00	0,00	0,52	0,39	0,00	0,00	0,00	0,00	0,00	0,00	0,00	0,00
In	0,03	0,00	0,00	0,00	0,17	0,12	0,03	0,05	0,06	0,06	0,05	0,14
Sb	0,12	0,00	0,00	0,00	0,00	0,00	0,00	0,00	0,00	0,00	0,00	0,00
Pb	0,23	0,22	0,29	0,00	0,09	0,18	0,00	0,14	0,17	0,10	0,23	0,18
Total	100,04	100,36	99,16	99,48	99,66	100,24	100,22	100,24	100,36	100,22	99,96	100,45
S	1,05	1,02	1,08	1,06	1,08	1,08	1,07	1,07	1,08	1,07	1,10	1,08
Fe	0,17	0,17	0,15	0,10	0,14	0,20	0,19	0,19	0,20	0,20	0,21	0,20
Cu	0,00	0,00	0,01	0,00	0,00	0,00	0,00	0,00	0,00	0,00	0,00	0,00
Zn	0,86	0,87	0,83	0,90	0,86	0,82	0,83	0,83	0,82	0,82	0,79	0,83
As	0,00	0,00	0,00	0,00	0,00	0,00	0,00	0,00	0,00	0,00	0,00	0,00
Ag	0,00	0,00	0,00	0,00	0,00	0,00	0,00	0,00	0,00	0,00	0,00	0,00
Cd	0,00	0,00	0,00	0,00	0,00	0,00	0,00	0,00	0,00	0,00	0,00	0,00
Sn	0,00	0,00	0,00	0,00	0,00	0,00	0,00	0,00	0,00	0,00	0,00	0,00
In	0,00	0,00	0,00	0,00	0,00	0,00	0,00	0,00	0,00	0,00	0,00	0,00
Sb	0,00	0,00	0,00	0,00	0,00	0,00	0,00	0,00	0,00	0,00	0,00	0,00
Pb	0,00	0,00	0,00	0,00	0,00	0,00	0,00	0,00	0,00	0,00	0,00	0,00

show a negative correlation ( $r^2 = 0.93$ ) between Fe+Cu+In and Zn (Fig. 25).

Other sulfides are pyrite, arsenopyrite, pyrrhotite, stibnite and marcasite. Pyrite is present in all deposits. The grain size varies from several microns up to 5 mm. Pyrite occurs in two types: i) as association with ore minerals and ii) as diagenetic mineral in association in the sedimentary stage.



**Figure 25.** Binary plots of Fe+Cu+In vs. Zn (top), and frequency diagram of indium contents in sphalerite from the SFD. Histogram showing In wt.% in sphalerite from the SFD. Electron microprobe measurements  $n = 51$  (below). In wt% was estimated not considering interference correction of 22 ppm of In per 1% of Sn.

In the ore assemblages, pyrite is mainly associated with quartz and cassiterite and sometimes assembles also galena, sphalerite, arsenopyrite, stannite and sulfosalts. Arsenopyrite occurs as crystals up to a few millimeters, some of them show anomalous anisotropy. Arsenopyrite was found in association with pyrrhotite, covellite and marcasite. Acicular stibnite and boulangerite crystals, up to several millimeters in length, are found mostly filling cavities (Fig. 24d).

### Stannite Group

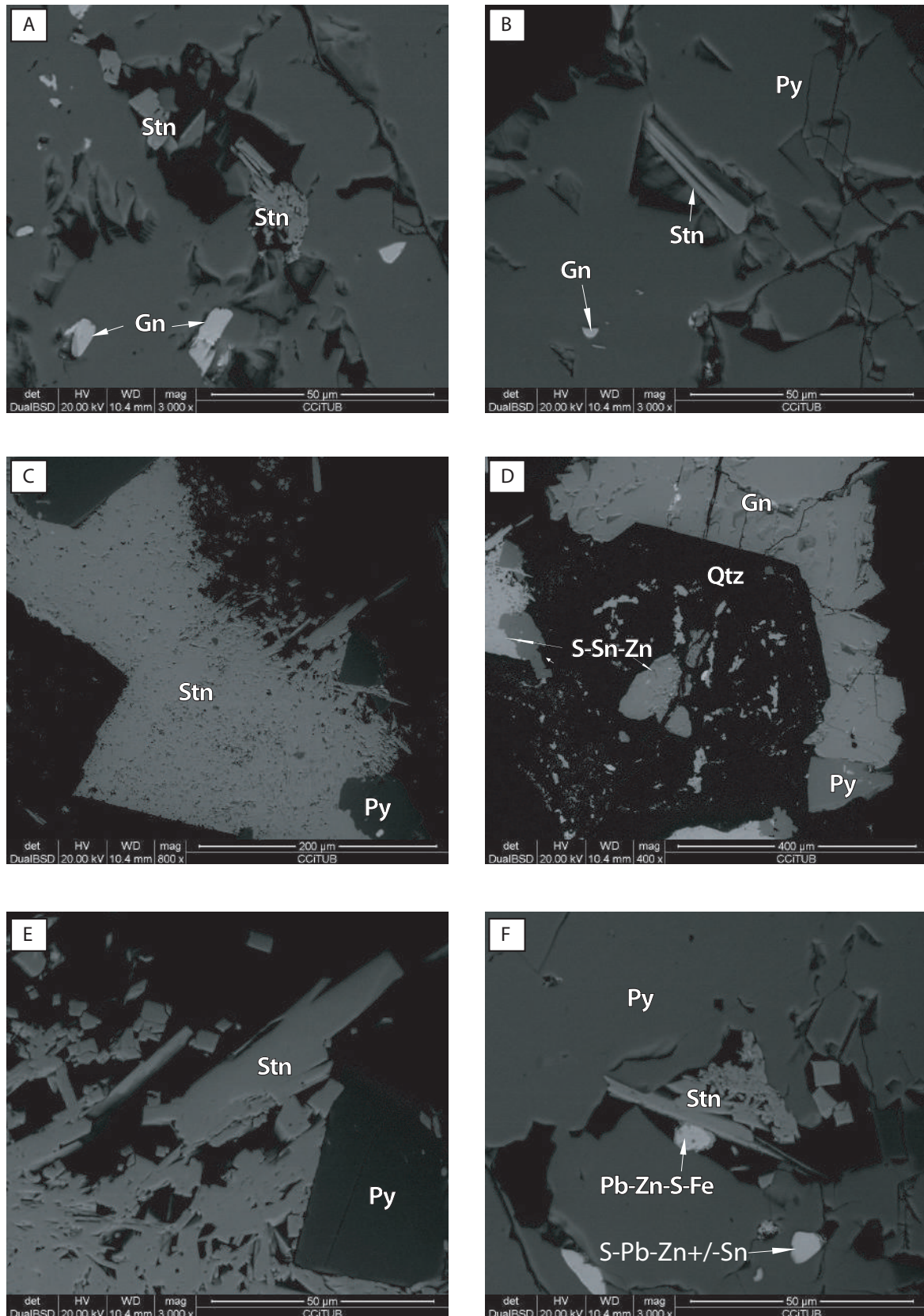
As already mentioned, some sulfosalts fit perfectly in specific sulfide groups (e.g. sulfo-stannates). In the SFD, sulfo-stannates play an important role because additionally to cassiterite, Sn occurs largely as a variety of minerals of the stannite group. The most abundant are stannite  $Cu_2FeSnS_4$ , k esterite  $Cu_2(Zn,Fe)SnS_4$ , sakuraiite as well as other sulfides of the S-Sn-Cu-Zn-Fe system.

Sakuraiite was first named in 1965. Currently, IMA define sakuraiite as  $(\text{Cu,Zn,Fe})_3(\text{In,Sn})\text{S}_4$ , but the formula is also given as  $(\text{Cu,Zn,Fe,In,Sn})\text{S}$ . The formula appears uncertain since the crystal structure has not been determined yet. Kato (1965) described sakuraiite as an indium analogue of k esterite, in which  $\text{Cu} > \text{Zn} > \text{Fe} > \text{Ag}$  and  $\text{In} > \text{Sn}$ . After, Shimizu, et al (1986) proposed that stannite and kesterite compositions are nearly stoichiometric  $(\text{Cu,Fe,Zn})_3(\text{Sn,In})\text{S}_4$ , with a coupled substitution of  $\text{ZnIn}$  and they also mentioned a continuous substitution of  $\text{In}$  for  $\text{Sn}$  is seen in sakuraiite and the associated stannite and kesterite. This means that sakuraiite is compositionally a  $\text{ZnIn}$ -substituted kesterite rather than a mere  $\text{In}$  analogue of kesterite, and that the present  $\text{In}$ -bearing kesterite assumes an intermediate position between  $\text{In}$ -bearing stannite and sakuraiite. On the other hand, Kissin and Owens (1986) proposed a cubic structure for sakuraiite, made a comparison

between them observations and observations made by Kato, and concluded that relationships between the space groups of sphalerite and sakuraiite may not be as simple as they found. Meanwhile, Hall et al. (1978) proposed use the name k esterite in stannite members with  $\text{Zn} > \text{Fe}$ .

In the SFD, stannite occurs filling cavities and within the cleavage in silicates, in association with quartz and pyrite (Fig. 26). Stannite from Japo and Morococala is rich in  $\text{In}$ , up to 2.36 wt.%, whereas that of Santa Fe is depleted in this element (under detection limit) (Table 5). Stannite group crystals are found in considerable amounts, but the grain size usually is  $< 100 \mu\text{m}$ . K esterite is the most scarce; all analyzed crystals were found in Japo.

In this study the sakuraiite formula was calculated as  $(\text{Cu,Zn,Fe})_3(\text{In,Sn})\text{S}_4$ , according to that of Shimizu et al. (1986). Sakuraiite was found in Japo and, more widely distributed, in Morococala. It occurs as very fine



**Figure 26.** Backscattered SEM images of A) Stannite crystals filling cavities; B) Stannite crystals inside exfoliation of a pyrite crystal; C) Prismatic crystals of stannite associated with pyrite; D) Ore minerals associated to euhedral quartz; E) Euhedral crystals of stannite showing tetrahedral prisms, and F) minerals of stannite group with composition variable. Gn, galena; Py, pyrite; Qtz, quartz; Stn, stannite.

**Table 5.** Chemical composition (wt.%) and atomic proportions (apfu) of representative stannite from the Santa Fe District (EMPA).

	Japo					Morococala						
	Stannite											
	1	2	3	4	5	6	7	8	9	10	11	12
S	29,61	29,81	29	28,9	30,05	30,16	29,94	30,3	30,13	30,11	30,73	29,85
Fe	12,8	12,94	12,24	14,37	11,95	11,93	12,22	12,57	12,86	13,14	13,12	13,52
Cu	25,69	26,12	28,56	28,41	21,97	25,98	27,23	27,03	28,38	28,4	27,26	27,97
Zn	7,1	6,82	2,01	2,57	17,03	5,53	3,3	3,13	1,55	1,47	2,44	1,54
As	0	0	0	0,01	0	0,05	0,02	0	0	0	0	0
Se	0,03	0	0,03	0,05	0,04	0	0,07	0	0,01	0,07	0,1	0
Ag	0,18	0	0,08	0	0,08	0,68	0,34	0,61	0,33	0,38	0,47	0,44
Cd	0	0	0	0	0,02	0,09	0	0,01	0	0	0	0
In	0,2	0,18	0,2	0,11	0,14	0,34	0,31	0,36	0,45	0,41	0	0,01
Sn	23,58	23,2	27,36	24,76	18,3	25,1	26,37	25,9	26,71	26,55	26,01	26,3
Nb	0,02	0	0,04	0	0,01	0	0	0,17	0	0	0	0,12
Pb	0,08	0,16	0	0,05	0,1	0,16	0,1	0,01	0,18	0,07	0,06	0,08
Bi	0,03	0	0,64	0	0,06	0	0,07	0,08	0	0,02	0,15	0
Total	99,65	99,26	100,24	99,44	99,76	100,16	100,14	100,3	100,75	100,77	100,5	99,99
S	3,998	4	3,998	3,997	3,998	4	4	4	4	4	4	4
Fe	0,992	0,997	0,969	1,141	0,913	0,909	0,937	0,953	0,98	1,002	0,981	1,04
Cu	1,751	1,769	1,987	1,983	1,475	1,739	1,836	1,801	1,901	1,904	1,791	1,891
Zn	0,47	0,449	0,136	0,174	1,111	0,36	0,216	0,203	0,101	0,096	0,156	0,101
As	0	0	0	0,001	0	0,003	0,001	0	0	0	0	0
Ag	0,007	0	0,003	0	0,003	0,027	0,013	0,024	0,013	0,015	0,018	0,017
Cd	0	0	0	0	0	0,003	0	0	0	0	0	0
In	0,008	0,007	0,008	0,004	0,005	0,013	0,012	0,013	0,017	0,015	0	0
Sn	0,86	0,841	1,019	0,925	0,658	0,899	0,952	0,924	0,958	0,953	0,915	0,952

Structural formulas were estimated not considering interference correction of In per Sn.

grains with composition corresponding as an intermediate member in stannite  $\text{Cu}_{1,9}(\text{Fe Zn})_{1,0}\text{Sn}_{1,0}\text{S}_{4,0}$ —kärsterite  $\text{Cu}_{1,5}(\text{Zn Fe})_{2,0}\text{Sn}_{0,7}\text{S}_{4,0}$  solid solution (Table 6).

The highest In value, 2.03 wt.%, was found in sakuraiite from Morococala. In the Santa Fe mine, an Ag-rich (up to 39.47 wt.%) phase of the hocartite—pirquitasite series ( $\text{Ag}_2\text{FeSnS}_4$ — $\text{Ag}_2\text{ZnSnS}_4$ ) occurs. It

forms crystals of ~200  $\mu\text{m}$ , found filling cavities associated with galena (Table 6). A few crystals assignable to petrukite  $(\text{Cu,Fe,Zn})_2(\text{Sn,In})\text{S}_4$  and stannoidite  $\text{Cu}_8\text{Fe}_3\text{Sn}_2\text{S}_{12}$  were also found.

## Sulfosalts

A thorough analysis of the sulfosalt phases was carried on in the ore mineralization of the SED. An

**Table 6.** Chemical composition (wt.%) and atomic proportions (apfu) of composition and atomic proportions of representative sakuraiite and k rsterite from the Santa Fe District (EMPA).

	Sakuraiite										K�rsterite	
	Japo			Morococala							Japo	
	1	2	3	4	5	6	7	8	9	10	1	2
S	29.50	30.05	29.62	29.24	31.07	30.63	27.26	30.18	31.57	31.11	29.02	30.05
Fe	14.03	11.95	11.66	12.50	13.00	12.75	14.94	14.04	12.65	13.01	12.76	11.95
Cu	25.14	21.97	22.62	25.12	21.95	25.72	21.79	27.54	21.68	22.51	21.88	21.97
Zn	6.19	17.03	10.80	1.62	12.17	5.92	1.40	1.84	14.58	13.50	12.81	17.03
As	0.00	0.00	0.00	0.00	0.00	0.00	0.08	0.05	0.03	0.00	0.00	0.00
Se	0.07	0.04	0.10	0.00	0.00	0.05	0.00	0.00	0.11	0.00	0.05	0.01
Ag	0.09	0.08	0.10	0.86	0.75	0.78	0.51	0.85	0.73	0.34	0.00	0.08
Cd	0.00	0.02	0.00	0.00	0.05	0.05	0.11	0.00	0.00	0.08	0.08	0.02
In	0.12	0.14	0.14	0.90	2.03	1.68	0.07	0.08	0.19	0.23	0.13	0.14
Sn	24.21	18.30	23.12	24.93	20.30	24.26	20.26	26.67	20.71	20.39	20.24	18.30
Pb	0.03	0.10	0.19	0.03	0.10	0.02	0.11	0.05	0.08	0.05	0.07	0.10
Total	99.42	99.76	98.42	95.22	101.56	102.00	88.32	101.45	102.64	101.54	97.11	99.76
S	3.996	3.998	3.995	4.000	4.000	4.000	4.000	4.000	4.000	4.000	3.997	3.999
Fe	1.091	0.913	0.903	0.982	0.961	0.956	1.259	1.069	0.920	0.961	1.009	0.913
Cu	1.719	1.475	1.539	1.734	1.426	1.695	1.614	1.842	1.386	1.461	1.521	1.476
Zn	0.411	1.111	0.714	0.109	0.768	0.379	0.101	0.120	0.906	0.851	0.865	1.111
As	0.000	0.000	0.000	0.000	0.000	0.000	0.005	0.003	0.002	0.000	0.000	0.000
Ag	0.004	0.003	0.004	0.035	0.029	0.030	0.022	0.034	0.027	0.013	0.000	0.003
Cd	0.000	0.001	0.000	0.000	0.002	0.002	0.005	0.000	0.000	0.003	0.000	0.000
In	0.005	0.005	0.005	0.034	0.073	0.061	0.003	0.003	0.007	0.008	0.005	0.005
Sn	0.886	0.658	0.842	0.921	0.706	0.856	0.803	0.955	0.709	0.708	0.753	0.658

Structural formulas were estimated not considering interference correction of In per Sn.

outstanding variety of phases has been a constant stoichiometric formal as found, and the phases were grouped  $\text{Ag}(\text{Zn},\text{Fe})\text{Bi}_3\text{S}_6$ ,  $\text{Cu}(\text{Sn},\text{Fe})_2\text{S}_4$  and  $\text{PbBiAg}$ , according to the proportion between were continuous recognized in the Sn, Pb, Ag, Cu, Sb and Bi, based in Mo lo EPMA analysis.

et al (2008). The table 7 enumerates Besides to stannite group minerals the different types of sulfosalts and the described previously, other Sn-rich mineral species corresponding. sulfosalts were also found such as

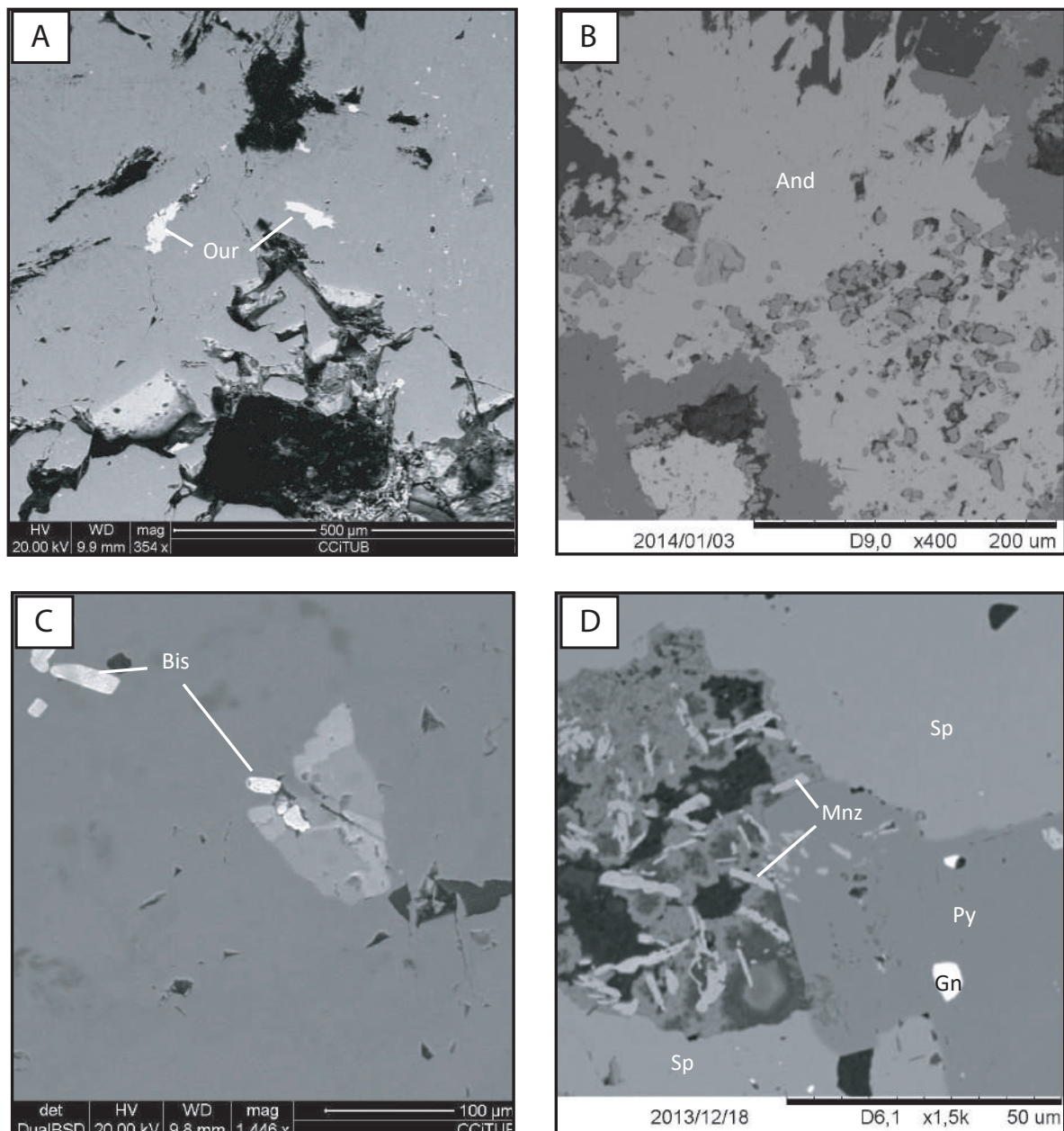
In addition, several solid solutions potosi ite  $\text{Pb}_6\text{FeSn}_2\text{Sb}_2\text{S}_{14}$  and franckeite were found in the SFD. Specifically,  $(\text{Pb},\text{Sn})_6\text{FeSn}_2\text{Sb}_2\text{S}_{14}$ . Berndtite  $\text{SnS}_2$  (member of the melonite group) and at least three different phases with teallite  $\text{PbSnS}_2$  can be mentioned.

**Table 7.** Summary of sulfosalts from the Santa Fe District (EMPA) and their structural formula.

Mineralogical Group	Mineral Name	Theoretical Formula	This study	Reference
Stannite Group	Stannite	$Cu_2(Fe,Zn)SnS_4$	$Cu_{1,9}(Fe,Zn)_{1,0}Sn_{1,0}S_{4,0}$	Hall et al, (1978)
	K�esterite	$Cu_2(Zn,Fe)SnS_4$	$Cu_{1,5}(Zn,Fe)_{2,0}Sn_{0,7}S_{4,0}$	Hall et al, (1978)
	Sakuraiite	$(Cu,Zn,Fe)_3(In,Sn)S_4$	$(Cu,Zn,Fe)_{3,2}(In,Sn)_{0,8}S_{4,0}$	Shimizu et al, (1986)
	Hocartite	$Ag_2FeSnS_4$	$Ag_{1,9}Fe_{0,4}Sn_{1,0}S_{4,0}$	Fleischer (1969)
	Piriquitasite	$Ag_2ZnSnS_4$	$Ag_{1,9}Zn_{0,9}Sn_{1,0}S_{4,0}$	Johan and Picot (1982)
	Petrukite	$(Cu,Ag)_2(Fe,Zn)(Sn,In)S_4$	$(Cu,Ag)_{1,95}(Fe,Zn)_{1,2}(Sn,In)_{0,98}S_{4,0}$	Petruk (1973)
Franckeite group	Franckeite	$Fe^{2+}(Pb,Sn^{2+})_6Sn_2^{4+}Sb_2S_{14}$	$Fe^{2+}_{1,1}(Pb,Sn^{2+})_{6,1}Sn_{2,0}^{4+}Sb_{2,0}S_{14,0}$	Williams and Hyde (1988)
	Potosiite	$Pb_6Sn_3FeSb_3S_{16}$	$Pb_{6,3}Sn_{2,7}Fe_{1,9}Sb_{2,3}S_{16,0}$	Williams and Hyde (1988)
Melanite group	Berndtite	$SnS_2$		Moh and Bernat (1965)
Tetraedrite group	Tetraedrite	$Cu_{12}Sb_4S_{13}$		Johnson et al, (1988)
	Freibergite	$Ag_6Cu_4Fe_2Sb_4S_{13-x}$	$Ag_{2,5}Cu_{7,3}Fe_{2,0}Sb_{3,9}S_{13,0}$	Fleischer et al, (1975)
	Tennantite	$Cu_{12}As_4S_{13}$	$(Cu,Fe)_{12}As_4S_{13}$	Seal et al, (1990)
Lillianite Group	Gustavite	$AgPbBi_3S_6$	$Ag_{0,3}Pb_{2,2}Bi_{1,5}S_{5,9}$	Makovicky and Karup-M�oller (1977)
	Ourayite	$Ag_3Pb_4Bi_5S_{13}$	$Ag_{2,0}Pb_{3,3}Bi_{4,9}S_{13,0}$	Makovicky and Karup-M�oller (1977)
	Andorite	$AgPbSb_3S_6$		Makovicky and Karup-M�oller (1977)
Cylindrite group	Cylindrite	$FePb_3Sn_4Sb_2S_{14}$	$Fe_{1,4}Pb_{5,3}Sn_{2,8}Sb_{2,0}S_{14,0}$	Williams and Hyde (1988)
Stibnite Group	Stibnite	$Sb_2S_3$		Kuze et al, (2004)
	Bismuthinite	$Bi_2S_3$	$Bi_{1,9}S_{3,0}$	Kuze et al, (2004)
	Stannoidite	$Cu_8(Fe,Zn)_3Sn_2S_{12}$		Fleischer (1969)
	Teallite	$PbSnS_2$	$Pb_{2,0}Sn_{1,6}S_{2,0}$	Ahlfeld (1926)
	Argentite	$Ag_2S$	$Ag_{1,5}S_{1,0}$	Petruk et al, (1974)
	Matildite	$AgBiS_2$	$Ag_{0,7}Bi_{1,9}S_{4,0}$	Shimizu, et al, (1998)
	Myargyrite	$AgSbS_2$		Effenberger, et al, (2002)
	Boulangerite	$Pb_5Sb_4S_{11}$		Khargish and Jele�n (2016)
	Jamesonite	$FePb_4Sb_6S_{14}$	$Fe_{1,9}Pb_{3,8}Sb_{5,7}S_{14,0}$	Khargish and Jele�n (2016)
	Zinckerite	$Pb_9Sb_{22}S_{42}$		Khargish and Jele�n (2016)
	Vianite	$(Fe,Pb)_4S_8O$	$(Fe,Pb)_{4,2}S_{8,0}O_{1,0}$	Kucha et al, (1995)
	Laitakarite	$Bi_4Se_3$	$Bi_{3,1}Se_{3,3}$	Cook, et al, (2007)
	Cosalite	$Pb_2Bi_2S_5$	$Pb_{2,3}Bi_{1,5}S_{5,9}$	Topa and Makovicky (2010)
	Bismite	$Bi_2O_3$	$Bi_{1,3}O_{3,0}$	Frondel (1943)

Structural formulas were estimated not considering interference correction of 22 ppm of In per 1 wt% of Sn.

Furthermore, a bunch of sulfosalts  $(\text{Cu,Fe})_{12}\text{As}_4\text{S}_{13}$  with silver was found not only in the Santa Fe mine but also in samples from Morococala deposit. These include the tetrahedrite group as tetrahedrite  $(\text{Cu,Fe})_{12}\text{Sb}_4\text{S}_{13}$ , freibergite  $(\text{Ag,Cu,Fe})_{12}(\text{Sb,As})_4\text{S}_{13}$  and tennantite  $(\text{Cu,Fe})_{12}\text{As}_4\text{S}_{13}$ . EPMA analyses of freibergite revealed up to 14.95 wt.% Ag. Ag-Bi phases belonging (or related) to the lillianite group were recognized in Morococala, as gustavite  $\text{PbAgBi}_3\text{S}_6$ , andorite  $\text{PbAgSb}_3\text{S}_6$  and ourayite  $\text{Pb}_4\text{Ag}_3\text{Bi}_5\text{S}_{13}$  (Fig. 24a, b). Ourayite



**Figure 27.** Backscattered SEM images of: A) Ourayite filling cavities in a pyrite crystal; B) Acicular crystals of andorite; C) Bismuthinite crystals in a galena crystal; D) Acicular monazite crystals associated to ore mineralization.



crystals show up to 8.58 wt.% Ag. Ahlfeld and Schneider-Scherbina (1964) reported miargyrite  $\text{AgSbS}_2$  in the Santa Fe mine; it was also recognized in samples of this study.

Pb-rich sulfosalts are very fine, with grain size under 30  $\mu\text{m}$ . They include cylindrite  $\text{Pb}_3\text{Sn}_4\text{FeSb}_2\text{S}_{14}$  and phases of  $\text{SbS}_3$  series as boulangerite  $\text{Pb}_5\text{Sb}_4\text{S}_{11}$ , jamesonite  $\text{Pb}_4\text{FeSb}_6\text{S}_{14}$  and zinckenite  $\text{Pb}_9\text{Sb}_{22}\text{S}_{42}$ . Viaeneite  $(\text{Fe,Pb})_4\text{S}_8\text{O}$  is an unusual oxysulfide that was also recognized in samples from Santa Fe deposit. Until now, Viaeneite had been only reported by Kucha et al. (1996).

A complex cases encountered in the sulfosalt group are exsolution aggregates of the bismuthinite series. In the SFD, bismuthinite  $\text{Bi}_2\text{S}_3$  and bismite  $\text{Bi}_2\text{O}_3$  crystals found are elongated, of  $\sim 50 \mu\text{m}$  (Fig. 27c). Cosalite  $\text{Pb}_2\text{Bi}_2\text{S}_5$  was only recognized in Morococala. It belongs to lead–bismuth sulfosalts and accepts substitutions of Cu, Ag, Pb and Bi (Topa and Makovicky, 2010). Analyzed crystals of cosalite show substitution of Bi by As.

## Phosphates

Phosphates occur in cavities and small fractures and formed during two different stages: (a) earlier, metasomatic stage (greisen), where monazite  $(\text{Ce,La,Nd,Th})\text{PO}_4$  was formed (Fig. 27d), and (b) later, supergene stage, where alteration minerals as plumbogummite  $\text{PbAl}_3(\text{PO}_4)_2(\text{OH})_5 \cdot (\text{H}_2\text{O})$  and crandallite  $\text{CaAl}_3(\text{PO}_4)_2(\text{OH})_5 \cdot (\text{H}_2\text{O})$  occur.

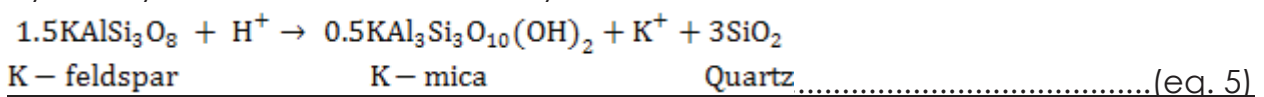
## 6.5. Alteration

In hydrothermal systems, alteration is a prime indicator of fluid paths involving mineralogical, chemical and textural changes, resulting from the interaction of fluids with the rocks, under evolving physico-chemical conditions. As a consequence, the geochemistry of altered rocks has commonly been used to characterize the intensity of hydrothermal alteration in almost all types of deposits, including massive sulfide, meso-thermal gold, epithermal and porphyry deposits and greisen (Piché and Jébrak, 2004). Alteration

mineral assemblages constrain the pressure and temperature conditions of ore formations; they also can reveal the pH and redox conditions of the hydrothermal fluid. Henley and Ellis (1983) emphasized the fundamental role played by the nature and composition of wall rocks in hydrothermal alteration processes. In hydrothermal alteration, H<sup>+</sup> (or OH<sup>-</sup>) is consumed during reaction with the silicate minerals, so that the ratio H<sup>+</sup>/OH<sup>-</sup> changes. A typical example of hydrolytic decomposition of feldspar is presented in equation 5.

Thus, hydrogen ion metasomatic process, hydration and base exchange control the stability of silicate minerals, the pH of the solution, and the transfer of cations into the solution (Pirajno, 2009). They are responsible for alteration mineral assemblages, which are so typical of hydrothermal mineral deposits.

Alteration in the SFD was studied by X-ray diffraction. We analyzed



several samples in order to recognize cryptocrystalline or clay minerals, which cannot be recognized by other conventional techniques. The terms used to classify alterations can be expressed as a function of recognized mineral assemblage. In the mineral assemblage studied minerals are list in order of decreasing abundances, for example quartz > sericite > K-feldspar. Results of the X-ray diffraction analysis of the selected samples are presented in Table 8.

### 6.6. Ore distribution in mineral processing

Distribution of ore minerals (especially Sn-bearing minerals) were studied in samples from Morococala and Japo, in order to know the efficiency in the recovery process in the SFD. In the Santa Fe mine, it was not possible because mineral processing is carry on in a different place. Samples of ore mineralization, concentrate and tailings

**Table 8.** Alteration assemblages recognized in selected samples from the Santa Fe District.

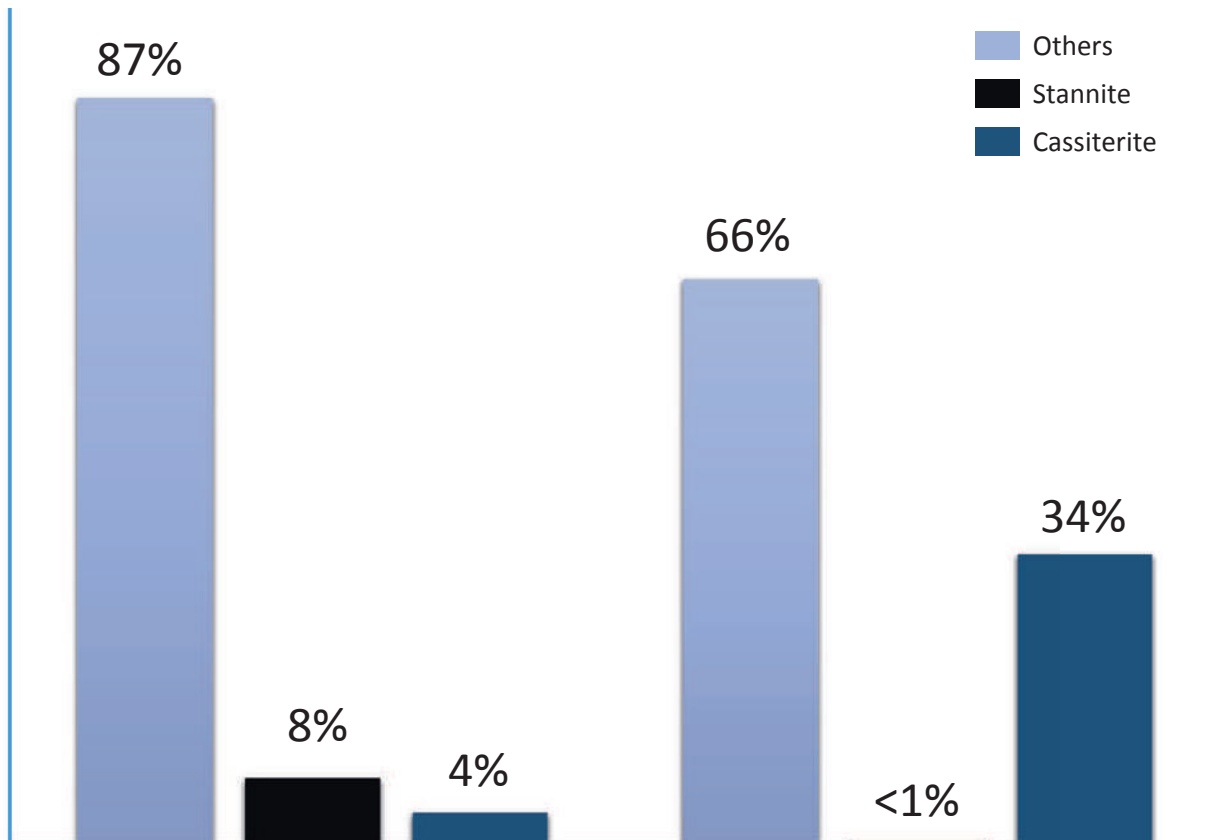
#	Clave	Mineral assemblage	Alteration
1	J-2b	Quartz, illite-montmorillonite, kaolinite, alunite, pyrite	Advanced argillic
2	J-2c	Quartz, kaolinite, rhomboclase, illite, anhydrite	Potasic
3	J-2e	Quartz, rhomboclase, cassiterite, kaolinite, gypsum, alunite, montmorillonite, vermiculite	Advanced argillic
5	J-3d	Quartz, kaolinite, rhomboclase, sericite, biotite	Argillic
6	J-4	Quartz, vermiculite, sericite, illite, jarosite, monazite, gypsum	Greisen
7	J-7a	Quartz, vermiculite, sericite, illite, jarosite, monazite, gypsum	Greisen
8	J-7b	Cassiterite, vermiculite, quartz, oligoclase, monazite	Greisen
9	ASF-01	Quartz, monazite, kaolinite, illite, sericite	Argillic
10	ASF-02	Hematite, cassiterite, quartz, sericite, illite, jarosite	Greisen
11	ASF-03	Sulfur, sericite, hematite, rhomboclase	Argillic
12	ASF-04	Orthoclase, anhydrite, sericite, chlorite, plumbojarosite	Potasic
13	ASF-05	Biotite, rhomboclase, illite, anhydrite, kaolinite	Potasic
15	MCC-13	Quartz, sphalerite, cassiterite, pyrite, kaolinite	Greisen
16	MCC-17	Goethite, melanterite, dickite, alunite, quartz, cassiterite	Advanced argillic
17	MCC-18	Pyrite, quartz, dickite, jarosite	Advanced argillic

Samples 1 to 8 from Japo mine, 9 to 13 from Santa Fe mine and 15 to 17 from Morococala

were analyzed by X-ray diffraction in order to identify even very fine phases. In the analyzed ore samples (before concentrate processing) is evident that proportion between stannite vs cassiterite phases is 2:1. However, processing mineral in all mines in the

Central Andean Tin Belt (especially in artisanal mines) is carrier on by high oxide minerals as cassiterite.

Theoretical cassiterite density is 6.993 g/cm<sup>3</sup>, meanwhile in stannite case is 4.49 g/cm<sup>3</sup>, this represents a weight ratio of 3:2 of cassiterite vs stannite. Thus, loss



**Figure 28.** Content (wt.%) of ore minerals before and after recovery concentration. Concentrate shows poor efficiency in recovery of cassiterite and total loss of stannite. Most of the “others” are gangue minerals.

of the stannite crystals is predictable. Results reveal that concentration processing is not efficient in any case. In ideal conditions, cassiterite percent by gravity recovery should be ~60% (Turner and Hallewell, 1993). In the analyzed samples, cassiterite recovery is only of 34% in the concentrate, where stannite percent recovery is negligible (Fig. 28).

## 6.7. Fluids characterization

### Fluid Inclusions

The analyzed FI have regular morphology and are distributed following growth zones of crystals or isolated, ranging in size from 5 to 20  $\mu\text{m}$ . In the veins of the SFD, most of the FI are aqueous with two phases (liquid+vapor) (Fig. 29), however in some inclusions

daughter minerals can be found (specially in FIA 1). CO<sub>2</sub> was detected in some FI, through the formation of clathrates, which implies that this gas is above 3.7 wt.% (cf. Hedenquist and Henley 1985).

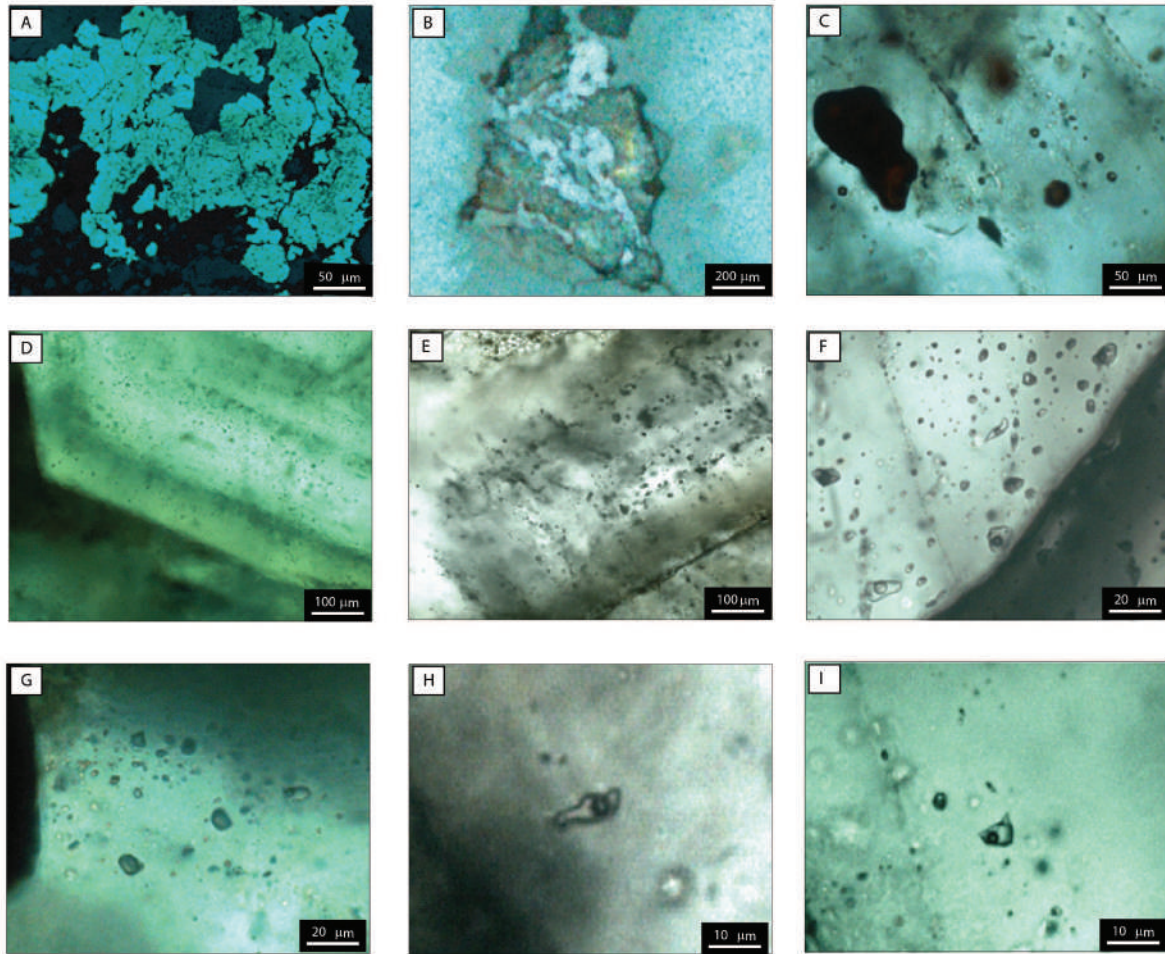
The obtained microthermometric data are summarized in Table 9 and plot on a T<sub>H</sub> vs. salinity diagram shown in Fig. 30. FI hosted by quartz crystals yield the highest TH, from 420° to 455°C, and salinity values of 18.8 to 19.45 wt.% NaCl eq. In calcite, T<sub>H</sub> is lower than quartz, varies from 238° to 269°C.

In the SFD, we found analyzable quartz and calcite-hosted FI exclusively in vein samples, corresponding to the post magmatic stage; from them, it was obtained a wide range of TH of 145°-438°C and salinity of 12.96 to 23.63 wt.% NaCl eq.

Microthermometric measurements were obtained in two clusters of FI appeared in the T<sub>H</sub> vs. salinity plot, possibly corresponding to different fluid inclusion assemblages (FIA) (Fig. 29): (a) T<sub>H</sub> between 249° and 438°C and salinity of 17.79-23.63 wt.% NaCl eq.; (b) T<sub>H</sub> of

**Table 9.** Summary of microthermometric data of fluid inclusions of the Santa Fe District.

Sample	Stage of formation	FIA	#	Th (°C)	Tm (°C)	Salinity
				min./mean/ max.	max./mean/min.	(wt.% NaCl equiv.) min./mean/max
SFM14 (1)	Greisen	1	7	275/282/288	-12.2/-14.0/-13.0	16/17/18
JDC-06-2	Greisen	1	6	420/438/455	-15.2/-15.5/-16.0	19/19/19
JDC-05-25	Greisen	1	29	380/400/410	-14.8/-16.4/-17.4	18/20/21
JDC-06-12	Greisen	2	26	280/294/310	-17.2/-18.3/-20.0	20/21/22
JDC-05-7 (1)	Greisen	2	14	210/223/240	-12.2/-13.5/-14.4	16/17/18
JDC-06-12	Greisen	2	26	280/294/310	-17.2/-18.3/-20.0	20/21/22
SFM14 (2)	Veins	4	11	304/307/311	-14.0/-14.8/-15.5	18/18/19
JDC-06-1	Veins	4	7	211/297/319	-12.0/-12.7/-13.0	16/17/17
JDC-05-7 (2)	Veins	D	13	320/345/390	-18.0/-18.5/-19.2	21/21/22
JAPO-13	Veins	D	25	200/215/225	-12.0/-13.3/-14.0	16/17/18
JDC-06-22	Veins	D	15	225/228/230	-12.7/-12.7/-12.7	17/17/17
JDC-05-23	Veins	D	40	143/172/205	-9.1/-10.6/-12.0	13/15/16



**Figure 29.** Photomicrographs of fluid inclusions from the SFD. A) Fluid inclusions associate with ore mineralization; B) sphalerite with quartz; C) primary fluid inclusions (negative crystals) on quartz and ore associate; D) primary fluid inclusion on growth zoning from Japo; E) primary fluid inclusion on growth zoning from Santa Fe; F) liquid+vapor inclusion in heterogeneous trapping zone from Japo; G) liquid+vapor inclusion in heterogeneous trapping zone from Santa Fe; H) liquid+vapor+solid, from Japo; (I) fluid inclusion with liquid+vapor+solid, from Santa Fe.

143-319°C and salinity of 17.79 to 18.13 wt.% NaCl eq.

The FIA (a) corresponds to the greisen stage, in with three groups can be recognized, each one of them can represented a different pulses:

(1) the hottest TH and low salinity, with 444°-275°C, and 20.52-16.15 wt.% NaCl eq., respectively;

(2) medium  $T_H$  and medium salinity, with 390°-280°C, and 22.38-20.37 wt.%

NaCl eq., respectively; and

(3) of less  $T_H$  and high salinity, with 266°-248°C, and 23.63-23.11 wt.% NaCl eq., respectively.

On the other hand, the FIA (b) corresponds with the veins stage, where a pulse was also recognized

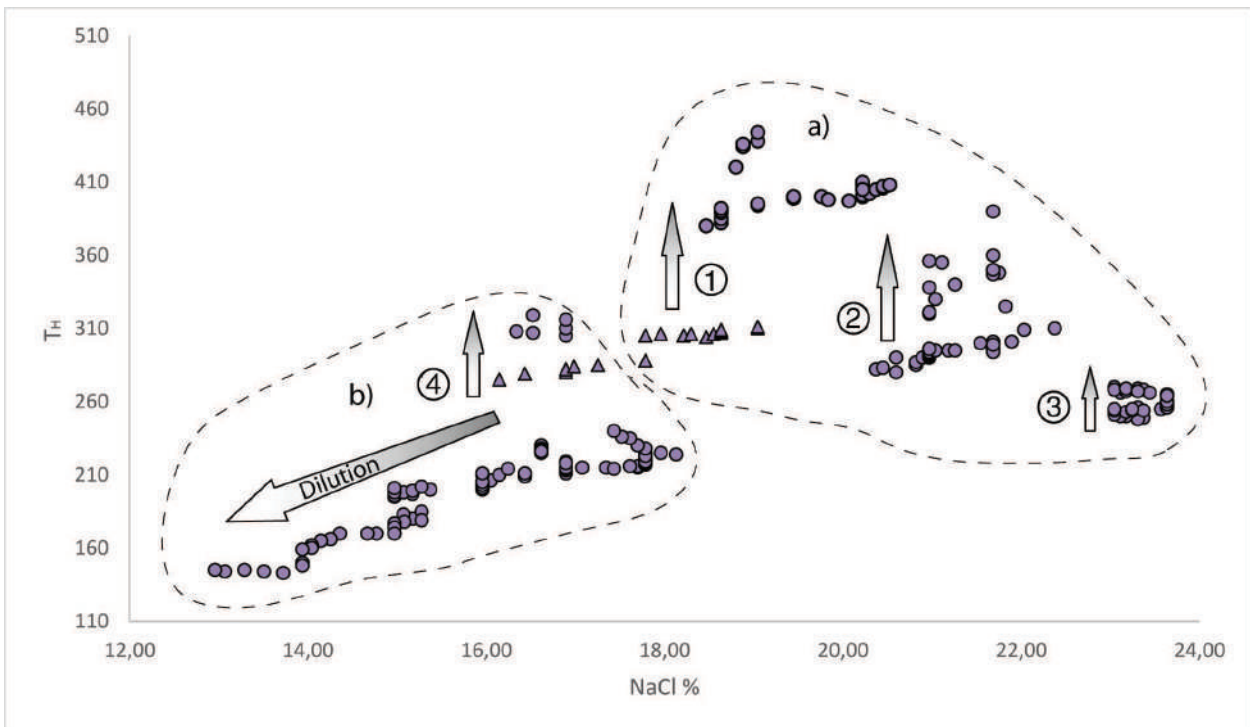
(4). However, in the FIA (b) the main process was interpreted as dilution. This process occurs to  $T_H$  of 319°C and 18.13 wt.% NaCl eq salinity, and conclude to  $T_H$  of 145°C and 12.96 wt.% NaCl eq of salinity. This behavior was observed in both in Japo as in Santa Fe mineralized zones.

### Sulfur Isotopes

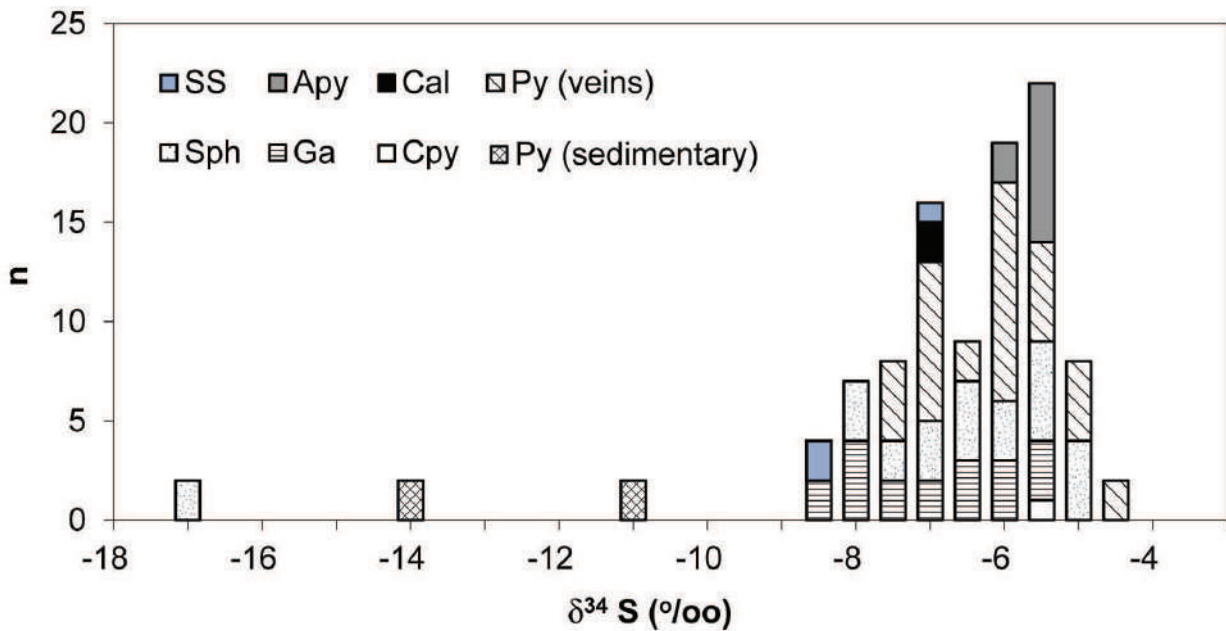
In the SFD, an extensive analysis of the isotopic values have revealed that most of the  $\delta^{34}S$  values in sulfides from the mineralization are distributed in a range, between -8.4 and -4.2 ‰ (n=99), with a mode value of -5.5‰ and an average of -6.6‰. An exceptional value of -16.8 ‰ was reported, in sphalerite from Morococala ore zone.  $\delta^{34}S$  values

of pyrite from the host shale are -13.5 and -10.9 ‰.

Sphalerite ranges from -16.8‰ to -4.8‰.  $\delta^{34}S$  values of galena range from -8.4‰ to -5.1‰, and  $\delta^{34}S$  values of arsenopyrite range from -5.6‰ to -5.1‰. The two analyzed chalcocite grains returned coincident values of -6.6‰, meanwhile, the chalcopyrite grain analyzed returned a value of -5.4‰. Sulfosalt crystals, obtained in samples from the Santa Fe mine, yield  $\delta^{34}S$  values of -6.7‰ and -8.4‰. Sulfur isotopic composition of sulfides is presented in Fig. 31 and Table 10. The isotopic fractionation among the different sulfide mineral pair suggests a lack of isotopic equilibrium.



**Figure 30.** Diagram showing salinity (wt.% NaCl eq.) vs. homogenization temperatures ( $T_H$ ) of the individual fluid inclusions analyzed in the SFD.



**Figure 31.** Histograms showing  $^{34}\text{S}_{\text{CDT}}$  (in ‰) values of sulfides from the SFD.



**Table 10.**  $\delta^{34}\text{S}\text{‰}$  values of sulfides from the mineralization and pyrite from the host shale (JP-1, JA-1, MCC-5 and MC-2) of the Santa Fe District

Sample	Ga	Sph	Py	Apy	Cal	SS	Sample	Cpy	Ga	Sph	Py	Apy	Cal	SS
$d^{34}\text{S}$							$d^{34}\text{S}$							
JP-1			-13,5				JA-7				-5,6			
S-2			-5,7				JA-8			-5,3				
J-17			-5,3	-5,6			JA-9		-7,6					
J-19			-5,8				MC-1			-16,8				
J-41			-4,5				MC-2				-10,9			
JPO 5	-7,6	-5,3	-5,6				MC-3					-5,1		
Jpo 8	-5,4	-5,4	-5,1				MC-13				-7			
MCC-5		-16,8	-10,9				MC-14			-7,7				
MCC-6		-7,7	-7	-5,1			MC-15				-5,7			
MCC-7		-5,2	-5,7				MC-4			-5,2				
MCC-8		-6,9	-6,2				MC-5				-6,2			
MCC-9		-5,8	-6,8				MC-6			-6,9				
MCC-18			-5,7				MC-7				-6,8			
MCC-20		-7,2	-7,3	-5,2			MC-8				-5,8			
SF-3	-7,3	-6,1	-5,1				MC-9				-5,7			
SF-4	-6,1				-6,6		MC-10			-7,2				
SF-8	-5,9	-4,8	-4,8			-8,4	MC-11					-5,2		
SF-9	-5,1						MC-12				-7,3			
SF-10			-4,2				SA-1				-5,1			
SF-11	-7,6	-4,9					SA-2		-7,3					
SF-13		-6,2					SA-3			-6,1				
SF-14	-8,4		-6,8				SA-4						-6,6	
SF-6		-6,7					SA-5		-6,1					
JA-31	-5,62	-5,95	-7,21	-5,35			SA-6							-8,4
JA-64	-6,98						SA-7				-4,8			
JA-96			-7,16				SA-8		-5,9					
JA-101	-6,92						SA-9			-4,8				
SF-7						-6,7	SA-10		-5,1					
SF-8	-6,24	-7,56	-5,75	-5,28			SA-11				-4,2			
JA-1			-13,5				SA-12			-4,9				
JA-2			-5,7				SA-13		-7,6					
JA-3				-5,6			SA-14			-6,2				
JA-4			-5,3				SA-15		-8,4					
JA-5			-5,8				SA-16				-6,8			
JA-6			-4,5				MCC-4	-5,4			-6,7	-5,4		

# 7. DISCUSSION: THE GREISEN DEPOSIT OF THE SANTA FE MINING DISTRICT AND ITS INDIUM POTENTIAL

## 7.1. Paragenetic sequence formation with sulfides deposition (In-

The mineralization in the SFD is related to igneous activity, since it is formed in or around the stock or dikes. The San Pablo stock show replacement of phenocrystals by aggregates of cassiterite and sulfides. These textural analyses suggests that mineral deposition started in the last stage of the intrusive activity.

In the Santa Fe deposit, three main paragenetic stages can be inferred, from old to young:

(1) Magmatic stage and injection of hydrothermal fluids rich in metals, especially in Sn (resulting in cassiterite precipitation);

(2) Metasomatism, producing the alteration of metasedimentary sequence as a greisen stage and vein

bearing minerals, mostly stannite); and (3) Supergene alteration that formed a replacive paragenesis rich in phosphates.

The magmatic stage is represented by association of quartz + albite + rutile + tourmaline and monacite, were cassiterite is also found. The postmagmatic event can be divided in two parts; greisen/metasomatic activity, which is characterized by an extensive deposition of, not only cassiterite but also sulfurs as pyrite + arsenopyrite + chalcopyrite + chalcocite +marcasite and pyrrotite.

Likewise, in the vein formation took place an assemblage of galena + sphalerite ± stannite group + stibnite and sulfosalts. Proportion of stannite

and sulfosalts is similar than the others sulfides but in contrast, the size of crystals is very fine. Some veins of calcite and gypsum also occurred in this stage. Finally, supergene alteration is represented by formation of several

phosphates, mostly, melanterite and vivianite, and subordinated amounts of sulfates as plumbogummite.

The results of the present study are consistent with the Sugaki et al. (1988) mineral sequence interpretation.

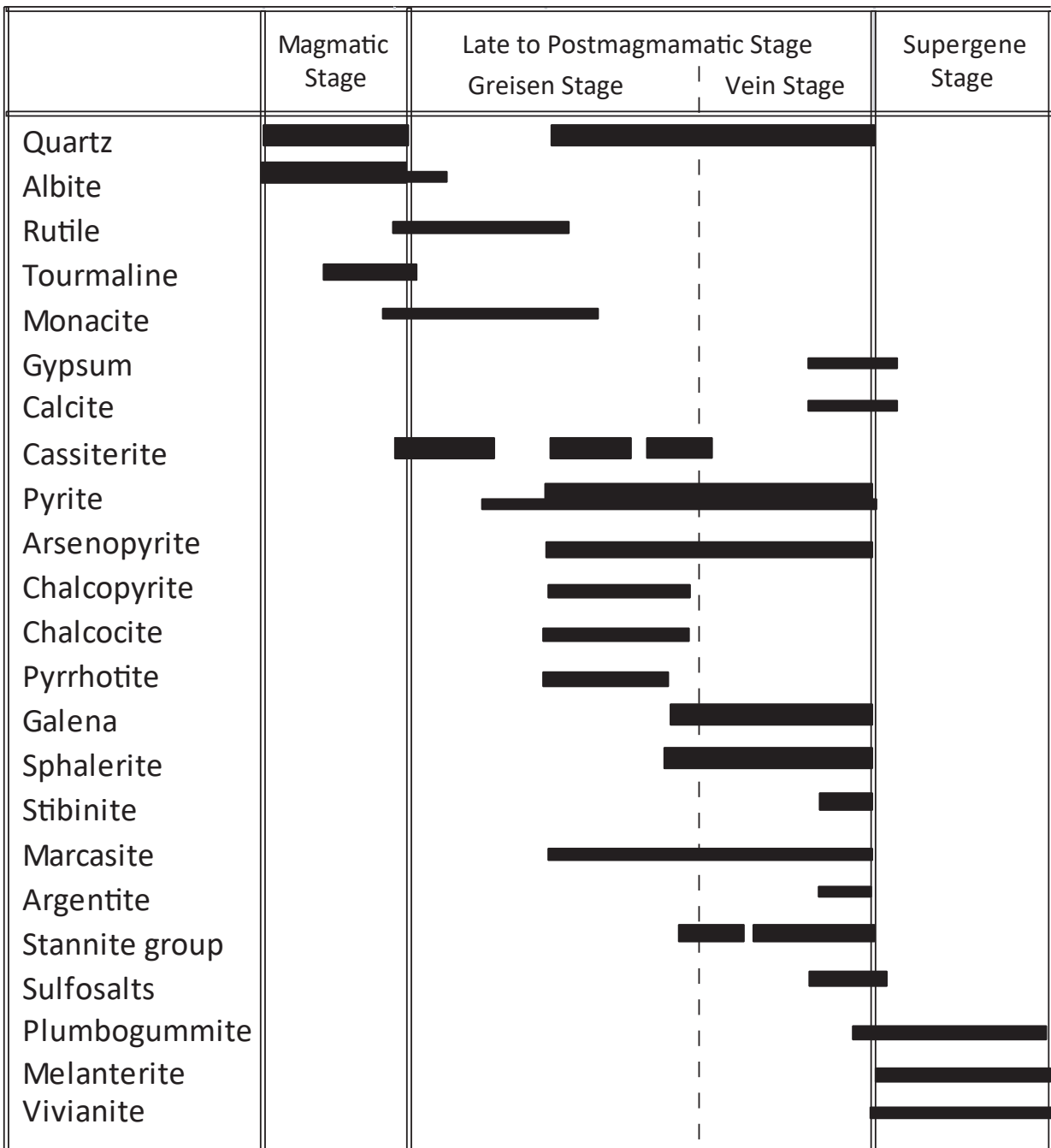


Figure 32. Paragenetic sequence of the Santa Fe District.

They proposed for first time a genetic link between Japo, Santa Fe and Morococala deposits, intimately related to Miocene magmatic activity (San Pablo stock), not so to all the rest of deposits in the Oruro district. The paragenetic sequence present in Fig. 32 summarizes and complements the vast mineralogy of the SFD.

## 7.2. Fluids evolution and sulfur source

Fluid inclusions analysis revealed TH of 145°-438°C and salinity of 12.96 to 23.63 wt.% NaCl eq. (Table 9). Meanwhile, Sugaki et al. (1988) found in these deposits (Japo, Santa Fe and Morococala) TH of 202 to 359°C and salinity of 4.2 to 26.0 wt.% NaCl eq. They observed that relatively high TH because inclusions in quartz associated with cassiterite generally corresponded with inclusions of three-phases (liquid + vapor + daughter mineral); this phenomenon was corroborated in this study (Fig 29h). Boiling is referred to the process of rapid separation of a gas

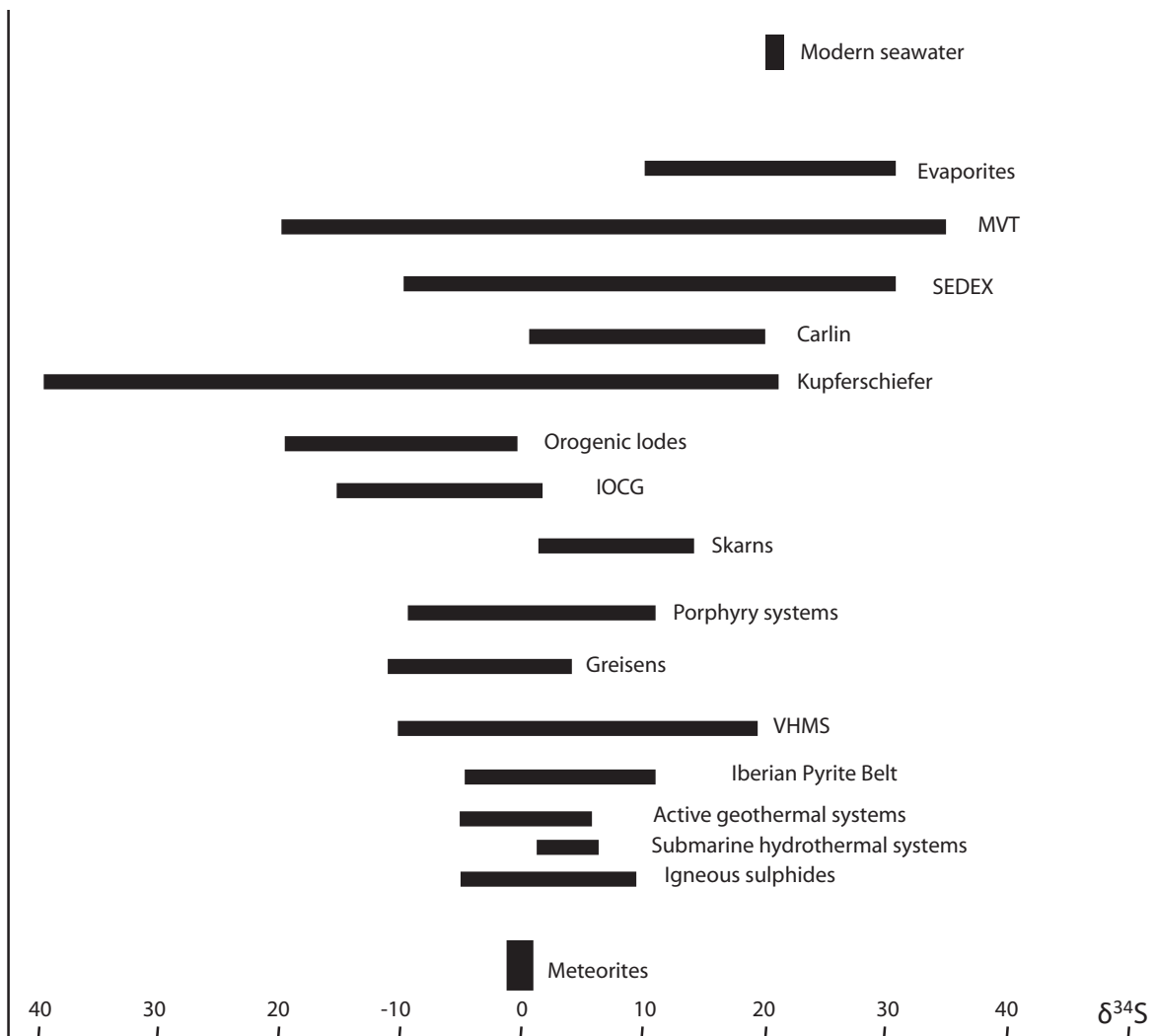
phase largely consisting in water-vapor from a water(-salt) system, because of a temperature increase or a pressure decrease (Roedder, 1984; Henley et al., 1984).

Boiling is the most important process triggering metal deposition in many ore deposit settings, in active and fossils hydrothermal systems (e.g. Cruz-Pérez et al., 2016). In the shallowest 2 km of the hydrothermal systems, boiling is the main process controlling the key chemical parameters for mineral precipitation such as pH, fluid composition and mineral solubility. On the contrary, other processes such as simple conductive cooling by wall rocks and mixing with cold, dilute groundwater are much less influential in ore formation (Drummond and Ohmoto, 1985; Hedenquist, 1991; Canet, 2011). In the FI analyzed, this phenomenon can be interpreted at least in four different pulses (Fig 30). Additionally, in the FI from the SFD evidence of CO<sub>2</sub> as clathrates formation also was reported.

On the other hand, Moura et al. (2007 and 2014) report the only Sn-In deposit in Brazil. High temperature fluid inclusions reported in this (350-200 °C, in quartz and cassiterite) are interpreted in the evolution of a greisen system. Consequently, the fluids cooled to temperatures as low as 100 °C, are interpreted as interaction with meteoric

water, as recorded in the secondary low-salinity aqueous fluid inclusions.

Sulfur isotopic fraction is a particularly useful application for the fluid-rock ratio. Fluid-rock ratios typically have extreme variations within a hydrothermal system and with time (Shanks, 2014). Fig. 33 illustrates a range of  $\delta^{34}\text{S}$  for sulfides from selected ore systems, compared



**Figure 33.** Range of  $\delta^{34}\text{S}_{\text{CDT}}$  (‰) values of sulfides in selected ore systems and reservoirs, compiled by Pirajno (2009).

with meteorites, seawater and igneous sulfides.

Two sample of pyrite from the host shale of the Llalagua Fm. was obtained in order to compare  $\delta^{34}\text{S}_{\text{CDT}}$  sedimentary vs  $\delta^{34}\text{S}_{\text{CDT}}$  hydrothermal values.  $\delta^{34}\text{S}_{\text{CDT}}$  values of about 0‰ are relative to igneous process, and large negative  $\delta^{34}\text{S}_{\text{CDT}}$  are relative to sedimentary reservoir (Ohmoto, 1986; Rollinson, 1993). Sedimentary pyrite revealed a -13.5‰ value, additionally sphalerite shows the most negative value of -16.8 ‰. Isotopic values obtained in this work could be explained by interaction of the fluid of two sulfur sources: i) one igneous (related to hydrothermal-magmatic stage), and ii) the other sedimentary (related to hosted sedimentary sequence). In addition, evidences of  $\text{CO}_2$  were observed in the fluid inclusions of the SFD. Mair et al. (2006) suggested that high  $\text{CO}_2$  contents could be linked with magmas that have interacted with sedimentary rocks.

Time of the interaction (residence) of fluids is also a factor that interfering in the final isotopic values obtained (Shanks, 2014). On the SFD, magmatism was established at ~23.3 Ma. (Grant et al., 1979; Sugaki et al., 2003); on the other hand, mineralization age was assigned at  $20.1 \pm 1.1$  Ma. (Sugaki et al., 2003). Thus, interaction between host-rock and fluids was continue during a considerable period ( $\pm 3$  Ma), promoting changes in the isotopic sulfur composition.

### 7.3. Type of deposit

The economic mineralization is associated to the San Pablo stock (Turneure 1960; Ahlfeld, 1967; Sillitoe et al., 1975; Grant et al., 1979; Sugaki et al., 2003 and Mlynarczyk and Williamsjones, 2005). The San Pablo stock has an association of quartz-feldspars-micas, K-feldspar phenocrysts are replaced by aggregates of tourmaline, pyrite, and cassiterite accompanied by variable amounts of rutile and monazite. Subsequently, magmatic activity

changed eventually to a metasomatic stage. Burt (1981) defined greisen as hydrothermally altered granitic rocks consisting of an association of quartz and micas with variable topaz, tourmaline and fluorite or other F- or B-rich minerals. Greisen result from complex metasomatic processes that affect and take place within a nearly granitic mass and the adjacent country rocks (Pirajno, 2009).

According with Pirajno (2009), metasomatism is a very important phenomenon involving the ionic decomposition of  $H_2O$  into  $H^+$  and  $OH^-$ . The conversion of anhydrous silicates to micas or clays, which consumes  $H^+$  and releases metal ions into the solution. This is related to the dissociation of complexes containing  $H^+$ , the degree of association of compounds such as NaCl, and consequently the formation of chloride complexes and the solubility of metallic elements. Sericitic alteration is represented by the assemblage quartz-sericite-pyrite. Mineral phases

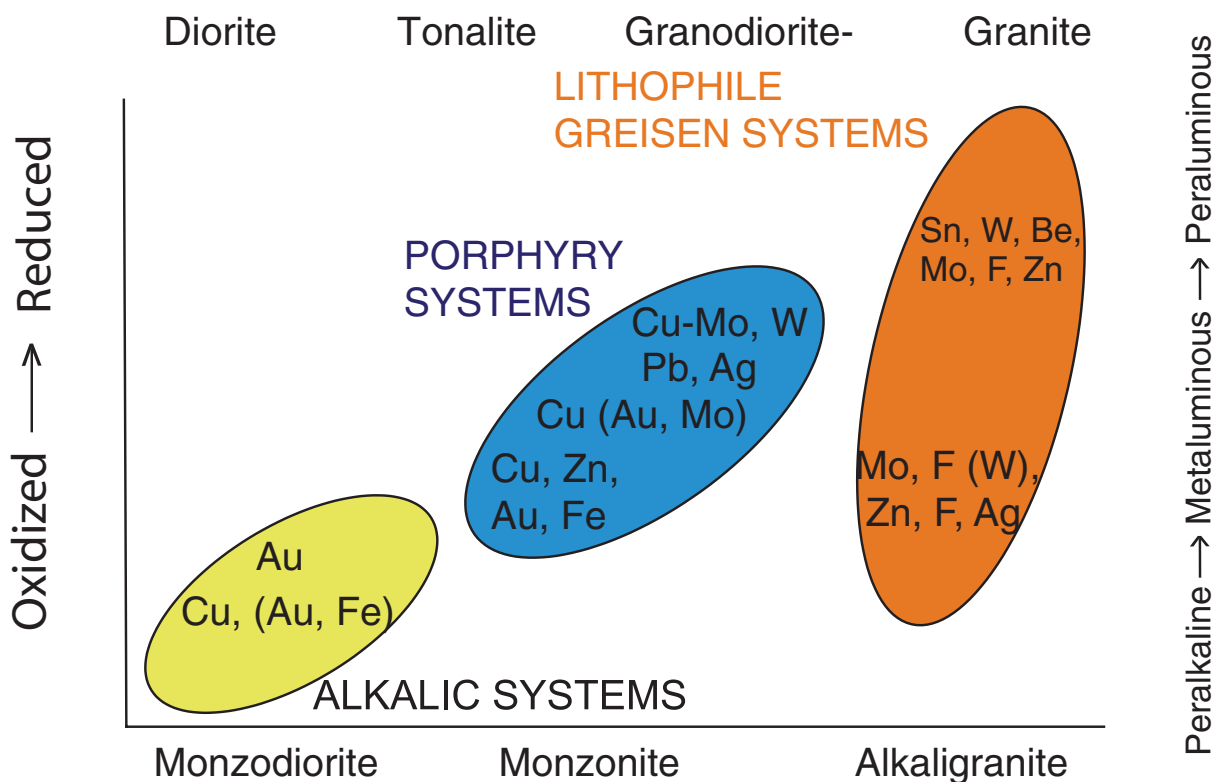
usually associated with this alteration are K-feldspar, kaolinite, calcite, biotite, rutile, anhydrite and apatite. Increasing amounts of topaz, tourmaline and quartz herald a transition to greisen-type alteration. Hydro-muscovite and illite are also associated with this type of alteration (Fleet, 2003).

Sericitic alteration is due to the destabilization of feldspars in the presence of  $H^+$ ,  $OH^-$ , K and S, to form quartz, white mica, pyrite and some chalcopyrite (sulfide content can be up to 20% by volume). This association in samples from San Pablo stock and dikes was found by X-ray analyses and described in Table 8.

Several authors (Groves and McCarthy, 1978; Hall, 1971; Lehmann, 1981; Pirajno, 2009) also points out, although greisen alteration is common in continental porphyry systems, its most favorable environment is a granite stock or sheet emplaced within argillaceous-arenaceous rock sequences, and associated with Sn-W mineralization.

Proposes that greisen alteration is alteration during and after, evidenced preceded by metasomatism. This by the common quartz flooding of involves the destabilization and the greisen altered rocks. Quartz + destruction of feldspar and biotite to form muscovite greisens may be followed the assemblage of quartz+muscovite, by progressive stages of F- and/or and with the introduction of B, F, Li result B-metasomatism, and in the latter case, in new series of reactions that may take the development of tourmaline may place to form topaz, tourmaline, and be so extensive that quartz-tourmaline oxide minerals (Figs. 18c and f, Table 8). assemblages may dominate altogether

According to Shcherba (1970), greisen sequence of events include an early alkaline stage, a greisen stage itself and a vein-depositing stage. Silicification is common in greisen Conceptual models of intrusion-related systems have been proposed by several authors (e.g. Sillitoe, 1996; Sillitoe and Thompson, 1998; Lang et



**Figure 34.** Ore systems and metal associations in relation to the nature of magma and redox conditions (after Barton, 1996; Thompson et al., 1999; Lang and Baker, 2001).



al., 2000; Lang and Baker, 2001). Figure 34, schematically these models, from an intrusion-related environment, to a greisen model.

These intrusion-related hydrothermal systems exhibit a spectrum of polymetallic ore assemblages, with the causative intrusions being surrounded by regional aureoles, from 2 to >5km wide, characterized by arrays of polymetallic veins, replacement, breccia pipes, disseminated, sedimentary rock-hosted to greisen systems. The causative intrusions have intermediate to felsic compositions (I-, S- and A-type granitoids), range from metaluminous to alkalic, are reduced to relatively oxidized (Barton; 1996; Thompson et al., 1999; Lang and Baker, 2001). This contrast to Fe oxides-Cu-Au systems, they are usually characterized by reduced ore mineral assemblages (arsenopyrite, pyrrhotite, and pyrite) and tend to lack in oxidized minerals, such as magnetite or hematite (Lang and Baker 2001).

In the South American context, Moura et al., (2007 and 2014) reported the Mangabeira tin-indium greisen deposit in Central Brazil. They proposed that the formation of this deposit and related Sn-In mineralization is genetically related to fluorine enrichment in the hydrothermal fluids, favoring the transport of Sn and In at temperature and pH conditions typical of greisen mineralization.

In the SFD, Grant et al. (1979) and Sugaki et al. (2003) obtained geochronological data from the San Pablo stock (~23.3 Ma,) and ore mineralization (~20 Ma), respectively. In consequence, it is pointed out that, the timing of tin-polymetallic mineralization in SFD is limited at two specific ages:

i) The post magmatic event was temporary the longest for ore mineralization, i) after metasomatic stage,

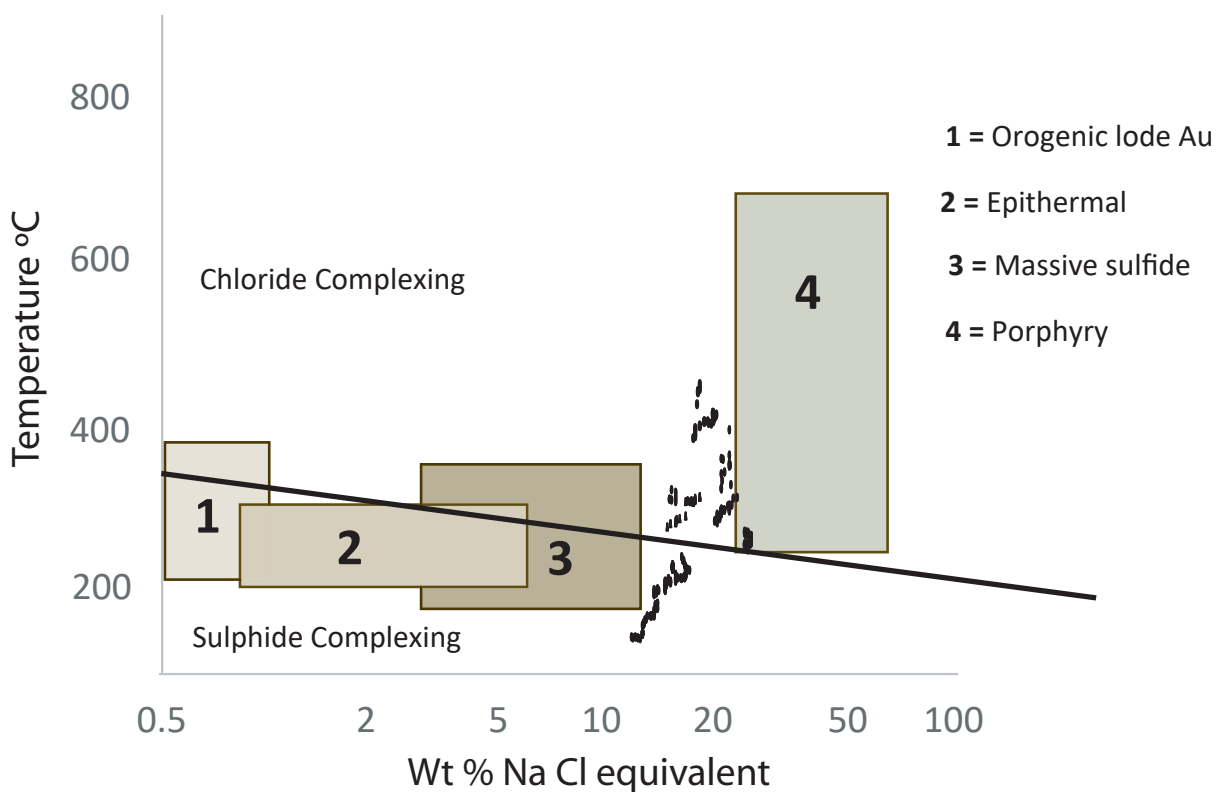
ii) Several episodes of metal deposition occurred forming veins or filling discontinuities as lithological contacts or shear zones. Veins are

infilled by an association of galena, argentite, sphalerite, stibnite marcasite, stannite and sulfosalts.

In addition, Hanson (1980) and Michard (1989) agreed with the fact of the REE abundances are significantly affected only if fluids flushed through the system several times. Thus, REE patterns may not sufficiently different from those of the unaltered rocks. In the mobilization of REE occurs under conditions of large-scale fluid flow. In the Fig. 22, the flat REE pattern corresponds

to altered rocks (e.g. pattern of advanced argillic alteration, Arribas et al. 1995). In contrast, REE results from this work and patterns of the Llallagua, Chorolque, and Oruro (Dietrich et al., 2000) correspond to unaltered plotting out of the REE altered field associated to porphyry systems.

Moreover, FI from the SFD were compared with the diagram in Fig. 35 where, it is reflected the range of salinities vs temperatures of a range of mineral deposits (Large et al., 1988). FI from the



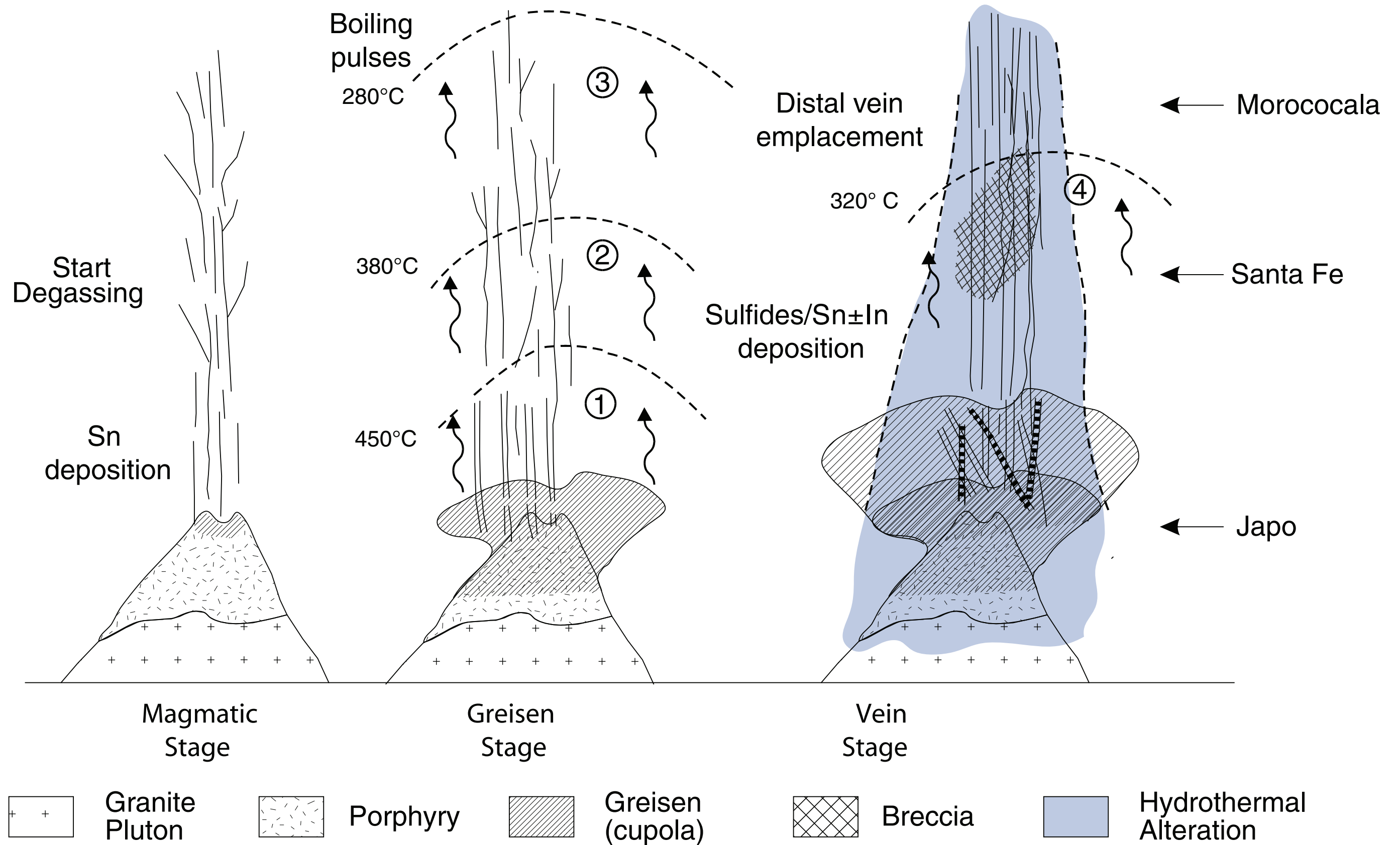
**Figure 35.** Temperature-salinity fields and mean gradient curve for a range of hydrothermal ore systems: 1) Archaean orogenic Au; 2) Epithermal Au-Ag; 3) volcanogenic massive sulfides and 4) Porphyry Cu-Au. After Large et al. (1988). Dots in black represent FI values from The SFD.

SFD plotted between the massive sulfides and porphyry.

Chloride complexing plays an important role in transporting of metals such as sulfides of tin, lead and zinc (e.g., Jackson and Helgeson 1985; Eugster, 1986), this zonal arrangement of minerals probably was caused by cooling and dilution of high-salinity ore fluid in the veins stage (Fig. 30), which is also consistent with conclusions of Sugaki et al. (1988). Aqueous-carbonic fluids reported in tin deposits of Brazil suggesting that CO<sub>2</sub>-bearing magmatic fluids are related to the genesis of these types of tin deposits. The aqueous-carbonic fluid inclusions may have resulted from immiscibility of the carbonic fluid from the dominant aqueous fluid under conditions of high temperature and low pressure due to the shallow emplacement of the granites (Moura et al., 2014). This propose is supported by the models of Burnham and Ohmoto (1980) and Lowenstern (2001).

$\delta^{34}\text{S}_{\text{CDT}}$  values obtained in sulfides of the SFD range mainly between -8.4 and -4.2‰, which is close to greisen/intrusion related isotopic values presented in different and greisen deposits (e.g. Mair et al., 2006; Moura et al., 2014, Fig. 33). Isolated values of -16.8 (sphalerite) and -13.5‰ (pyrite) are interpreted as a sedimentary reservoir source (Ohmoto; 1986; Rollinson, 1993). In addition, evidences of CO<sub>2</sub> were observed in the fluid inclusions of the SFD. Mair et al. (2006) suggested that high CO<sub>2</sub> contents could be linked with magmas that have interacted with sedimentary rocks. Major element and REE models proposed by Simons et al. (2016) indicated that 20% and 30% partial melting of a greywacke source would be sufficient to increase the element abundances in granites (particularly Li, Be, Ga, Nb, Ta, In, Sn, Sb, W and Bi).

Based on the above, Fig. 36 schematizes a conceptual greisen genetic model for the Santa Fe mining District. As is illustrated the mineralization was formed at different levels above



**Figure 36.** Conceptual genetic model of the Santa Fe District, illustrates the three different stages in deposit evolution. In this model, volatile-rich granitic cupola-like intrusions are emplaced in metasedimentary rocks. Stages of degassing and fluid evolution range from incipient through to advanced, from left to right in the figure, resulting in different levels of mineralization-alteration above the San Pablo stock. 1 to 4 represent different pulses of mineralization and dotted line the isothermal curves according to the fluid inclusions results in this work.

greisen development. The Santa Fe greisen (*sensu stricto*) and veins were formed in three main stages, wherein four boiling-pulses took place. First Sn deposition ( $\text{SnO}_2$ ) is more evident in proximity to San Pablo stock (Japo deposit). In contrast, In-bearing sulfides are related to distal veins (cooler) stage of post-magmatic stage (Morococala deposit).

#### 7.4. Indium-bearing in the Santa Fe Mining District

A few studies have been done about indium crustal distribution (Taylor and McLennan, 1985; Rudnick and Gao, 2014; Werner et al., 2017). Werner et al. (2017) propose an indium average of 0.0556 ppm in the crust, based on the correlation between Sn and In concentrations in the deposits reported in the current literature. Only few minerals with indium are known in nature (e.g. Taylor and McLennan, 1985; Schwarz-Schampera and Herzig, 2002; Cook et al., 2011b): Indite  $\text{FeIn}_2\text{S}_4$ , cadmoindite  $\text{CdIn}_2\text{S}_4$ , roquesite  $\text{CuInS}_2$ , laforêtite

$\text{AgInS}_2$ , sakuraiite  $(\text{Cu,Zn,Fe})_3(\text{In,Sn})\text{S}_4$ , petrukite  $(\text{Cu,Fe,Zn})_2(\text{Sn,In})\text{S}_4$ , damiaoite  $\text{PtIn}_2$  and yixunite  $\text{Pt}_3\text{In}$ . Native indium was first found on 1963 in a tin-bearing greisen deposit of the Ukrainian Shield.

According to Seifert and Sandmann (2006), polymetallic and base metal vein deposits as well as granite-related tin-base metal deposits (vein and greisen-type orebodies) are among the most important hosts for In-bearing mineralization.

Recently, a granite related In-bearing occurrence has been reported in Finland (Cook et al., 2011b; Valkama et al., 2016). However, the vast majority of indium is obtained from sphalerite, where it occurs by ionic substitution of Zn (Cook et al., 2011a; Cook et al., 2011b).

Meanwhile, Pavlova et al. (2015) reported an extend study of indium content in several deposits of Russia, Vietnam and Germany, in cassiterite and other tin minerals. They reported until 485 ppm of In in cassiterite, 100–

25,000 ppm in sphalerite and up to 1000 ppm in chalcopyrite, and, in the case of stannite, up to 60,000 ppm. Meanwhile, Serranti et al. (2002) reported up to 394 ppm of In in cassiterite from the Neves-Corvo deposit, Portugal.

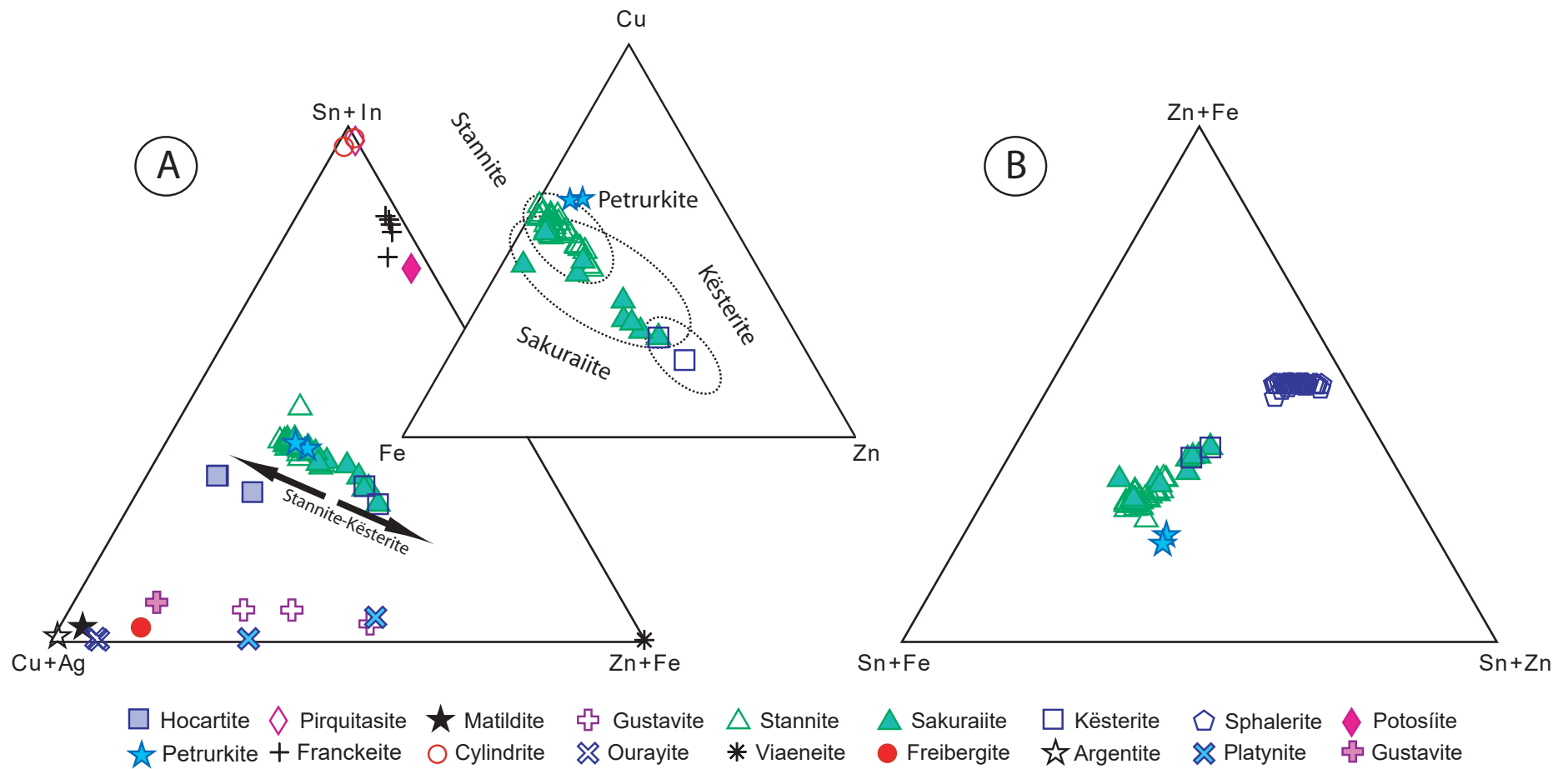
In comparison, in SFD, indium occurs mostly in stannite group, as phases belonging to a complex stannite-sakuraiite-k esterite solid solution and other phases of the S-Sn-Cu-Zn-Fe system. Few analyses from cassiterite reported up to 0.25 wt.% In amount (Table 3), however most of them show subordinated contents. Sphalerite is also depleted in In (Fig. 25, table 4).

Stannite group has several members; some of them are currently cause of controversy. According to Shimizu et al. (1986), stannite-k esterite composition shows substitutions of (Zn Fe) In for Cu-Sn, which is consistent with results from this study. Fig. 37 illustrates these compositional variations, which have a stannite-k esterite trend and their relationship with sulfosalts.

Sakuraiite compositions plot as solid solutions along the stannite-k esterite continuous compositional series. The SEM-EDS and microprobe results in this study, show that sakuraiite forms tetrahedral crystals with a general structural formula as  $(\text{Cu,Zn,Fe})_3(\text{Sn,In})_4\text{S}_4$ , which is consistent to Shimizu et al. (1986). Sakuraiite has up to 2.03 wt.% of In (Figs. 26f, 37b; Tables 6, 7).

On one hand, In-bearing minerals have been reported from localities world-wide (Valkama et al., 2016; Murakami and Ishihara, 2013; Dill et al., 2013; Ishihara et al., 2011; Cook et al., 2011b; Sinclair et al., 2006; Murao and Furuno, 1991; Murao et al., 2008; Ohta, 1989; Seifert and Sandmann, 2006). A summary of results of In-content reported by these authors is shown in Fig. 38.

Japanese deposits have significant In, up to 1030 ppm. Ishihara et al. (2006) reported in samples of different Japanese ore deposits, that indium was found to correlate best with Sn, then Ga,



**Figure 37.** A) Ternary Cu+Ag-Sn+In-Zn+Fe plot of indium-rich minerals from the SFD; B) Ternary diagram Fe-Cu-Zn, plot compositional difference between Stannite-Sakuraiite-Petrurkite-K esterite-Sphalerite phases.



**Figure 38.** Summary of the ppm content of major Indium deposit around the world (Valkama et al., 2016; Murakami and Ishihara, 2013; Dill et al., 2013; Ishihara et al., 2011; Cook et al., 2011b; Sinclair et al., 2006; Murao and Furuno, 1991; Murao et al., 2008, Ohta, 1989; Seifert and Sandmann, 2006).

and most poorly with Zn. In the South American context, like Argentinian deposits of San Roque and Pingüinos, for example indium is strongly related to Sn. In the San Roque deposit 5437 ppm of In was reported (Ishihara et al., 2011), whereas that in the Pingüinos deposit, Jovic et al. (2011) reported up to 1184 ppm.

On the other hand, in the Bolivian deposits Ishihara et al. (2011) reported up to 3080 ppm in the Huari Huari deposit; the maximum 1000×In/Zn ratios in this country are of 22.19 (Potosí), 11.2 (Huari Huari) and 7.42 (Bolivar) (Murakami and Ishihara, 2013). Murakami and

Ishihara (2013) also reported the estimated indium production in major Sn-polymetallic deposits in Bolivia and the corresponding inferred tonnage. The Bolivar deposit has 1,092 indium tons and an inferred tonnage of 45.0 MT; Colquiri has 484 tons of In and an inferred tonnage of 2.0 MT; Porco has 997 tons of In and an inferred tonnage of 3.7 MT; and Potosí has 4,037 tons of In and an inferred tonnage of 541.0 MT. Finally, a total of 1,106.7 MT of inferred resources of indium in Bolivia were estimated with data provided by Arce (2009). In comparison, in the SFD the In content reach up to 54.5 ppm and the



1000×In/Zn ratio vary from 26 up to 1298 in the ore (Table 2).

Furthermore, Werner et al. (2017) point the fact that higher grades of Sn are associated with higher grades of Indium suggests that this correlation may be used to more accurately estimate the grade of indium where Sn grades are reported. They also propose that indium grades can be highly variable within particular mineral hosts, and that a greater number of reporting deposits do not reduce statistical uncertainty. In addition, they recommend for mineralogical information to be reliable, it would then need to link it to other geological factors that would be more likely known about a deposit. Besides, Cook et al. (2011a) emphasize that due to increased

demand for indium in a number of high- technology applications, In has attracted considerable attention in recent years. Additionally, indium-tin oxide (ITO) is mostly used as a thin-film coating on flat-screens (LCDs). In 2014, global ITO production capacity was about 2090 t/yr. Capacity utilization at global ITO facilities was estimated to be about 70% in 2014 (Tolcin, 2016).

According to results from the SFD, indium is mostly found in Sn-bearing minerals; it was also found in high amounts in ore concentration (200 ppm). Thus, the significant potential of obtaining Sn and In in the SFD from the same ore concentrate is itself a key target, not only in exploration but also in the improvement of the processing mineral techniques.

# CONCLUSION REMARKS AND RECOMMENDATIONS

The paragenetic sequence and the mineral assemblage of the SFD are consistent with a greisen ore system. Petrographic observations show greisenization events. The tin-polymetallic mineralization in the SFD is associated in main proportion to post magmatic activity. In the Santa Fe deposit, three main paragenetic stages can be inferred, from former to latter:

(1) Magmatic stage and injection of hydrothermal fluids rich in metals, especially in Sn (resulting in cassiterite precipitation);

(2) Metasomatic event, producing the alteration of metasedimentary sequence as a greisen stage and vein formation with sulfides deposition (In-bearing minerals, mostly stannite); and

(3) Supergene alteration that formed a replacive paragenesis rich in phosphates.

The SFD is known by the tin mineralization; however, an important number of metal associations, including base, alloy, noble and critical metals, have been found in this ore deposit. The most important ore associations from the point of view of their economic interest are: (i) tin mineralization, and (ii) sulfides In-bearing. There is an important relationship between sulfide In-bearing minerals (stannite group) and sulfosalts. Japo and Morococala deposits have exceptional In values, which occur in sakuraiite.

Nowadays, the IMA admits that more than 50 sulfosalts structures remain unsolved, among which about half probably correspond to new structure types. Sakuraiite was found in tetrahedral crystals in this deposit show evidences for a link between stannite—k esterite solid solution, the highest indium content is 2.03 wt.%; however,

the analysis of In-tin minerals by EPMA is problematic, due to intense line interference of InLa and SnLh. In order to obtain lower detection limits and precise information on the In distribution use of nanometrical technics is strongly recommended.

On the other hand, a specific study about the mineral processing in all artisanal mines of the Central Andean tin belt is mandatory. Improve Sn recovery as cassiterite and, at the same time, implementing recovery of stannite as In-bearing mineral could considerably increase the economic and strategic potential of similar ore deposits in the Andean region.

The European Commission of CRMs has not considered tin between the group of CRMs. However, in order to improve to recovery of Indium is essential to study both. It should be

noted that currently, China domains the indium world productions. Likewise, indium-tin oxide (ITO) is mostly used as an important material because technological implications. Thus, the significant potential of obtaining Sn and In in the Santa Fe mining District in the same ore product is itself an key target. Additionally, other mineral phases can also result attractive from the point of view economic (e.g. REE in monazite; Al in alunite, Cu in chalcopyrite).

Quantification of the potential ore reserves was not part of this study, however, results of the mineralogical study and semi-quantitative results are (*a priori*) a target in CRMs terms.

There is an obvious exploration/exploitation potential for strategic metals in this deposit and in similar deposits in the Central Andean Belt.

# REFERENCES

- Adam, J.; Green, T. 2006. Trace element partitioning between mica- and amphibole-bearing garnet lherzolite and hydrous basanitic melt 1: experimental results and the investigation of controls on partitioning behaviour. *Contributions to Mineralogy and Petrology* 152 (1-5): 1-17.
- Andersen, J.C.Ø.; Stickland, R.J.; Rollinson, G.K.; Shail, R.K. 2016. Indium mineralisation in SW England: Host parageneses and mineralogical relations. *Ore Geology Reviews* 78: 213–238.
- Ahlfeld, F. 1926. Zinkteallite und alaskaite aus Bolivia. (Zincteallite and alaskaite from Bolivia). *Centralblatt für Mineralogie, Geologie und Paläontologie* 12: 388-390.
- Ahlfeld, F. 1967. Metallogenic epochs and provinces of Bolivia. *Mineralium Deposita* 2 (4-4): 291-311.
- Ahlfeld, F.; Schneider-Scherbina, A. 1964. Los yacimientos minerales y de hidrocarburos de Bolivia. Ministerio de minas y petróleo. Departamento Nacional de Geología.
- Alderton, D.H.M.; Moore, F. 1981. New determinations of tin and tungsten in granites from south-west England. *Mineralogical Magazine* 44 (335): 354-356.
- Arce-Burgoa, O.R.; Goldfarb, R.J. 2009. Metallogeny of Bolivia. *Society of Economic Geologists Newsletter* 79 (4-4): 1-15.
- Arribas, A.; Cunningham, C.G.; Rytuba, J.J.; Rye, R.O.; Kelly, W.C.; Podwysocki, M.H.; Mckee, E.H.; Tosdal, R.M. 1995. Geology, geochronology, fluid inclusions, and isotope geochemistry of the Rodalquilar gold alunite deposit, Spain. *Economic Geology* 90 (4-8): 795-822.
- Barton, M. D. 1996. Granitic magmatism and metallogeny of southwestern North America. *Transactions of the Edinburgh*

- Geological Society. *Earth Sciences* 87: 261-280.
- Benzaazoua, M.; Marion, P.; Pinto, A.; Migeon, H.; Wagner, F.E. 2003. Tin and indium mineralogy within selected samples from the Neves Corvo ore deposit (Portugal): a multidisciplinary study. *Mineral Engineering* 16 (11-12): 1291–1302.
- Bodnar, R.J.; Reynolds, T.J.; Kuehn, C.A. 1985. Fluid inclusion systematics in epithermal systems. In: *Geology and Geochemistry of Epithermal Systems*: (Berger, B.R. and Bethke, P.M. editors). *Reviews in Economic Geology* 2:73–97.
- Bodnar, R.J.; Sterner, S.M.; Hall, D.L. 1989. SALTY: a FORTRAN program to calculate compositions of fluid inclusions in the system NaCl-KCl-H<sub>2</sub>O. *Computers & Geosciences*, 15(1): 19-41.
- Bodnar, R.J.; Vityk, M.O. 1994. Interpretation of microthermometric data for NaCl-H<sub>2</sub>O fluid inclusions. In: *Fluid Inclusions in Minerals: Methods and Applications* (De Vivo, B. and Frezzotti, M.L. editors) Virginia Polytechnic Institute, State University. 117–130 p. Blacksburg.
- Breiter, K. 2014. Trace element composition of quartz from different types of pegmatites: a case study from the Moldanubian Zone of the Bohemian Massif (Czech Republic). *Mineralogical Magazine* 78 (3-7): 703-722.
- Burnham, C. W. 1997. Magmas and hydrothermal fluids. In: *Geochemistry of hydrothermal deposits* (Barnes, H. L. editor) Wiley third edition. 63-123 p. New York.
- Burnham, C.; Ohmoto, H. 1980. Late-stage processes of felsic magmatism. *Society of Mining Geologists of Japan* 8: 1-11.
- Burt, D. 1981. Acidity-salinity diagrams - Application to greisen and porphyry deposits. *Economic Geology* 76 (4-8): 832-843.
- Canet, C.; Franco, S.I.; Prol-Ledesma, R.M.; González-Partida, E.; Villanueva-Estrada, R.E. 2011. A model of boiling for fluid inclusion studies: Application

- to the Bolaños Ag-Au-Pb-Zn epithermal deposit, Western Mexico. *Journal of Geochemical Exploration* 110 (2): 118-125.
- Claypool, G.E., Holser, W.T., Kaplan, I.R., Sakai, H., Zak, I. (1980): The age curves of sulfur and oxygen isotopes in marine sulfate and their mutual interpretation. *Chemical Geology* 28, 199–260.
- Clark, A.H.; Farrar, E.; Kontak, D.J.; Langridge, R.J.; Arenas, M.J.; France, L.J.; McBride, S.L.; Woodman, P.L.; Wasteneys, H.A.; Sandeman, H.A.; Archibald, D.A. 1990. Geologic and geochronologic constraints on the metallogenic evolution of the Andes of south-eastern Peru. *Economic Geology* 85 (7-8): 1520–1583.
- Cook, N.J.; Ciobanu, C.L.; Wagner, T.; Stanley, C.J. 2007. Minerals of the system Bi-Te-Se-S related to the tetradymite archetype: review of classification and compositional variation. *The Canadian Mineralogist* 45 (4-6): 665-708.
- Cook, N.J.; Ciobanu, C.L.; Williams, T. 2011a. The mineralogy and mineral chemistry of indium in sulphide deposits and implications for mineral processing. *Hydrometallurgy* 108 (3-4): 226-228.
- Cook, N.J.; Sundblad, K.; Valkama, M.; Nygård, R.; Ciobanu, C.L.; Danyushevsky, L. 2011b. Indium mineralisation in A-type granites in southeastern Finland: Insights into mineralogy and partitioning between coexisting minerals. *Chemical Geology* 284 (1-2): 62-73.
- Cruz-Pérez, M.A.; Canet, C.; Franco, S.I.; Camprubí, A.; González-Partida, E.; Rajabi, A. 2016. Boiling and depth calculations in active and fossil hydrothermal systems: A comparative approach based on fluid inclusion case studies from Mexico. *Ore Geology Review* 72: 603–611.
- Díaz Martínez, E. 1997. Facies y ambientes sedimentarios de la Formación Cancañiri (Silúrico inferior) en La Cumbre de La Paz, norte de la Cordillera Oriental de Bolivia *Geogaceta* 22: 55-57.

- Dietrich, A.; Lehmann, B.; Wallianos, A. 2000. Bulk rock and melt inclusion geochemistry of Bolivian tin porphyry systems. *Economic Geology* 95 (2-8): 313–326.
- Dill, H.G.; Garrido, M.M.; Melcher, F.; Gomez, M.C.; Weber, B.; Luna, L.I.; Bahr, A. 2013. Sulfidic and non-sulfidic indium mineralization of the epithermal Au-Cu-Zn-Pb-Ag deposit San Roque (Provincia Rio Negro, SE Argentina) — with special reference to the “indium window” in zinc sulfide. *Ore Geology Reviews* 51: 103-128.
- Drummond, S. E.; Ohmoto, H. 1985. Chemical evolution and mineral deposition in boiling hydrothermal systems. *Economic geology*, 80(1-8): 126-147.
- Duclos, S.J.; Otto, J.P.; Konitzer, D.G. 2010. Design in an era of constrained resources. *Mechanical Engineering*, 132(9): 36-40.
- Eadington, P.J. 1983. A fluid inclusion investigation of ore formation in a tin-mineralized granite, New England, New South Wales. *Economic Geology* 78 (6-8): 1204-1221.
- Effenberger, H.; Paar, W.H.; Topa, D.; Criddle, A.J.; Fleck, M. 2002. The new mineral baumstarkite and a structural reinvestigation of aramayoite and miargyrite. *American Mineralogist* 87 (5-6): 753-764.
- Espinoza-Morales, J. E. 2010. Minería boliviana: su realidad. Plural editors. Bolivia
- Eugster, H. P. 1985. Granites and hydrothermal ore deposits: a geochemical framework. *Mineral Magazine* 49 (350):7-23.
- Eugster, H. P. 1986. Minerals in hot water. *American Mineralogist* 71 (1-2):655-673.
- European Commission 2014. Report on critical raw materials for the EU Report of the Ad-hoc Working Group on Defining Critical Raw Materials. pp 41.
- Evernden, J.F.; Kriz, S.J.; Cherroni, C. 1977. Potassium argon ages of some Bolivian rocks. *Economic Geology* 72 (6-8): 1042-1061.

- Fleet, M.E. 2003. Sheet silicates: Geological Society of London Special Publication 7: 117-126.
- Micas. In: Rock-forming minerals (Deer, W.A.; Howie, R.A.; Zussman, J., editors) The Geological Society of London. 3A. London
- Fleischer, M. 1969. New mineral names. *American Mineralogist* 54: 573.
- Fleischer, M.; Chao G.Y.; Kato, I. 1975. New mineral names. *American Mineralogist* 60: 485-489.
- Flinter, B.H. 1971. Tin in acid granitoids: the search for a geochemical scheme of mineral exploration. In Proceedings of the 3rd International Geochemical Exploration Symposium: 323-330.
- FrondeL, C. 1943. Mineralogy of the oxides and carbonates of bismuth. *American Mineralogist* 28: 521-535.
- Frost, B. R. 1991 Introduction to oxygen fugacity and its petrologic importance. *Reviews in Mineralogy and Geochemistry* 25 (1-1): 1-9.
- Grant, J.N.; Halls, C.; Avila, W.; Avila, G. 1977. Igneous geology and the evolution of hydrothermal systems in some subvolcanic tin deposits of Bolivia: Grant, J.N.; Halls, C.; Avila-Salinas, W.; Snelling, N.J. 1979. K-Ar ages of igneous rocks and mineralization in part of the Bolivian tin belt. *Economic Geology* 74 (4-8): 838-851.
- Grant, J.N.; Halls, C.; Sheppard, S.M.F.; Avila-Salinas, W. 1980. Evolution of the porphyry tin deposits of Bolivia: *Mining Geology Special Issue* (8) 151-173.
- Groves, D.I. 1972. The geochemical evolution of tin-bearing granites in the Blue Tier Batholith, Tasmania. *Economic Geology* 67(4-8): 445-457.
- Groves, D.I.; McCarthy, T.S. 1978. Fractional crystallization and the origin of tin deposits in granitoids. *Mineralium Deposita* 13 (1-3): 11-26.
- Groves, D.I., Bierlein, F.P. 2007. Geodynamic settings of mineral deposit systems. *Journal of the Geological Society*, 164 (1): 19-30.
- Haapala, I. 1997. Magmatic and postmagmatic processes in tin-



- mineralized granites: topaz-bearing leucogranite in the Eurajoki Rapakivi Granite Stock, Finland. *Journal of Petrology* (38): 1645-1659.
- Hall, A. 1971. Greisenisation in the granite of Cligga Head, Cornwall. *Proceedings of the Geologists' Association* 82 (2-4): 209-230.
- Hall, D.L.; Sterner, S.M.; Bodnar, R.J. 1988. Freezing point depression of NaCl-KCl-H<sub>2</sub>O solutions. *Economic Geology* 83(1-8): 197-202.
- Hall, S.R.; Szymanski, J.T.; Stewart, J.M. 1978. Kesterite, Cu<sub>2</sub>(Zn,Fe)SnS<sub>4</sub>, and stannite, Cu<sub>2</sub>(Fe,Zn)SnS<sub>4</sub>, structurally similar but distinct minerals. *The Canadian Mineralogist* 16 (2-4): 131-137.
- Hanson, G.N. 1980. Rare earth elements in petrogenetic studies of igneous systems. *Annual Review of Earth and Planetary Sciences* 8: 371-406.
- Hedenquist, J.W. 1991. Boiling and dilution in the shallow portion of the Waiotapu geothermal system, New Zealand. *Geochimica et Cosmochimica Acta* 55: 2753-2765.
- Hedenquist, J.W.; Henley, R. 1985. The importance of CO<sub>2</sub> on freezing point measurements of fluids inclusions: evidence from active geothermal systems and implications for epithermal ore deposition. *Economic Geology* 80 (5-8): 1379-1406.
- Hedenquist, J.W. and Lowenstern, J.B. 1994. The role of magmas in the formation of hydrothermal ore deposits. *Nature* 370: 519-527.
- Hemley, J.J., Hunt J.P. 1992. Hydrothermal Ore-Forming Processes in the Light of Studies in Rock-Buffered Systems: II. Some General Geologic Application. *Economic Geology* 87 (1-8): 23-43.
- Henley, R. W.; Ellis, A. J. 1983. Geothermal systems ancient and modern: a geochemical review. *Earth Science Review* 19 (1-4): 1-50.
- Hoefs, J., Hoefs, J. (1997). Stable isotope geochemistry. Vol. 201. Berlin: Springer.
- Holland, H.D., 1972. Granites, solutions, and base metal deposits. *Economic Geology* 67(3-8): 281-301.

- Holloway, J.R. 1976. Fluids in the evolution of granitic magmas: Consequences of finite CO<sub>2</sub> solubility. *Geological Society of America Bulletin* 87 (10-12): 1513-1518.
- Ishihara, S. 1977. The magnetite-series and ilmenite-series granitic rocks. *Mining Geology* 27 (5-6): 293-305.
- Ishihara, S. 1981. The granitoid series and mineralization. *Economic Geology 75th Anniversary Volume*: 458-484
- Ishihara, S.; Sawata, H.; Arornsuwan, S.; Busaracome, P.; Bungbrakearti, N. 1979. The magnetite series and ilmenite series granitoids and their bearing on tin mineralisation, particularly of the Malay peninsula region. *Geological Society of Malaysia Bulletin* 11: 103-110.
- Ishihara, S.; Hoshino, K.; Murakami, H.; Endo, Y. 2006. Resource evaluation and some genetic aspects of indium in the Japanese ore deposits. *Resource Geology* 56 (3-4): 347-364.
- Ishihara, S.; Murakami, H.; Marquez-Zavalia, M.F. 2011. Inferred Indium Resources of the Bolivian Tin-Polymetallic Deposits. *Resource Geology* 61 (2-4): 174-191.
- Ivanova, G. F. 1969. Conditions of concentration of tungsten during greisenization. *Geokhimiya* 1: 22-36 (in Russian).
- Jasinski, S.M. 1993. Indium: U.S. Bureau of Mines Mineral Commodity Summaries 1993, 84-85.
- Jackson, K.J., Helgeson, H.C. 1985. Chemical and thermodynamic constraints on the hydrothermal transport and deposition of tin: I. Calculation of the solubility of cassiterite at high pressures and temperatures. *Geochimica et Cosmochimica Acta* 49 (1-12): 1-22.
- Johan, Z.; Picot, P. 1982. La pirquitasite, Ag<sub>2</sub>ZnSnS<sub>4</sub>, un nouveau membre du groupe de la stannite. *Bulletin de minéralogie* (105): 229-235.
- Johnson, N.E.; Craig, J.R.; Rimstidt, J.D. 1988. Crystal chemistry of tetrahedrite. *American Mineralogist* 73 (3-4): 389-397.
- Jovic, S.M.; Guido, D.M.; Ruiz, R.; Páez, G.N.; Schalamuk, I.B. 2011.

- Indium distribution and correlations in polymetallic veins from Pingüino deposit, Deseado Massif, Patagonia, Argentina. *Geochemistry: Exploration, Environment, Analysis* 11 (2-4): 107–115.
- Kato, A. 1965. Sakuraiite, a new mineral. *Chigaku Kenkyu (Earth Science Studies): Sakurai* (1-5) (in Japanese).
- Kelly, W.C.; Turneure, F.S. 1970. Mineralogy, paragenesis and geothermometry of the tin and tungsten deposits of the eastern Andes, Bolivia. *Economic Geology* 65 (5-8): 609-680.
- Kerrick, R.; Goldfarb, R.J.; Richards, J. 2005. Metallogenic provinces in an evolving geodynamic framework. *Economic Geology 100th Anniversary Volume*: 1097-1136.
- Kharbish, S.; Jeleň, S. 2016. Raman spectroscopy of the Pb-Sb sulfosalts minerals: Boulangerite, jamesonite, robinsonite and zinkenite. *Vibrational Spectroscopy* 85: 157-166.
- Kissin, S.A.; Owens, D.A. 1986. The crystallography of sakuraiite. *The Canadian Mineralogist* 24 (4-4): 679-683.
- Kontak, D.J.; Clark, A.H.; Farrar, E.; Strong, D.F. 1984a. The rift-associated Permo-Triassic magmatism of the Eastern Cordillera: A precursor to the Andean orogeny. In: *Magmatism at a plate edge: The Peruvian Andes* (Pitcher, W.S.; Atherton, M.P.; Cobbing, E. J.; Beckinsale, R.D., editors) Blackie. 36-44 p. Glasgow.
- Kontak, D.J., Clark, A.H., Farrar, E. 1984b. The magmatic evolution of the Cordillera Oriental, southeastern Peru. In: *Andean magmatism: Chemical and isotopic constraints* (Harmon, R.S. and Barreiro, B.A., editors) 203- 219 p. Nantwich, Shiva.
- Kucha, H.; Osuch, W.; Elsen, J. 1996. Viaeneite, (Fe, Pb)  $4S_8O$ , A new mineral with mixed sulphur valencies from Engis, Belgium. *European Journal of Mineralogy* 8 (1-5): 93-102.
- Kuze, S.; Du Boulay, D.; Ishizawa, N.; Saiki, A.; Pring, A. 2004. X-ray diffraction evidence for a monoclinic form of stibnite,  $Sb_2S_3$ , below 290 K. *American Mineralogist* 89 (7-12): 1022-1025.

- Lang, J.R.; Baker, T.; Hart, C.J.R.; Mortensen, J.K. 2000. An exploration model for intrusion-related gold systems. SEG Newsletter 40: 1-15.
- Lang, J.R.; Baker, T. 2001. Intrusion-related gold systems: the present level of understanding. Mineral Deposita 36 (6-8): 477-489.
- Large R., Huston D., McGoldrich P., McArthur G., Ruxton P. 1988. Gold distribution and genesis in Paleozoic volcanogenic massive sulphide systems. Bicentennial Gold 88. Geological Society of Australia Abstract 22: 121-126.
- Lavenu, A.; Bonhomme, M. G.; Vatin-Perignon, N.; De Pachtere, P. 1985. Neogene magmatism in the Bolivian Andes (between 16° and 18°S). Part 1: Numerical stratigraphy (K-Ar) and tectonics. Comunicaciones, Departamento de Geología, Universidad de Chile 35: 121-124.
- Lehmann, B. 1978. Memoria explicativa del mapa geológico de Milluni, Cordillera Real (Bolivia): Univerdisad Mayor de San Andres, La Paz, Bolivia, Revista Geociencias 2: 187-257.
- Lehmann, B. 1979. Schichtgebundene Sn-Lagerstätten in der Cordillera Real/Bolivien: Berlin, Dietrich Reimer, Berliner geowissenschaften Abhandlungen, Reihe A 14: 135pp. (Geologic map 1:50,000)
- Lehmann, B. 1981. A discussion of the paper by M. Boissavy-Vinau and G. Roger "the TiO<sub>2</sub>/Ta ratio as an indicator of the degree of differentiation of tin granites". Mineralium Deposita 16 (2-3): 329-331.
- Lehmann, B. 1982. Metallogeny of tin: magmatic differentiation versus geochemical heritage. Economic Geology 77 (1-8): 50-59.
- Lehmann, B. 1985. Formation of the strata-bound Kellhuani tin deposits, Bolivia. Mineralium Deposita 20 (3-4): 169-176.
- Lehmann, B.; Pichler, H. 1980. Tin distribution in mid-Andean volcanic rocks. Mineralium Deposita 15 (1-3): 35-39.
- Lehmann, B.; Willgallis, A.; Heyer, H. 1978. Anomalous Sn-rutiles in wall rocks

- of Bolivian tin deposits. *Neues Jahrbuch für Mineralogie Monatshefte* 11: 498-505.
- Lehmann, B.; Ishihara, S.; Michel, H.; Miller, J.; Rapela, C.W.; Sanchez, A.; Tistl, M.; Winkelmann, L. 1990. The Bolivian tin province and regional tin distribution in the Central Andes; a reassessment. *Economic Geology* 85 (5-8): 1044-1058.
- Lehmann, B.; Dietrich, A.; Heinhorst, J.; Metrich, N.; Mosbah, M.; Palacios, C.; Schneider, H.-J.; Wallianos, A.; Webster, J.D.; Winkelmann, L. 2000a. Boron in the Bolivian tin belt. *Mineralium Deposita* 35 (4-8): 223-232.
- Lehmann, B.; Dietrich, A.; Wallianos, A.; 2000b. From rocks to ore. *International Journal of Earth Sciences* 89 (2-4): 284-294.
- Lowenstern, J.B. 2001. Carbon dioxide in magmas and implications for hydrothermal systems. *Mineralium Deposita* 36(6): 490-502.
- Ludwick, M.T. 1959. Indium, discovery, occurrence, development, and characteristics: Utica, N.Y., Indium Corporation of America, 770 p.
- Makovicky, E.; Karup-Møller, S. 1977. Chemistry and crystallography of the lillianite homologous series. II. Definition of new minerals eskimoite, vikingite, ourayite and treasurite. Redefinition of schirmerite and new data on the lillianite-gustavite solid-solution series. *Neues Jahrbuch für Mineralogie, Abhandlungen* 131: 56-82.
- Marks, M.A.W.; Marschall, H.R.; Schühle, P.; Guth, A.; Wenzel, T.; Jacob, D.E.; Barth, M.; Markl, G. 2013. Trace element systematics of tourmaline in pegmatitic and hydrothermal systems from the Variscan Schwarzwald (Germany): the importance of major element composition, sector zoning, and fluid or melt composition. *Chemical Geology* 344: 73-90.
- Melgarejo, J.C.; Proenza, J.A.; Galí, S.; Llovet, X. 2010. Técnicas de caracterización mineral y su aplicación en exploración y explotación minera. *Boletín de la Sociedad Geológica Mexicana*, 62: 1-23.
- Michard, A. 1989. Rare earth element systematics in hydrothermal fluids.

- Geochimica et Cosmochimica Acta 53 (3-12): 745-750.
- Miroshnichenko, L.A. 1965. New data on distribution of indium in ore deposits of Central Kazakhstan. International Geology Review 7 (2-12): 233-240.
- Mitchell, A. H.G.; Garson, M. S. 1981. Mineral deposits and global tectonic settings. Academic Press, London.
- Mlynarczyk, M.; William-Jones, A. 2005. The role of collisional tectonics in the metallogeny of the Central Andean tin belt. Earth and Planetary Science Letters 240 (3-4): 656-667.
- Moëlo, Y.; Makovicky, E.; Mozgova, N.N.; Jambor, J.L.; Cook, N.; Pring, A.; Paar, W.; Nickel, E.H.; Graeser, S.; Karup-Møller, S.; Balic-Žunic, T.; Mumme, W.G.; Vurro, F.; Topa, D., Bindi, L.; Bente, K.; Shimizu, M. 2008. Sulfosalt systematics: a review. Report of the sulfosalt sub-committee of the IMA Commission on Ore Mineralogy. European Journal of Mineralogy 20: 7-46.
- Moh, G.H.; Berndt, F. 1964. Two new natural tin sulfides, Sn<sub>2</sub>S<sub>3</sub> and SnS<sub>2</sub>. Neues Jahrbuch für Mineralogie, Abhandlungen 3: 94-95.
- Morgan, G.B.; London, D.; Luedke, R.G. 1998. Petrochemistry of late Miocene peraluminous silicic volcanic rocks from the Morococala field, Bolivia. Journal of Petrology 39 (4-12): 601-632.
- Moura, M.A.; Botelho, N.F. Carvalho de Medonca, F. 2007. The indium-rich sulfides and rare arsenates of the Sn-In-mineralized Mangabeira A-type granite, Central Brazil. Canadian Mineralogist 45: 485-496.
- Moura, M.A.; Botelho, N.F.; Olivo, G.R.; Kyser, K.; Pontes, R.M. 2014. Genesis of the Proterozoic Mangabeira tin-indium mineralization, Central Brazil: Evidence from geology, petrology, fluid inclusion and stable isotope data. Ore Geology Review 60: 36-49.
- Murakami, H.; Ishihara, S. 2013. Trace elements of Indium-bearing sphalerite from tin-polymetallic deposits in Bolivia, China and Japan: A femto-second LA-ICPMS study. Ore Geology Reviews 53: 223-243.

- Murao, S.; Furuno, M. 1991. Roquesite from the Akenobe tin-polymetallic deposits, Southwest Japan. *Bulletin of the Geological Survey of Japan* 42 (1-12): 1-10.
- Murao, S., Deb, M., Furuno, M., 2008. Mineralogical evolution of indium in high grade tin-polymetallic hydrothermal veins—a comparative study from Tosham, Haryana state, India and Goka, Naegi district, Japan. *Ore Geology Reviews* 33 (3-4): 490-504.
- Neiva, A.M.R.; Silva, M.M.V.G.; Gomes, M.E.P.; Campos, T.F.C. 2002. Geochemistry of coexisting biotite and muscovite of Portuguese peraluminous granitic differentiation series. *Chemie der Erde - Geochemistry* 62 (3-4): 197-215.
- Ohmoto H., Rye, R.O. (1979): Isotopes of sulfur and carbon, en: Barnes, H.L. (ed.) *Geochemistry of Hydrothermal Ore Deposits*, 2nd ed. Willey, New York, pp 509–567.
- Ohmoto, H., 1986. Stable isotope geochemistry of ore deposits. In: *Stable isotopes in high temperature geological processes* (Valley, J.W.; Taylor, H.P.; O'Neil, J.R. Editors). *Mineralogical Society of America, Reviews in Mineralogy* 16: 491-599 p.
- Ohmoto H., Lasaga, A., (1982). Kinetics of reactions between aqueous sulfates and sulfides in hydrothermal systems. *Geochim Cosmochim. Acta* 46:1727–745
- Ohmoto, H.; Goldhaber, M.B. 1997. Sulfur and carbon isotopes. In: *Geochemistry of hydrothermal ore deposits* (Barnes, H.L, editor) third edition . John Wiley & Sons: 517–612 p. New York.
- Ohta, E., 1989. Occurrence and chemistry of indium-containing minerals from the Toyoha mine, Hokkaido, Japan. *Mining Geology* 39: 355-372.
- Pat Shanks, W.C. 2014. Stable Isotope Geochemistry of Mineral Deposits In: *Treatise on Geochemistry* (Turekian, H.D.; Holland, K.K.; Editors). Second edition Elsevier: 59-85 p. Oxford.
- Paterson, D. J.; Ohmoto, H.; Solomon, M. 1981. Geologic setting and genesis

- of cassiterite-sulfide mineralization at Renison Bell, western Tasmania. *Economic Geology* 76 (2-8): 393-438.
- Pavlova, G.G., Palessky, S.V., Borisenko, A.S., Vladimirov, A.G., Seifert, T., Phan, L.A., 2015. Indium in cassiterite and ores of tin deposits. *Ore Geology Reviews* 66: 99-113.
- Petruk, W. 1973. Tin sulphides from the deposit of Brunswick Tin Mines, Limited. *The Canadian Mineralogist* 12 (1-7): 46-54.
- Petruk, W.; Owens, D.R.; Stewart, J.M.; Murray, E.J. 1974. Observations on acanthite, aguilarite and naumannite. *The Canadian Mineralogist* 12 (6-7): 365-369.
- Pirajno, F. 2009. *Hydrothermal Processes and Mineral Systems*. Springer: 1250 p. Netherlands.
- Radelli, L. 1966. New data on tectonics of Bolivian Andes from a photograph by Gemini 5, and field knowledges: *Universite de Grenoble, Faculte des Sciences, Laboratoire de Geologie Travaux* (42): 237-261.
- Roedder, E. 1984. Fluid inclusions. *Reviews in mineralogy, Mineralogical Society of America* 12: 644p.
- Roedder, E.; Bodnar, R.J. 1997. Fluid inclusion studies of hydrothermal ore deposits. In: *Geochemistry of hydrothermal ore deposits* (Barnes, H.L. editor). Third edition John Wiley & Son: 657–697 p. New York.
- Rollinson, H. 1993. *Using geochemical data: evaluation, presentation, interpretation*. Longman Scientific & Technical, John Wiley & Sons: 352p. New York.
- Romer, R.L.; Meixner, A.; Förster, H.J. 2014. Lithium and boron in late-orogenic granites— isotopic fingerprints for the source of crustal melts? *Geochimica et Cosmochimica Acta* 131: 98-114.
- Rudnick, R.L.; Gao, S. 2014. Composition of the continental crust. In: *Treatise on Geochemistry* (Turekian, H.D.; Holland, K.K.; Editors). Second edition Elsevier: 1-64 p. Oxford.
- Schmitt, B. 1989. Pentagon report urges stockpiling of indium, rhodium,



- and ruthenium: American Metal Market, 97 (78): 1.
- Schwartz, M. O.; Rajah, S. S.; Askury, A. K.; Putthapiban, P., Djaswadi, S. 1995 The Southeast Asian tin belt. *Earth Sciences Review* 38 (2-4): 95-293.
- Schwarz-Schampera, U.; Herzig, P.M. 2002. Indium: Geology, Mineralogy and Economics. Springer-Verlag: 262 p. Heidelberg.
- Seal, R.R.; Essene, E.J.; Kelly, W.C. 1990. Tetrahedrite and tennantite: evaluation of thermodynamic data and phase equilibria. *The Canadian Mineralogist* 28 (4-4): 725-738.
- Sebrier, M., Soler, P. 1991. Tectonics and magmatism in the Peruvian Andes from late Oligocene time to the Present in *Andean Magmatism and Its Tectonic Setting* Geological Society of America Special paper (Harmon, R.S. and Rapela C.W. Editors) 265: 259-278.
- Seifert, T.; Sandmann, D. 2006. Mineralogy and geochemistry of indium-bearing polymetallic vein-type deposits: Implications for host minerals from the Freiberg district, Eastern Erzgebirge, Germany. *Ore Geology Reviews* 28 (1-4): 1-31.
- Serranti, S.; Ferrini, V.; Masi, U.; Cabri, L.J. 2002. Trace-element distribution in cassiterite and sulfides from Rubané and massive ores of the Corvo deposit, Portugal. *The Canadian Mineralogist* 40 (3-6): 815-835.
- Shcherba, G.N. 1970. Greisens. *International Geology Review* 12 (2-2): 114-150.
- Shimizu, M.; Kato, A.; Shiozawa, T. 1986. Sakuraiite: chemical composition and extent of (Zn,Fe)In-CuSn substitution. *The Canadian Mineralogist* 24 (2-4): 405-409.
- Shimizu, M.; Kato, A.; Matsuyama, F. 1998. Two Se-bearing Ag-Bi sulphosalts, benjaminite and matildite from the Ikuno Deposits, Hyogo Prefecture, Japan -Au-Ag mineralization in polymetallic Zone. *Resource Geology* 48 (2-4) 117-124.
- Sillitoe, R.H.; Halls, C.; Grant, J.N. 1975. Porphyry tin deposits in Bolivia. *Economic Geology* 70 (5-8): 913-927.

Sillitoe, R.H. 1976. Andean collisional peraluminous magmatism mineralization: a model for the in the Rhenohercynian Zone of SW metallogeny of convergent plate England. *Lithos* 260: 76-94. margins. Geological association of Canada special paper (14): 59-100. Sinclair, W.D.; Kooiman, G.; Martin, D.; Kjarsgaard, I.M. 2006. *Geology, geochemistry and mineralogy of indium resources at Mount Pleasant, New Brunswick, Canada. Ore Geology Reviews* 28 (1-3): 123-145.

Sillitoe, R.H. 1996. Granites and metal deposits. *Episodes Journal of International Geoscience* 19 (4-4): 126-133. Slattery, J.A. 1995. Indium and indium compounds, in encyclopedia of chemical technology (Kirk-Othmer editors) fourth edition John Wiley: (14) 155-160. New York.

Sillitoe, R.H.; Thompson, J.F.H. 1998. Intrusion-related vein gold deposits: types, tectono-magmatic settings and difficulties of distinction from orogenic gold deposits. *Resource Geology* 48 (4-4):237-250. Soler, P.; Bonhomme, M.G. 1990. Relation of magmatic activity to plate dynamics in central Peru from Late Cretaceous to present. In: *Plutonism from Antarctica to Alaska* (Kay, S.M. and Rapela, C.W., editors). Geological Society of America Special Paper 241: 173-192.

Simons, B.; Andersen, J.C.Ø.; Shail, R.K.; Jenner, F. 2017. Fractionation of Li, Be, Ga, Nb, Ta, In, Sn, Sb, W and Bi in the peraluminous Early Permian Variscan granites of the Cornubian Batholith: precursor processes to magmatic-hydrothermal mineralisation. *Lithos* (278-281): 491–512. Solomon, M.; Groves, D.I. 1994. The geology and origin of Australia's Mineral Deposits. *Oxford Monographs in Geology and Geophysics*, 24.

Simons, B.; Shail, R.K.; Andersen, J.C.Ø. 2016. The petrogenesis of the Early Permian Variscan granites of the Cornubian Batholith — lower plate post-

---

- Stepanov, A.S.; Hermann, J. 2013. Fractionation of Nb and Ta by biotite and phengite: implications for the "missing Nb paradox". *Geology* 41: 303-306.
- Sterner, S.M.; Hall, D.L.; Bodnar, R.J. 1988. Synthetic fluid inclusions. V. Solubility relations in the system NaCl-KCl-H<sub>2</sub>O under vapor-saturated conditions. *Geochimica et Cosmochimica Acta*, 52(5-12): 989-1005.
- Sugaki, A., Ueno, H., Shimada, N., Kitakaze, A.; Hayashi, K., Shima H., Sanjines, O.V., Saavedra A.M. 1981. Geological study on poly metallic hydrothermal deposits in the Oruro District Bolivia. *Science Reports of the Tohoku University III (XV-1)* 1-52.
- Sugaki, A.; Kitakaze, A.; Shima, H. 1982. Synthesis of cosalite and its phase relations in the Cu-Pb-Bi-S quaternary system. In *Crystal Chemistry of Minerals, Proceedings 13th General Meeting of the International Mineralogical Association*, 291-298. Varna, Germany.
- Sugaki, A.; Kojima, S.; Shimada, N. 1988. Fluid inclusion studies of the polymetallic hydrothermal ore deposits in Bolivia. *Mineralium Deposita* 23 (1-4): 9-15.
- Sugaki, A.; Shimada, N.; Ueno, H.; Kano, S. 2003. K-Ar Ages of Tin-Polymetallic Mineralization in the Oruro Mining District, Central Bolivian Tin Belt. *Resource Geology* 53: (4-4): 273-282.
- Sun S.S., McDonough W.F. 1989. Chemical and isotopic systematics of oceanic basalts: implications for mantle compositions and processes. *Geological Society, London, Special Publications* 42: 313-345.
- Taylor, R. G. 1979. *Geology of tin deposits*. Elsevier: 544p. Amsterdam.
- Taylor, J.R.; Wall, V.J. 1992. The behavior of tin in granitoid magmas. *Economic Geology* 87(2-8): 403-420.
- Taylor, S.R.; McLennan S.M. 1985. *The continental crust: its composition and evolution*. Springer: 312 p. Oxford.
- Thompson, J.F.H.; Sillitoe, R.H.; Baker, T.; Lang, J.R.; Mortensen, J.K. 1999. Intrusion-related gold deposits associated with tungsten-tin provinces. *Mineral Deposita* 34 (4-8): 323-334.

Thormann, W., Ljunggren, P., Virreira, M. 1966. Investigaciones preliminares sobre la geotectónica y metalogénesis de la zona Challapata-Caxata (Bolivia). Servicio Geológico de Bolivia 7: 118 p.

Tischendorf, G.; Förster, H.J.; Gottesmann, B. 2001. Minor and trace-element composition of trioctahedral micas: a review. *Mineralogical Magazine* 65 (2-6): 249-276.

Tolcin, A.C. 2016. Indium. In 2014 Minerals Yearbook. (Lee-Bray, E.; editor). United States Geological Survey: 35.1-35.7.

Tolcin, A.C. 2013. Indium (In). In U.S. Geological Survey, Metal prices in the United States through 2010. U.S. Geological Survey Scientific Investigations Report 204 p. available on-line at <http://pubs.usgs.gov/sir/2012/5188>.

Tomkins, A. G.; Mavrogenes, J. A. 2003. Generation of metal-rich felsic magmas during crustal anatexis. *Geology* 31 (9-12): 765-768.

Topa, D.; Makovicky, E. 2010. The crystal chemistry of cosalite based on new electron-microprobe data and single-crystal determinations of the structure. *The Canadian Mineralogist* 48 (5-6): 1081-1107.

Turekian, K.K.; Wedepohl, K.H. 1961. Distribution of the elements in some major units of the earth's crust. *Geological Society of America Bulletin* 72 (2-12): 175-192.

Turneure, F.S. 1960. A comparative study of major ore deposits of central Bolivia. *Economic Geology* 55 (2-8): 217-254.

Turner, J.W.G.; Hallewell, M.P. 1993. Process improvements for fine cassiterite recovery at Wheal Jane. *Mineral Engineering* 6 (8-10): 817-829.

Urabe, T. 1987. The effect of pressure on the partitioning ratios of lead and zinc between vapor and rhyolite melts. *Economic Geology* 82(4-8): 1049-1052.

U.S. Department of Energy (DOE). 2010. Critical Materials Strategy 166 p. available on-line at <https://energy.gov/>

---

sites/prod/files/edg/news/documents/criticalmaterialsstrategy.pdf

Valkama, M.; Sundblad, K.; Nygård, R.; Cook, N. 2016. Mineralogy and geochemistry of indium-bearing polymetallic veins in the Sarvlaxviken area, Lovisa, Finland. *Ore Geology Reviews* 75: 206-219.

Van den Kerkhof, A.M.; Hein, U.F. 2001. Fluid inclusion petrography. *Lithos* 55 (1-4): 27-47.

Van Kranendonk, M.J., Pirajno, F. 2004. Geochemistry of metabasalts and hydrothermal alteration zones associated with c. 3.45 Ga chert and barite deposits: implications for the geological setting of the Warrawoona Group, Pilbara Craton, Australia. *Geochemistry: Exploration, Environment, Analysis* 4 (3-4): 253-278.

Webster, J.D.; Kinzler, R.J.; Mathez, E.A. 1999. Chloride and water solubility in basalt and andesite melts and implications for magmatic degassing. *Geochimica et Cosmochimica Acta* 63 (5): 729-738.

Werner, T.T.; Mudd, G.M.; Jowitt, S.M. 2017. The world's by-product and critical metal resources part II: A method for quantifying the resources of rarely reported metals. *Ore Geology Reviews* 80: 658-675.

Wilkinson, J.J. 2001. Fluid inclusions in hydrothermal ore deposits. *Lithos* 55 (1-4):229–272.

Williams, T.B., Hyde, B.G. 1988. Electron microscopy of cylindrite and franckeite. *Physics and Chemistry of Minerals* 15 (6-6): 521-544.

William-Jones, A. E.; Heinrich, C. A. 2005. Vapor transport of metals and the formation of magmatic-hydrothermal ore deposits. *Economic Geology 100th Anniversary Volume*: 1287-1312.

#### Websites:

ActLab Ltd., 2017. 4Lithores - Lithium Metaborate/Tetraborate Fusion - ICP and ICP/MS (online) Available:

<http://www.actlabs.com/page.aspx?page=517&app=226&cat1=549&tp=12&lk=no&menu=64>

Indium. 2012. Chemicool Periodic Table. Chemicool.com. Web access: 3/14/2017 <<http://www.chemicool.com/elements/indium.html>>.

Tin. 2015. Chemicool Periodic Table. Chemicool.com. Web access: 6/6/2017 <<http://www.chemicool.com/elements/tin.html>>.



## APPENDIX 1

#	Sample	Depth (m)	Description
1	JAPO 1a	0	Massive sulfides with py, apy and cst in tailing
2	JAPO 2c	0	Alteration in ore zone
3	JAPO 2d	0	White alteration in ore zone
4	JAPO 2e	0	Yellow alteration in ore zone (adit)
5	JAPO 3a	0	Yellow alteration in ore zone (adit)
6	JAPO 3d	0	White alteration in ore zone
7	JAPO 4	0	Alteration in contact zone
8	JDC-06-001	Unknown	Vein
9	JDC-06-001	Unknown	Quartz vein with py and cts filling cavities
10	JDC-06-001	Unknown	Massive sulfides
11	JDC-06-001	Unknown	Quartz vein in intrusive rock
12	JDC-06-001	12	Massive sulfures
13	JDC-06-001	Unknown	Intrusive rock with silicification
14	JDC-06-001	Unknown	Vein
15	JDC-06-001	Unknown	Contact zone between sedimentary and intrusive rock
16	JDC-06-001	Unknown	Different vein generations
17	JDC-06-001	43	Sulfides and sulfosalts
18	JDC-06-001	43.8	Veins
19	JDC-06-001	46	Ore mineralization
20	JDC-06-001	50.7	Ore mineralization in breccia zone
21	JDC-06-001	59.3	Ore mineralization in breccia zone
22	JDC-06-001	68.2	Ore mineralization in breccia zone
23	JDC-06-001	79.6	Ore mineralization in breccia zone
24	JDC-06-001	80.6	Ore mineralization in breccia zone
25	JDC-06-001	111	Massive sulfides
26	JDC-06-001	116	Ore veins
27	JDC-06-001	42	Ore veins
28	JDC-05-006	81	Vein with cst and sulfides
29	JDC-05-006	210	Massive sulfides
30	JDC-06-001	265	Ore mineralization in breccia zone
31	JAPO 5	Unknown	Shear zone with Sn and sulfides, hosted in shale
32	JAPO 6	Mine	San Salvador level
33	JAPO 7	Unknown	Tailing
34	JAPO 8	30	" Gomez" vein with sphalerite and sulfosalts
35	JAPO 9	30	Stockwork
36	JAPO 10	30	Cassiterite(adit gate)
37	JAPO 11	30	Massive sulfides
38	JAPO 12	30	Vein N78°E/50°W
39	JAPO13	30	Dyke
40	JAPO 14	30	Shale
41	JDC-06-003	90	Shear zone with ore mineralizaion
42	JDC-06-002	22	Ore veins
43	JDC-06-003	118	Porphyritic stock with phenocrystals of feldespars
44	JDC-06-003	132	Ore vein
45	JDC-06-003	140	Vein with turmaline
46	JDC-06-003	146	Ore mineralization
47	JDC-06-002	105	Vein of 40 cm of thickness
48	JDC-06-002	60	Quartz vein woth ore mineralization
49	JD-2	Unknown	Shear zone with alteration
50	JDC-06-002	117	Sedimentary rock with dissemination
51	JDC-06-002	170	Shale with ore mineralization filling cavities




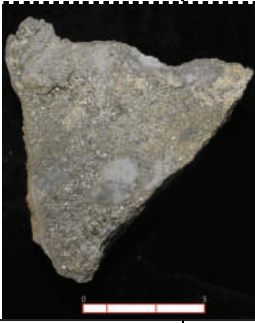


#	Sample	Depth (m)	Description
53	JDC-06-002	175	Vein in shale
54	JDC-06-002	250	Dike with veins and tourmaline crystals
55	JDC-05-007	39	ore mineralization
56	JDC-05-007	73	Sedimentary rock with dissemination
57	JDC-05-007	150	Quartz vein with massive sulfides
58	JAPO 7a	200	Shear zone with ore mineralization and alteration
59	JAPO 7b	Unknown	Alteration undermine
60	JDC-06-007	231	Porphyritic rock with sulfides reemplaced phenocrystals
61	JDC-06-007	252	Intrusive rock with massive sulfides veins of 2-3 cm of thickness
62	JDC-06-008	8	Shale with very fine dissemination (~5%)
63	JDC-06-008	50	Intrusive rock with massive sulfides veins of 2-3 cm of thickness
64	JDC-06-008	64	massive sulfides
65	JDC-06-008	113	Shear zone with ore mineralizaion
66	JDC-06-008	227	Meta-Greywacke with sulfides dissemination
67	JDC-06-016	22	Dicke
68	JDC-06-016	220	Veins in intrusive rock
69	JDC-06-016	177	Veins in intrusive rock
70	JDC-06-016	161	Mineralized intrusive rock and veins
71	JDC-06-016	139	Intrusive rock with massive sulfides veins of 2-3 cm of thickness
72	JDC-06-016	133	Vein in contact zone
73	JDC-06-016	76-78	Upper and lower contact
74	JDC-06-016	48	Ore vein
75	JDC-06-016	30	Contact zone
76	JDC-06-016	Unknown	Sedimentary rock with big rock fragment
77	JDC-06-015	15	Dyke
78	JDC-06-015	147	Massive sulfides
79	JDC-06-015	171	Shear zone with ore mineralizaion
80	JDC-06-015	44	Shear zone with ore mineralizaion
81	JDC-06-015	203	Shear zone with ore mineralizaion
82	JDC-06-015	261	Massive sulfides and cassiterite
83	JDC-06-015	271	Ore vein
84	JDC-06-012	12	Mineralization in breccia
85	JDC-06-012	2	Quartz vein
86	JDC-06-012	128	Quartz vein
87	JDC-06-012	225	Massive sulfides
88	JDC-05-23	270	Vein
89	JDC-05-23	229	Vein-shear with ore mineralizaion
90	JDC-05-23	105	Quartz vein with ore mineralization
91	JDC-05-23	76	Quartz vein with ore mineralization
92	JDC-05-23	43	Ore mineralization in contact between two meta-sedimentary rock
93	JDC-05-23	34	Host rock (barren)
94	JDC-05-22	187	Ore vein with chalcantite
95	JDC-06-22	190	Ore vein
96	JDC-06-22	180	Quartz vein
97	JDC-06-22	130	Very massive mineralization
98	JDC-06-22	109	Oxided breccia


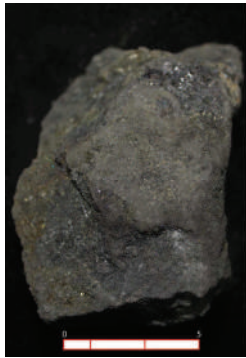


#	Sample	Depth (m)	Description
99	JDC-06-22	85	Dyke
100	JDC-06-22	10	Quartz vein
101	JDC-05-25	71	Quartz vein
102	JDC-05-25	68	Ore vein
103	JDC-05-25	23	Quartz vein
105	JDC-05-26	55-58	Sphalerite vein
106	JDC-06-34	228	Vein on galena with anomalous anisotropy
107	JDC-06-34	212	Vein on galena with anomalous anisotropy
108	JDC-06-34	208	Vein
109	JDC-06-34	210	Cst in alteration zone
110	JDC-06-34	86	Dyke
111	JDC-06-34	176	Intrusive rock with veins
112	JDC-06-34	163	Massive sulfides
113	JDC-06-34	105	Vein
114	JDC-06-34	40	Shale with sulfides dissemination
115	JDC-06-36	166	Shear zone with ore mineralizaion
116	JDC-06-36	100	Dyke in shale rock
117	JDC-06-36	72	Ore vein
118	JDC-06-36	69	Aplitic dyke
119	JDC-06-36	42	Sedimentary rock with bands
120	JDC-06-36	31	Ore vein
121	JDC-06-44	212	Porphyritic rock
122	JDC-06-44	223	Shear zone with ore mineralizaion
123	JDC-06-44	180	Sedimentary rock with bands
124	JDC-06-44	106	Sedimentary rock with bands
125	JDC-06-44	95	Silicified breccia
126	JDC-06-44	93	Breccia with mineralization
127	JP-1	Outcrop	Shale with sedimentary pyrite
128	JP-2	Unknown	Tailings
129	JP-3	Unknown	Concentate
130	JP-4	Unknown	Tailings
131	JP-5	Unknown	Final concentrate
132	JP-6	Outcrop	Dome
133	SPS-1	Outcrop	San Pablo stock
134	SPS-2	Outcrop	Tin mineralization in granite





## APPENDIX 1.

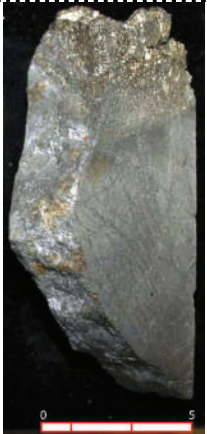
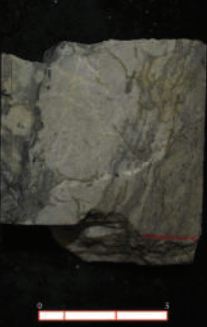


#	Sample	Depth (m)	Description
1	SFM-1	50	Rosario vein
2	SFM-2	50	"Venta nueva" vein
3	SFM-3	26	Ag vein
4	SFM-4	26	Zn vein
5	SFM-5	26	End of the Zn vein
6	SFM-6	26	Meta-Greywacke
7	ASF-1	Outcrop	Alteration tailings
8	ASF-2	Outcrop	Alteration tailings
9	ASF-3	Outcrop	Alteration tailings
10	ASF-4	50	Rosario vein
11	ASF-5	50	Rosario vein
12	SF-01	Outcrop	Tailing
13	SF-02	42-75	Underground vein
14	SF-03	26	Rosario Vein N40°E/65°NW
15	SF-04	26	Vein
16	SF-05	26	Vein
17	SF-06	26	Adit gate
18	SF-07	Unknown	Alteration
19	SF-08	26	Galena and sulfosalts
20	SF-09	26	Gn vein EW/N42°
21	SF-10	26	Gn and Ag veins
22	SF-11	50	Vein 70°/30°NW
23	SF-12	50	Vein with sulfosalts
24	SF-13	50	Vein with low ore grade
25	SF-14	50	Vein with high ore grade
26	SF-15	50	Stockwork and gypsum
27	SF-16	50	Gn and Ag veins in oxidation zone





#	Sample	Depth (m)	Description
1	MCC-1	160	"San Fco" level green alteration
2	MCC-2	160	Vein 222°
3	MCC-3	160	Vein 250° NE subvertical
4	MCC-4	160	Vein in the adit end 220°
5	MCC-5	160	Vein in the adit end
6	MCC-6	160	Same vein
7	MCC-7	160	Vein 218° subvertical
8	MCC-8	160	Sphalerite vein 86°
9	MCC-9	160	Vein parallel
10	MCC-10	160	Vein in the adit end
11	MCC-11	50	Before concentrate
12	MCC-12	50	Concentrate
13	MCC-13	50	White alteration
14	MCC-14	160	Concentrate 2
15	MCC-15	160	Sn vein "cuadro San Miguel"
16	MCC-16	160	Green and yellow alteration
17	MCC-17	160	White alteration
18	MCC-18	120	Vin 29° with white alteration and host-rock
19	MCC-19	26	Quartz vein with sulfides
20	MCC-20	26	Sphalerite vein 35°/70°E

HAND-SAMPLES DESCRIPTION OF THE JAPO DEPOSIT		
<b>JAPO 1</b>	<b>MASSIVE SULFIDES</b>	<i>Superficial</i>
<p>Massive sulfides with pyrite, arsenopyrite and cassiterite hosted in meta-sedimentary rock.</p>		
<b>JAPO 2</b>	<b>VEIN WITH MASSIVE SULFIDES</b>	<i>Superficial</i>
<p>Ore vein with massive sulfides.</p>		
<b>JAPO-05</b>	<b>SHEAR ZONE</b>	<i>Superficial</i>
<p>Shale with Sn-minerals and sulfides hosted in a shear zone. The rock shows several fractures.</p>		
<b>JAPO-06</b>	<b>QUARTZ VEIN</b>	<i>Undermine</i>
<p>Quartz vein with sulfides. Mostly, Pyrite and arsenopyrite.</p>		


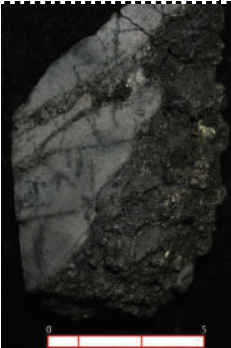
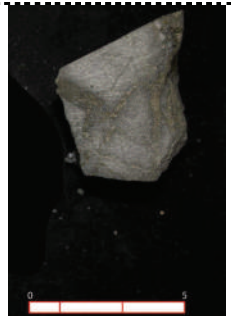

HAND-SAMPLES DESCRIPTION OF THE JAPO DEPOSIT		
<b>JAPO-07</b>	<b>HOST ROCK (BARREN)</b>	<i>Superficial</i>
Meta-sedimentary host rock without ore mineralization		
<b>JAPO-08</b>	<b>SPHALERITE VEIN WITH SULFOSALTS</b>	<i>Undermine</i>
Quartz vein with massive sulfides. Mostly sphalerite with sulfosalts.		
<b>JAPO-09</b>	<b>STOCKWORK</b>	<i>Undermine</i>
Stockwork with massive sulfides. Very alternated sample.		
<b>JAPO-10</b>	<b>HOST ROCK WITH ORE MINERALIZATION</b>	<i>Undermine</i>
Meta-sedimentary host rock with mostly cassiterite and sulfides.		





HAND-SAMPLES DESCRIPTION OF THE JAPO DEPOSIT		
<b>JAPO-11</b>	<b>MASSIVE SULFIDES</b>	<i>Undermine</i>
<p>Massive mineralization in altered meta-sedimentary rock.</p>		
<b>JAPO-12</b>	<b>QUARTZ VEIN</b>	<i>Undermine</i>
<p>Quartz vein with dissemination of sulfides. Very fractured.</p>		
<b>JAPO-14</b>	<b>SHALE</b>	<i>Undermine</i>
<p>Shale of fine-grained mainly composed of clay minerals.</p>		
<b>JDC-03-03 C-31</b>	<b>SHEAR ZONE</b>	<i>Drill-core</i>
<p>Shear zone with sulfide dissemination. Very altered.</p>		





HAND-SAMPLES DESCRIPTION OF THE JAPO DEPOSIT		
JDC-03-06 C-50	HOST ROCK WITH ORE MINERALIZATION	<i>Drill-core</i>
<p>Meta-sedimentary host-rock with ore mineralization infillings fractures.</p>		
JDC-05-07 C-14	HOST ROCK WITH ORE MINERALIZATION	<i>Drill-core</i>
<p>Meta-sedimentary host-rock with ore dissemination.</p>		
JDC-05-07 C-26	HOST ROCK WITH ORE MINERALIZATION	<i>Drill-core</i>
<p>Meta-sedimentary host-rock with massive ore mineralization.</p>		
JDC-05-23 C-13	QUARTZITE	<i>Drill-core</i>
<p>Quartzite apparently without ore mineralization.</p>		




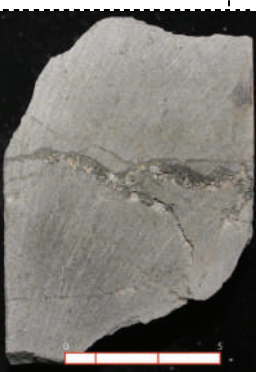
HAND-SAMPLES DESCRIPTION OF THE JAPO DEPOSIT		
<b>JDC-05-23 C-14</b>	<b>CONTACT ZONE</b>	<i>Drill-core</i>
<p>Ore mineralization in contact between shale and phyllite rock. Ore mineralization infillings fractures in two different directions, following lamination direction.</p>		
<b>JDC-05-23 C-24</b>	<b>HOST ROCK WITH ORE MINERALIZATION</b>	<i>Drill-core</i>
<p>Meta-sedimentary host-rock with massive sulfides mineralization infillings fractures.</p>		
<b>JDC-05-23 C-26</b>	<b>BRECCIA</b>	<i>Drill-core</i>
<p>Breccia-vein cemented by quartz without ore mineralization</p>		
<b>JDC-05-23 C-100</b>	<b>HOST ROCK WITH ORE MINERALIZATION</b>	<i>Drill-core</i>
<p>Meta-sedimentary host-rock with ore dissemination.</p>		

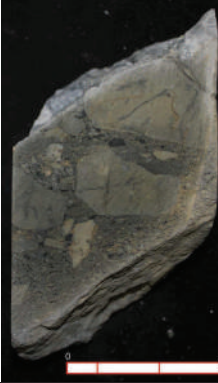


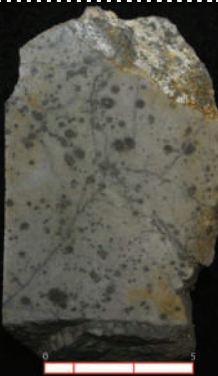



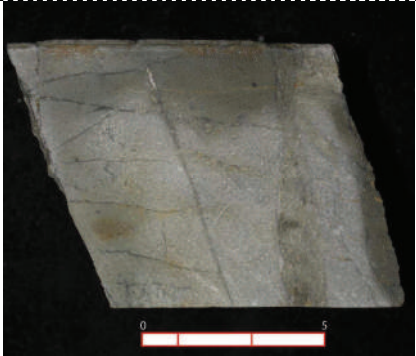

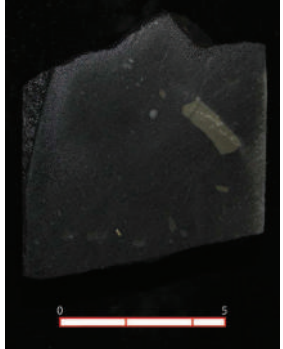
HAND-SAMPLES DESCRIPTION OF THE JAPO DEPOSIT		
JDC-05-25 C-04	<b>BRECCIA</b>	<i>Drill-core</i>
Breccia-vein cemented by quartz without ore mineralization		
JDC-05-25 C-24	<b>QUARTZ VEIN</b>	<i>Drill-core</i>
Very fractured quartz vein with dissemination of sulfides.		
JDC-06-01 C-1	<b>QUARTZITE WITH ORE MINERALIZATION</b>	<i>Drill-core</i>
Quartzite with sulfides mineralization infillings fractures.		
JDC-06-01 C-3	<b>HOST ROCK WITH ORE MINERALIZATION</b>	<i>Drill-core</i>
Meta-sedimentary host-rock with massive sulfides mineralization.		





HAND-SAMPLES DESCRIPTION OF THE JAPO DEPOSIT		
<b>JDC-06-01 C-7</b>	<b>HOST ROCK WITH ORE MINERALIZATION</b>	<i>Drill-core</i>
Meta-sedimentary host-rock with ore dissemination.		
<b>JDC-06-01 C-12</b>	<b>HOST ROCK WITH ORE MINERALIZATION</b>	<i>Drill-core</i>
Meta-sedimentary host-rock with ore dissemination.		
<b>JDC-06-01 C-13</b>	<b>SHEAR ZONE</b>	<i>Drill-core</i>
Shear zone with sulfide dissemination. Very altered.		
<b>JDC-06-01 C-15</b>	<b>HOST ROCK WITH ORE MINERALIZATION</b>	<i>Drill-core</i>
Meta-sedimentary host-rock with dissemination of sulfides and sulfosalts		




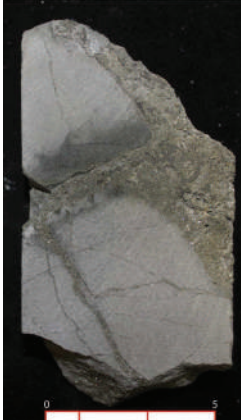
HAND-SAMPLES DESCRIPTION OF THE JAPO DEPOSIT		
<b>JDC-06-01 C-16</b>	<b>MASSIVE SULFIDES</b>	<i>Drill-core</i>
Massive sulfides with pyrite, arsenopyrite and cassiterite hosted in meta-sedimentary rock.		
<b>JDC-06-01 C-17</b>	<b>BRECCIA</b>	<i>Drill-core</i>
Breccia-vein cemented by quartz without ore mineralization		
HAND-SAMPLES DESCRIPTION OF THE JAPO DEPOSIT		
<b>JDC-06-01 C-21</b>	<b>BRECCIA</b>	<i>Drill-core</i>
Breccia cemented by quartz with ore mineralization		
<b>JDC-06-01 C-24</b>	<b>BRECCIA</b>	<i>Drill-core</i>
Ore mineralization in breccia zone		

HAND-SAMPLES DESCRIPTION OF THE JAPO DEPOSIT		
JDC-06-01 C-31	<b>MASSIVE SULFIDES</b>	<i>Drill-core</i>
<p>Massive sulfides with pyrite, arsenopyrite and cassiterite hosted in meta-sedimentary rock.</p>		
JDC-06-01 C-38	<b>HOST ROCK WITH ORE MINERALIZATION</b>	<i>Drill-core</i>
<p>Meta-sedimentary host-rock with ore mineralization in fractures.</p>		
JDC-06-01 C-40	<b>QUARTZITE WITH ORE MINERALIZATION</b>	<i>Drill-core</i>
<p>Quartzite with sulfides mineralization infillings fractures</p>		
JDC-06-01 C-42	<b>QUARTZITE WITH ORE MINERALIZATION</b>	<i>Drill-core</i>
<p>Quartzite with massive sulfides mineralization infillings fractures</p>		





HAND-SAMPLES DESCRIPTION OF THE JAPO DEPOSIT		
<b>JDC-06-01 C-92</b>	<b>BRECCIA</b>	<i>Drill-core</i>
Breccia cemented by quartz without ore mineralization		
<b>JDC-06-02 C-8</b>	<b>HOST ROCK WITH ORE MINERALIZATION</b>	<i>Drill-core</i>
Meta-sedimentary host-rock with ore dissemination.		
<b>JDC-06-02 C-38</b>	<b>HOST ROCK WITH ORE MINERALIZATION</b>	<i>Drill-core</i>
Meta-sedimentary host-rock with massive sulfides mineralization infillings fractures		
<b>JDC-06-02 C-42</b>	<b>META-GREYWACKE WITH ORE DISSEMINATION</b>	<i>Drill-core</i>
Meta-greywacke with sulfides dissemination		

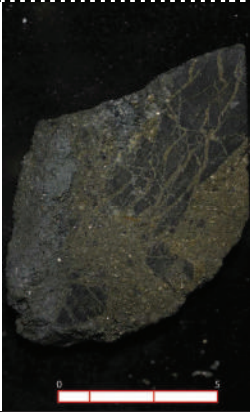


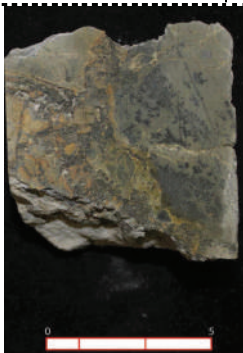
HAND-SAMPLES DESCRIPTION OF THE JAPO DEPOSIT		
JDC-06-02 C-61	HOST ROCK	<i>Drill-core</i>
<p>Meta-sedimentary host-rock apparently without ore mineralization.</p>		
JDC-06-02 C-90	HOST ROCK WITH VEINS	<i>Drill-core</i>
<p>Meta-sedimentary host-rock apparently with tourmaline infilling very fine veins.</p>		
JDC-06-03 C-33	MASSIVE SULFIDES	<i>Drill-core</i>
<p>Massive sulfides and cassiterite hosted in meta-sedimentary rock.</p>		
JDC-06-03 C-41	HOST ROCK (BARREN)	<i>Drill-core</i>
<p>Meta-sedimentary host-rock apparently without ore mineralization.</p>		





HAND-SAMPLES DESCRIPTION OF THE JAPO DEPOSIT		
JDC-06-03 C-45	<b>VEIN WITH MASSIVE SULFIDES</b>	<i>Drill-core</i>
Ore vein with massive sulfides.		
JDC-06-03 C-48	<b>HOST ROCK (BARREN)</b>	<i>Drill-core</i>
Meta-sedimentary host-rock apparently without ore mineralization.		
JDC-06-06 C-28	<b>SHEAR ZONE</b>	<i>Drill-core</i>
Vein with cassiterite and sulfides		
JDC-06-06 C-75	<b>HOST ROCK WITH ORE MINERALIZATION</b>	<i>Drill-core</i>
Massive sulfides and cassiterite hosted in meta-sedimentary rock.		

HAND-SAMPLES DESCRIPTION OF THE JAPO DEPOSIT		
<b>JDC-06-07 C-84</b>	<b>META-GREYWACKE WITH ORE DISSEMINATION</b>	<i>Drill-core</i>
Meta-greywacke dissemination	with sulfides	
<b>JDC-06-07 C-92</b>	<b>META-GREYWACKE WITH ORE MINERALIZATION</b>	<i>Drill-core</i>
Meta-greywacke mineralization in veins	with massive	
<b>JDC-06-08 C-3</b>	<b>META-GREYWACKE WITH ORE DISSEMINATION</b>	<i>Drill-core</i>
Meta-greywacke mineralization in micro-veins	with very fine	
<b>JDC-06-08 C-17</b>	<b>META-GREYWACKE WITH ORE MINERALIZATION</b>	<i>Drill-core</i>
Meta-greywacke mineralization in quartz veins	with massive	



HAND-SAMPLES DESCRIPTION OF THE JAPO DEPOSIT		
<b>JDC-06-08 C-24</b>	<b>META-GREYWACKE WITH MASSIVE SULFIDES</b>	<i>Drill-core</i>
Meta-greywacke with massive mineralization.		
<b>JDC-06-08 C-40</b>	<b>SHEAR ZONE</b>	<i>Drill-core</i>
Shear zone with massive sulfide mineralization. Very altered.		
<b>JDC-06-08 C-82</b>	<b>META-GREYWACKE WITH SULFIDES DISSEMINATION</b>	<i>Drill-core</i>
Meta-Greywacke with sulfides dissemination and pyrolusite.		
<b>JDC-06-12 C-9</b>	<b>BRECCIA</b>	<i>Drill-core</i>
Mineralization in breccia		

HAND-SAMPLES DESCRIPTION OF THE JAPO DEPOSIT		
<b>JDC-06-12 C-78</b>	<b>MASSIVE SULFIDES</b>	<i>Drill-core</i>
Massive sulfides with pyrite, arsenopyrite and cassiterite hosted in meta-sedimentary rock.		
HAND-SAMPLES DESCRIPTION OF THE JAPO DEPOSIT		
<b>JDC-06-15 C-10</b>	<b>META-GREYWACKE WITH ORE DISSEMINATION</b>	<i>Drill-core</i>
Meta-greywacke with sulfides dissemination and micro-veins.		
<b>JDC-06-15 C-53</b>	<b>MASSIVE SULFIDES</b>	<i>Drill-core</i>
Massive sulfides with pyrite, arsenopyrite and cassiterite hosted in meta-sedimentary rock.		
<b>JDC-06-15 C-62</b>	<b>BRECCIA</b>	<i>Drill-core</i>
Breccia cemented by quartz without ore mineralization.		

HAND-SAMPLES DESCRIPTION OF THE JAPO DEPOSIT		
JDC-06-15 C-74	<b>MASSIVE SULFIDES</b>	<i>Drill-core</i>
<p>Massive sulfides with pyrite, arsenopyrite and cassiterite hosted in meta-sedimentary rock.</p>		
JDC-06-15 C-95	<b>HOST ROCK WITH ORE MINERALIZATION</b>	<i>Drill-core</i>
<p>Cassiterite and bornite dissemination in meta-sedimentary rock.</p>		
JDC-06-15 C-99	<b>SHEAR ZONE</b>	<i>Drill-core</i>
<p>Shear zone with sulfide mineralization.</p>		
JDC-06-16 C-8	<b>APLITIC DYKE</b>	<i>Drill-core</i>
<p>Intrusive rock with quartz and feldspar in a fine matrix.</p>		

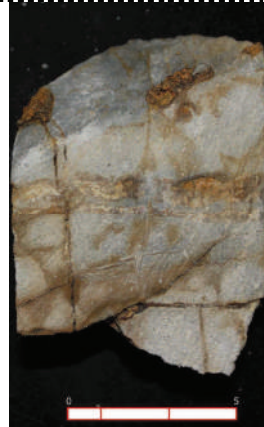
HAND-SAMPLES DESCRIPTION OF THE JAPO DEPOSIT

JDC-06-16 C-11

CONTACT ZONE

Drill-core

Contact between two meta-sedimentary rocks



JDC-06-16 C-8

SHEAR ZONE

Drill-core

Vein in shear zone with massive sulfide mineralization.

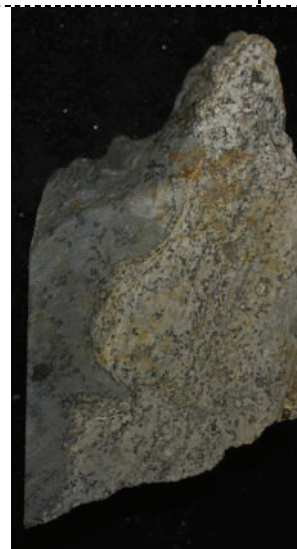






JDC-06-16 C-28

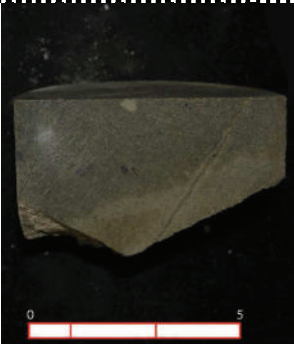


CONTACT ZONE

Drill-core





Contact between two meta-sedimentary rocks



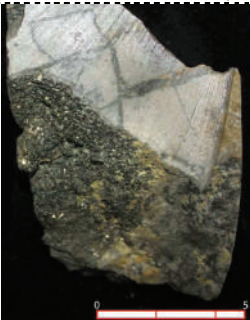


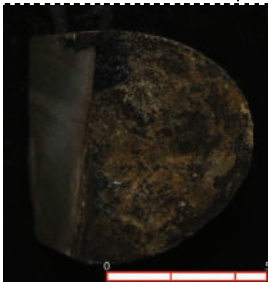
HAND-SAMPLES DESCRIPTION OF THE JAPO DEPOSIT		
JDC-06-16 C-49	<b>HOST ROCK WITH ORE MINERALIZATION</b>	<i>Drill-core</i>
Meta-sedimentary host-rock with ore vein.		
JDC-06-16 C-52	<b>HOST ROCK WITH ORE DISSEMINATION</b>	<i>Drill-core</i>
Meta-sedimentary host-rock without ore mineralization.		
JDC-06-16 C-53	<b>VEIN WITH SULFIDES AND TOURMALINE</b>	<i>Drill-core</i>
Meta-sedimentary host-rock with ore vein and tourmaline.		
JDC-06-16 C-59	<b>HOST ROCK WITH ORE MINERALIZATION</b>	<i>Drill-core</i>
Meta-sedimentary host-rock with ore mineralization infillings fractures.		


HAND-SAMPLES DESCRIPTION OF THE JAPO DEPOSIT		
JDC-06-16 C-65	CONTACT ZONE	<i>Drill-core</i>
<p>Contact between two meta-sedimentary rocks and micro-veins</p>		
JDC-06-16 C-69	HOST ROCK WITH ORE DISSEMINATION	<i>Drill-core</i>
<p>Meta-sedimentary rock with big rock fragment and micro-vein of sulfides (mostly pyrite). Alteration in the vein zone.</p>		
JDC-06-16 C-83	CONTACT ZONE	<i>Drill-core</i>
<p>Contact between two meta-sedimentary rocks</p>		

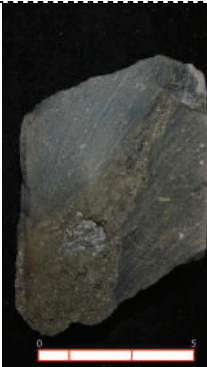

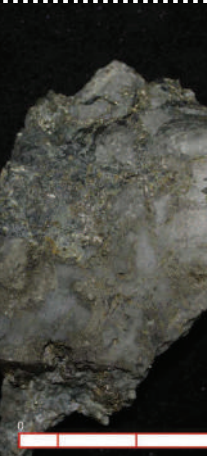
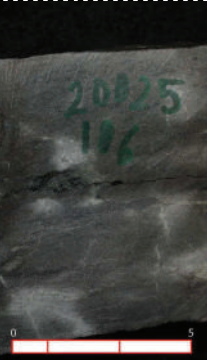
HAND-SAMPLES DESCRIPTION OF THE JAPO DEPOSIT		
JDC-06-22 C-28	<b>PORPHYRITIC ROCK</b>	<i>Drill-core</i>
Intrusive acid rock with porphyritic texture		
JDC-06-22 C-44	<b>MASSIVE SULFIDES</b>	<i>Drill-core</i>
Massive sulfides with pyrite, arsenopyrite and cassiterite hosted in meta-sedimentary rock.		
JDC-06-22 C-65	<b>VEIN WITH MASSIVE SULFIDES</b>	<i>Drill-core</i>
Ore vein with massive sulfides in meta-sedimentary host rock.		
JDC-06-34 C-12	<b>HOST ROCK (BARREN)</b>	<i>Drill-core</i>
Meta-sedimentary rock with a big rock fragment.		




HAND-SAMPLES DESCRIPTION OF THE JAPO DEPOSIT		
<b>JDC-06-34 C-35</b>	<b>VEIN IN ALTERED HOST ROCK</b>	<i>Drill-core</i>
<p>Mineralization in altered meta-sedimentary rock.</p>		
<b>JDC-06-34 C-57</b>	<b>MASSIVE SULFIDES</b>	<i>Drill-core</i>
<p>Massive sulfides with pyrite, arsenopyrite and cassiterite hosted in meta-sedimentary rock.</p>		
<b>JDC-06-34 C-61</b>	<b>QUARTZITE</b>	<i>Drill-core</i>
<p>Quartzite with sulfides mineralization infillings fractures</p>		
<b>JDC-06-34 C-65</b>	<b>HOST ROCK (BARREN)</b>	<i>Drill-core</i>
<p>Meta-sedimentary rock with a rock fragment of quartzite.</p>		




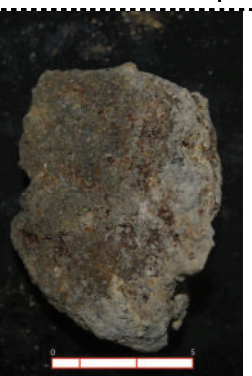






HAND-SAMPLES DESCRIPTION OF THE JAPO DEPOSIT		
<b>JDC-06-34 C-73</b>	<b>HOST ROCK WITH ORE MINERALIZATION</b>	<i>Drill-core</i>
Meta-sedimentary host-rock with ore vein and tourmaline infilling very fine veins.		
HAND-SAMPLES DESCRIPTION OF THE JAPO DEPOSIT		
<b>JDC-06-34 C-74</b>	<b>SHALE WITH MICRO-VEINS</b>	<i>Drill-core</i>
Shale with very fine mineralization (mostly pyrite) in micro-veins		
<b>JDC-06-34 C-75</b>	<b>SHALE (BARREN)</b>	<i>Drill-core</i>
Shale of fine-grained mainly composed of clay minerals.		
<b>JDC-06-34 C-80</b>	<b>SHALE</b>	<i>Drill-core</i>
Shale with vein of cassiterite and tourmaline.		




HAND-SAMPLES DESCRIPTION OF THE JAPO DEPOSIT		
<b>JDC-06-36 C-5</b>	<b>APLITIC DYKE</b>	<i>Drill-core</i>
<p>Intrusive rock with quartz and feldspar in a fine matrix.</p>		
<b>JDC-06-36 C-12</b>	<b>HOST ROCK WITH ORE MINERALIZATION</b>	<i>Drill-core</i>
<p>Meta-sedimentary host-rock with ore vein,</p>		
<b>JDC-06-36 C-15</b>	<b>HOST ROCK WITH BANDS</b>	<i>Drill-core</i>
<p>Meta-sedimentary rock with bands and faults.</p>		
<b>JDC-06-36 C-36</b>	<b>CONTACT ZONE</b>	<i>Drill-core</i>
<p>Contact between two meta-sedimentary rocks</p>		

HAND-SAMPLES DESCRIPTION OF THE JAPO DEPOSIT		
JDC-06-36 C-60	<b>HOST ROCK WITH ORE MINERALIZATION</b>	<i>Drill-core</i>
<p>Meta-sedimentary host-rock with ore mineralization infilling fractures.</p>		
JDC-06-44 C-78	<b>SHEAR ZONE</b>	<i>Drill-core</i>
<p>Shear zone with massive sulfide mineralization.</p>		
JDC-06-44 C-32	<b>VEIN WITH MASSIVE SULFIDES</b>	<i>Drill-core</i>
<p>Quartz vein with massive sulfides in meta-sedimentary host rock.</p>		
JDC-06-44 C-37	<b>SHALE (BARREN)</b>	<i>Drill-core</i>
<p>Shale of fine-grained mainly composed of clay minerals.</p>		

HAND-SAMPLES DESCRIPTION OF THE JAPO DEPOSIT		
JDC-06-44 C-63	VEINS	<i>Drill-core</i>
<p>Different generations of vein. Para and post mineralization.</p>		
JDC-06-44 C-75	META-GREYWACKE WITH ORE DISSEMINATION	<i>Drill-core</i>
<p>Meta-greywacke with sulfides dissemination</p>		
HAND-SAMPLES DESCRIPTION OF THE SANTA FE DEPOSIT		
SF-01	QUARTZ VEIN	<i>Undermine</i>
<p>Quartz vein with sulfides. Mostly, Galena, pyrite and arsenopyrite.</p>		

HAND-SAMPLES DESCRIPTION OF THE SANTA FE DEPOSIT		
SF-02	RIOLITE (BARREN)	<i>Superficial</i>
<p>Extrusive igneous rock. Riolitic lava flow with phenocrysts of quartz, glass, plagioclase, k-feldspar and mica (mostly biotite)</p>		
SF-03	SPHALERITE VEIN WITH SULFOSALTS	<i>Undermine</i>
<p>Quartz vein with massive sulfides. Mostly sphalerite with sulfosalts.</p>		
SF-04	QUARTZ VEIN	<i>Undermine</i>
<p>Quartz vein with sulfides. Mostly, Galena, pyrite and arsenopyrite.</p>		
SF-05	QUARTZ VEIN	<i>Undermine</i>
<p>Quartz vein with sulfides. Mostly, Galena, pyrite and arsenopyrite in bands.</p>		

HAND-SAMPLES DESCRIPTION OF THE SANTA FE DEPOSIT		
SF-08	MASSIVE SULFIDES	<i>Undermine</i>
<p>Massive mineralization (mostly galena) in meta-sedimentary host-rock.</p>		
HAND-SAMPLES DESCRIPTION OF THE SANTA FE DEPOSIT		
SF-09	SULFIDES DISSEMINATION	<i>Undermine</i>
<p>Dissemination of ore mineralization (mostly galena) in meta-sedimentary host-rock.</p>		
SF-11	MASSIVE SULFIDES	<i>Undermine</i>
<p>Massive mineralization (mostly galena and sphalerite) in meta-sedimentary host-rock.</p>		
SF-12	QUARTZ VEIN	<i>Undermine</i>
<p>Quartz vein with sulfides. Mostly, Galena, pyrite and arsenopyrite.</p>		

HAND-SAMPLES DESCRIPTION OF THE SANTA FE DEPOSIT		
<b>SF-13</b>	<b>SHEAR ZONE</b>	<i>Undermine</i>
Shear zone with sulfide dissemination. Very altered.		
<b>SF-14</b>	<b>QUARTZ VEIN</b>	<i>Undermine</i>
Quartz vein with sulfides of Galena, sphalerite, pyrite and arsenopyrite in bands.		
<b>SF-15</b>	<b>HOST ROCK WITH ORE MINERALIZATION</b>	<i>Undermine</i>
Meta-sedimentary host-rock with ore mineralization infillings fractures.		

## APPENDIX 2

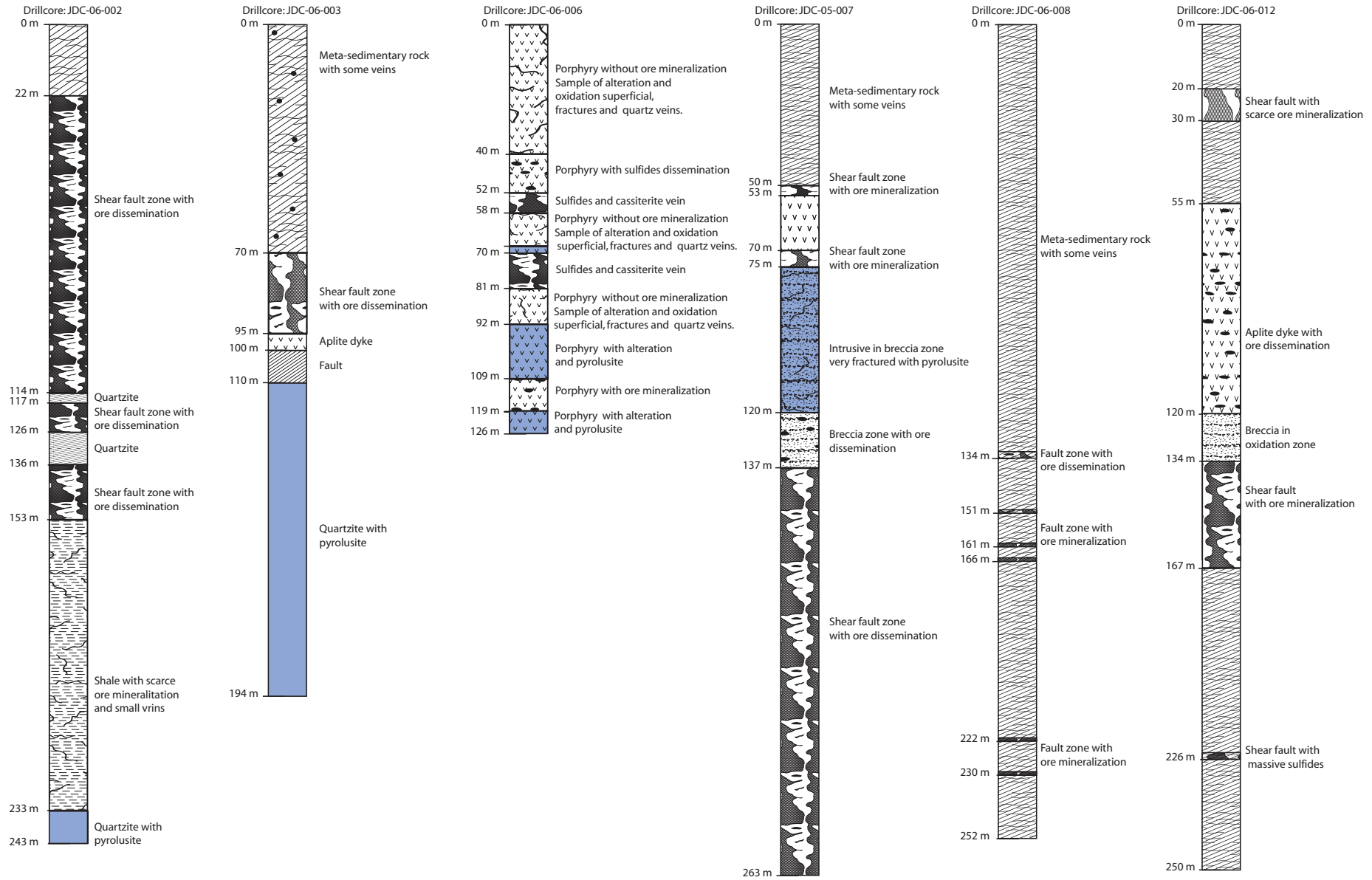
Appendix 2- It should be noted that despite being available it was not possible to log several drill-cores because was impossible to have access to them; in other cases, the drill-holes were no longer found

Table of the drill-hole

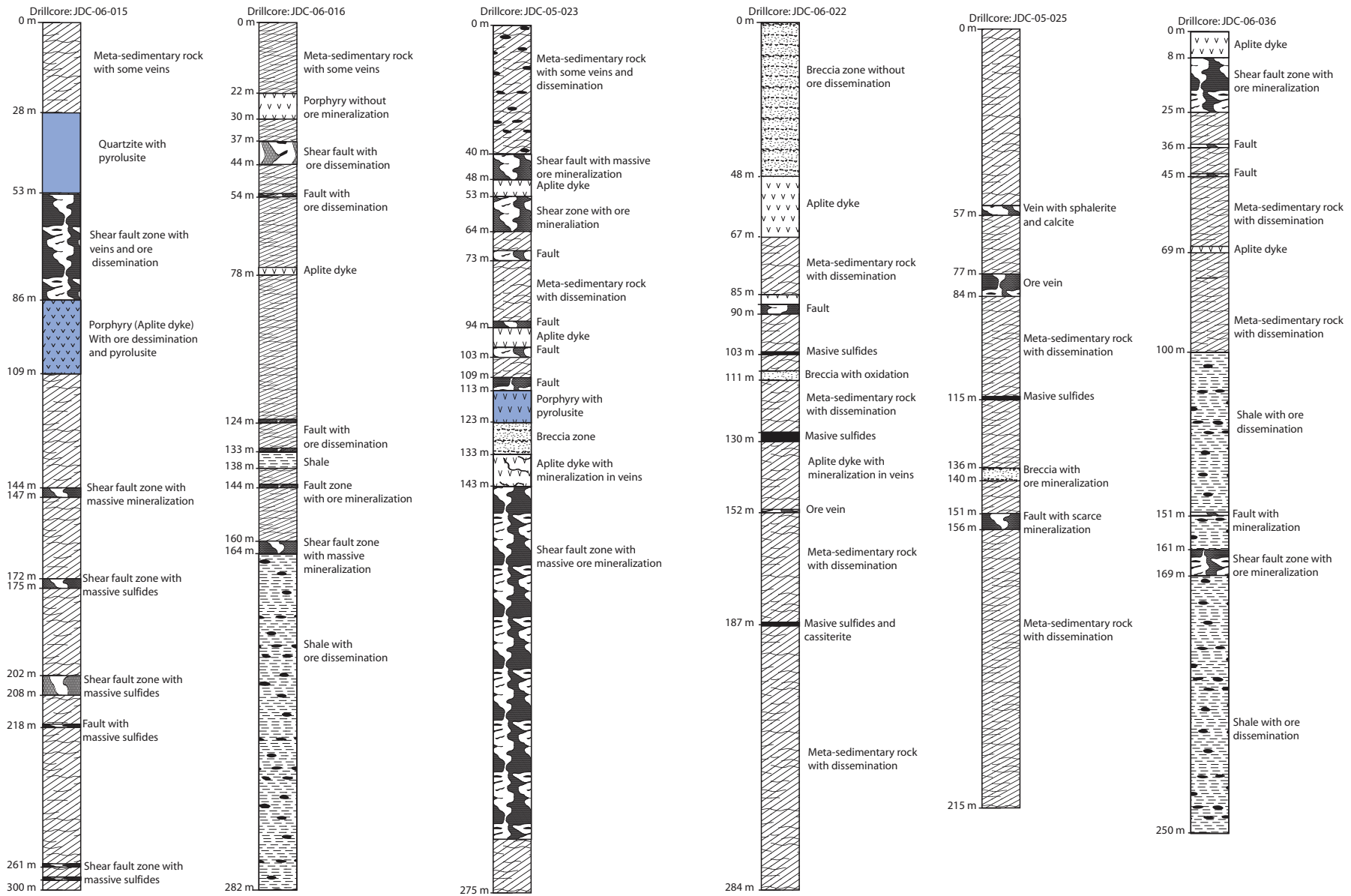
Drill hole	Observations	Drill hole	Observations
JDC-06-001	Inaccessible	JDC-06-023	OK
JDC-06-002	OK	JDC-06-024	Not exists
JDC-06-003	OK	JDC-06-025	OK
JDC-06-004	Inaccessible	JDC-06-026	Inaccessible
JDC-06-005	Inaccessible	JDC-06-027	Inaccessible
JDC-06-006	OK	JDC-06-028	Not exists
JDC-06-007	OK	JDC-06-029	Inaccessible
JDC-06-008	OK	JDC-06-030	Not exists
JDC-06-009	Inaccessible	JDC-06-031	Not exists
JDC-06-010	Inaccessible	JDC-06-032	Not exists
JDC-06-011	Inaccessible	JDC-06-033	Not exists
JDC-06-012	OK	JDC-06-034	Incomplete
JDC-06-013	Not exists	JDC-06-035	Inaccessible
JDC-06-014	Not exists	JDC-06-036	OK
JDC-06-015	OK	JDC-06-037	Inaccessible
JDC-06-016	OK	JDC-06-038	Inaccessible
JDC-06-017	Not exists	JDC-06-039	Inaccessible
JDC-06-018	Not exists	JDC-06-040	Inaccessible
JDC-06-019	Inaccessible	JDC-06-041	Inaccessible
JDC-06-020	Inaccessible	JDC-06-042	Inaccessible
JDC-06-021	Not exists	JDC-06-043	Inaccessible
JDC-06-022	OK	JDC-06-044	Incomplete



APPENDIX 2.



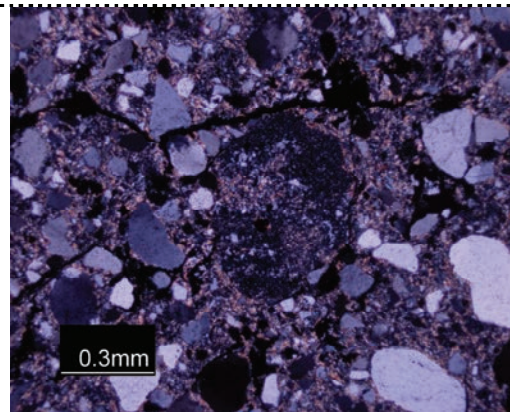
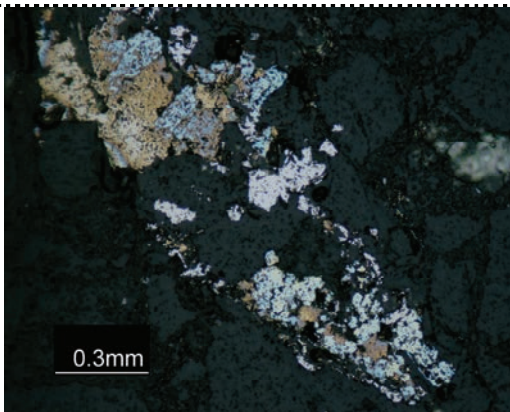
APPENDIX 2.





## APPENDIX 3

<b>B-00</b>	<b>QUARTZITE</b>
<b>METALLIC</b>	Mostly pyrite
<b>NO METALLIC</b>	<i>Essentials:</i> quartz, feldspar, rock fragment. <i>Accessories:</i> chlorite, epidote, micas, sillimanite, augite, hornblende.
<b>MODE</b>	Qtz 50 %; Fds 10 %; Lit 5 %; Matrix: 35 %
<b>TEXTURE</b>	Phanerocrystalline (250 $\mu\text{m}$ – 1 mm), granular, Madura, poorly graded.

**DESCRIPTION**

None foliated metamorphic rock composed almost entirely of quartz.

Quartz is the majority mineral; it is colorless with gray interference colors of the first order. The grain size ranging from some millimeters to 100  $\mu\text{m}$ , heterogeneous rounding, from sub-rounded to sub-angular, some crystals have overgrown apparently from the silica matrix, with very irregular edges, and other crystals show engulfed morphologies, characteristic of volcanic. Most of the crystals present parallel extinction, however, in some crystals it is observed undulating extinction. Some crystals have inclusions of tabular crystals (micas?) and zircon.

K-feldspar crystals are scarce, present anhedral form, irregular, rounded, of micrometric size ( $\sim 500 \mu\text{m}$ ), with edges of overgrowth, usually present twinning.

Matrix is clayey, cryptocrystalline, altered and metamorphosed. It is composed of some crystals of micas, sillimanite, chlorite and epidote, a slight alignment in the crystals is evident, product of metamorphism.

Sillimanite is widely distributed in the matrix. Generally, in entangled sections surrounding quartz and feldspar crystals, it presents first order yellow-brown interference colors and moderate relief.

Micas in some sectors are shown alignment, in other cases without preferential order, the interference colors are red to blue of first and second order. The maximum size is 2 mm in the

-----  
elongation direction.

Chlorite is arranged in well-defined crystals of micas that have been altered. It presents green pleochroism very evident, relief medium to high.

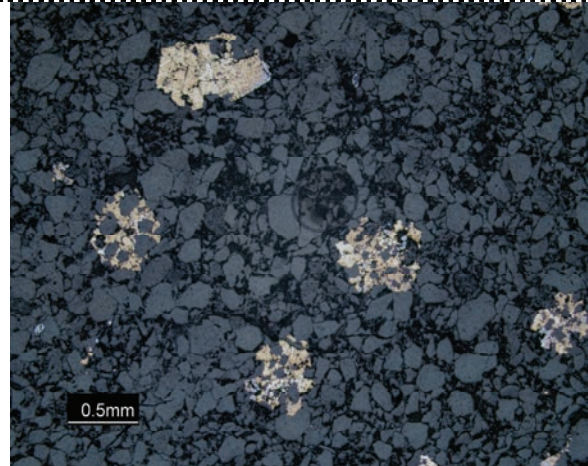
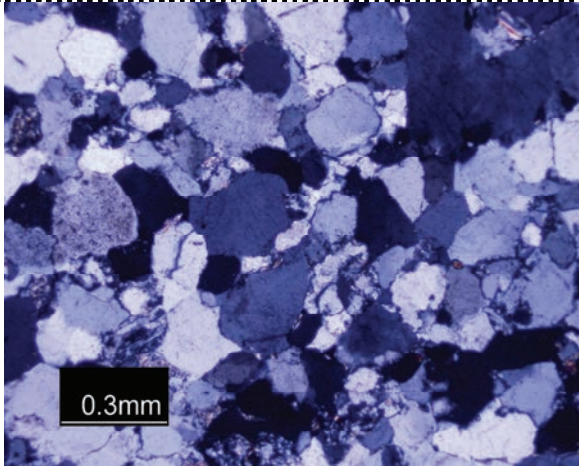
Epidote crystals are interceded with metallic mineralization and quartz in veinlets. They are rectangular crystals of 100 to 50  $\mu\text{m}$  in the cross-section, with moderate relief and interference colors of 3rd order.

Hornblende occurs very occasionally (<1%) with high relief, green pleochroism very evident and cleavage at  $120^\circ$ .

Rock fragments are scarce, composed of quartz and feldspars, with very irregular edges and sometimes difficult to appreciate, the sizes are  $\sim 500 \mu\text{m}$ .

---

<b>B-01</b>	<b>META-GREYWACKE OF QUARTZ WITH SULFIDES DISSEMINATION</b>
<b>METALLIC</b>	Mostly pyrite 10%
<b>NO METALLIC</b>	<i>Essentials:</i> quartz, feldspar, rock fragment. <i>Accessories:</i> chlorite, epidote, micas, sillimanite, augite, hornblende.
<b>MODE</b>	Qtz 35 %; Fds 25 %; Lit 10 %; Matrix: 20 %
<b>TEXTURE</b>	Phanerocrystalline (250 $\mu\text{m}$ – 1 mm), granular, mature, poorly graded.



## DESCRIPTION

Sedimentary rock affected by a moderate metamorphism, grain size of fine sand, supported by an altered cryptocrystalline matrix, micas and sillimanite.

Quartz is the majority mineral; it is colorless with gray interference colors of first order. Size grains varies from some millimeters to 700  $\mu\text{m}$ , rounding is heterogeneous, from sub-rounded to sub-angular, very irregular edges and some engulfed crystals, some crystals have overgrown apparently from the silica matrix, with very irregular edges. Most of the crystals present parallel extinction; however, in some crystals there is undulating extinction, which may indicate volcanic and metamorphic origin.

K-feldspars and plagioclase are both anhedral crystals and in irregular, rounded, irregular, rounded, idiomorphic sections of micrometric size ( $\sim 500 \mu\text{m}$ ), as in quartz crystals with overgrowth edges.

Matrix is clayey, cryptocrystalline, altered and metamorphosed. It is composed of some crystals of micas, sillimanite, chlorite and epidote, crystals are slight alignment by low metamorphism.

Sillimanite is widely distributed in the matrix. Generally, in entangled sections surrounding quartz and feldspar crystals, it presents first order yellow-brown interference colors and moderate relief.

Micas in some sectors are aligned, in other cases without preferential order, the interference colors are red to blue of first and second order. Maximum size of the crystals is 2 mm in the

-----  
elongation direction.

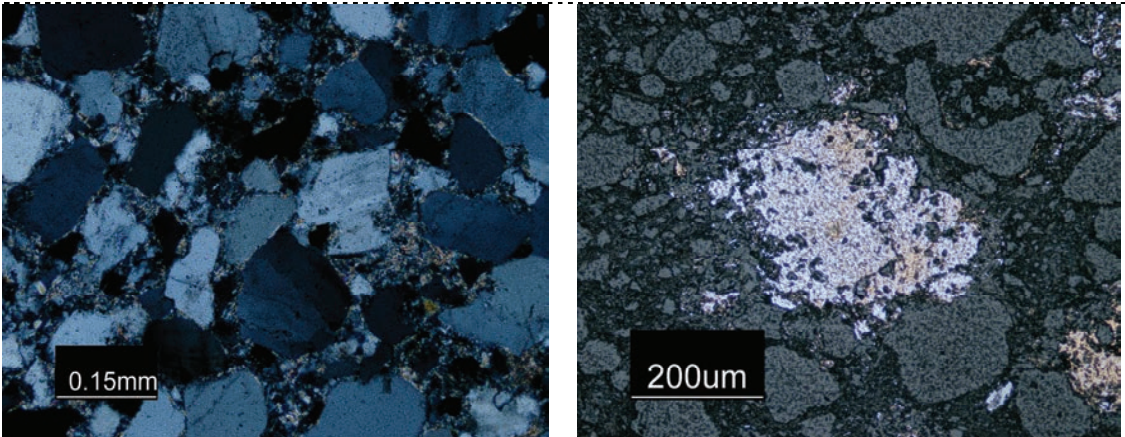
Chlorite is arranged in well-defined crystals of micas that have been altered. It presents green pleochroism very marked, relief medium to high.

Epidote crystals are interceded with metallic mineralization and quartz in veinlets. They are rectangular crystals of 100 to 50  $\mu\text{m}$  in the cross-section, with moderate relief and interference colors of 3rd order.

Hornblende occurs very occasionally (<1%) with high relief, green pleochroism very marked, and cleavage at 120  $^{\circ}$ .

Rock fragments are scarce, composed of quartz and feldspars, with very irregular edges and sometimes difficult to appreciate, the sizes are  $\sim 500 \mu\text{m}$ .

---

<b>B-02</b>	<b>META-GREYWACKE OF QUARTZ WITH SULFIDES DISSEMINATION</b>
<b>METALLIC</b>	Mostly pyrite 20%
<b>NO METALLIC</b>	<i>Essentials:</i> quartz, feldspar, rock fragment. <i>Accessories:</i> chlorite, epidote, micas, sillimanite, augite, hornblende.
<b>MODE</b>	Qtz 30 %; Fds 15 %; Lit <1 %; Matrix: 30 %; Micas 5%
<b>TEXTURE</b>	Phanerocrystalline (250 $\mu\text{m}$ – 1 mm), granular, Madura, poorly graded.
	

## DESCRIPTION

Sedimentary rock affected by a moderate metamorphism, grain size of fine sand, supported by an altered cryptocrystalline matrix, micas and sillimanite.

Quartz is the majority mineral; it is colorless with gray interference colors of first order. Size grains varies from some millimeters to 700  $\mu\text{m}$ , rounding is heterogeneous, from sub-rounded to sub-angular, very irregular edges and some engulfed crystals, some crystals have overgrown apparently from the silica matrix, with very irregular edges. Most of the crystals present parallel extinction; however, in some crystals there is undulating extinction, which may indicate volcanic and metamorphic origin.

K-feldspars and plagioclase are both anhedral crystals and in irregular, rounded, irregular, rounded, idiomorphic sections of micrometric size ( $\sim 500 \mu\text{m}$ ), as in quartz crystals with overgrowth edges.

Matrix is clayey, cryptocrystalline, altered and metamorphosed. It is composed of some crystals of micas, sillimanite, chlorite and epidote, crystals are slight alignment by low metamorphism.

Sillimanite is widely distributed in the matrix. Generally, in entangled sections surrounding quartz and feldspar crystals, it presents first order yellow-brown interference colors and moderate relief.



Micas in some sectors are aligned, in other cases without preferential order, the interference colors are red to blue of first and second order. Maximum size of the crystals is 2 mm in the elongation direction.

Chlorite is arranged in well-defined crystals of micas that have been altered. It presents green pleochroism very marked, relief medium to high.

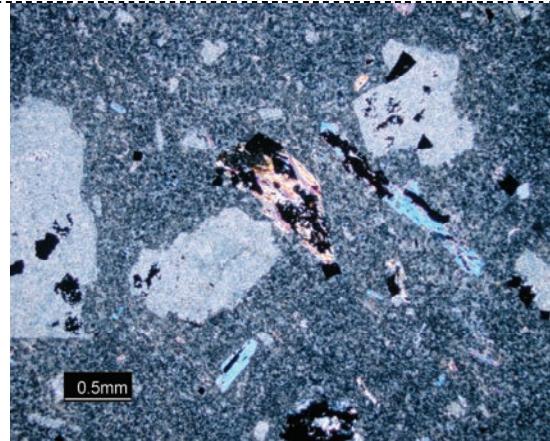
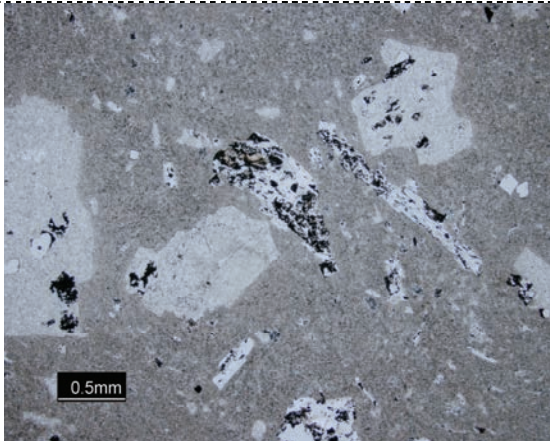
Epidote crystals are interceded with metallic mineralization and quartz in veinlets. They are rectangular crystals of 100 to 50  $\mu\text{m}$  in the cross-section, with moderate relief and interference colors of 3rd order.

Hornblende occurs very occasionally (<1%) with high relief, green pleochroism very marked, and cleavage at 120  $^{\circ}$ .

Rock fragments are scarce, composed of quartz and feldspars, with very irregular edges and sometimes difficult to appreciate, the sizes are  $\sim 500 \mu\text{m}$ .

---

<b>B-03</b>	<b>PORPHYRY (SAN PABLO STOCK)</b>
<b>METALLIC</b>	Mostly pyrite and cassiterite
<b>NO METALLIC</b>	<i>Essentials:</i> quartz, k-feldspar, plagioclase. <i>Accessories:</i> biotite, chlorite, tourmaline, monazite, sericite.
<b>MODE</b>	Qtz 40 %; k-Fds 40 %; plag 20%
<b>TEXTURE</b>	Porphyritic



## DESCRIPTION

Igneous, intrusive rock of granitic composition and porphyritic texture. It is composed by anhedral to euhedral crystals of quartz, 200  $\mu\text{m}$  to 5mm; plagioclase, 500  $\mu\text{m}$  to 4mm; k-feldspar 300  $\mu\text{m}$  to 5 mm; and micas, up to 2 mm. Matrix is cryptocrystalline and it was found considerably altered to sericite.

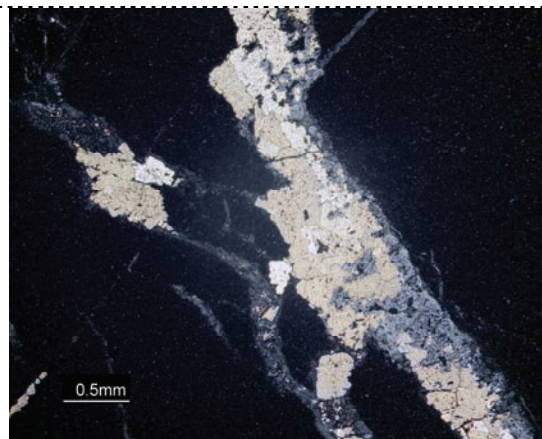
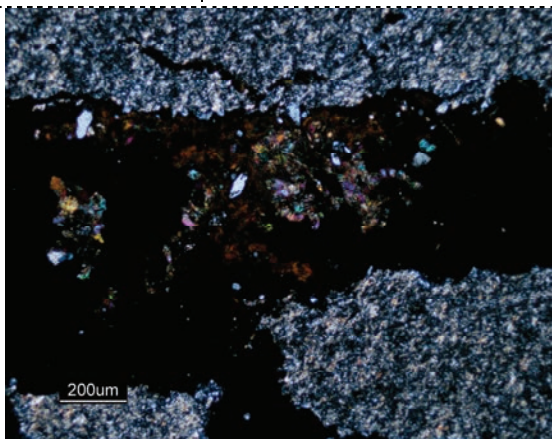
Quartz crystals are found as isolate crystals or forming agglomerates. In general, phenocrystals are pervasively sericitized. K-feldspar is more abundant of plagioclase. Mica crystals have been replaced by illite and chlorite.

Dark tourmaline with elongated forms or acicular crystals were found as accessory mineral. Tourmaline is more abundant in veins and altered zones in the sample.

Monazite is also found as an accessory mineral, crystals are very fine (>10  $\mu\text{m}$ ). Sulfide and cassiterite crystals were found replacing phenocrystals.

Micas show interference colors of red to blue of first and second order. Maximum size of the crystals is 2 mm in the elongation direction. Chlorite is arranged in well-defined crystals of micas that have been altered. It presents green pleochroism very marked, relief medium to high

<b>B-04</b>	<b>SHALE</b>
<b>METALLIC</b>	Infilling fractures mostly pyrite
<b>NO METALLIC</b>	<i>Essentials:</i> clay minerals
<b>MODE</b>	-
<b>TEXTURE</b>	Fine



## DESCRIPTION

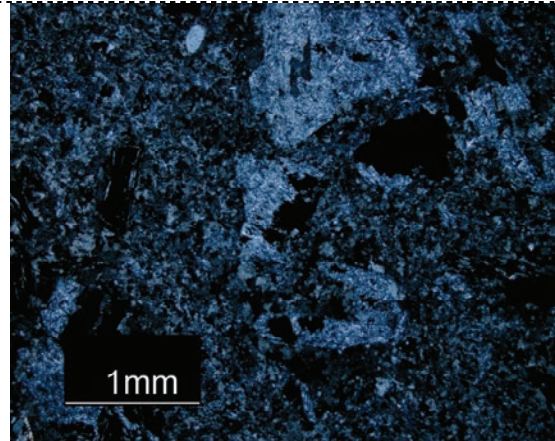
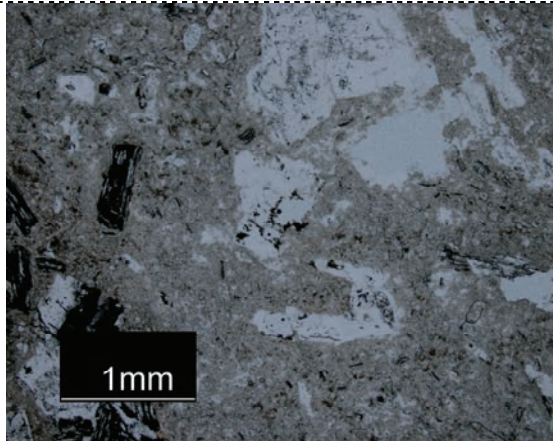
Metamorphic rock composed essentially by clay.

In this sample can be distinguished lamination as changes in the sedimentation regimen in different layers (change in the size of grain of clay to fine-sand). Also can be recognized an abrupt change in the lamination direction.

Infilling porosity and micro-fractures, acicular agglomerates of actinolite-tremolite crystals were found.

Two pyrite types were also observed, i) pyrite in different layer related to diagenesis process and ii) pyrite magmatic associated with ore mineralization in porosity zones and micro-veins.

<b>B-05</b>	<b>APLITIC DIKE</b>
<b>METALLIC</b>	Mostly pyrite
<b>NO METALLIC</b>	<i>Essentials:</i> quartz, k-feldspar, plagioclase. <i>Accessories:</i> tourmaline, apatite
<b>MODE</b>	Qtz 40 %; k-Fds 40 %; plag 20%
<b>TEXTURE</b>	Porphyritic



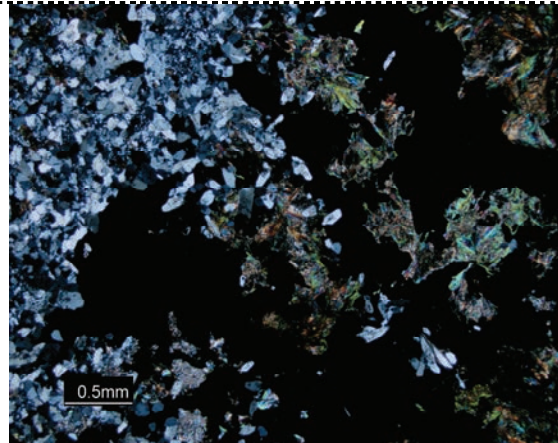
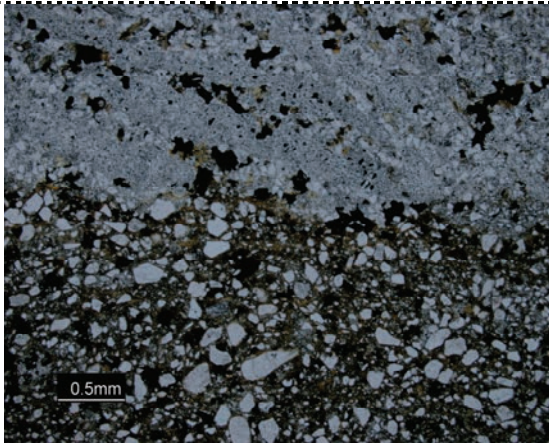
**DESCRIPTION**

Igneous, intrusive rock of quartz-feldspar composition and porphyritic fine texture. It is composed by anhedral to euhedral crystals of quartz, 200 µm to 5mm; plagioclase, 500 µm to 1mm; k-feldspar 300 µm to 1 mm. Matrix is cryptocrystalline and it was found considerably altered to sericite.

Quartz crystals are found as isolate crystals also as secondary mineral. Primary quartz is finer in size (up to 500 µm). Secondary quartz crystals were found up to 5mm. In general, phenocrystals are pervasively sericitized. K-feldspar is more abundant of plagioclase.

Dark tourmaline and apatite crystals were also found as accessory minerals. Apatite crystals were found in acicular forms, size of 100 to 200 µm. Some oxides were found in fractures.

<b>B-06</b>	<b>TRANSITION ZONE</b>
<b>METALLIC</b>	Infilling fractures mostly pyrite
<b>NO METALLIC</b>	<i>Essentials:</i> clay minerals, rock fragments, quartz, feldspars
<b>MODE</b>	-
<b>TEXTURE</b>	Very fine to fine



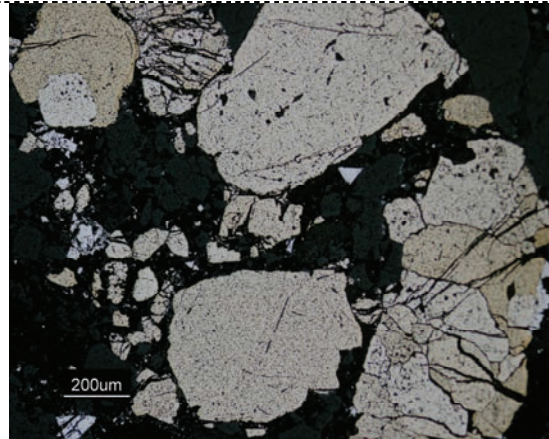
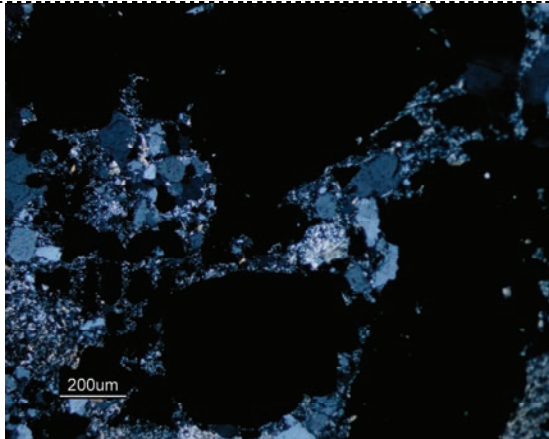
## DESCRIPTION

Sedimentary rock affected by metamorphism.

It is evident a contact transitional zone of clay to sand grains. Infilling porosity and micro-fractures have been found fibrous, acicular crystals, with interfered colors of red to blue of 2<sup>nd</sup> order (probably actinolite).

Sulfides mineralization also was recognized infilling porosity and fractures.

<b>B-07</b>	<b>META-GREYWACKE OF QUARTZ WITH SULFIDES DISSEMINATION</b>
<b>METALLIC</b>	Pyrite, arsenopyrite, sphalerite
<b>NO METALLIC</b>	<i>Essentials:</i> quartz, feldspar, rock fragment. <i>Accessories:</i> chlorite, epidote, micas, sillimanite, augite, hornblende.
<b>MODE</b>	Qtz 35 %; Fds 25 %; Lit 10 %; Matrix: 20 %
<b>TEXTURE</b>	Phanerocrystalline (250 µm – 1 mm), granular, mature, poorly graded.



**DESCRIPTION**

Sedimentary rock affected by a moderate metamorphism, grain size of fine sand, supported by an altered cryptocrystalline matrix, micas and sillimanite.

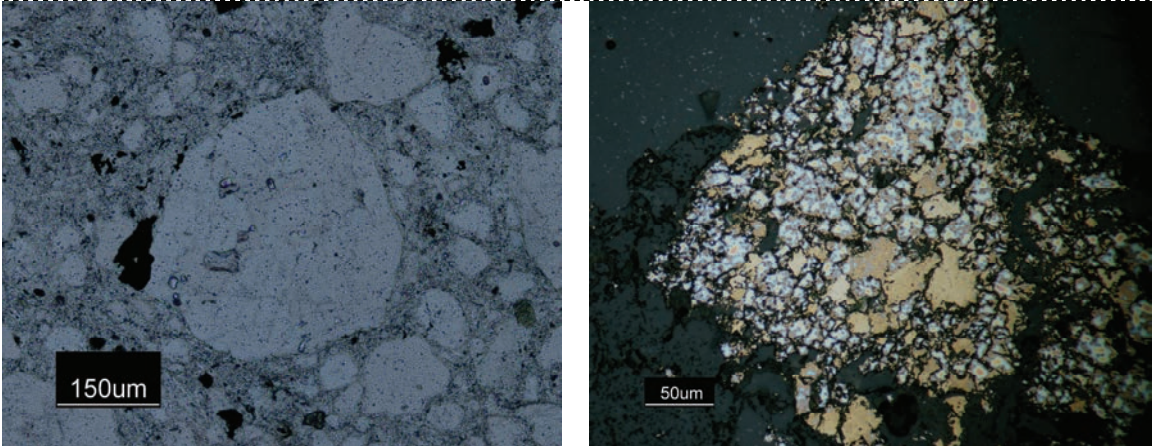
Quartz is the majority mineral; it is colorless with gray interference colors of first order. Size grains varies from some millimeters to 700 µm, rounding is heterogeneous, from sub-rounded to sub-angular, very irregular edges and some engulfed crystals, some crystals have overgrown apparently from the silica matrix, with very irregular edges. Most of the crystals present parallel extinction; however, in some crystals there is undulating extinction, which may indicate volcanic and metamorphic origin.

K-feldspars and plagioclase are both anhedral crystals and in irregular, rounded, irregular, rounded, idiomorphic sections of micrometric size (~ 500 µm), as in quartz crystals with overgrowth edges. Actinolite crystals are also found.

Matrix is clayey, cryptocrystalline, altered and metamorphosed. It is composed of some crystals of micas, sillimanite, chlorite and epidote, crystals are slight alignment by low metamorphism.

Rock fragments are scarce, composed of quartz and feldspars, with very irregular edges and sometimes difficult to appreciate, the sizes are ~ 500 µm.

Sulfides as pyrite, arsenopyrite and sphalerite have found in micro-fracture zones and alteration zones, the crystals are of 50 µm up to 1 mm.

<b>B-08</b>	<b>META-GREYWACKE OF QUARTZ WITH SULFIDES DISSEMINATION</b>
<b>METALLIC</b>	Pyrite, arsenopyrite
<b>NO METALLIC</b>	<i>Essentials:</i> quartz, feldspar, rock fragment. <i>Accessories:</i> chlorite, epidote, micas, sillimanite, augite, hornblende.
<b>MODE</b>	Qtz 35 %; Fds 15 %; Lit 20 %; Matrix: 20 %
<b>TEXTURE</b>	Phanerocrystalline (250 $\mu\text{m}$ – 1 mm), granular, mature, poorly graded.
	

## DESCRIPTION

Sedimentary rock affected by a moderate metamorphism, grain size of fine sand, supported by an altered cryptocrystalline matrix, micas and sillimanite.

Quartz is the majority mineral; it is colorless with gray interference colors of first order. Size grains varies from some millimeters to 700  $\mu\text{m}$ , rounding is heterogeneous, from sub-rounded to sub-angular, very irregular edges and some engulfed crystals, some crystals have overgrown apparently from the silica matrix, with very irregular edges. Most of the crystals present parallel extinction; however, in some crystals there is undulating extinction, which may indicate volcanic and metamorphic origin.

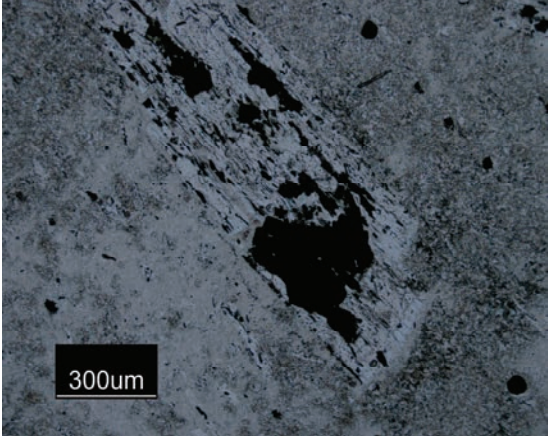
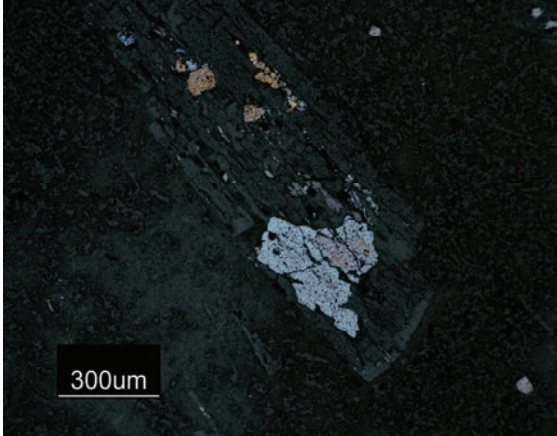
K-feldspars and plagioclase are both anhedral crystals and in irregular, rounded, irregular, rounded, idiomorphic sections of micrometric size ( $\sim 500 \mu\text{m}$ ), as in quartz crystals with overgrowth edges.

Matrix is clayey, cryptocrystalline, altered and metamorphosed. It is composed of some crystals of micas, sillimanite, chlorite and epidote, crystals are slight alignment by low metamorphism.

Rock fragments are more abundant, composed of quartz and feldspars, with very irregular edges, rock fragments up to some centimeters in size.

Sulfides as pyrite, arsenopyrite have found mainly in micro-fracture zones and alteration zones, the crystals are of 50  $\mu\text{m}$  up to 1 mm.

<b>B-09</b>	<b>PORPHYRY (SAN PABLO STOCK)</b>
<b>METALLIC</b>	Sulfides and cassiterite
<b>NO METALLIC</b>	<i>Essentials:</i> quartz, k-feldspar, plagioclase. <i>Accessories:</i> biotite, chlorite, tourmaline, monazite, sericite.
<b>MODE</b>	Qtz 40 %; k-Fds 40 %; plag 20%
<b>TEXTURE</b>	Porphyritic

## DESCRIPTION

Igneous, intrusive rock of granitic composition and porphyritic texture. It is composed by anhedral to euhedral crystals of quartz, 200  $\mu\text{m}$  to 5mm; plagioclase, 500  $\mu\text{m}$  to 4mm; k-feldspar 300  $\mu\text{m}$  to 5 mm; and micas, up to 2 mm. Matrix is cryptocrystalline and it was found considerably altered to sericite.

Quartz crystals are found as isolate crystals or forming agglomerates. In general, phenocrysts are pervasively sericitized. K-feldspar is more abundant of plagioclase. Mica crystals have been replaced by illite and chlorite.

Dark tourmaline with elongated forms or acicular crystals were found as accessory mineral. Tourmaline is more abundant in veins and altered zones in the sample.

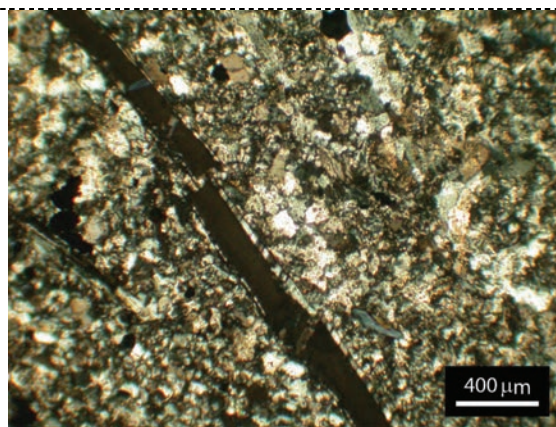
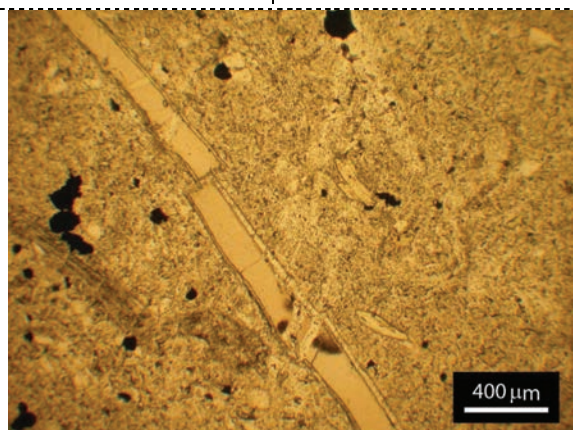
Monazite is also found as an accessory mineral, crystals are very fine (>10  $\mu\text{m}$ ). Sulfide and cassiterite crystals were found replacing phenocrysts.

Micas show interference colors of red to blue of first and second order. Maximum size of the crystals is 2 mm in the elongation direction. Chlorite is arranged in well-defined crystals of micas that have been altered. It presents green pleochroism very marked, relief medium to high.

Sulfides are found replacing phenocrysts of mica and quartz.



<b>B-10</b>	<b>META-SANDSTONE</b>
<b>METALLIC</b>	Infilling fractures mostly pyrite
<b>NO METALLIC</b>	<i>Essentials:</i> rock fragments, quartz, feldspars
<b>MODE</b>	Qtz 65%; rocks fragments 20%; feldspars 15
<b>TEXTURE</b>	Fine

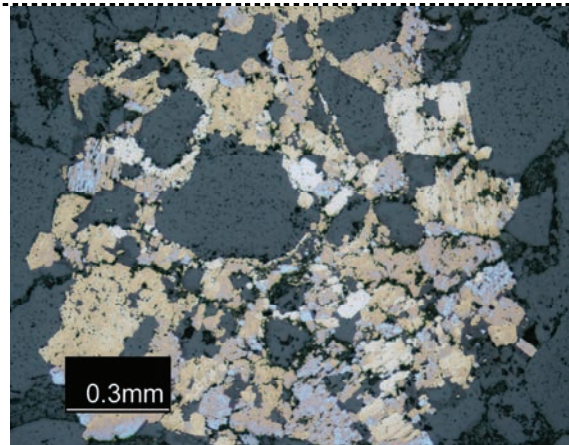
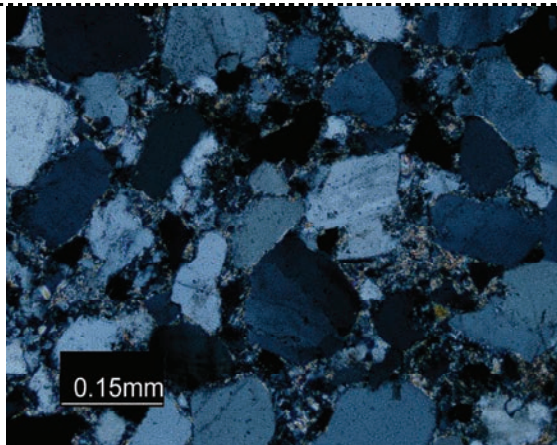


#### DESCRIPTION

Sedimentary rock affected by metamorphism.

Litharenite affected by metamorphism. Grains up to 300  $\mu\text{m}$ . Dissemination of pyrite, and chalcopyrite was found in micro-veins. Very fine crystals of sphalerite <50  $\mu\text{m}$  were also recognized infilling porosity.

<b>B-11</b>	<b>META-GREYWACKE OF QUARTZ WITH SULFIDES DISSEMINATION</b>
<b>METALLIC</b>	Mostly pyrite 10%
<b>NO METALLIC</b>	<i>Essentials:</i> quartz, feldspar, rock fragment. <i>Accessories:</i> chlorite, epidote, micas, sillimanite, augite, hornblende.
<b>MODE</b>	Qtz 35 %; Fds 25 %; Lit 10 %; Matrix: 20 %
<b>TEXTURE</b>	Phanerocrystalline (250 µm – 1 mm), granular, mature, poorly graded.



**DESCRIPTION**

Sedimentary rock affected by a moderate metamorphism, grain size of fine sand, supported by an altered cryptocrystalline matrix, micas.

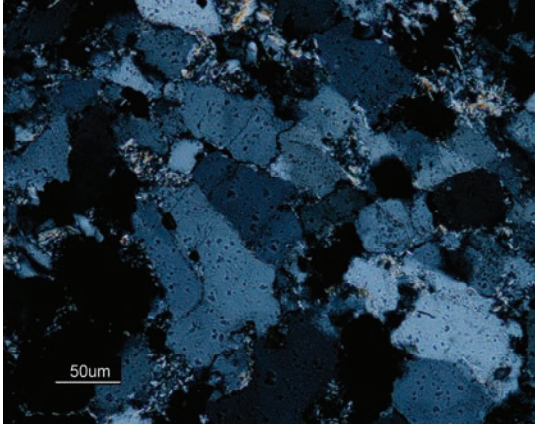
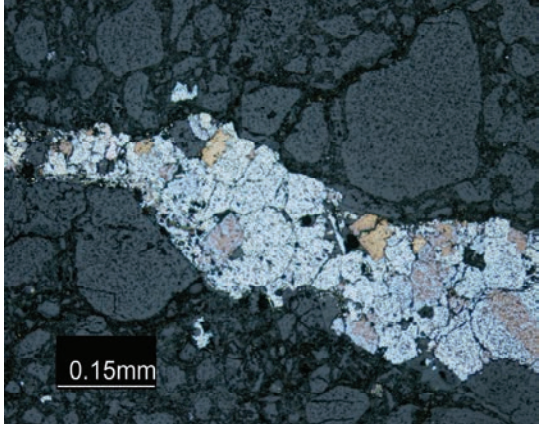
Quartz is the majority mineral; it is colorless with gray interference colors of first order. Size grains varies from some millimeters to 700 µm, rounding is heterogeneous, from sub-rounded to sub-angular, very irregular edges and some engulfed crystals, some crystals have overgrown apparently from the silica matrix, with very irregular edges. Most of the crystals present parallel extinction; however, in some crystals there is undulating extinction, which may indicate volcanic and metamorphic origin.

K-feldspars and plagioclase are both anhedral crystals and in irregular, rounded, irregular, rounded, idiomorphic sections of micrometric size (~ 500 µm), as in quartz crystals with overgrowth edges.

Matrix is clayey, cryptocrystalline, altered and metamorphosed. It is composed of some crystals of micas, sillimanite, chlorite and epidote, crystals are slight alignment by low metamorphism.

Micas in some sectors are aligned, in other cases without preferential order, the interference colors are red to blue of first and second order. Maximum size of the crystals is 2 mm in the elongation direction.

Rock fragments are scarce, composed of quartz and feldspars, with very irregular edges and sometimes difficult to appreciate, the sizes are ~ 500 µm.

B-12	QUARTZITE
METALLIC	Mostly pyrite
NO METALLIC	<i>Essentials:</i> quartz, feldspar, rock fragment. <i>Accessories:</i> micas
MODE	Qtz 75 %; Fds 10 %; Lit 5 %; Matrix: 10 %
TEXTURE	Phanerocrystalline (250 $\mu\text{m}$ – 1 mm), granular, Madura, poorly graded.
	

## DESCRIPTION

None foliated metamorphic rock composed almost entirely of quartz.

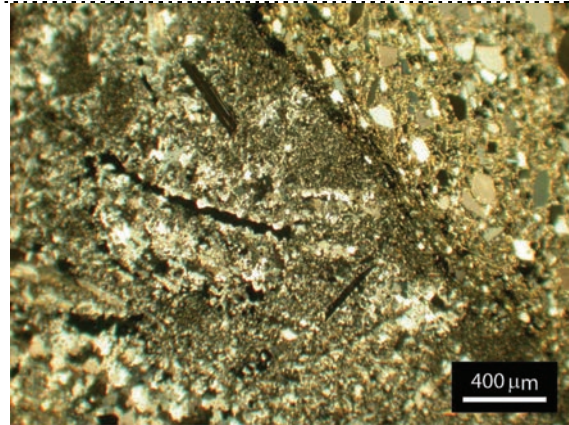
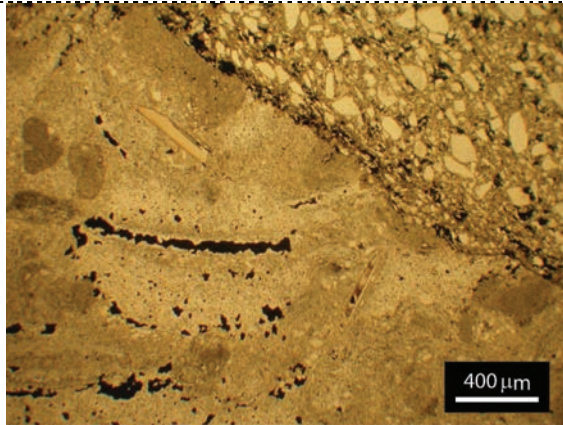
Quartz is the majority mineral; it is colorless with gray interference colors of the first order. The grain size ranging from some millimeters to 100  $\mu\text{m}$ , heterogeneous rounding, from sub-rounded to sub-angular, some crystals have overgrown apparently from the silica matrix, with very irregular edges, and other crystals show engulfed morphologies, characteristic of volcanic. Most of the crystals present parallel extinction, however, in some crystals it is observed undulating extinction. Some crystals have inclusions of tabular crystals (micas?) and zircon.

K-feldspar crystals are scarce, present anhedral form, irregular, rounded, of micrometric size ( $\sim 500 \mu\text{m}$ ), with edges of overgrowth, usually present twinning.

Matrix is clayey, cryptocrystalline, altered and metamorphosed. It is composed of some crystals of micas product of metamorphism.

Rock fragments are scarce, composed of quartz and feldspars, with very irregular edges and sometimes difficult to appreciate, the sizes are  $\sim 500 \mu\text{m}$ .

<b>B-13</b>	<b>META-SANDSTONE</b>
<b>METALLIC</b>	Infilling fractures mostly pyrite
<b>NO METALLIC</b>	<i>Essentials:</i> rock fragments, quartz, feldspars
<b>MODE</b>	Qtz 65%; rocks fragments 20%; feldspars 15
<b>TEXTURE</b>	Fine

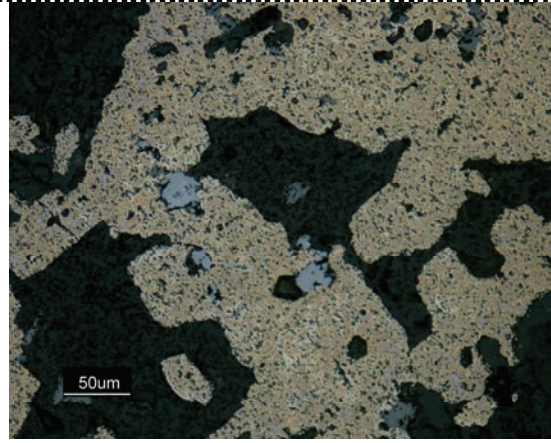
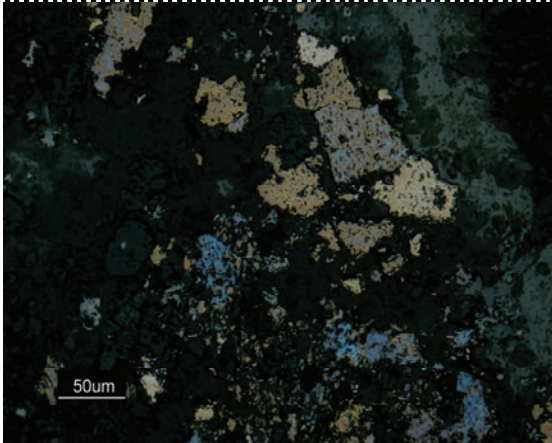


**DESCRIPTION**

Sedimentary rock affected by metamorphism.

Litharenite affected by metamorphism. Grains up to 300 μm. Dissemination of pyrite, and chalcopyrite was found in micro-veins. Very fine crystals of sphalerite <50 μm were also recognized infilling porosity.

<b>B-014</b>	<b>META-GREYWACKE OF QUARTZ WITH SULFIDES DISSEMINATION</b>
<b>METALLIC</b>	Mostly pyrite 10%
<b>NO METALLIC</b>	<i>Essentials:</i> quartz, feldspar, rock fragment. <i>Accessories:</i> micas
<b>MODE</b>	Qtz 45 %; Fds 15 %; Lit 20 %; Matrix: 20 %
<b>TEXTURE</b>	Phanerocrystalline (250 $\mu\text{m}$ – 1 mm), granular, mature, poorly graded.



### DESCRIPTION

Sedimentary rock affected by a moderate metamorphism, grain size of fine sand, supported by an altered cryptocrystalline matrix, micas and sillimanite.

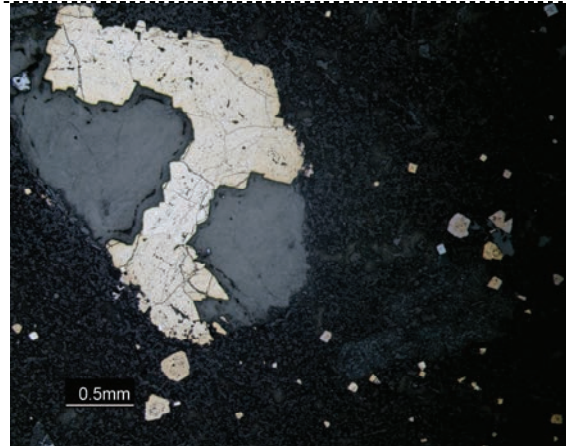
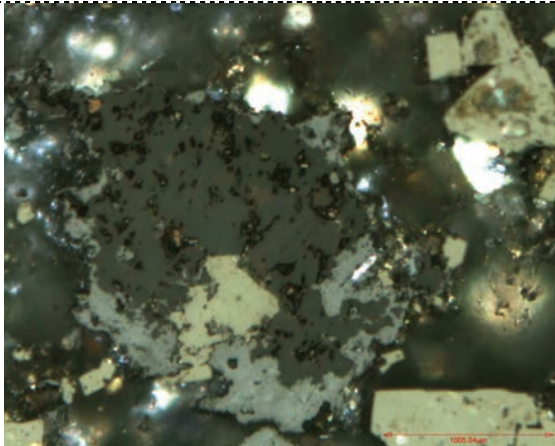
Quartz is the majority mineral; it is colorless with gray interference colors of first order. Size grains varies from some millimeters to 700  $\mu\text{m}$ , rounding is heterogeneous, from sub-rounded to sub-angular, very irregular edges and some engulfed crystals, some crystals have overgrown apparently from the silica matrix, with very irregular edges. Most of the crystals present parallel extinction; however, in some crystals there is undulating extinction, which may indicate volcanic and metamorphic origin.

K-feldspars and plagioclase are both anhedral crystals and in irregular, rounded, irregular, rounded, idiomorphic sections of micrometric size ( $\sim 500 \mu\text{m}$ ), as in quartz crystals with overgrowth edges.

Matrix is clayey, cryptocrystalline, altered and metamorphosed. It is composed of some crystals of micas. Micas in some sectors are aligned.

Rock fragments are more abundant.

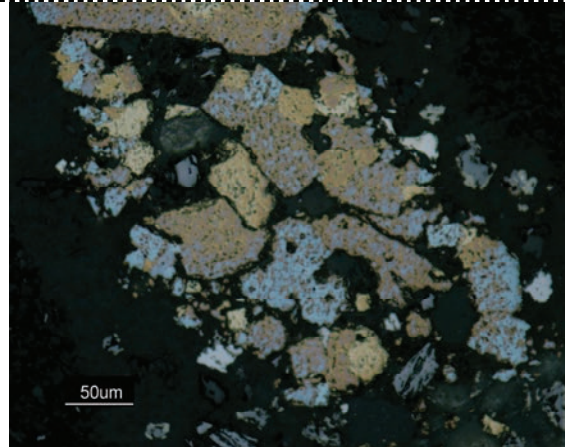
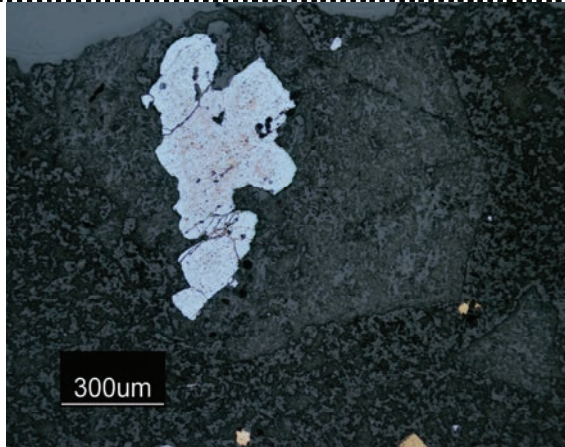
<b>B-015</b>	<b>MINERALIZED BRECCIA</b>
<b>METALLIC</b>	Cassiterite, galena, sphalerite, pyrite
<b>NO METALLIC</b>	Rock fragment and quartz
<b>MODE</b>	-
<b>TEXTURE</b>	Breccia



**DESCRIPTION**

Magmatic breccia in contact zone between porphyry body and meta-sedimentary sequence. Grains are cemented by silica. Most of grains are of igneous rocks.

<b>B-16</b>	<b>META-GREYWACKE OF QUARTZ WITH SULFIDES DISSEMINATION</b>
<b>METALLIC</b>	Mostly pyrite 10%
<b>NO METALLIC</b>	<i>Essentials:</i> quartz, feldspar, rock fragment. <i>Accessories:</i> chlorite, epidote, micas, sillimanite, augite, hornblende.
<b>MODE</b>	Qtz 35 %; Fds 25 %; Lit 10 %; Matrix: 20 %
<b>TEXTURE</b>	Phanerocrystalline (250 $\mu\text{m}$ – 1 mm), granular, mature, poorly graded.



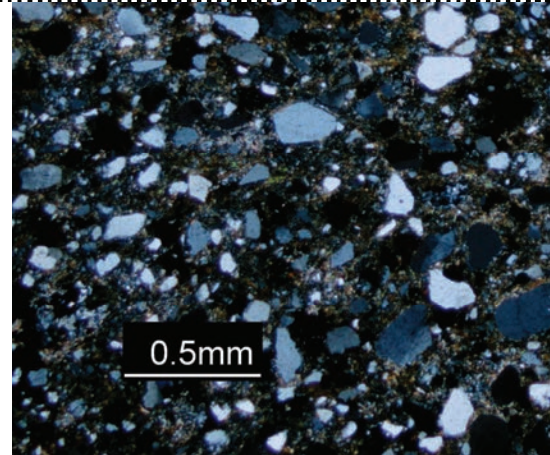
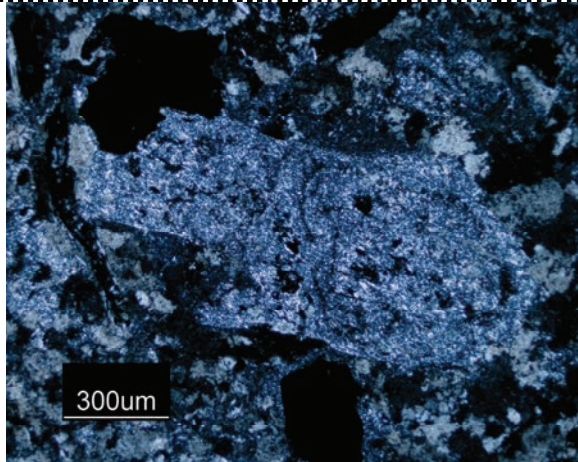
### DESCRIPTION

Sedimentary rock affected by a moderate metamorphism, grain size of fine sand, supported by an altered cryptocrystalline matrix, micas and sillimanite.

Quartz is the majority mineral; it is colorless with gray interference colors of first order. Size grains varies from some millimeters to 700  $\mu\text{m}$ , rounding is heterogeneous, from sub-rounded to sub-angular, very irregular edges and some engulfed crystals, some crystals have overgrown apparently from the silica matrix, with very irregular edges. Most of the crystals present parallel extinction; however, in some crystals there is undulating extinction, which may indicate volcanic and metamorphic origin.

Rock fragments are scarce, composed of quartz and feldspars, with very irregular edges and sometimes difficult to appreciate, the sizes are  $\sim 500 \mu\text{m}$ .

<b>B-17</b>	<b>META-GREYWACKE OF QUARTZ WITH SULFIDES DISSEMINATION</b>
<b>METALLIC</b>	Mostly pyrite 10%
<b>NO METALLIC</b>	<i>Essentials:</i> quartz, feldspar, rock fragment. <i>Accessories:</i> chlorite, epidote, micas, sillimanite, augite, hornblende.
<b>MODE</b>	Qtz 35 %; Fds 25 %; Lit 10 %; Matrix: 20 %
<b>TEXTURE</b>	Phanerocrystalline (250 $\mu\text{m}$ – 1 mm), granular, mature, poorly graded.



## DESCRIPTION

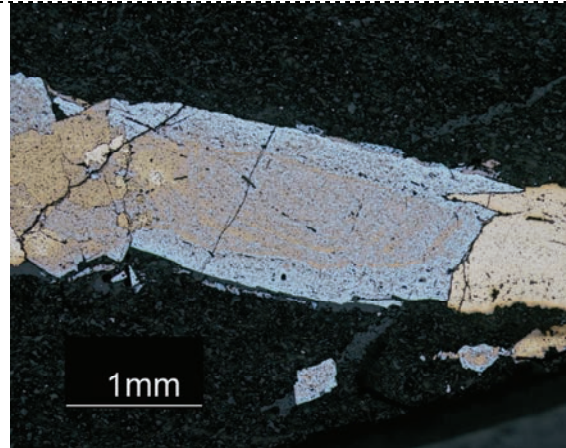
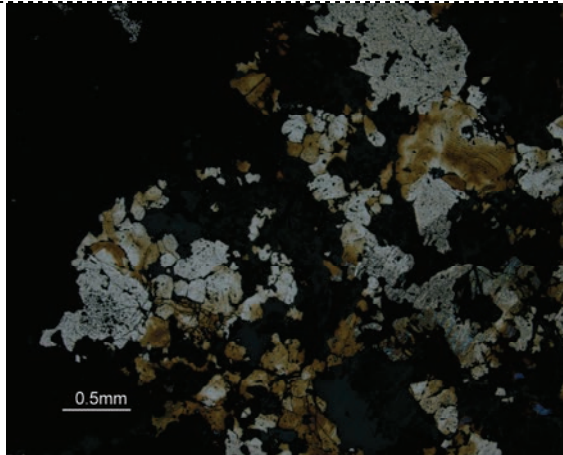
Sedimentary rock affected by a moderate metamorphism, grain size of fine sand, supported by an altered cryptocrystalline matrix, micas and sillimanite.

Quartz is the majority mineral; it is colorless with gray interference colors of first order. Size grains varies from some millimeters to 700  $\mu\text{m}$ , rounding is heterogeneous, from sub-rounded to sub-angular, very irregular edges and some engulfed crystals, some crystals have overgrown apparently from the silica matrix, with very irregular edges. Most of the crystals present parallel extinction; however, in some crystals there is undulating extinction, which may indicate volcanic and metamorphic origin.

Rock fragments are scarce, composed of quartz and feldspars, with very irregular edges and sometimes difficult to appreciate, the sizes are  $\sim 500 \mu\text{m}$ .



<b>B-18</b>	<b>META-GREYWACKE OF QUARTZ WITH SULFIDES DISSEMINATION</b>
<b>METALLIC</b>	Mostly pyrite 10%
<b>NO METALLIC</b>	<i>Essentials:</i> quartz, feldspar, rock fragment. <i>Accessories:</i> chlorite, epidote, micas, sillimanite, augite, hornblende.
<b>MODE</b>	Qtz 35 %; Fds 25 %; Lit 10 %; Matrix: 20 %
<b>TEXTURE</b>	Phanerocrystalline (250 $\mu$ m – 1 mm), granular, mature, poorly graded.



### DESCRIPTION

Sedimentary rock affected by a moderate metamorphism, grain size of fine sand, supported by an altered cryptocrystalline matrix, micas and sillimanite.

Quartz is the majority mineral; it is colorless with gray interference colors of first order. Size grains varies from some millimeters to 700  $\mu$ m, rounding is heterogeneous, from sub-rounded to sub-angular, very irregular edges and some engulfed crystals, some crystals have overgrown apparently from the silica matrix, with very irregular edges. Most of the crystals present parallel extinction; however, in some crystals there is undulating extinction, which may indicate volcanic and metamorphic origin.

Rock fragments are scarce, composed of quartz and feldspars, with very irregular edges and sometimes difficult to appreciate, the sizes are  $\sim$  500  $\mu$ m.

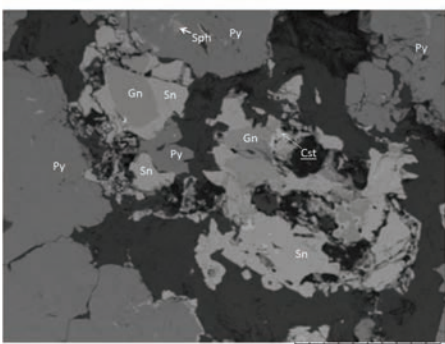
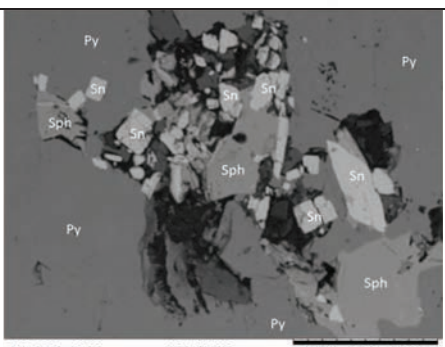
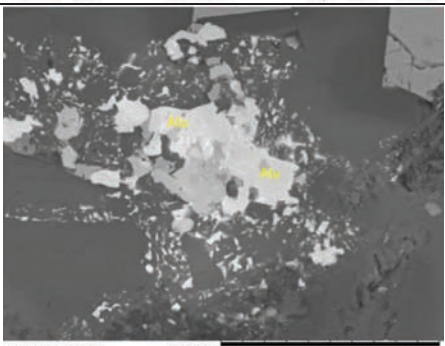
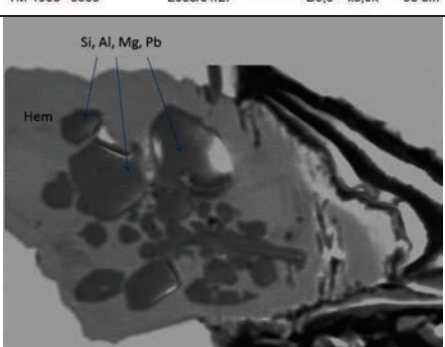
## APPENDIX 4

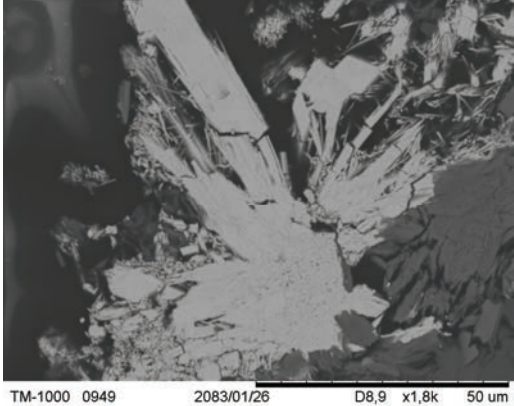
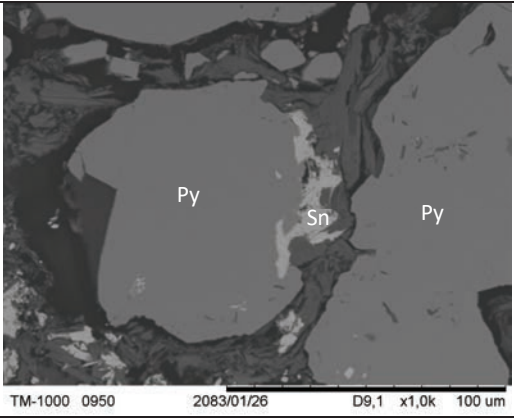
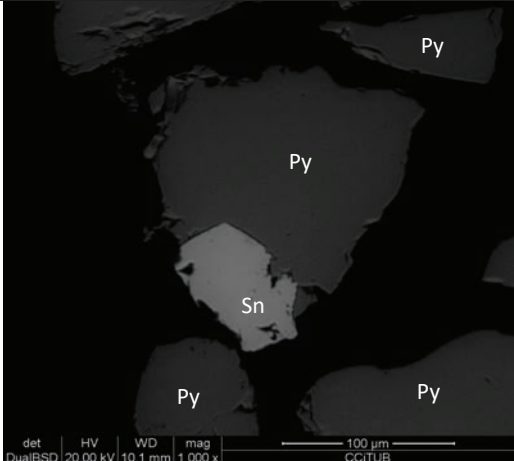
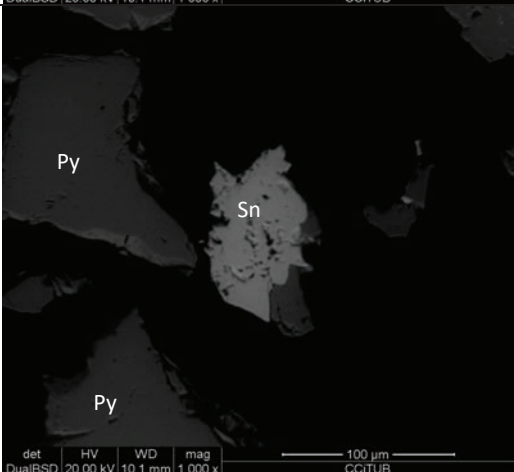
Sample	Minerals	Formula
J-2b	Quartz, Illite, Illite-Montmorillonite, Kaolinite, Alunite, Pyrite	Si O2 K <sub>0.7</sub> Al <sub>2</sub> ( Si , Al ) <sub>4</sub> O <sub>10</sub> ( O H ) <sub>2</sub> K - Al <sub>4</sub> ( Si Al ) <sub>8</sub> O <sub>20</sub> ( O H ) <sub>4</sub> !x H <sub>2</sub> O Al <sub>2</sub> ( Si <sub>2</sub> O <sub>5</sub> ) ( O H ) <sub>4</sub> K ( Al <sub>3</sub> ( O H ) <sub>6</sub> ( S O <sub>4</sub> ) <sub>2</sub> ) Fe S <sub>2</sub>
J-2c	Quartz, Kaolinite, Rhomboclase, Illite, Anhydrite	Si O2 Al <sub>2</sub> Si <sub>2</sub> O <sub>5</sub> ( O H ) <sub>4</sub> ( H <sub>5</sub> O <sub>2</sub> ) Fe ( S O <sub>4</sub> ) <sub>2</sub> ( H <sub>2</sub> O ) <sub>2</sub> K Al <sub>2</sub> Si <sub>3</sub> Al O <sub>10</sub> ( O H ) <sub>2</sub> Ca ( S O <sub>4</sub> )
J-2e	Quartz, Rhomboclase, Cassiterite, Kaolinite 1\T\RG, Gypsum, Alunite, Montmorillonite, Vermiculite	Si O2 ( H <sub>5</sub> O <sub>2</sub> ) Fe ( S O <sub>4</sub> ) <sub>2</sub> ( H <sub>2</sub> O ) <sub>2</sub> Sn O <sub>2</sub> Al <sub>2</sub> Si <sub>2</sub> O <sub>5</sub> ( O H ) <sub>4</sub> Ca ( S O <sub>4</sub> ) ( H <sub>2</sub> O ) <sub>2</sub> K <sub>2</sub> O ! <sub>3</sub> Al <sub>2</sub> O <sub>3</sub> ! <sub>4</sub> S O <sub>3</sub> ! <sub>6</sub> H <sub>2</sub> O Si <sub>3.74</sub> Al <sub>2.03</sub> Fe <sub>0.03</sub> Mg <sub>0.02</sub> ! O <sub>11</sub> ( Mg <sub>2.36</sub> Fe <sub>.48</sub> Al <sub>.16</sub> ) ( Al <sub>1.28</sub> Si <sub>2.72</sub> ) O <sub>10</sub> ( O H ) <sub>2</sub> ( H <sub>2</sub> O ) <sub>4.32</sub> Mg <sub>0.32</sub>
J-3a	Quartz low, Rhomboclase, Vermiculite 2\TM\RG,  Plumbojarosite, Sulfur, Okenite, Siderophyllite 1\TM\RG	Si O2 ( H <sub>5</sub> O <sub>2</sub> ) Fe ( S O <sub>4</sub> ) <sub>2</sub> ( H <sub>2</sub> O ) <sub>2</sub> ( Mg <sub>2.36</sub> Fe <sub>.48</sub> Al <sub>.16</sub> ) ( Al <sub>1.28</sub> Si <sub>2.72</sub> ) O <sub>10</sub> ( O H ) <sub>2</sub> ( H <sub>2</sub> O ) <sub>4.32</sub> Mg <sub>0.32</sub> Pb ( Al <sub>3</sub> ( O H ) <sub>6</sub> ( S O <sub>4</sub> ) <sub>2</sub> ) <sub>2</sub> S <sub>8</sub> Ca <sub>10</sub> Si <sub>18</sub> O <sub>46</sub> ( H <sub>2</sub> O ) <sub>18</sub> K <sub>.99</sub> ( Fe <sub>1.92</sub> Al <sub>1.08</sub> ) ( Al <sub>1.05</sub> Si <sub>2.71</sub> O <sub>10</sub> ) ( O H F )
J-3d	Illite, Quartz, Kaolinite 1T, Rhomboclase, Sericite, Biotite 2M1	K Al <sub>2</sub> Si <sub>3</sub> Al O <sub>10</sub> ( O H ) <sub>2</sub> Si O2 K Al <sub>2</sub> Si <sub>3</sub> Al O <sub>10</sub> ( O H ) <sub>2</sub> ( H <sub>5</sub> O <sub>2</sub> ) Fe ( S O <sub>4</sub> ) <sub>2</sub> ( H <sub>2</sub> O ) <sub>2</sub> K Al <sub>2</sub> ( Si <sub>3</sub> Al ) O <sub>10</sub> ( O H , F ) <sub>2</sub> K Mg <sub>2</sub> Al <sub>2</sub> Si <sub>3</sub> O <sub>11</sub> ( O H )
J-4	Quartz low, Sericite 2M1,  Vermiculite 2\TM\RG, Alunite, Illite, Jarosite, Argentojarosite, Monazite-(La), Anhydrite, Gypsum,	Si O2 ( K <sub>0.727</sub> Na <sub>0.170</sub> Ca <sub>0.011</sub> ) ( Al <sub>0.933</sub> Fe <sub>0.016</sub> Mg <sub>0.011</sub> ) <sub>2</sub> ( Si <sub>0.782</sub> Al <sub>0.221</sub> Ti <sub>0.005</sub> ) <sub>4</sub> O <sub>10</sub> ( O H ) <sub>2</sub> Mg <sub>3.41</sub> Si <sub>2.86</sub> Al <sub>1.14</sub> O <sub>10</sub> ( O H ) <sub>2</sub> ( H <sub>2</sub> O ) <sub>3.72</sub> K ( Al <sub>3</sub> ( S O <sub>4</sub> ) <sub>2</sub> ( O H ) <sub>6</sub> ) K Al <sub>2</sub> Si <sub>3</sub> Al O <sub>10</sub> ( O H ) <sub>2</sub> K Fe <sub>3</sub> ( S O <sub>4</sub> ) <sub>2</sub> ( O H ) <sub>6</sub> Ag Fe <sub>3</sub> ( S O <sub>4</sub> ) <sub>2</sub> ( O H ) <sub>6</sub> La P O <sub>4</sub> Ca ( S O <sub>4</sub> ) Ca ( S O <sub>4</sub> ) ( H <sub>2</sub> O )
J-7a	Quartz low, Sericite 2M1,  Vermiculite 2\TM\RG, Alunite, Illite, Jarosite, Argentojarosite, Monazite-(La), Anhydrite, Gypsum,	Si O2 ( K <sub>0.727</sub> Na <sub>0.170</sub> Ca <sub>0.011</sub> ) ( Al <sub>0.933</sub> Fe <sub>0.016</sub> Mg <sub>0.011</sub> ) <sub>2</sub> ( Si <sub>0.782</sub> Al <sub>0.221</sub> Ti <sub>0.005</sub> ) <sub>4</sub> O <sub>10</sub> ( O H ) <sub>2</sub> Mg <sub>3.41</sub> Si <sub>2.86</sub> Al <sub>1.14</sub> O <sub>10</sub> ( O H ) <sub>2</sub> ( H <sub>2</sub> O ) <sub>3.72</sub> K ( Al <sub>3</sub> ( S O <sub>4</sub> ) <sub>2</sub> ( O H ) <sub>6</sub> ) K Al <sub>2</sub> Si <sub>3</sub> Al O <sub>10</sub> ( O H ) <sub>2</sub> K Fe <sub>3</sub> ( S O <sub>4</sub> ) <sub>2</sub> ( O H ) <sub>6</sub> Ag Fe <sub>3</sub> ( S O <sub>4</sub> ) <sub>2</sub> ( O H ) <sub>6</sub> La P O <sub>4</sub> Ca ( S O <sub>4</sub> ) Ca ( S O <sub>4</sub> ) ( H <sub>2</sub> O )
J-7b	Cassiterite, Vermiculite,  Cristobalite, Andesine, Oligoclase, Monazite (Pr)	Sn O <sub>2</sub> ( Mg <sub>2.36</sub> Fe <sub>.48</sub> Al <sub>.16</sub> ) ( Al <sub>1.28</sub> Si <sub>2.72</sub> ) O <sub>10</sub> ( O H ) <sub>2</sub> ( C <sub>6</sub> H <sub>14</sub> N O <sub>2</sub> ) Si O2 Na <sub>.499</sub> Ca <sub>.491</sub> ( Al <sub>1.488</sub> Si <sub>2.506</sub> O <sub>8</sub> ) ( Na , Ca ) Al ( Al , Si ) Si <sub>2</sub> O <sub>8</sub> Pr ( P O <sub>4</sub> )
ASF-01	Quartz, Coesite,	Si O2 Si O2

	<b>Sulfur, Monazite-(Nd), Kaolinite, Illite, sodian brammallite Sericite 2M1 (heated)</b>	S ( Nd , Ca , Ce ) P O <sub>4</sub> , K Al <sub>2</sub> Si <sub>3</sub> Al O <sub>10</sub> ( O H ) <sub>2</sub> ( Na , K ) <sup>1-x</sup> ( Al , Mg , Fe ) <sub>2</sub> ( Si , Al ) <sub>4</sub> O <sub>10</sub> ( O H ) <sub>2</sub> ( K <sub>0.776</sub> Na <sub>0.181</sub> Ca <sub>0.011</sub> ) ( Al <sub>0.916</sub> Fe <sub>0.016</sub> Mg <sub>0.011</sub> ) <sub>2</sub> ( Si <sub>0.787</sub> Al <sub>0.223</sub> Ti <sub>0.005</sub> ) <sub>4</sub> O <sub>11</sub>
<b>ASF-02</b>	<b>Hematite, Cassiterite, Quartz, Sericite 2M1 (heated),  Illite Sulfur, Jarosite</b>	Fe <sub>2</sub> O <sub>3</sub> Sn O <sub>2</sub> Si O <sub>2</sub> ( K <sub>0.776</sub> Na <sub>0.181</sub> Ca <sub>0.011</sub> ) ( Al <sub>0.916</sub> Fe <sub>0.016</sub> Mg <sub>0.011</sub> ) <sub>2</sub> ( Si <sub>0.787</sub> Al <sub>0.223</sub> Ti <sub>0.005</sub> ) <sub>4</sub> O <sub>11</sub> K Al <sub>2</sub> ( Si <sub>3</sub> Al O <sub>10</sub> ) ( O H ) <sub>2</sub> S K ( Fe <sub>3</sub> ( S O <sub>4</sub> ) <sub>2</sub> ( O H ) <sub>6</sub> )
<b>ASF-03</b>	<b>Sulfur, Sericite [NR], Hematite, Rhomboclase</b>	S <sub>8</sub> K Al <sub>2</sub> ( Si <sub>3</sub> Al ) O <sub>10</sub> ( O H , F ) <sub>2</sub> Fe <sub>2</sub> O <sub>3</sub> ( H <sub>5</sub> O <sub>2</sub> ) Fe ( S O <sub>4</sub> ) <sub>2</sub> ( H <sub>2</sub> O ) <sub>2</sub>
<b>ASF-04</b>	<b>Orthoclase, Gypsum, Anhydrite, Sericite,  Chlorite, Hydrobiotite (Chlorite), Plumbojarosite</b>	K ( Al , Fe ) Si <sub>2</sub> O <sub>8</sub> Ca ( S O <sub>4</sub> ) ( H <sub>2</sub> O ) <sub>2</sub> Ca ( S O <sub>4</sub> ) ( K <sub>0.727</sub> Na <sub>0.170</sub> Ca <sub>0.011</sub> ) ( Al <sub>0.933</sub> Fe <sub>0.016</sub> Mg <sub>0.011</sub> ) <sub>2</sub> ( Si <sub>0.782</sub> Al <sub>0.221</sub> Ti <sub>0.005</sub> ) <sub>4</sub> O <sub>10</sub> ( O H ) <sub>2</sub> Al - Fe - Si O <sub>2</sub> - O Al - Fe - Si - O - O H Pb Fe <sub>6</sub> ( S O <sub>4</sub> ) <sub>4</sub> ( O H ) <sub>12</sub>
<b>ASF-05</b>	<b>Biotite, Rhomboclase, Illite-2, Anhydrite, Gypsum, Kaolinite</b>	K Mg <sub>2</sub> Al <sub>2</sub> Si <sub>3</sub> O <sub>11</sub> ( O H ) ( H <sub>5</sub> O <sub>2</sub> ) Fe ( S O <sub>4</sub> ) <sub>2</sub> ( H <sub>2</sub> O ) <sub>2</sub> ( K , H <sub>3</sub> O ) Al <sub>2</sub> Si <sub>3</sub> Al O <sub>10</sub> ( O H ) <sub>2</sub> Ca ( S O <sub>4</sub> ) Ca S O <sub>4</sub> ( H <sub>2</sub> O ) <sub>2</sub> Al <sub>2</sub> Si <sub>2</sub> O <sub>5</sub> ( O H ) <sub>4</sub>
<b>MCC-1</b>	<b>Melanterite</b>	Fe S O <sub>4</sub> ( H <sub>2</sub> O ) <sub>7</sub>
<b>MCC-13</b>	<b>Bianchite, Quartz, Sphalerite, Cassiterite, Pyrite, Kaolinite</b>	Zn ( S O <sub>4</sub> ) ( H <sub>2</sub> O ) <sub>6</sub> Si O <sub>2</sub> Zn S Sn O <sub>2</sub> Fe S <sub>2</sub> Al <sub>4</sub> ( O H ) <sub>8</sub> ( Si <sub>4</sub> O <sub>10</sub> )
<b>MCC-17</b>	<b>Goethite, Melanterite, Dickite, Alunite, Quartz, Calcite, Ilmenite, Cassiterite</b>	Fe O ( O H ) Fe S O <sub>4</sub> ( H <sub>2</sub> O ) <sub>7</sub> Al <sub>2</sub> Si <sub>2</sub> O <sub>5</sub> ( O H ) <sub>4</sub> ( H C O N H <sub>2</sub> ) K ( Al <sub>3</sub> ( O H ) <sub>6</sub> ( S O <sub>4</sub> ) <sub>2</sub> ) Si O <sub>2</sub> Ca ( C O <sub>3</sub> ) Fe Ti O <sub>3</sub> Sn O <sub>2</sub>
<b>MCC-18</b>	<b>Pyrite, Quartz, Dickite, Jarosite</b>	Fe S <sub>2</sub> Si O <sub>2</sub> Al <sub>2</sub> Si <sub>2</sub> O <sub>5</sub> ( O H ) <sub>4</sub> ( H C O N H <sub>2</sub> ) K ( Fe <sub>3</sub> ( S O <sub>4</sub> ) <sub>2</sub> ( O H ) <sub>6</sub> )

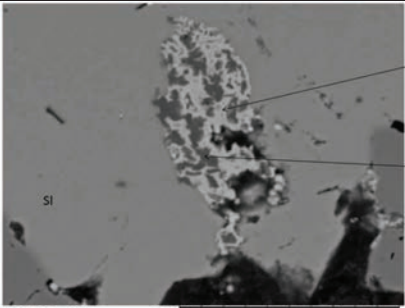
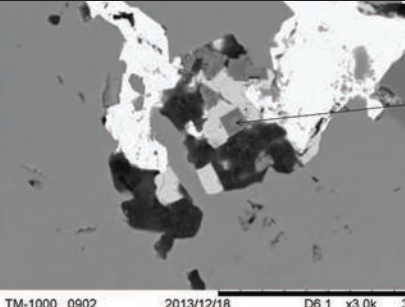
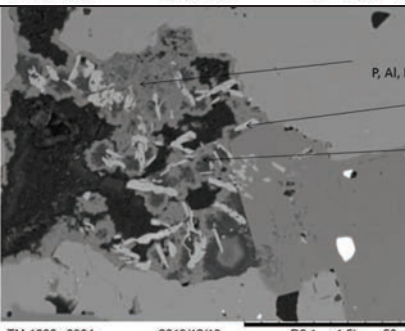
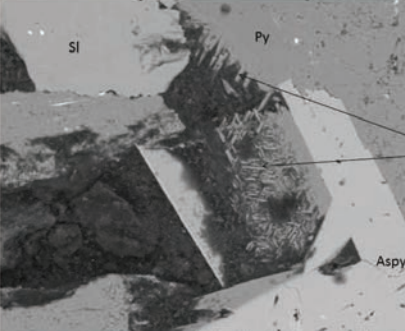
# APPENDIX 5

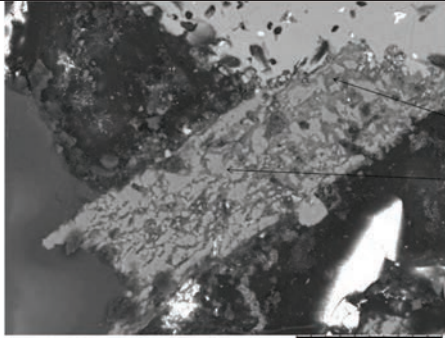
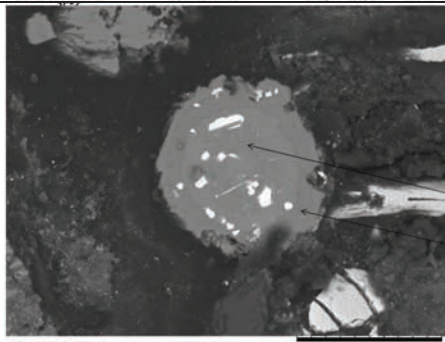
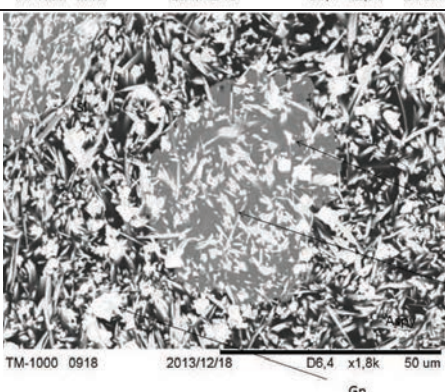
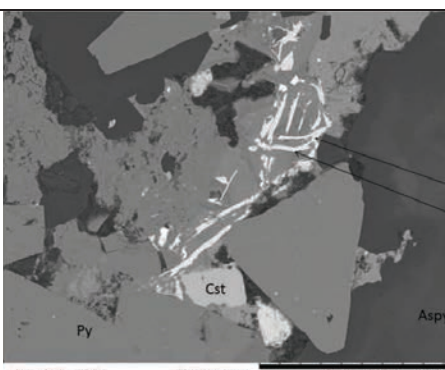
## ISEM-BSE-EDS OF THE SANTA FE DISTRICT

#1	<b>Japo</b>	
METALLIC	Sphalerite ( <i>Sph</i> ), galena ( <i>Gn</i> ), cassiterite ( <i>Cst</i> ), pyrite ( <i>Py</i> ), stannite ( <i>Sn</i> )	
TEXTURE	Paragenetic assemblage of sulfides	
#2	<b>Japo</b>	
METALLIC	Sphalerite pyrite ( <i>Py</i> ), stannite ( <i>Sn</i> )	
TEXTURE	Paragenetic assemblage of sulfides	
#3	<b>Japo</b>	
NO METALLIC	Alunite ( <i>Alu</i> )	
TEXTURE	Alteration	
#4	<b>Japo</b>	
METALLIC	Hematite	
TEXTURE	Exolution (?)	

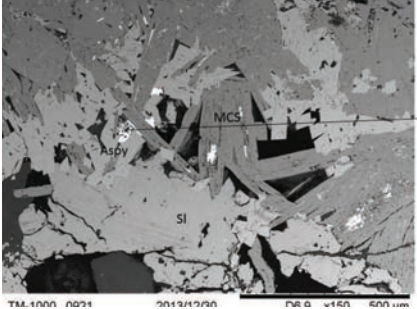
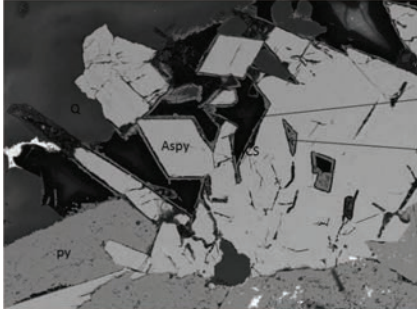
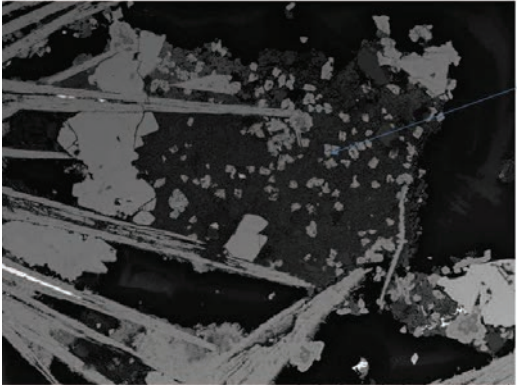
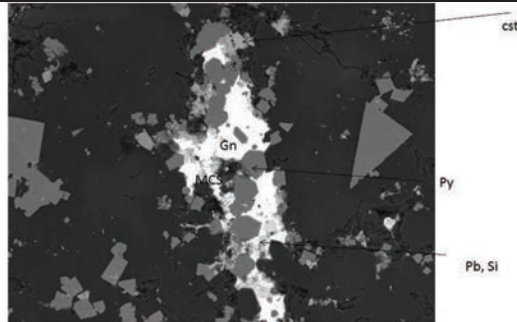
<b>#5</b>	<b>Japo</b>	 <p>TM-1000 0949 2083/01/26 D8,9 x1,8k 50 um</p>
METALLIC	Stannite	
TEXTURE	Idiomorphic, acicular	 <p>TM-1000 0950 2083/01/26 D9,1 x1,0k 100 um</p>
METALLIC	Stannite (Sn), pyrite (Sy)	
TEXTURE	Idiomorphic	 <p>det HV WD mag DualBSD 20.00 kV 10.1 mm 1 000 x</p> <p>100 µm CCITUB</p>
METALLIC	Stannite (Sn), pyrite (Sy)	
TEXTURE	Idiomorphic	 <p>det HV WD mag DualBSD 20.00 kV 10.1 mm 1 000 x</p> <p>100 µm CCITUB</p>
METALLIC	Stannite (Sn), pyrite (Sy)	

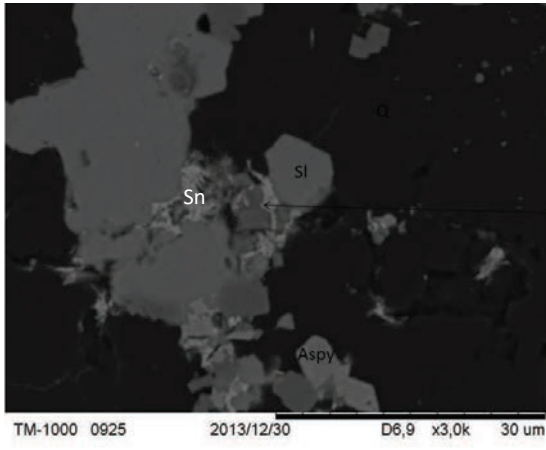
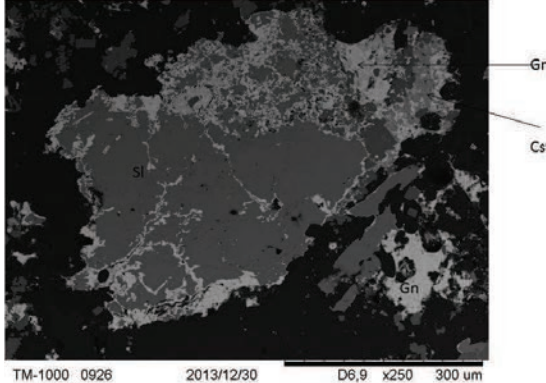
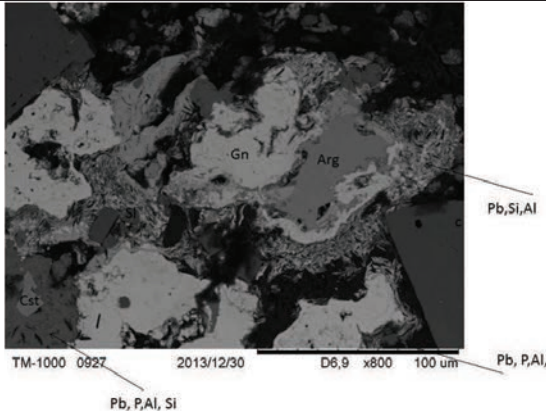
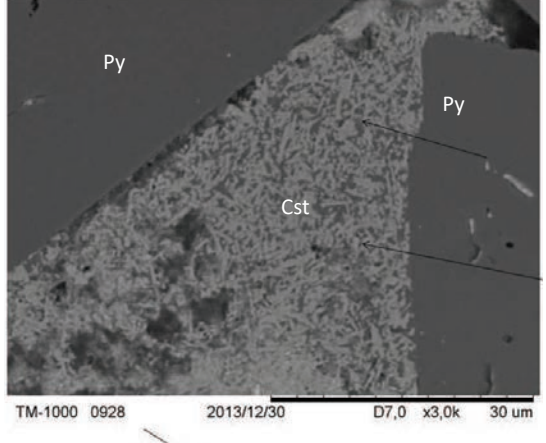


TEXTURE	Idiomorphic	
<b>#10</b>	<b>Japo</b>	
METALLIC	Stannite (Sn), pyrite (Sy)	
TEXTURE	Idiomorphic	
<b>#11</b>	<b>Santa Fe</b>	
METALLIC	Argentite (Arg), tennantite (Ten), pyrite (Py), galena (Gn), sphalerite (Sp)	
TEXTURE	Infilling holes	
<b>#12</b>	<b>Santa Fe</b>	
METALLIC	Rutile (Ti), pyrite (Py), Sn (Stannite)	
TEXTURE	Acicular	

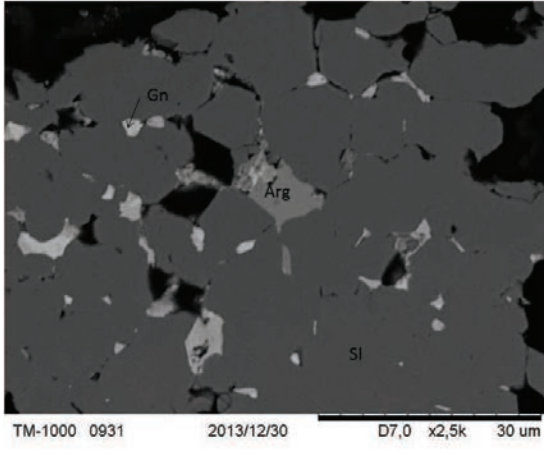
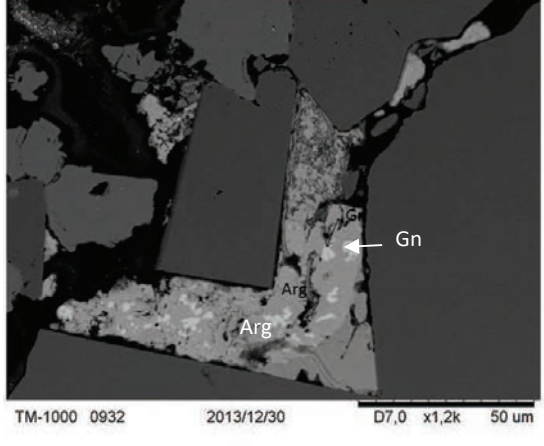
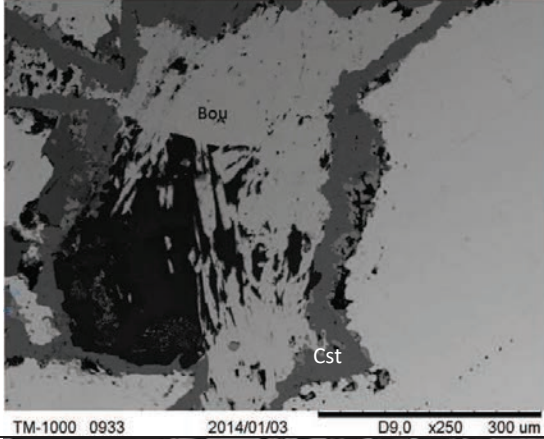
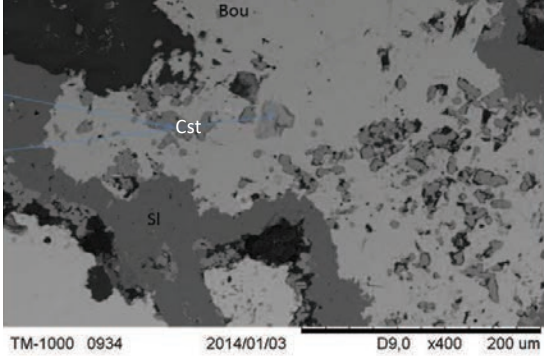
<b>#13</b>	<b>Santa Fe</b>	
METALLIC	Rutile (Ti), pyrite (Py), Sn (Stannite)	
TEXTURE	Idiomorphic, acicular	<p>TM-1000 0901 2013/12/18 D6,1 x5,0k 20 um</p>
<b>#14</b>	<b>Santa Fe</b>	
NO METALLIC	Phosphate	
TEXTURE	Idiomorphic	<p>TM-1000 0902 2013/12/18 D6,1 x3,0k 30 um</p>
<b>#15</b>	<b>Santa Fe</b>	
NO METALLIC	Phosphates: monazite	
TEXTURE	Infilling holes	<p>TM-1000 0904 2013/12/18 D6,1 x1,5k 50 um</p>
<b>#16</b>	<b>Santa Fe</b>	
METALLIC	Sphalerite (SI), pyrite (Py), Apy (arsenopyrite)	
TEXTURE	Exolution (?)	<p>TM-1000 0912 2013/12/18 D6,5 x1,0k 100 um</p>

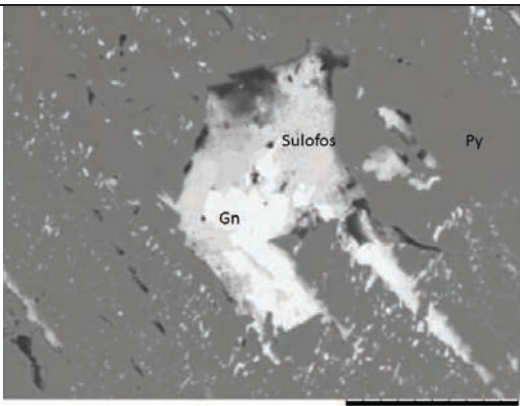
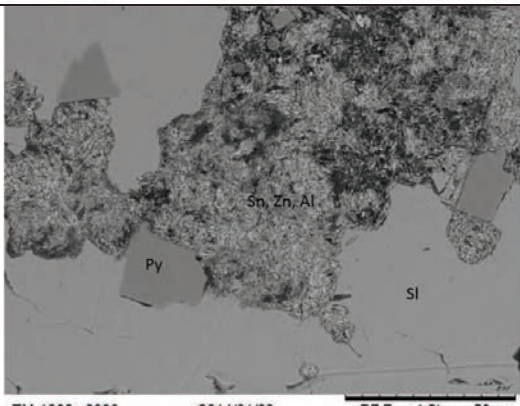
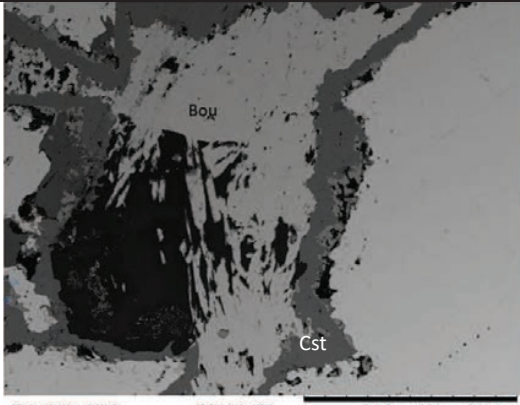
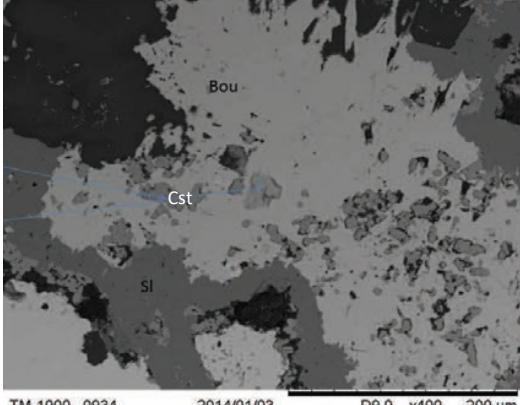
#17	<b>Santa Fe</b>	 <p>TM-1000 0913 2013/12/18 D6,4 x2,0k 30 um</p>
METALLIC	Stannite???	
TEXTURE	Solid solution???	
#18	<b>Santa Fe</b>	 <p>TM-1000 0915 2013/12/18 D6,4 x2,0k 30 um</p>
NO METALLIC	Phosphate	
TEXTURE	Zonation	
#19	<b>Santa Fe</b>	 <p>TM-1000 0918 2013/12/18 D6,4 x1,8k 50 um</p>
NO METALLIC	Phosphates and sulfosalts	
TEXTURE	Alteration	
#20	<b>Santa Fe</b>	 <p>TM-1000 0920 2013/12/18 D6,4 x800 100 um</p>
METALLIC	Sulfosal	
TEXTURE	Exolution (?)	

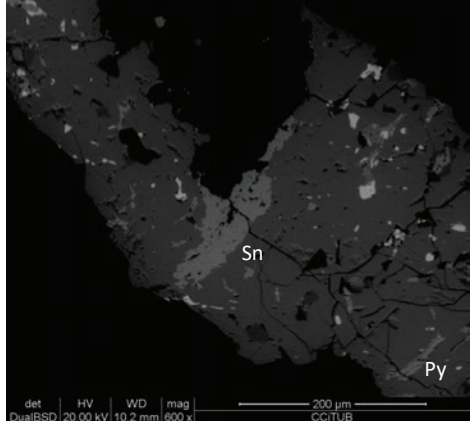
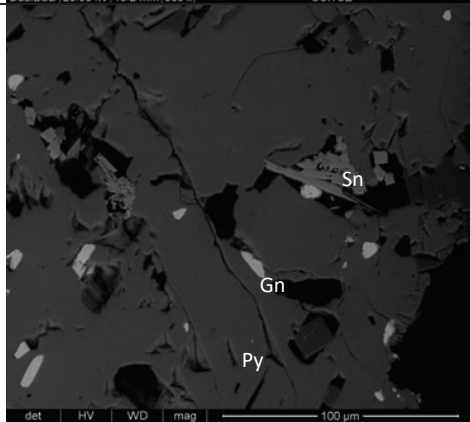
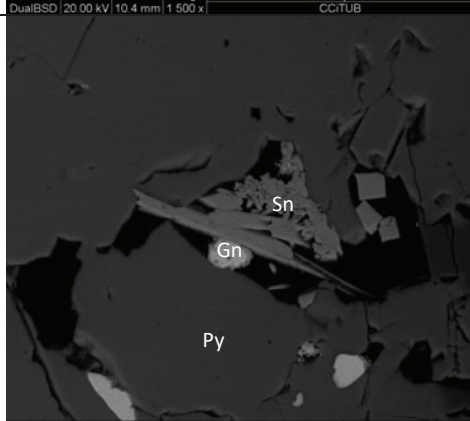
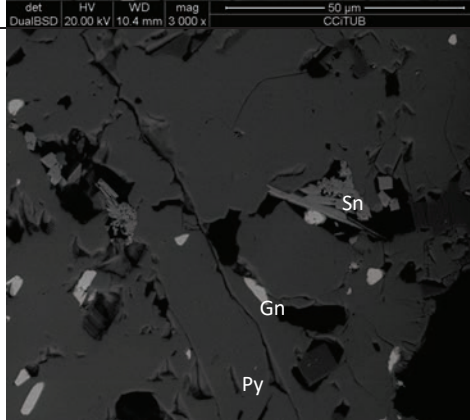


<p><b>#21</b></p> <p>METALLIC</p> <p>TEXTURE</p>	<p><b>Santa Fe</b></p> <p>Marcasite (MCS), arsenopyrite (Aspy), galena (Gn), sphalerite (SI)</p> <p>Paragenetic assemblage</p>	 <p>TM-1000 0921 2013/12/30 D6,0 x400 100 um</p>
<p><b>#22</b></p> <p>METALLIC</p> <p>TEXTURE</p>	<p><b>Santa Fe</b></p> <p>Pyrite (Py), arsenopyrite (Aspy),</p> <p>Zonation</p>	 <p>TM-1000 0922 2013/12/30 D6,7 x800 100 um</p>
<p><b>#23</b></p> <p>METALLIC</p> <p>TEXTURE</p>	<p><b>Santa Fe</b></p> <p>Sulfosalts</p> <p>Replacement</p>	 <p>TM-1000 0923 2013/12/30 D6,7 x250 300 um</p>
<p><b>#24</b></p> <p>METALLIC</p> <p>TEXTURE</p>	<p><b>Santa Fe</b></p> <p>Cassiterite (cst), galena (Gn), pyrite (Py)</p> <p>Paragenetic assemblage</p>	 <p>TM-1000 0924 2013/12/30 D7,0 x800 100 um</p>

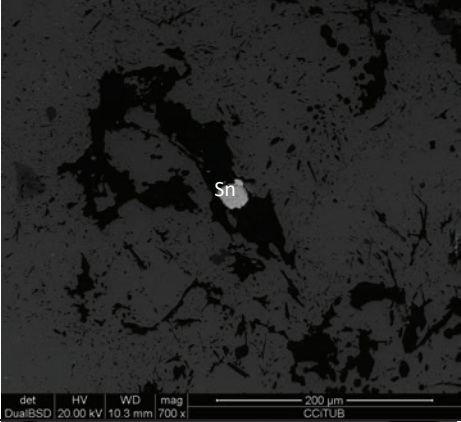

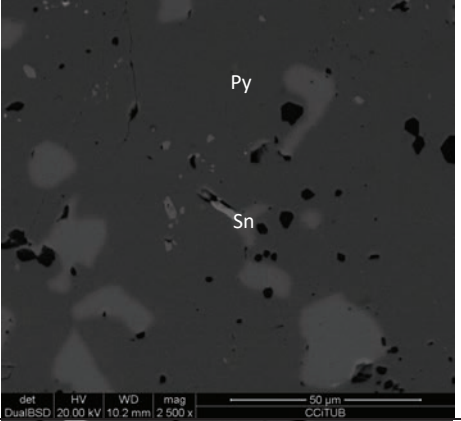

#25	<b>Santa Fe</b>	
METALLIC	Arsenopyrite (Aspy), galena (Gn), sphalerite (Sl), Quartz (Q)	
TEXTURE	Paragenetic assemblage	
METALLIC	#26 <b>Santa Fe</b> Cassiterite (Cst), galena (Gn), sphalerite (Sl)	
TEXTURE	#27 <b>Santa Fe</b> Cassiterite (Cst), galena (Gn), argentite (Arg)	
METALLIC	#28 <b>Santa Fe</b> Cassiterite (cst), pyrite (Py)	
TEXTURE	Infilling	

#29	<b>Santa Fe</b>	
METALLIC	Galena (Gn), sphalerite (Sl), argentite (Arg)	
TEXTURE	Paragenetic assemblage	
#30	<b>Santa Fe</b>	
METALLIC	Galena (Gn), argentite (Arg)	
TEXTURE	Infilling	
#31	<b>Santa Fe</b>	
METALLIC	Cassiterite (cst), boulangerite (Bou)	
TEXTURE	Replacement	
#32	<b>Santa Fe</b>	
METALLIC	Cassiterite (cst), boulangerite (Bou)	
TEXTURE	Replacement	

#33	Santa Fe	 <p>TM-1000 0935 2014/01/03 D7,8 x2,0k 30 um</p>
METALLIC	Galena (Gn), pyrite (Py), sulfosalts	
TEXTURE	Infilling	 <p>TM-1000 0938 2014/01/03 D7,7 x1,2k 50 um</p>
METALLIC	Sphalerite (Sl), pyrite (Py)	
TEXTURE	Infilling	 <p>TM-1000 0933 2014/01/03 D9,0 x250 300 um</p>
METALLIC	Cassiterite (cst), boulangerite (Bou)	
TEXTURE	Replacement	 <p>TM-1000 0934 2014/01/03 D9,0 x400 200 um</p>
METALLIC	Cassiterite (cst), boulangerite (Bou)	

#37	<b>Morococala</b>	
METALLIC	Stannite (Sn), pyrite (Sy)	
TEXTURE	Idiomorphic	
#38	<b>Morococala</b>	
METALLIC	Stannite (Sn), pyrite (Sy), galena (Gn)	
TEXTURE	Idiomorphic	
#39	<b>Morococala</b>	
METALLIC	Stannite (Sn), pyrite (Sy), galena (Gn)	
TEXTURE	Idiomorphic	
#38	<b>Morococala</b>	
METALLIC	Stannite (Sn), pyrite (Sy), galena (Gn)	
TEXTURE	Idiomorphic	

#39	<b>Morococala</b>	
METALLIC	Stannite (Sn), pyrite (Sy)	
TEXTURE	Idiomorphic	
METALLIC	Stannite (Sn), pyrite (Sy)	
TEXTURE	Idiomorphic	
#41	<b>Morococala</b>	
METALLIC	Stannite (Sn), pyrite (Sy), galena (Gn)	
TEXTURE	Idiomorphic	
#42	<b>Morococala</b>	
METALLIC	Stannite (Sn), pyrite (Sy), quartz (Q)	
TEXTURE	Idiomorphic	

#43	<b>Morococala</b>	
METALLIC	Stannite (Sn)	
TEXTURE	Idiomorphic	
METALLIC	Stannite (Sn), pyrite (Sy)	
TEXTURE	Idiomorphic	
METALLIC	Stannite (Sn), pyrite (Sy)	
TEXTURE	Idiomorphic	
METALLIC	Stannite (Sn), pyrite (Sy), galena (Gn)	
TEXTURE	Idiomorphic	

## APPENDIX 6

JAPO													
	Sp	Sp	Sp	Sp	Sp	sp	sp	sp	sp	sp	sp	sp	sp
	1	2	3	4	5	6	7	8	9	10	11	12	13
S	33,070	32,770	32,600	34,580	33,000	33,060	32,490	31,870	32,480	32,390	31,740	32,980	32,840
Fe	12,190	11,460	11,000	13,390	11,610	11,150	12,000	12,230	12,230	12,990	12,280	11,390	10,960
Cu	0,090	0,420	0,700	0,200	0,460	0,710	0,140	3,660	0,360	0,100	0,620	0,430	1,450
Zn	51,740	52,090	51,980	49,440	53,630	50,170	51,330	44,670	51,620	51,250	51,750	51,060	50,390
Ag	0,040	0,050	0,040	0,030	0,000	0,000	0,000	0,030	0,020	0,000	0,000	0,000	0,000
Cd	0,630	0,680	0,400	0,390	0,370	0,730	0,610	0,670	0,670	0,730	0,780	0,540	0,560
Sn	0,000	0,000	0,000	0,000	0,000	0,180	0,060	0,160	0,110	0,130	0,280	0,350	0,110
In	0,120	0,160	0,090	0,240	0,000	0,120	0,030	0,000	0,000	0,020	0,000	0,020	0,110
Pb	0,150	0,030	0,100	0,070	0,100	0,000	0,100	0,130	0,020	0,130	0,050	0,140	0,030
Total	98,300	97,690	97,020	98,390	99,180	97,050	97,870	97,590	98,280	97,890	98,580	97,480	97,260
S	1,031	1,022	1,017	1,078	1,029	1,031	1,013	0,994	1,013	1,010	0,990	1,028	1,024
Fe	0,218	0,205	0,197	0,240	0,208	0,200	0,215	0,219	0,219	0,233	0,220	0,204	0,196
Cu	0,001	0,007	0,011	0,003	0,007	0,011	0,002	0,058	0,006	0,002	0,010	0,007	0,023
Zn	0,791	0,796	0,795	0,756	0,820	0,767	0,785	0,683	0,789	0,784	0,791	0,781	0,770
Ag	0,000	0,000	0,000	0,000	0,000	0,000	0,000	0,000	0,000	0,000	0,000	0,000	0,000
Cd	0,006	0,006	0,004	0,003	0,003	0,006	0,005	0,006	0,006	0,006	0,007	0,005	0,005
Sn	0,000	0,000	0,000	0,000	0,000	0,002	0,001	0,001	0,001	0,001	0,002	0,003	0,001
In	0,001	0,001	0,001	0,002	0,000	0,001	0,000	0,000	0,000	0,000	0,000	0,000	0,001
Pb	0,001	0,001	0,000	0,001	0,000	0,001	0,000	0,000	0,000	0,000	0,000	0,000	0,001

	sp	Sp	Sp	Sp	Sp	Sp	sp	sp	Sp	Sp	Sp	Sp	Sp
	1	2	3	4	5	6	7	8	9	10	11	12	13
S	32,670	33,630	34,770	32,820	33,240	32,760	33,490	33,050	33,637	34,388	34,620	33,899	34,322
Fe	9,270	9,580	13,940	9,740	9,610	9,270	11,010	7,770	6,460	8,284	8,644	5,654	8,233
Cu	0,090	0,160	0,170	0,080	0,000	0,210	0,170	0,010	0,078	0,014	0,372	0,210	0,118
Zn	56,520	56,220	49,210	54,460	55,690	57,090	53,390	55,570	57,859	55,736	54,308	58,919	55,162
Ag	0,000	0,030	0,050	0,000	0,000	0,340	0,000	0,000	0,000	0,000	0,000	0,000	0,000
Cd	0,260	0,060	0,200	0,380	0,280	0,000	0,280	0,250	0,039	0,000	0,009	0,048	0,000
Sn	0,000	0,000	0,000	0,000	0,000	0,000	0,150	0,020	0,094	0,014	0,519	0,388	0,144
In	0,000	0,030	0,000	0,000	0,000	0,000	0,000	0,070	0,000	0,011	0,000	0,000	0,000
Pb	0,010	0,230	0,070	0,220	0,170	0,220	0,180	0,060	0,029	0,000	0,287	0,000	0,000
Total	99,340	100,040	98,520	97,730	99,050	100,360	99,020	97,230	98,426	98,620	99,163	99,477	98,183
S	1,019	1,049	1,084	1,023	1,036	1,022	1,044	1,031	1,049	1,072	1,080	1,057	1,070
Fe	0,166	0,172	0,250	0,174	0,172	0,166	0,197	0,139	0,116	0,148	0,155	0,101	0,147
Cu	0,001	0,003	0,003	0,001	0,000	0,003	0,003	0,000	0,001	0,000	0,006	0,003	0,002
Zn	0,864	0,860	0,752	0,833	0,851	0,873	0,816	0,850	0,885	0,852	0,830	0,901	0,843
Ag	0,000	0,000	0,000	0,000	0,000	0,003	0,000	0,000	0,000	0,000	0,000	0,000	0,000
Cd	0,002	0,001	0,002	0,003	0,002	0,000	0,002	0,002	0,000	0,000	0,000	0,000	0,000
Sn	0,000	0,000	0,000	0,000	0,000	0,000	0,001	0,000	0,001	0,000	0,004	0,003	0,001
In	0,000	0,000	0,000	0,000	0,000	0,000	0,000	0,001	0,000	0,000	0,000	0,000	0,000
Pb	0,000	0,000	0,000	0,000	0,000	0,000	0,000	0,000	0,000	0,000	0,000	0,000	0,000



APPENDIX 6.

MOROCOCALE																				
	Sp	Sp	Sp	Sp	Sp	Sp	Sp	Sp	Sp	Sp	Sp	Sp	Sp	Sp	Sp	Sp	Sp	Sp	Sp	Sp
	1	2	3	4	5	6	7	8	9	10	11	12	13	14	15	16	17	18	19	20
S	34,266	34,491	34,245	34,016	34,775	34,723	34,374	34,385	34,490	34,340	34,340	34,940	34,930	34,550	34,370	35,360	34,570	34,370	34,490	33,570
Fe	7,811	7,964	8,017	7,993	7,724	7,709	7,819	8,904	11,040	10,890	10,820	11,060	10,870	11,360	11,350	11,930	11,090	10,900	11,110	10,440
Cu	0,964	0,078	0,070	0,099	0,031	0,117	0,091	0,682	0,133	0,000	0,039	0,028	0,045	0,040	0,024	0,054	0,051	0,044	0,093	0,000
Zn	54,865	56,086	55,342	55,562	56,245	56,540	56,406	54,261	53,860	54,550	54,510	54,480	54,160	53,690	53,930	51,960	54,420	54,500	54,100	54,000
Ag	0,000	0,000	0,000	0,000	0,000	0,000	0,000	0,000	0,012	0,000	0,009	0,020	0,010	0,000	0,015	0,006	0,000	0,006	0,002	0,003
Cd	0,000	0,033	0,003	0,000	0,019	0,000	0,003	0,059	0,392	0,349	0,327	0,386	0,364	0,389	0,372	0,364	0,344	0,352	0,329	0,342
Sn	0,936	0,000	0,000	0,000	0,007	0,000	0,003	0,017	0,000	0,000	0,000	0,000	0,000	0,000	0,000	0,000	0,000	0,000	0,000	0,000
In	0,126	0,139	0,051	0,128	0,104	0,170	0,113	0,080	0,118	0,030	0,046	0,070	0,051	0,063	0,064	0,055	0,090	0,053	0,144	0,056
Pb	0,000	0,000	0,074	0,000	0,000	0,089	0,060	0,025	0,177	0,000	0,145	0,175	0,162	0,172	0,096	0,227	0,047	0,230	0,184	0,000
Total	99,103	99,188	97,939	98,119	99,224	99,662	98,990	98,562	100,241	100,224	100,236	101,230	100,623	100,361	100,221	99,961	100,641	100,480	100,452	98,412
S	1,068	1,075	1,068	1,061	1,084	1,083	1,072	1,072	1,075	1,071	1,071	1,089	1,089	1,077	1,072	1,103	1,078	1,072	1,075	1,047
Fe	0,140	0,143	0,144	0,143	0,138	0,138	0,140	0,159	0,198	0,195	0,194	0,198	0,195	0,203	0,203	0,214	0,199	0,195	0,199	0,187
Cu	0,015	0,001	0,001	0,002	0,000	0,002	0,001	0,011	0,002	0,000	0,001	0,000	0,001	0,001	0,000	0,001	0,001	0,001	0,001	0,000
Zn	0,839	0,857	0,846	0,849	0,860	0,864	0,862	0,830	0,823	0,834	0,833	0,833	0,828	0,821	0,824	0,794	0,832	0,833	0,827	0,826
Ag	0,000	0,000	0,000	0,000	0,000	0,000	0,000	0,000	0,000	0,000	0,000	0,000	0,000	0,000	0,000	0,000	0,000	0,000	0,000	0,000
Cd	0,000	0,000	0,000	0,000	0,000	0,000	0,000	0,001	0,003	0,003	0,003	0,003	0,003	0,003	0,003	0,003	0,003	0,003	0,003	0,003
Sn	0,008	0,000	0,000	0,000	0,000	0,000	0,000	0,000	0,000	0,000	0,000	0,000	0,000	0,000	0,000	0,000	0,000	0,000	0,000	0,000
In	0,001	0,001	0,000	0,001	0,001	0,001	0,001	0,001	0,001	0,000	0,000	0,001	0,000	0,001	0,001	0,000	0,001	0,000	0,001	0,000
Pb	0,001	0,001	0,000	0,001	0,001	0,001	0,001	0,000	0,001	0,000	0,000	0,000	0,000	0,000	0,000	0,000	0,000	0,000	0,001	0,000

MOROCOCALE																				
	Sp	Sp	Sp	Sp	Sp	Sp	Sp	Sp	Sp	Sp	Sp	Sp	Sp	Sp	Sp	Sp	Sp	Sp	Sp	Sp
	21	22	23	24	25	26	27	28	29	30	31	32	33	34	35	36	37	38	39	40
S	34,680	34,390	34,780	34,740	34,060	34,600	34,350	34,520	34,460	32,110	34,530	34,280	34,300	34,550	33,680	35,060	34,130	34,090	34,010	33,360
Fe	11,530	10,250	11,450	11,450	11,340	11,220	10,570	5,880	5,020	4,640	11,670	11,010	11,150	10,970	11,320	10,700	8,730	10,010	10,050	7,520
Cu	0,000	0,037	0,003	0,026	0,086	0,088	0,390	0,000	0,000	0,034	2,740	0,106	0,056	1,510	5,980	0,075	0,059	1,000	1,050	0,136
Zn	53,810	53,330	54,050	53,800	53,330	53,510	53,690	57,710	60,250	58,250	49,350	54,550	54,240	51,850	43,800	54,110	55,920	53,480	53,120	56,680
Ag	0,000	0,020	0,027	0,003	0,000	0,010	0,015	0,000	0,000	0,000	0,028	0,028	0,000	0,050	0,149	0,026	0,000	0,016	0,000	0,035
Cd	0,326	0,366	0,350	0,362	0,329	0,300	0,374	0,323	0,303	0,264	0,387	0,443	0,403	0,279	0,358	0,457	0,286	0,197	0,078	0,248
Sn	0,000	0,000	0,047	0,000	0,077	0,000	0,290	0,079	0,170	2,250	2,770	0,000	0,015	1,640	5,580	0,000	0,043	0,252	0,249	0,125
In	0,049	0,041	0,030	0,052	0,083	0,111	0,000	0,000	0,000	0,000	0,261	0,108	0,092	0,090	0,124	0,093	0,022	0,006	0,033	0,033
Pb	0,055	0,000	0,060	0,057	0,121	0,044	0,000	0,226	0,280	0,056	0,146	0,093	0,104	0,095	0,035	0,111	0,151	0,100	0,086	0,074
Total	100,455	98,477	100,842	100,549	99,455	99,993	99,777	98,752	100,496	97,644	101,916	100,788	100,735	101,144	101,346	100,9	99,746	99,260	98,946	98,222
S	1,081	1,072	1,085	1,083	1,062	1,079	1,071	1,076	1,075	1,001	1,077	1,069	1,070	1,077	1,050	1,093	1,064	1,063	1,060	1,040
Fe	0,206	0,184	0,205	0,205	0,203	0,201	0,189	0,105	0,090	0,083	0,209	0,197	0,200	0,196	0,203	0,192	0,156	0,179	0,180	0,135
Cu	0,000	0,001	0,000	0,000	0,001	0,001	0,006	0,000	0,000	0,001	0,043	0,002	0,001	0,024	0,094	0,001	0,001	0,016	0,017	0,002
Zn	0,823	0,815	0,826	0,823	0,815	0,818	0,821	0,882	0,921	0,891	0,754	0,834	0,829	0,793	0,670	0,827	0,855	0,818	0,812	0,867
Ag	0,000	0,000	0,000	0,000	0,000	0,000	0,000	0,000	0,000	0,000	0,000	0,000	0,000	0,000	0,001	0,000	0,000	0,000	0,000	0,000
Cd	0,003	0,003	0,003	0,003	0,003	0,003	0,003	0,003	0,003	0,002	0,003	0,004	0,004	0,002	0,003	0,004	0,003	0,002	0,001	0,002
Sn	0,000	0,000	0,000	0,000	0,001	0,000	0,002	0,001	0,001	0,019	0,023	0,000	0,000	0,014	0,047	0,000	0,000	0,002	0,002	0,001
In	0,000	0,000	0,000	0,000	0,001	0,000	0,000	0,000	0,000	0,000	0,002	0,001	0,001	0,014	0,047	0,000	0,000	0,002	0,002	0,001
Pb	0,000	0,000	0,000	0,000	0,001	0,001	0,000	0,000	0,000	0,000	0,002	0,001	0,001	0,001	0,001	0,001	0,000	0,000	0,000	0,000

APPENDIX 6.

Santa Fe																						
	Hoc	Hoc	Hoc	Pir	Pot	Cyl	Cyl	Cyl	Frei	Frak	Frak	Frak	Frak	Frak	Via	Arg	Arg	Arg	Mat	Mat	Mat	Mat
	1	2	3	4	5	6	7	8	9	10	11	12	13	14	15	16	17	18	1	2	3	4
S	24,75	24,99	24,49	5,49	20,36	4,35	4,85	5,61	23,08	20,56	20,27	19,73	19,04	20,10	48,18	16,88	17,72	13,26	9,06	18,82	18,73	18,70
Fe	6,83	6,83	3,79	0,80	4,12	0,58	0,36	0,60	6,06	2,26	2,66	2,77	3,37	2,39	40,44	0,10	0,07	0,20	0,20	1,51	1,55	1,16
Cu	1,59	1,62	0,23	0,02	0,04	0,04	0,72	0,00	25,63	0,02	0,07	0,03	0,12	0,00	0,00	0,17	0,24	0,21	4,17	0,05	0,03	0,00
Zn	2,05	1,99	11,18	0,03	0,14	0,11	0,16	0,00	0,76	0,12	0,05	0,13	0,33	0,07	0,04	0,57	0,63	2,03	0,27	6,15	6,15	5,35
As	0,00	0,00	0,06	0,05	0,00	0,00	0,07	0,00	0,00	0,00	0,00	0,00	0,17	0,04	0,00	0,29	0,27	0,26	0,00	0,05	0,00	0,04
Se	0,17	0,00	0,09	0,10	0,09	0,13	0,11	0,02	0,00	0,00	0,00	0,05	0,05	0,02	0,05	0,00	0,00	0,00	0,00	0,07	0,06	0,11
Ag	39,56	39,96	39,47	0,07	0,53	0,00	0,21	0,00	14,95	0,38	0,33	0,46	1,05	0,35	0,05	63,82	61,22	66,81	6,78	10,30	10,24	10,59
Cd	0,00	0,00	0,00	0,10	0,31	0,03	0,38	0,00	0,12	0,87	0,00	0,00	0,21	0,05	0,11	0,00	0,00	0,07	0,00	0,21	0,00	0,00
In	0,00	0,00	0,00	0,09	0,02	0,06	0,07	0,05	0,00	0,07	0,00	0,05	0,00	0,02	0,00	0,00	0,00	0,00	0,00	0,00	0,00	0,00
Sn	23,64	23,81	22,09	29,92	12,57	27,04	32,37	16,59	1,21	12,98	13,11	12,96	14,21	12,56	0,09	0,00	0,00	0,00	0,32	0,00	0,00	0,00
Sb	0,00	0,00	0,00	0,00	11,13	0,00	0,00	0,00	26,53	11,14	10,94	10,97	10,50	11,59	0,12	24,48	22,64	17,64	0,31	0,14	0,11	0,00
W	0,00	0,00	0,00	0,00	0,00	0,00	0,00	0,00	0,00	0,00	0,00	0,00	0,00	0,00	0,00	0,00	0,00	0,00	0,00	0,00	0,00	0,10
Pb	0,05	0,02	0,07	43,72	51,58	37,52	36,10	57,81	0,29	52,79	52,48	52,17	46,68	51,85	11,23	0,05	0,04	0,00	0,11	3,72	3,61	3,45
Bi	0,00	0,00	0,00	0,00	0,00	0,00	0,00	0,00	0,05	0,00	0,00	0,00	0,00	0,00	0,00	0,00	0,00	0,00	60,59	61,47	61,90	62,46
Total	98,65	99,32	101,63	82,66	102,22	70,6	76,6	81,5	98,78	101,47	100,70	100,31	96,24	99,35	100,60	106,36	102,88	100,73	81,81	102,51	102,40	101,96
S	3,99	4,00	3,99	3,97	16,0	4,0	4,0	4,0	13,00	14,00	14,00	13,99	13,99	15,99	8,00	1,00	1,00	1,00	5,00	3,99	3,99	3,99
Fe	0,63	0,63	0,35	0,33	1,9	0,3	0,2	0,2	1,96	0,88	1,05	1,13	1,42	1,09	3,85	0,00	0,00	0,01	0,06	0,18	0,19	0,14
Cu	0,13	0,13	0,02	0,01	0,0	0,0	0,3	0,0	7,29	0,01	0,02	0,01	0,04	0,00	0,00	0,01	0,01	0,01	1,16	0,00	0,00	0,00
Zn	0,16	0,16	0,89	0,01	0,1	0,0	0,1	0,0	0,21	0,04	0,02	0,05	0,12	0,03	0,00	0,02	0,02	0,07	0,07	0,64	0,64	0,56
As	0,00	0,00	0,00	0,02	0,0	0,0	0,0	0,0	0,00	0,00	0,00	0,00	0,05	0,01	0,00	0,01	0,01	0,01	0,00	0,00	0,00	0,00
Ag	1,90	1,90	1,91	0,02	0,1	0,0	0,1	0,0	2,50	0,08	0,07	0,10	0,23	0,08	0,00	1,12	1,03	1,50	1,11	0,65	0,65	0,67
Cd	0,00	0,00	0,00	0,00	0,0	0,0	0,0	0,0	0,00	0,00	0,00	0,00	0,00	0,00	0,00	0,00	0,00	0,00	0,00	0,01	0,00	0,00
In	0,00	0,00	0,00	0,02	0,0	0,0	0,0	0,0	0,00	0,01	0,00	0,01	0,00	0,00	0,00	0,00	0,00	0,00	0,00	0,00	0,00	0,00
Sn	1,03	1,03	0,97	5,85	2,7	6,6	7,1	3,2	0,18	2,39	2,45	2,48	2,82	2,70	0,00	0,00	0,00	0,00	0,05	0,00	0,00	0,00
Sb	0,00	0,00	0,00	0,00	2,3	0,0	0,0	0,0	3,94	2,00	1,99	2,05	2,03	2,43	0,01	0,38	0,34	0,35	0,04	0,01	0,01	0,00
Se	0,00	0,00	0,01	0,03	0,0	0,0	0,0	0,0	0,00	0,00	0,00	0,01	0,01	0,01	0,00	0,00	0,00	0,00	0,00	0,01	0,01	0,01
Pb	0,00	0,00	0,00	4,89	6,3	5,3	4,6	6,4	0,03	5,56	5,61	5,72	5,31	6,39	0,29	0,00	0,00	0,00	0,01	0,12	0,12	0,11
Bi	0,00	0,00	0,00	0,00	0,0	0,0	0,0	0,0	0,00	0,00	0,00	0,00	0,00	0,00	0,00	0,00	0,00	0,00	5,13	2,00	2,03	2,05

APPENDIX 6.

Morococala									
Mat	Lill	Lill	Lill	Lill	Gus	Our	Our	Plat	Plat
5	6	7	8	9	10	11	12	13	14
18,07	16,60	17,11	17,07	15,09	16,55	16,38	16,54	12,82	13,05
0,93	0,86	1,16	3,24	2,03	1,64	0,68	0,74	0,59	1,22
0,22	0,68	0,66	0,65	0,03	0,06	0,02	0,00	0,02	0,05
6,03	1,14	0,20	0,03	0,01	0,02	0,00	0,00	0,14	0,03
0,08	0,00	0,01	0,01	0,00	0,00	0,01	0,01	0,06	0,00
0,53	0,59	0,60	0,52	0,45	0,82	0,91	1,13	1,18	0,99
11,22	2,33	2,33	2,16	8,21	9,22	8,56	8,58	1,45	0,98
0,31	0,02	0,00	0,10	0,00	0,00	0,00	0,00	0,00	0,00
0,00	0,01	0,00	0,00	0,00	0,00	0,00	0,00	0,00	0,02
0,00	0,31	0,28	0,21	0,00	0,89	0,05	0,02	0,01	0,09
0,02	6,43	7,01	6,43	0,97	6,16	3,50	3,55	0,03	0,12
0,00	0,00	0,00	0,00	0,00	0,00	0,00	0,00	0,00	0,00
6,44	44,29	42,84	42,05	16,97	16,71	26,71	25,82	78,38	81,55
57,81	26,66	28,46	27,83	52,08	42,80	40,51	42,52	3,90	2,83
101,68	99,92	100,67	100,33	95,85	94,9	97,34	98,92	98,59	100,98
17,78	5,91	5,91	5,92	5,92	5,9	29,3	29,1	0,96	3,87
0,52	0,18	0,23	0,65	0,46	0,3	0,7	0,8	0,03	0,21
0,11	0,12	0,12	0,11	0,01	0,0	0,0	0,0	0,00	0,01
2,91	0,20	0,03	0,01	0,00	0,0	0,0	0,0	0,00	0,00
0,04	0,00	0,00	0,00	0,00	0,0	0,0	0,0	0,00	0,00
3,28	0,25	0,24	0,22	0,96	1,0	4,6	4,5	0,03	0,09
0,09	0,00	0,00	0,01	0,00	0,0	0,0	0,0	0,00	0,00
0,00	0,00	0,00	0,00	0,00	0,0	0,0	0,0	0,00	0,00
0,00	0,03	0,03	0,02	0,00	0,1	0,0	0,0	0,00	0,01
0,00	0,60	0,64	0,59	0,10	0,6	1,6	1,6	0,00	0,01
0,22	0,09	0,09	0,08	0,08	0,1	0,7	0,9	0,04	0,13
0,98	2,44	2,29	2,26	1,03	0,9	7,4	7,0	0,91	3,75
8,73	1,46	1,51	1,48	3,14	2,3	11,1	11,5	0,04	0,13

